Inaugural – Dissertation

zur

Erlangung der Doktorwürde

der

Naturwissenschaftlichen – Mathematischen Gesamtfakultät

der

Ruprecht – Karls – Universität

Heidelberg

vorgelegt von

Master of Science Ilka Maria Bartsch

aus Mainz

Tag der mündlichen Prüfung: 22.06.2020

Dynamics of the human T cell response to repeated immunization with irradiated malaria parasites

Gutachter:

Prof. Dr. Hans-Reimer Rodewald

Prof. Dr. Hedda Wardemann

Abstract

Plasmodium falciparum (*Pf*) is a unicellular parasite and the major causative agent of human malaria. The sporozoite form of the parasite is transferred from mosquitos to humans and can infect hepatocytes in the liver. Both *Pf*-specific antibodies, generated with the help of $CD4^+$ T follicular helper cells, and $CD8^+$ T cells can limit disease progression at an early stage by preventing the infection of hepatocytes and eliminating infected cells, respectively. However, so far no vaccine is capable of eliciting strong humoral and cellular immune responses that can reliably confer long-term protection. Therefore, a better understanding of immune responses induced by current vaccines is necessary to guide the development of alternative vaccination strategies. While many studies focused on the evolution of protective B cell responses during malaria immunizations, little is known about the kinetics of emergence and maintenance of T cell subsets. In this study, a newly developed platform for the single-cell, high-throughput sequencing and expression-cloning of human T cell receptors (TCRs) was applied to characterize the TCR repertoire of $CD8^+$ effector memory T (T_{EM}) cells and $CD4^+$ circulating T follicular helper (cT_{FH}) cells induced during immunization with radiation-attenuated sporozoites (*Pf* RAS). This study revealed that the two subsets show contrary dynamics in their repertoire upon immunization. In activated $CD8^+$ T_{EM} cells, the repertoire was dominated by large, persistent clones which did not respond to *Pf* RAS immunization. The recruitment of smaller, highly diverse clones of yet unknown specificity resulted in the diversification of the repertoire upon immunization. In contrast, in the cT_{FH} cell compartment the *Pf* RAS immunization led to the clonal expansion of activated cells, which dominated the otherwise highly polyclonal repertoire. The activated cT_{FH} cells were highly enriched for clones reacting to the C-terminal region of the circumsporozoite protein (C-CSP), the most abundant protein on the surface of sporozoites. While most of the C-CSP-reactive cT_{FH} cells carried diverse TCRs, some formed clusters of highly similar TCRs that could be detected within but also between donors, indicating convergence in the otherwise highly diverse TCR repertoire. Identification of epitopes targeted by the *Pf*-specific TCRs could complement the information about the dynamics of *Pf*-specific clones and would thereby provide helpful insight into how different T cell epitopes shape the T cell repertoire during immunizations. This information could help to optimize existing vaccines, e.g. by reducing subunit vaccines to epitopes which dominate the *Pf*-specific T cell responses and are highly conserved between *Pf* strains, thereby enhancing protection from heterologous infection.

Zusammenfassung

Plasmodium falciparum (*Pf*) ist ein einzelliger Parasit und der wichtigste Erreger der Malaria im Menschen. Die Parasiten werden im Sporozoiten-Stadium von Mücken auf den Menschen übertragen und können dort Hepatozyten in der Leber infizieren. Sowohl *Pf*-spezifische Antikörper, die unter Hilfe von $CD4^+$ follikulären T-Helferzellen gebildet wurden, als auch $CD8^+$ T-Zellen können den Krankheitsverlauf in einem frühen Stadium eingrenzen, indem sie die Infektion von Hepatozyten verhindern oder infizierte Zellen eliminieren. Allerdings gibt es bis jetzt keinen Impfstoff, der starke humorale und zelluläre Immunantworten hervorrufen kann, welche einen zuverlässigen Langzeitschutz vermitteln. Daher ist ein besseres Verständnis der durch derzeitige Impfstoffe hervorgerufenen Immunantworten erforderlich, um die Entwicklung von alternativen Impfstrategien zu ermöglichen. Während sich die meisten Studien auf die Entstehung von schützenden B-Zell-Antworten in Malaria-Immunisierungen fokussiert haben, ist weiterhin wenig über die Kinetik der Entstehung sowie Aufrechterhaltung von T-Zell-Antworten bekannt. In dieser Studie wurde eine neu entwickelte Plattform für die Hochdurchsatz-Einzelzell-Sequenzierung und Expressionsklonierung von humanen T-Zell-Rezeptoren (TCRs) angewendet, um das TCR Repertoire von $CD8^+$ Effektor-Gedächtnis-T-Zellen (T_{EM}) und $CD4^+$ zirkulierenden follikulären T-Helferzellen (cT_{FH}) zu charakterisieren, welche durch die Immunisierung mit bestrahlten Sporozoiten hervorgerufen wurden. Diese Studie verdeutlicht, dass die zwei T-Zellpopulationen nach Immunisierung entgegengesetzte Veränderungen in ihrem Repertoire aufweisen. In aktivierten $CD8^+$ T_{EM}-Zellen wurde das Repertoire von großen, langlebigen Klonen dominiert, die nicht auf die *Pf* RAS Immunisierung reagiert haben. Die Rekrutierung von kleinen, sehr diversen Klonen von unbekannter Spezifität resultierte in einer Diversifizierung des Repertoires nach der Immunisierung. Im Gegensatz dazu führte die *Pf* RAS Immunisierung im cT_{FH}-Zell-Kompartiment zu einer klonalen Expansion aktivierter Zellen, welche das ansonsten sehr polyklonale Repertoire dominierten. Aktivierten cT_{FH}-Zellen waren stark angereichert mit Klonen, die reaktiv gegen die C-terminale Region des Circumsporozoit Proteins (C-CSP) waren, welches das häufigste Protein auf der Oberfäche von Sporozoiten ist. Während die meisten der C-CSP-reaktiven cT_{FH}-Zellen sehr diverse TCRs aufwiesen, konnten Gruppen von TCRs mit hoher Ähnlichkeit innerhalb und zwischen Spendern entdeckt werden, was auf eine Konvergenz in dem ansonsten sehr diversen TCR Repertoire hindeutet. Die Identifizierung von Epitopen, die von diesen *Pf*-spezifischen TCRs erkannt werden, könnte die Informationen über die Dynamik der *Pf*-spezifischen Klone komplettieren und dadurch hilfreiche Einblicke darüber geben, wie verschiedene Epitope das T-Zell-Repertoire nach Immunisierung verändern. Diese Information könnte dabei helfen bestehende Impfstoffe zu verbessern, indem zum Beispiel

Untereinheiten-Impfstoffen auf Epitope reduziert werde, welche die *Pf*-spezifischen T-Zell-Antworten dominieren und zudem hochkonserviert sind zwischen *Pf* Stämmen, wodurch der Schutz gegen heterologe Infektionen erhöht werden kann.

Abbreviations

7-AAD	7-aminoactinomycin D
aa	amino acid
ABTS	2,2'-azino-bis(3-ethylbenzthiazoline-6-sulphonic acid)
AmpR	ampicillin resistance
APC	antigen presenting cell
BCL-6	B-cell lymphoma 6
BCR	B cell receptor
bp	base pair
BSA	bovine serum albumin
$CaCl_2$	calcium chloride
CCR	C-C motif chemokine receptor
C-CSP	C-terminal domain of CSP
CD	cluster of differentiation
cDNA	complementary DNA
CDR	complementary determining region
CMV	cytomegalovirus
CSP	circumsporozoite protein
CSR	class-switch recombination
cT_{FH} cell	circulating T follicular helper cell
CTV	CellTrace™ Violet
CXCL	C-X-C motif chemokine ligand
CXCR	C-X-C motif chemokine receptor
DDX3Y	DEAD-box helicase 3 Y-linked
DMSO	dimethyl sulfoxide
DNA	deoxyribonucleic acid
dNTP	deoxynucleotid triphosphate
DTT	dithiothreitol
EBV	Epstein-Barr virus
E. coli	*Escherichia coli*
ELISA	enzyme-linked immunosorbent assay
FACS	fluorescence-activated cell sorting
FBS	fetal bovine serum
FDC	follicular dendritic cell
FSC	forward scatter

FWR	framework region
GC	germinal center
gDNA	genomic DNA
GFP	green fluorescent protein
GPI	glycosylphosphatidyl-inositol
HBS	HEPES buffered saline
HC-04 cells	human hepatocyte cells
HEPES	4-(2-hydroxyethyl)-1-piperazineethanesulfonic acid
HIV	human immunodeficiency virus
HRP	horseradish peroxidase
ICOS	inducible T-cell costimulator
IFN	interferon
Ig	immunoglobulin
IL	interleukin
IRES	internal ribosomal entry site
J76 cells	Jurkat76 T cells
LB	lysogeny broth
LTR	long terminal repeat
M1	matrix protein 1
MAIT cells	mucosal associated invariant T cells
MFI	mean fluorescence intensity
$MgCl_2$	magnesium chloride
MHC	major histocompatibility complex
mRNA	messenger RNA
NANP	repeat peptide consisting of asparagine-alanine-asparagine-proline
N-CSP	N-terminal domain of CSP
NGS	next-generation sequencing
OD	optical density
OVA	ovalbumin
PAC	puromycin N-acetyltransferase
P. berghei	*Plasmodium berghei*
PBMC	peripheral blood mononuclear cell
PBS	phosphate-buffered saline
PCR	polymerase chain reaction
PD-1	programmed cell death 1

Pf	*Plasmodium falciparum*
PFA	paraformaldehyde
Pf SPZ	*Pf* sporozoites
PGK	phosphoglycerate kinase
pre-T_{FH} cell	precursor T follicular helper cell
RAS	radiation-attenuated sporozoites
RHP	random hexamer primer
RNA	ribonucleic acid
RPMI	Roswell Park Memorial Institute (medium)
RT	reverse transcription
SEB	Staphylococcal enterotoxin B
SHM	somatic hypermutation
SLO	secondary lymphoid organs
SPR	surface plasmon resonance
SS	signal sequence
SSC	sideward scatter
T_{CM} cell	central memory T cell
TCR	T cell receptor
T_{EM} cell	effector memory T cell
T_{EMRA} cell	terminally differentiated effector memory T cell
T_{FH} cell	T follicular helper cell
T_H cell	T helper cell
TLR	toll-like receptor
TRA (V/J/C)	T Cell Receptor Alpha (Variable/Joining/Constant)
TRB (V/J/D/C)	T Cell Receptor Beta (Variable/Joining/Diversity/Constant)
T_{reg} cell	regulatory T cell

Table of Contents

1 Introduction

1.1 T cell responses

The human immune system protects the body from invading pathogens through two arms, the innate and adaptive immunity. While the innate immune system forms the first line of defense, the more specialized adaptive immune system requires several days until it can efficiently target pathogens. The adaptive immune system can be further subdivided into the humoral compartment, consisting of antibody-secreting B lymphocytes, and the cellular compartment, consisting of cytokine-secreting and cytotoxic T lymphocytes. Both B and T lymphocytes can specifically discriminate a great variety of different antigens and thereby target pathogens precisely.

1.1.1 T cell development

T cells develop in the thymus, where they mature and each T cell generates a unique membrane-bound T cell receptor (TCR). This TCR can recognize antigens presented by major histocompatibility complexes (MHCs) and thereby defines the specificity of a given T cell. To target a variety of different antigens, a large repertoire of highly diverse TCRs is generated. Each TCR consists of two chains, the alpha and beta chain. The TCR genes encoding both chains are formed by the assembly of variable (V), diversity (D) and joining (J) segments (Figure 1) [1]. This process involves the random selection of one V, one D (only in beta locus) and one J segment from a pool of germline segments, which are then joined together. The random selection and joining of segments generates a high combinatorial diversity. This diversity is further increased by the random addition and deletion of palindromic (P) and non-templated (N) nucleotides at the junctions of the V(D)J segments [2–4]. The combinatorial diversity, the junctional diversity and the pairing of the alpha and beta chains result in an overall diversity of 10^{15} different TCRs that could be theoretically generated during T cell development [5]. However, as this number exceeds the estimated total number of T cells in a human body (10^{13}), the actual TCR diversity in an individual is lower than the theoretical estimate [6]. Besides the great advantage of generating a high number of different TCR, this process also bears the risk of generating non-functional or auto-reactive T cells. During the development in the thymus, T cells are therefore screened for their ability to recognize self-peptides presented on MHC proteins of thymic stromal cells [7]. T cells that express a functional TCR and weakly bind self-antigens are positively selected (self-MHC restriction), whereas

auto-reactive T cells, strongly binding self-antigens, are eliminated. Positively selected T cells further develop into mature T cells and exit the thymus.

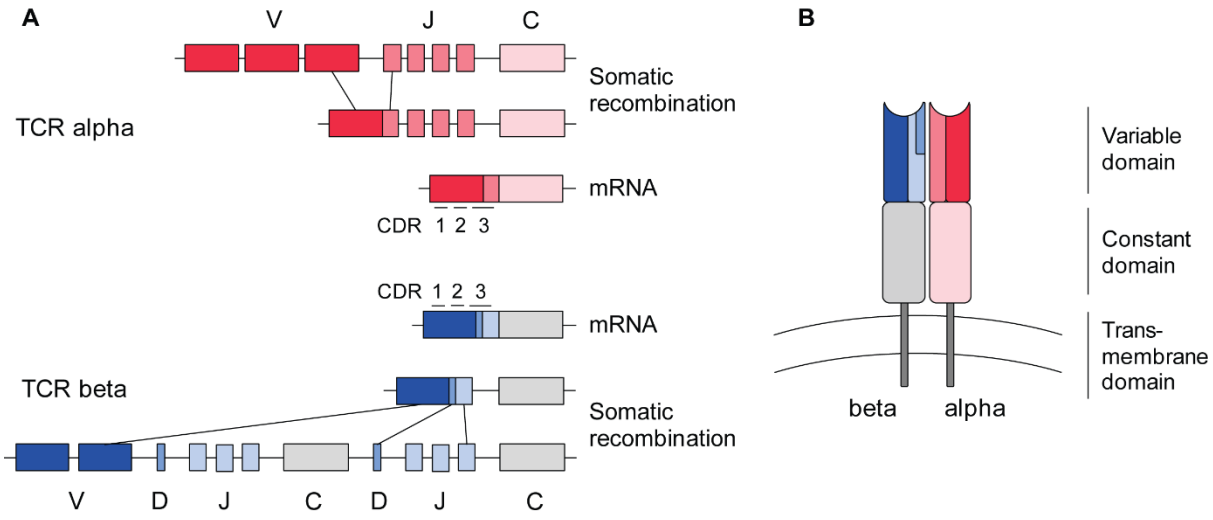

Figure 1: Somatic recombination of the TCR locus. (A) TCRs are generated by random recombination of V and J segments for the alpha locus or V, D and J segments for the beta locus. The V(D)J segments form the variable region of the TCR and contain three complementarity determining regions (CDRs) mediating the antigen recognition. (B) Schematic representation of the TCR structure. The TCR is formed by pairing of the alpha and beta chain and is anchored in the T cell membrane with a transmembrane domain. Each chain contains a constant domain and a variable domain, which is mediating antigen binding. Adapted from [8].

1.1.2 T cell activation and differentiation

T cells exit the thymus in a resting (naive) state and migrate through the peripheral circulation and the secondary lymphoid organs (SLOs) until they encounter their matching antigen and become activated. This activation is required for differentiation into effector cells that can efficiently target the invading pathogens. T cell activation takes place in the SLOs, where T cells interact with antigen presenting cells (APCs), including dendritic cells, macrophages and B cells, which have sampled antigens and present them on their MHC proteins. Two major subtypes of T cells exist, which can be differentiated by the expression of the co-receptors CD4 and CD8. While $CD4^+$ T cells recognize extracellular proteins presented on the MHC-II proteins of the APC, $CD8^+$ T cells are specific for intracellular proteins which are presented on MHC-I proteins [9–11]. This specific binding of TCRs to the peptide-MHC complex forms the basis for T cell activation and is mediated by so-called complementarity determining regions (CDRs) within the TCR. Each chain of the TCR contains three different CDR regions (Figure 1A). While the less variable CDR1 and CDR2 mainly form contacts to the MHC, the highly diverse CDR3 (encoded by the V(D)J segment junction) interacts primarily with the presented peptide [5,12–15].

However the TCR alone is not sufficient to mediate the peptide-MHC interaction as well as the subsequent intracellular signaling, but relies on the help of co-receptors (Figure 2). While the co-receptor CD3 forms a complex together with the TCR and mediates the intracellular signaling, the co-receptors CD4 and CD8 interact with the MHC-II an MHC-I, respectively, and stabilize the interaction between the T cell and APC as well as enhance the intracellular signaling [10,11,16–18]. Besides the interaction of the TCR with the peptide-MHC on the APC (signal 1), T cells require two other signals for complete activation and differentiation into effector cells (Figure 2). This includes on the one hand the interaction of co-stimulatory molecules like CD28 and 4-1BB with their respective ligands, CD80/86 and 4-1BBL, on the surface of APCs, which amplifies the intracellular signaling of the TCR (signal 2) [19–22]. On the other hand, cytokines released by the APC guide the T cell differentiation into different effector cells dependent on the type of infection (signal 3). After proper activation by all three signals, T cells proliferate and differentiate into various distinct effector cells to efficiently target the pathogens. $CD8^+$ effector T cells can eliminate pathogen-infected cells or cancer cells, presenting aberrant peptides on their MHC-I molecules, by the release of cytotoxic mediators. The function of $CD4^+$ effector T cells, however, is highly diverse and dependent on the subtype into which a T cell differentiated, i.e. T helper 1 (T_H1), T helper 2 (T_H2), T helper 17 (T_H17), T follicular helper (T_{FH}) and regulatory T (T_{reg}) cell [23]. While T_H1, T_H2 and T_H17 cells are specialized to respond to intracellular pathogens, helminths and extracellular bacteria or fungi, respectively, T_{FH} and T_{reg} fulfill more generalized functions independent of the type of infection [23–26]. T_{FH} cells play an important role in supporting the immune system by providing help to B cells, whereas T_{reg} cells are crucial for suppressing the immune system to prevent autoimmunity and silence immune responses after clearance of the pathogen [27–30]. This silencing leads to a strong decline of the T cell population after the primary immune response. However a small number of T cells persists and develops into memory T cells, which are classified by less stringent requirements for activation, a high proliferative capacity and a more rapid effector response upon antigen encounter [31]. Among the memory T cells, the effector memory T (T_{EM}) cells are the first responders upon antigen re-encounter as they patrol through the peripheral tissues and most rapidly activate their effector function [32,33]. In contrast, central memory T (T_{CM}) cells migrate to the SLOs and have an increased proliferative potential upon activation, thereby serving as a long-term reservoir of effector cells [32,33]. Together, T_{EM} and T_{CM} cells can efficiently attack pathogens upon the second encounter to prevent disease development.

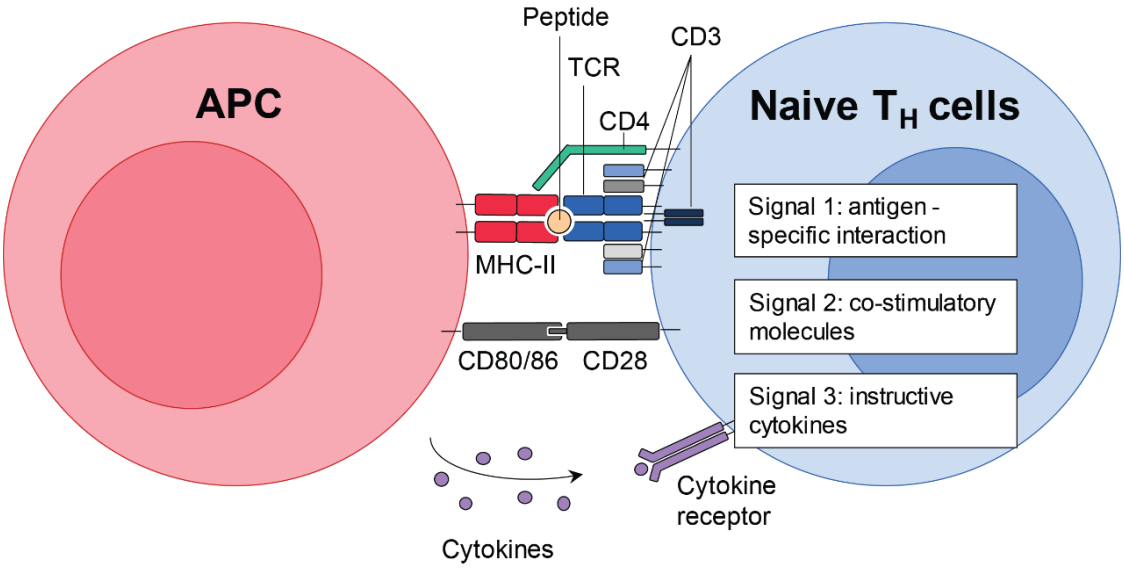

Figure 2: T cell activation and differentiation requires three signals. Activation of $CD4^+$ T cells in the lymphoid organs is initiated with the interaction of TCRs with peptides presented on the MHC-II proteins on the surface of antigen-presenting cells (APCs). The intracellular signaling is mediated by the co-receptor CD3, which is associated to the TCR. Binding of CD4 to the MHC-II stabilizes the interaction and enhances intracellular signaling. The interaction of co-stimulatory molecules (i.e. CD28) to its ligands (CD80/86) on the APC surface further amplifies the intracellular signaling within a T cell and is essential for proper T cell activation. Cytokines secreted by the APC guide T cell differentiation into different subsets. Adapted from [34]

1.1.3 The role of T follicular helper cells in B cell responses

The development of potent antibody responses largely relies on support by T_{FH} cells, which are specialized to provide help to B cells in the germinal centers (GCs) of SLOs. Within SLOs, T cells and B cells are localized in spatially separated niches known as T cell zone and B cell follicle, respectively (Figure 3). In the T cell zone, dendritic cells that sampled and processed antigens present them on their MHC molecules, resulting in the activation of antigen-specific T cells (Figure 3A). Activated $CD4^+$ T cells have two fates: they either exit the SLO as effector cells or develop into precursor T_{FH} (pre-T_{FH}) cells to eventually support B cell responses. The development of pre-T_{FH} cells is accompanied by the upregulation of the transcription factor BCL-6 (B-cell lymphoma 6) as well as the surface proteins PD-1 (programmed cell death 1), ICOS (inducible T-cell costimulator) and CXCR5 (C-X-C motif chemokine receptor 5) [35,36]. Expression of the chemokine receptor CXCR5 allows the migration of pre-T_{FH} cells to B cell follicles along a gradient of its ligand, CXCL13 (C-X-C motif chemokine ligand 13) [37,38]. At the border of the T cell zone and B cell follicle, pre-T_{FH} cells interact with B cells, which have previously taken up antigen and present it on their MHC-II molecules, resulting in the activation and proliferation of pre-T_{FH} and B cells as well as the development of pre-T_{FH} cells into T_{FH} cells (Figure 3B) [39–41]. Activated B cells can either develop into extra-follicular memory B cells or short-lived plasma cells and exit the SLOs, or migrate together with the T_{FH} cells into the B

cell follicles to form GCs, which become clearly visible 6 days after immunization (Figure 3C) [42]. Within GCs, T_{FH} cells provide guidance and survival signals to B cells that are undergoing class-switching and affinity maturation, processes required to improve B cell responses [43–45]. During class-switch recombination (CSR), the constant region of an antibody is irreversibly exchanged, thereby altering its effector function without affecting the specificity [46]. The switching to different constant regions is guided by cytokines secreted by T_{FH} cells and depends on the type of infection, hence T_{FH} cells are assuring that the effector functions matches the requirements for targeting the respective pathogen. In contrast to CSR, affinity maturation changes the specificity of a given antibody without altering the effector function. This is achieved by introduction of random mutations (somatic hypermutations, SHM) into the antigen-binding variable region of the antibody, resulting in a diversification of the antibody repertoire [47–49]. After acquiring SHM, B cells have to compete for limited antigen and help provided by follicular dendritic cells (FDCs) and T_{FH} cells, respectively. During this process, B cells take up antigens presented by FDCs, process it and present it on their MHC-II proteins to T_{FH} cells, which in turn provide survival signals [45,50–53]. The higher the affinity of a B cell is,

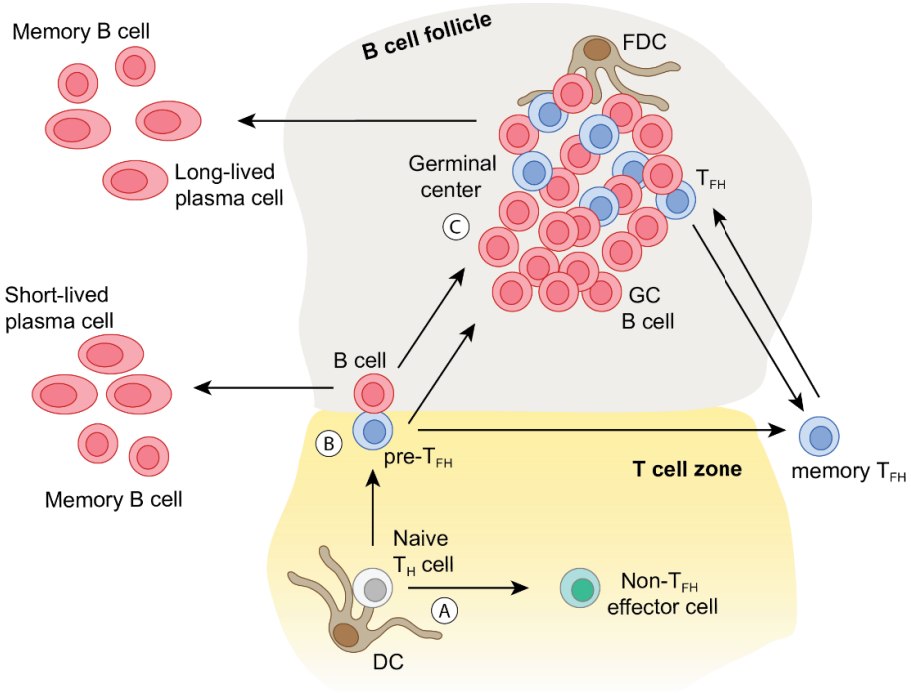

Figure 3: T_{FH} cell differentiation and their role in humoral immune responses. The differentiation of T_{FH} cells is initiated in the T cell zone of secondary lymphoid organs (SLOs), where naive T_H cells interact with dendritic cells (DCs) and get activated (A). They either differentiate into non-T_{FH} effector cells and exit the SLO or develop into pre-T_{FH} cells and migrate to the border of the T cell zone and B cell follicle, where they interact with antigen-specific B cells (B). Upon activation, B cells and T_{FH} cells can migrate together into the B cell follicle and form germinal centers (GCs) (C). Within the GCs, affinity maturation and class switching of B cells occurs and relies on positive selection by follicular dendritic cells (FDCs) and T_{FH} cells. Both, T_{FH} cells and B cells, can differentiate into effector or memory cells and exit the SLO either after the primary encounter (B) or after the GC-reaction (C). Adapted from [54]

the more antigen it can sample from FDCs and present to T_{FH} cells, and the more survival signals it receives. This affinity-based positive feedback promotes the selection of high-affine B cells, thereby serving as a quality control mechanism of affinity maturation. B cells encountering sufficiently high survival signals either continue proliferating and acquiring SHM or exit the germinal center and differentiate into memory B cells and long-lived plasma cells [55–57].

Recent progress in T_{FH} cell research showed that not only B cells, but also T_{FH} cells can develop into memory cells that exit the SLOs and can be detected in the circulation [27,28]. These circulating T_{FH} cells (cT_{FH} cells), defined by the expression of CXCR5, phenotypically and functionally resemble GC T_{FH} cells, despite an almost absent expression of the T_{FH} transcription factor BCL-6 [58–62]. In line with the function of GC T_{FH} cells, cT_{FH} cells are superior over $CXCR5^-$ cells in providing help to B cells by inducing class-switching as wells as the differentiation of B cells into antibody-secreting plasma cells in *in vitro* co-cultures [59–61,63]. The majority of cT_{FH} cells have a central memory phenotype and are in a resting state, in which they can persist for long time until they get rapidly re-activated upon antigen-encounter [27,28,60,64]. This re-activation results in a transient increase of activated cT_{FH} cells, defined by expression of activation markers like ICOS, PD-1 and CD38, in the blood, which peaks 7 days post antigen challenge and is synchronized with active differentiation of T_{FH} cells in SLOs of mice [60–62,64,65]. These activated cT_{FH} cells are highly enriched for antigen-specific cells and their frequencies correlate with antibody responses in various human studies [60,62,64,65]. cT_{FH} cells are further subdivided into $cT_{FH}1$, $cT_{FH}2$ and $cT_{FH}17$ cells dependent on the expression of lineage-specific chemokine receptors, transcription factors and cytokines [59]. The subset preferentially activated upon antigen-encounter depends on the type of pathogen and mimics the general T cell response. However, the cT_{FH} subsets differ in the capacity to provide help to B cells. While $cT_{FH}2$ and $cT_{FH}17$ cells are capable of providing efficient help to naive B cells as well as memory B cells, $cT_{FH}1$ cells are limited in their helper capacity and only provide help to memory B cells [59,62]. Although the phenotype of cT_{FH} cells has been extensively described, their role in the immune response is still incompletely understood. Studies blocking different stages of T_{FH} and GC development indicate that cT_{FH} cells can develop from both, pre-T_{FH} cells as well as GC T_{FH} cells [61,66,67]. Furthermore, cT_{FH} cells were shown to rapidly differentiate back into GC T_{FH} cells upon activation in mice [61]. This dynamic distribution of long-lived memory T_{FH} cells in the circulation and secondary lymphoid tissues seems to be a powerful mechanism for tackling pathogens at different sites of the body and controlling subsequent infections.

1.2 Malaria

Malaria is a vector-borne disease caused by the unicellular protozoan parasite *Plasmodium*. While five different *Plasmodium* species can cause malaria in humans, *Plasmodium falciparum* is the most prevalent species with the highest mortality, especially within the high-risk group of young children. The infection is often accompanied by diverse symptoms including fever, headaches, tiredness and nausea [68,69]. To control the symptoms and clear the infection, chemotherapeutics as Arthemisinin and Chloroquine are commonly used to defeat the parasite at different stages of its complex life cycle. However, the emergence of resistances against these anti-malarial drugs calls for a better understanding of the different developmental stages of *Plasmodium falciparum* as well as the protective host immune responses against them, which would provide important insights for the development of a protective vaccine [70–72].

1.2.1 The life cycle of *Plasmodium falciparum*

Plasmodium falciparum (*Pf*) has a complex life cycle alternating between mosquitos and human hosts (Figure 4). The parasites are transmitted to the human body by the bite of an infected female *Anopheles* mosquito (Figure 4A). During the blood meal, the *Pf* sporozoites are injected from the salivary gland of the mosquito into the human skin, from where they enter blood vessels to migrate through the blood stream into the liver [73–76]. In the liver, they infect hepatocytes, differentiate into a blood stage form called merozoites and start an asexual replication cycle (Figure 4B) [77,78]. After approximately one week, the merozoites are released from the hepatocytes and enter the blood stream, where they infect erythrocytes and initiate another round of asexual replication (Figure 4C) [79–81]. After 48 h, infected erythrocytes rupture, releasing high numbers of merozoites into the blood. These merozoites can infect other erythrocytes, resulting in an exponential replication of the parasites. This massive replication as well as rupture of erythrocytes leads to the development of clinical symptoms. A small proportion of merozoites can develop into a sexual form of the parasite, male and female gametocytes. These gametocytes can be taken up by mosquitos during their blood meal and fertilize to form an ookinete, which develops inside the mosquito midgut into an oocyst (Figure 4D). This oocyst can replicate and differentiate into sporozoites, which migrate to the salivary gland of the mosquito and can be transmitted to a human host upon the next blood meal, starting another round of the multistep life cycle (reviewed in [68,69]).

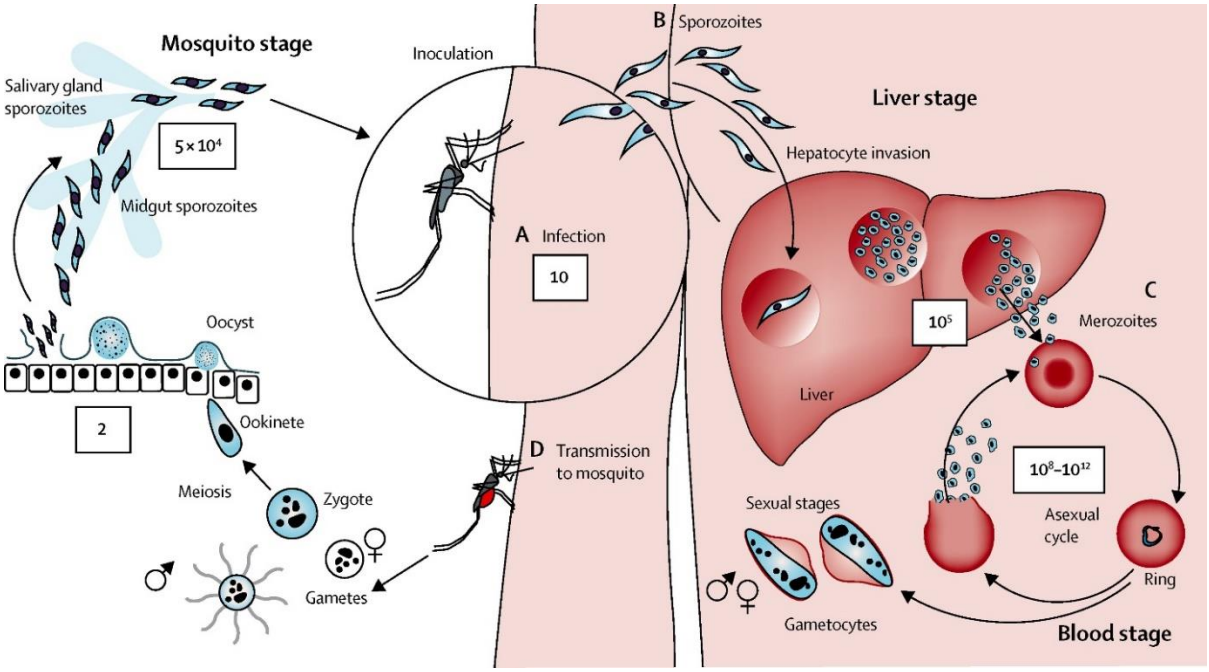

Figure 4: *Plasmodium falciparum* life cycle. *Pf* sporozoites are injected into the human skin by the bite of an infected female *Anopheles* mosquito (A). Sporozoites migrate through the blood stream to the liver, where they infect hepatocytes (B). Inside hepatocytes, sporozoites differentiate into merozoites and proliferate. After hepatocyte lysis, merozoites are released into the blood stream and can infect erythrocytes, initiating the symptomatic blood stage (C). After replication within the red blood cells, merozoites are released upon erythrocyte rupture and infect other erythrocytes, resulting in an exponential amplification. Some merozoites can further develop into male and female gametocytes, which are taken up by mosquitos during the next blood meal (D). The gametocytes fertilize to form an ookinete, which develops inside the mosquito midgut into an oocyst. The oocyst replicates and differentiates into sporozoites that migrate to the salivary glands and can be transmitted to a human host upon the next blood meal. Numbers in squares indicate the average parasite counts. The figure is adapted from [68].

1.2.2 Immunity to *Plasmodium falciparum* infection

Humoral and cellular immune responses act on different stages of the *P. falciparum* life cycle and are indispensable for the restriction of parasite replication as well as disease severity. While antibodies can block the infection of hepatocytes and erythrocytes in a $CD4^+$ T cell dependent manner, $CD8^+$ T cells can eliminate infected hepatocytes and thereby limit the disease burden [69,82]. However, naturally induced immunity develops only gradually over many years and requires repeated parasite exposures [83]. It is primarily directed against the erythrocytic stages of the parasite and hence can limit the emergence of symptoms but fails to provide sterile immunity [84–87]. The delayed emergence of protective immunity together with the absence of sterile immunity necessitates the development of effective vaccines inducing long-term sterile protection. Therefore, a major goal in the malaria vaccine field has been to redirect the immune responses towards the pre-erythrocytic stages of *P. falciparum* and eliminate the parasites before they develop to the symptomatic erythrocytic stage. Already

over fifty years ago Nussenzweig and colleagues succeeded in the induction of sterile immunity in mice by using radiation-attenuated sporozoites (RAS) as vaccine [88]. While RAS are live sporozoites that can infect liver cells, they fail to mature and form merozoites, thereby focusing the immune response solely on the pre-erythrocytic stages [89]. In the last decades, RAS have been shown to reliably induce sterile protection in mice and men, making them the golden standard in malaria vaccine development for a long time [90–93]. However the requirement of extremely large numbers of sporozoites as well as the failure in inducing long-term protection favored the investigation of alternative vaccine approaches. The current leading clinical candidate for malaria vaccine is a subunit vaccine, RTS,S/AS01 (Mosquirix™), which showed a protection efficacy between 25-55% in recent Phase III clinical trials conducted in endemic regions [94–97]. However, as RAS, RTS,S fails to induce long-term protection, raising the need for further improved vaccines [94]. This optimization process requires a better understanding of the immune responses induced with current vaccine strategies to identify possible targets for improvements.

1.2.3 T cell responses to *P. falciparum* pre-erythrocytic stages

While vaccine development often focuses primarily on the induction of humoral immune responses, growing evidence highlight the role of $CD8^+$ and $CD4^+$ T cell responses in protection against malaria [91,92,98]. *Plasmodium*-specific $CD8^+$ T cell responses, targeting infected hepatocytes either by direct lysis or via IFN-γ assisted clearance of the sporozoites, are raised during natural malaria infections as well as vaccinations and have been associated with protection in RAS immunizations [91,92,98–104]. The importance of $CD4^+$ T cell responses in protection from malaria can be attributed, at least partly, to their role in the induction of B cell responses, as antibodies can block the parasites at various stages and prevent hepatocyte invasion [105,106]. T_{FH} cells, specialized in promoting B cell responses, have been shown to expand in *Plasmodium* infections and play a profound role in promoting protective B cell responses [107,108]. However, T_{FH} cell responses are dysregulated in malaria as T_{FH} cells adopt a T_H1-like phenotype, secrete IFN-γ and provide comparably inferior help to B cells [108,109]. These aberrant T_{FH} responses seem to be induced by IFN-γ and may represent one explanation for the delayed acquisition and impaired maintenance of protective humoral immune responses in malaria. The high levels of IFN-γ are not only produced by $CD8^+$ T cells but can be largely attributed to T_H1 helper cells. While $CD4^+$ T cells can develop into different subsets dependent on the type of infection, a preferential T_H1 polarization is observed in *Plasmodium* infections and immunizations [110,111]. T_H1 cells release large amounts of IFN-γ, which not only supports parasite clearance from hepatocytes but also guides, together with

other T_H1-associated cytokines, the activation and modulation of innate and adaptive immune responses [111–113]. Together, $CD8^+$ T cell responses as well as T_{FH}-induced B cell responses, guided by T_H1 cells, form a promising direction for vaccine development. Hence, identifying sporozoite antigens that can be efficiently targeted by $CD8^+$ and $CD4^+$ T cells would help improving the composition of vaccines to elicit optimal T cell responses. However, the genome of *Plasmodium falciparum* encodes for around 5300 genes, resulting in an extremely large number of possible targets [114]. So far, T cell responses to only a limited number of proteins have been identified, which can be mainly attributed to the restricted availability of antigens for screenings [115,116]. The most studied protein of *P. falciparum* is the circumsporozoite protein (CSP). It is the most abundant protein on the surface of sporozoites and mediates the invasion of hepatocytes, making it a promising candidate for vaccine development (i.e. RTS,S) [117,118]. CSP consists of three main domains, the N-terminal domain, the central repeat region, consisting predominantly of multiple NANP amino acid repeats, and the C-terminal domain (Figure 5). It is anchored in the sporozoite membrane with a glycosylphosphatidyl-inositol (GPI) anchor [119,120]. Extensive studies identified a large number of epitopes within CSP that can be recognized by B and T cells. While the central repeat region is the immunodominant region for B cell epitopes, only little $CD4^+$ T cell and no $CD8^+$ T cell epitopes were detected there so far [116,121–125]. In contrast, the majority of identified T cell epitopes lay within the C-terminus and to a lesser extent in the N-terminus [115,116,123,126]. Although several immunogenic epitopes of CSP have been identified and studied in detail, the association between epitopes and the respective T cell receptors is still missing.

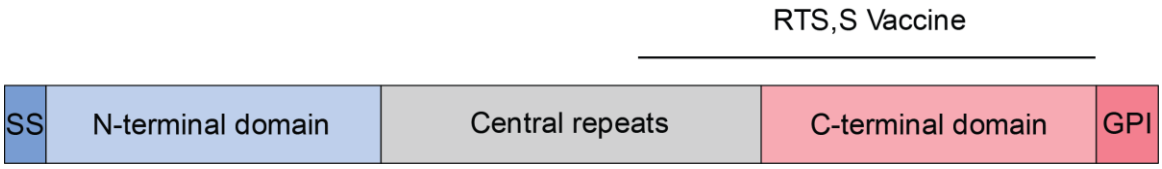

Figure 5: Schematic representation of *Pf* CSP. *Pf* CSP contains a signal sequence (SS), an N-terminal domain, a central repeat region and a C-terminal domain. It is anchored in the membrane by a glycosylphosphatidyl-inositol (GPI) anchor. The part present in the RTS,S/AS01 vaccine is indicated.

1.3 Characterization of the human T cell receptor repertoire

In the last years, characterization of the TCR repertoire has been proven to provide valuable insights into antigen-specific T cell responses induced during natural infections and immunizations [64,127–129]. For instance, as T cells proliferate upon antigen-specific activation, the degree of clonal expansion of T cells can be a good measure for antigen-specificity.

Moreover, TCR sequence features can provide insights into the mode of TCR-peptide-MHC binding. However, although clone size and TCR sequence features can indicate antigen-specificity, they cannot, so far, be used to distinguish immune responses to different antigens. Therefore it is indispensable to experimentally determine antigen-specificity along with TCR sequencing and directly link the TCR sequence to the respective epitope.

Different approaches allow the identification of antigen-specific T cells prior to TCR sequencing, with tetramer staining and *in vitro* proliferation assays being the most common ones. While staining of antigen-specific T cells with peptide-MHC tetramers can tag cells without altering their phenotype, it requires *a priori* knowledge of the antigen as well as MHC-alleles of each subject and only depicts a small fraction of the T cell response [130,131]. In contrast, *in vitro* stimulation of T cells with a variety of antigens circumvents these drawbacks, however alterations in T cell phenotype and composition due to stimulation impede a characterization of the native immune response. An alternative approach is the sequencing of TCRs of unselected T cells, followed by the determination of antigen-specificity through expression cloning and functional analysis. This approach provides a complete picture of the overall T cell response, including the unaltered cellular phenotype, clone sizes and TCR sequences that can be associated with antigen-specificity. However this requires the compatibility of the TCR sequencing platform with direct TCR expression cloning, which most of the common TCR sequencing platforms lack, as first efforts to characterize the TCR repertoire by high-throughput next-generation sequencing (NGS) were restricted to bulk T cells [132–134]. While the analysis of bulk T cells allows the sequencing of extremely high numbers of cells, the major drawback is the loss of cellular TCR alpha and beta gene pairing information, essential for functional analysis [135–139]. Attempts to estimate the pairing based on relative alpha and beta sequence abundance are problematic, as they bear the risk of introducing biases [140]. These limitations are overcome by newly developed strategies, characterizing T cells on a single-cell level and thereby preserving the correct chain pairing [141–145]. However, most of these strategies are still not compatible with direct cloning of the TCRs, as they either amplify only the CDR3 region, not full-length TCR sequences, or do not provide separated DNA products. Hence, exploring the link between TCR sequence and specificity without the limitations introduced by tetramer staining and in vitro stimulations would require the development of a strategy combining high-throughput sequencing of paired full-length TCR genes with direct expression cloning of TCR for functional assessments.

2 Objectives

The overall goal of this study was to quantitatively and qualitatively characterize the T cell repertoire of the functionally distinct, though for the anti-malaria immune response indispensable, populations of $CD8^+$ effector memory T cells and circulating T follicular helper cells over the course of successive malaria immunizations.

The specific aims were:

1) to develop a platform that enables the direct linkage of the cellular phenotype with the T cell receptor repertoire and functionality on single cell level.

2) to describe the molecular characteristics of the T cell repertoire of $CD8^+$ effector memory T cells as well as T follicular helper cells before and after repeated malaria immunizations.

3) to identify and characterize CSP-reactive T cells in the repertoire.

3 Methods

3.1 Human malaria immunization trial

The repertoire data generated and analyzed in this thesis were obtained from samples of the human malaria immunization trial MAVACHE Group A, conducted by Prof. Dr. Benjamin Mordmüller and colleagues in the Institute of Tropical Medicine, Tübingen, Germany. In this study, volunteers were intravenously immunized at day 0, 7 and 28 with $9x10^5$ radiation-attenuated *Plasmodium falciparum* (*Pf*) sporozoites (strain NF54), followed by challenge with 3200 live *Pf* sporozoites of the same strain at day 49. Blood samples were taken 3 days before the first immunization and 7 days after each immunization.

Ethical approval was granted by the ethics committee of the medical faculty and the university clinics of the University of Tübingen. The study was carried out according to the principles of the Declaration of Helsinki. The clinical trial was registered in the EudraCT database (2015-005123-11) and under https://clinicaltrials.gov/ct2/show/study/NCT02704533.

3.1.1 Isolation of peripheral blood mononuclear cells (PBMCs)

For PBMC preparation, blood samples were diluted 1:2 in RPMI medium and 35 ml of the diluted blood sample were carefully loaded onto 15 ml Ficoll in a 50 ml reaction tube. PBMCs were isolated by gradient density centrifugation for 40 min at 400g and room temperature (without break and acceleration). The buffy coat between the transparent Ficoll layer and the reddish RMPI layer was aspirated with a plastic Pasteur pipet. The cells were washed twice by addition of ice-cold RPMI followed by centrifugation for 10 min at 400 g and 4 °C. Subsequently, the PBMCs were resuspended in FBS containing 10% DMSO at a final concentration of $5x10^6$ cells per ml and frozen in a CoolCell cell freezing device at -80 °C. After 24 h, the tubes were transferred to the liquid nitrogen tank for long term storage.

3.1.2 Thawing PBMCs

PBMCs, stored in liquid nitrogen, were thawed at 37 °C and quickly transferred to a 50 ml falcon tube containing 30 ml pre-warmed RPMI medium. The cells were centrifuged with 400 g for 8 min at 4 °C and the supernatant was discarded. The cells were resuspended in AIM-V medium for stimulation (3.1.3) or FACS buffer (10% FBS in PBS) for flow cytometric analysis (3.2.1).

3.1.3 Stimulation of PBMCs with *Pf* antigens

PBMCs were resuspended in AIM-V medium at densities of $1x10^6$ cells per ml and rested over night by incubation at 37 ˚C and 5% CO_2. The next day, cells were harvested and washed in PBS by centrifugation at 400 g for 10 min and subsequent removal of the supernatant. To track proliferations, cells were resuspended in PBS containing 1 µM CellTrace™ Violet (CTV) dye at densities of $1x10^6$ cells per ml. After 20 min incubation at 37 ˚C, a 5 times higher volume of AIM-V medium was added to the cells and they were incubated for 5 min at 37 ˚C. Cells were washed in AIM-V medium and plated in 24-well or 6-well tissue culture plates at densities of $1x10^6$ cells per ml. The cells were stimulated by addition of 10 µg/ml CSP, lysate of 150,000 sporozoites per ml (prepared from the salivary gland of infected mosquitos) or an equivalent from uninfected mosquitos as negative control (kindly provided by Dr. Giulia Costa and Dr. Elena Levashina, MPI IB, Berlin). As positive control, cells were stimulated with 1 µg/ml Staphylococcal enterotoxin B. After 72 h incubation at 37 ˚C and 5% CO_2, the cells were harvested and used for fluorescence-activated single-cell sorting and T cell receptor sequencing.

3.2 T cell receptor repertoire sequencing

For the sequencing and analysis of human T cell receptor repertoires, single T cells from PBMCs were sorted into 384-well plates, the TCR genes were amplified from cDNA, sequenced with next generation sequencing and analyzed with an automated analysis pipeline.

3.2.1 Fluorescence-activated cell analysis and single-cell sorting

For flow cytometric analysis, freshly thawed or previously stimulated PBMCs were resuspended in 1 ml FACS buffer (10% FBS in PBS), transferred to a 1.5 ml Eppendorf tube and centrifuged with 1300 g for 3 min at 4 °C. The supernatant was discarded and the cell pellet was resuspended in 50 µl (<$1x10^6$ cells) or 100 µl (1-$5x10^6$ cells) staining cocktail containing fluorescently-labelled antibodies diluted in FACS buffer. Freshly thawed PBMCs were stained with the complete antibody cocktail whereas stimulated PBMCs were stained with a reduced antibody cocktail (Table 1). The cells were incubated for 30-60 min at 4 °C in the dark. Afterwards, the cells were washed by addition of 1 ml FACS buffer and subsequent centrifugation at 1300 g for 3 min (4 °C). The supernatant was discarded and the pellet was

resuspended in 50 or 100 µl FACS buffer containing the live-dead marker 7-aminoactinomycin D (7-AAD) at 1:400 dilution. The cells were incubated for 10 min at 4 °C in the dark, washed as before and resuspended in 1 ml FACS buffer for analysis. The cells were filtered before analysis and single-cell sorting with the FACS AriaIII (BD). Lymphocytes and single cells were identified via forward and sideward scatter area and height. For freshly thawed PBMCs stained with the complete antibody cocktail, either activated circulating T follicular helper (T_{FH}) cells (7-AAD$^-$ CD3$^+$ CD4$^+$ CD45RA$^-$ CXCR5$^+$ PD-1$^{+/hi}$ ICOS$^+$) or activated effector memory CD8$^+$ T cells (7-AAD$^-$ CD3$^+$ CD8$^+$ CD45RA$^-$ CCR7$^+$ PD-1$^+$ ICOS$^+$) were sorted. In contrast, for previously stimulated PBMCs stained with the reduced antibody cocktail, live, proliferating T cells (7-AAD$^-$ CD3$^+$ CTV ^{low}) were sorted. During the single-cell sort, index data were acquired to link the cell phenotype to the position on the plate. The cells were sorted into a 384-well plate containing 2 µl sort RHP mix in each well. The sort RHP mix (Table 2) consisted of the RNAse inhibitor RNAsin, the cell-lysing agent NP-40, the reducing agent DTT for denaturation of secondary structures of the RNA and random hexamer primers (RHP) for priming reverse transcription. After each sort, the plate was immediately sealed, frozen on dry ice and later stored at -80 °C.

Table 1: Fluorescently-labelled anti-human antibodies used for single-cell sorting

Antigen	Fluorochrome	Clone	Dilution	Staining panel
CD3	FITC	OKT3	1:250	Complete, reduced
CD4	APC-Cy7	A161A1	1:100	Complete
CD4	PE-Cy7	A161A1	1:200	Reduced
CD8a	Alexa700	SK1	1:200	Complete, reduced
CD45RA	BV510	HI100	1:200	Complete
CD45RA	PE	HI100	1:200	Reduced
PD-1 (CD279)	BV605	EH12.2H7	1:20	Complete
ICOS (CD278)	PE-Cy7	C398.4A	1:100	Complete
CXCR5 (CD185)	Alexa647	RF8B2	1:100	Complete, reduced
CXCR3 (CD183)	BV421	G025H7	1:20	Complete
CCR6 (CD196)	PE	G034E3	1:50	Complete
CCR7 (CD197)	BV710	G043H7	1:10	Complete, reduced

Table 2: Composition of the sort RHP mix

Reagent	Stock concentration	Volume (µl)
Nuclease-free water	-	1.4813
PBS	10x	0.0500
DTT	100 mM	0.1000
NP-40	10%	0.1375
RHP	300 ng/µl	0.1375
RNAsin	40 U/µl	0.0938
Total		2.0000

3.2.2 T cell receptor gene amplification

Reverse Transcription (RT)

For cDNA synthesis the frozen plates were thawed shortly on ice and incubated for 60 sec at 68 °C to denature secondary structures of the RNA. Afterwards the plate was centrifuged at 850 g for 1 min (4 °C) and 2 µl of RT mix (Table 3) were added to each well. The RT mix contained, besides DTT and RNAsin, components required for cDNA synthesis (dNTPs, RT buffer and the reverse transcriptase SuperScript IV). The plate was incubated on an Eppendorf Mastercycler at changing temperatures (see Table 4).

Table 3: Composition of the RT mix for cDNA synthesis

Reagent	Stock concentration	Volume (µl)
Water	-	0.6375
RT-Buffer	5x	0.8000
DTT	100 mM	0.3000
dNTPs	25 mM each	0.1375
RNAsin	40 U/µl	0.0563
SuperScript IV	200 U/µl	0.0688
Total		2.0000

Table 4: Reverse transcription program

Step	Temperature	Duration	Cycles
RNA denaturation	42 ˚C	5 min	1x
Primer annealing	25 ˚C	10 min	1x
Reverse transcription	50 ˚C	60 min	1x
Termination	94 ˚C	5 min	1x
Keeping cold	4 ˚C	Hold	1x

T cell receptor gene amplification by semi-nested PCR

To amplify the TCR genes, two subsequent semi-nested PCRs were run. If not stated differently, the amplification was performed as described below. For the first PCR, 2.5 µl pre-diluted cDNA (4 µl cDNA + 9 µl nuclease-free water) were used as template. Separate primer sets have been designed for alpha and beta, covering all V-segments and attaching a common linker sequence at the transcript start, which served as primer binding site in the second PCR. The amplified fragment covered large parts of the V-segment (excluding the signal sequence at the 5' end) and extended until the start of the C-region, where the reverse primers bound. The alpha and beta genes were amplified separately and the amplification efficiency was increased by performing duplicated first PCRs, resulting in two alpha and two beta PCR reactions. The primers used for the TCR gene amplification are listed in the Supplementary Table 6 and Supplementary Table 7 and the PCR reactions as well as the cycling conditions are stated in Table 5 and Table 6, respectively. For the second PCR 1 µl first PCR product (0.5 µl of each duplicate plate) was used as template. The forward primer bound the common linker region, attached to the V-segment, and the reverse primer bound to the C-segment in a nested way. Both forward and reverse primers contained 16 bp long barcodes encoding for unique rows and columns, thereby adding spatial information to the amplified TCR genes. The primers used for the second PCR are listed in the Supplementary Table 6 and Supplementary Table 7 and the PCR reactions and cycling conditions are stated in Table 7 and Table 8, respectively. The pipetting was carried out on a Tecan Evo200 automation platform. Successful amplification was verified by gel electrophoresis on a 2% agarose gel.

Table 5: Composition of first PCR reaction (TCR alpha and beta). The amount of the 5' primer set was dependent on the number of primers per set and was hence higher for the TCR alpha than the TCR beta PCR.

Reagent	Stock concentration	Final concentration	Volume (µl)
Nuclease-free water	-	-	10 - x
PCR Buffer	10x	1x	1.0000
5' primer set (alpha/beta)	50 µM	0.06 µM each	0.492/0.336
3' primer	50 µM	0.3 µM	0.0600
dNTPs	25 mM each	0.25 mM	0.1000
HotStarTaq	5 U/µl	0.025 U/µl	0.0500
Template (diluted with 9 µl nuclease-free water)	-		2.5000
Total			10.000

Table 6: PCR program for first PCR reaction (TCR alpha and beta)

Step	Temperature	Duration	Cycles
HotStarTaq activation	94 ˚C	15 min	1x
Denaturation	94 ˚C	30 sec	50x
Primer annealing	62 ˚C	1 min	50x
Elongation	72 ˚C	1 min	50x
Final elongation	72 ˚C	5 min	1x
Keeping cold	4 ˚C	Hold	1x

Table 7: Composition of second PCR reaction (TCR alpha and beta)

Reagent	Stock concentration	Final concentration	Volume (µl)
Nuclease-free water	-		6.7832
PCR Buffer	[10x]	1x	1.0000
$MgCl_2$	[25 mM]	4 mM	1.0000
5' primer	[50 µM]	0.167 µM	0.0334
3' primer	[50 µM]	0.167 µM	0.0334
dNTPs	[25 mM each]	0.25 mM	0.1000
HotStarTaq	[5 U/µl]	0.025 U/µl	0.0500
Template	-	-	1.0000
Total			10.000

Table 8: PCR program for second PCR reaction (TCR alpha and beta)

Step	Temperature	Duration	Cycles
HotStarTaq activation	94 ˚C	15 min	1x
Denaturation	94 ˚C	30 sec	50x
Primer annealing	62 ˚C	30 sec	50x
Elongation	72 ˚C	1 min	50x
Final elongation	72 ˚C	5 min	1x
Keeping cold	4 ˚C	Hold	1x

3.2.3 Next-generation sequencing of the TCR amplicons

To enable next generation sequencing by Illumina, sequencing adaptors were ligated to the TCR amplicons. The adaptor ligation was kindly performed by Dorien Foster and Julia Gärtner. In brief, 1 µl DNA from each well of the second PCR plate were diluted 1:1 – 1:3 with nuclease-free water and all wells corresponding to one matrix and one TCR locus were pooled. Subsequently, the pooled DNA was purified using the NucleoSpin Gel and PCR Clean-up kit (Macherey-Nagel GmbH), which is based on the binding of DNA to a silica membrane. The purification was performed as suggested by the provider, with a DNA:NTI ratio of 3:2 to enable efficient purification of 400 bp DNA fragments, corresponding to the size of amplicons. The DNA concentration and purity was determined by measuring the OD_{260}/OD_{280} and CD_{260}/OD_{230} ratio using a NanoQuant plate in a Tecan M1000 Pro plate reader. For further purification and size exclusion, the DNA sample was separated by agarose gel electrophoresis on a 4% agarose gel, run at low voltage (80 V) for 6 h at room temperature. Bands of the expected size (~ 400 bp) were cut out and purified with the NucleoSpin Gel and PCR Clean-up kit (Macherey-Nagel GmbH) using a gel:NTI ratio of 1:4, which allowed the addition of large amounts of gel to a single column without clogging the column. The DNA concentration and purity was determined as before. The purified DNA samples were used for library preparation, which was performed with the TruSeq Nano DNA LT Kit (Illumina). First, the purified amplicons were heated to 70 ˚C for 10 min and afterwards cooled down on ice. 1 µg of sample was filled up to 27 µl with nuclease-free water and 3 µl NEB 2.1 Buffer were added. The ligation of Illumina adaptors to the amplicons was performed as described in the TruSeq Nano DNA LT Kit manual, chapter Ligate Adaptors. Changes to the protocol were the exchange of resuspension buffer (RSB) by nuclease-free water during the adaptor ligation, as well as the reduction of the volume of resuspension buffer used to resolve the DNA amplicons after the magnetic bead-mediated amplicon purification (section Clean Up Ligated Fragments) from 52.5 µl to 25 µl, as

the amplicon concentrations were rather low. Furthermore only the Round 1 purification was performed. After adaptor ligation and purification, the DNA concentration was measured as before and the efficiency of adaptor ligation was quantified by qPCR with the KAPA Library Quant Kit (Roche), using 1:10,000 – 1:40,000 sample dilutions and strictly following the manuals instructions. The Illumina MiSeq300 sequencing was performed by Eurofins Genomics.

3.3 T cell receptor sequence analysis

The TCR sequence analysis and segment annotation was performed by a modified version of the automated analysis pipeline sciReptor [146], which was originally developed for the analysis of single-cell Ig gene sequences. This pipeline first assembles the paired end Illumina sequencing reads using the PandaSeq tool [147]. To capture all expected lengths of TCR sequences, the allowed maximal and minimal length of the assembled reads is 550 and 300 bp, respectively (parameters -L 550, -l 300). Furthermore, a minimal overlap of 50 bp is required for assembly (-o 50) and the minimal quality score of the assembled read is 0.8 (-t 0.8). The assembled sequences are aligned to the genome of the bacteriophage PhiX to filter out PhiX sequences added to the sample before sequencing to achieve a balanced base composition during sequencing. Afterwards, the reads are assigned to different wells according to their positional barcodes. V, D and J segments as well as CDR and FWR regions are identified by IgBLAST, performing an alignment to the reference library [148]. This reference library containing the germline sequences of all human TCR segments was generated during the establishment phase by integrating V, J and D segment sequences published on the Ensembl Genome Browser [149]. As a next step, the CDR3 regions are annotated according to conserved recognition motifs (Table 9). The flow cytometric index data as well as the meta-information are linked to the sequence information and stored in a relational MySQL database. The subsequent sequence analysis and plotting was performed using R.

Table 9: Amino acid recognition motifs required for CDR3 definition of human TCRs where '.' means any type of character (amino acid) and '*' means zero or more times ('.*' = variable number of unspecified amino acids)

	Alpha chain	Beta chain
CDR3 start	C	C
CDR3 end	.*FG.G	.*FG.G
	.*F..G	.*VG.G
	.*FG..	
	.*.G.G	

3.4 T cell receptor cloning

For the stable expression of TCRs of interest in target T cells, the TCRs were cloned into a retroviral expression vector. This was achieved by amplification of the TCR alpha and beta gene from the PCR products generated during the single-cell TCR gene amplification protocol described before. For equimolar expression, the alpha and beta gene were joined head-to-tail with the 2A self-cleaving element and introduced into the retroviral expression vector using Gibson assembly.

3.4.1 Specific amplification of TCR genes

To clone the TCR alpha and beta genes into the retroviral expression vector, a segment-specific PCR was performed to attach regions with sequence homology, required for Gibson assembly, to the TCR genes. As template, the PCR product of the first PCR (see section 3.2.2) was used. Importantly, as two first PCR reactions were performed per chain, 0.5 µl of each of the doubled reactions were pooled and used as template for the specific PCR. For alpha, forward primers containing 32 bp of the TRAV13-1 signal sequence attached to the 5' end were used, whereas the beta forward primers contained 19 bp of the TRBV5-1 signal sequence. Furthermore, some TCR beta forward primers also contained up to 26 bp of the corresponding V segment, which were not amplified during the first PCR. The reverse primers bound to the constant region of the alpha or beta genes. A complete list of specific PCR primers can be found in Supplementary Table 8 and Supplementary Table 9. The composition of the PCR reaction mix and the cycling conditions are listed in Table 10 and Table 11, respectively. The successful amplification was verified by gel electrophoresis on a 2% agarose gel. PCR products were purified from the gel using the NucleoSpin Gel and PCR Clean-up kit (Macherey-Nagel GmbH), which is based on the binding of DNA to a silica membrane. DNA concentration and purity was determined using a NanoQuant plate in a Tecan M1000 Pro plate reader.

Table 10: Composition of the specific PCR reaction for TCR alpha and beta cloning

Reagent	Stock concentration	Final concentration	Volume (µl)
Nuclease-free water	-		10.6
PCR Buffer	[5x]	1x	4.00
5' primer	[5 µM]	0.5 µM	2.00
3' primer	[5 µM]	0.5 µM	2.00
dNTPs	[25 mM each]	0.25 mM	0.20
Phusion	[2 U/µl]	0.02 U/µl	0.20
Template	-	-	1.00
Total			20.0

Table 11: PCR program for the specific PCR for TCR alpha and beta cloning

Step	Temperature	Duration	Cycles
Initial denaturation	98 ˚C	1 min	1x
Denaturation	98 ˚C	20 sec	5x
Primer annealing	65 ˚C	30 sec	5x
Elongation	72 ˚C	1 min	5x
Denaturation	98 ˚C	20 sec	35x
Primer annealing	72 ˚C	30 sec	35x
Elongation	72 ˚C	1 min	35x
Final elongation	72 ˚C	10 min	1x
Keeping cold	4 ˚C	Hold	1x

3.4.2 Restriction endonuclease digestion of vector and linker segment

The retroviral expression vectors pMSCV-PImC-TRBC1/2, containing either the TCR beta constant segment TRBC1 or TRBC2 (Supplementary Figure 17), were digested with the restriction enzyme MfeI at 37 ˚C overnight and dephoshorylated using the alkaline phosphatase CIP for 1 h at 37 ˚C to avoid religation. The pEX-A128-TRAC-2A-SSb vector, containing the linker segment for joining the TCR alpha and beta genes (Supplementary Figure 18), was digested with BsrGI for 2 h at 37 ˚C. The digested expression vector and pEX-A128-TRAC-2A-SSb were separated on a 1% and 2% agarose gel, respectively. The linearized expression vector and the 2500 bp large linker segment were excised and purified using the NucleoSpin Gel and PCR Clean-up kit (Macherey-Nagel GmbH). DNA concentration was determined using a NanoQuant plate in a Tecan M1000 Pro plate reader.

3.4.3 DNA assembly

The linearized expression vector, the linker segment as well as the specific PCR product of the TCR alpha and beta genes were joined together based on sequence homology using the NEBuilder HiFi DNA assembly kit (New England BioLabs). For this, 0.0125 pmol of each fragment were used and nuclease-free water was added to a total volume of 2.5 µl. The same volume of NEBuilder HiFi DNA Assembly Master Mix was added and the reaction was incubated for 1 h at 50 ˚C. Dependent on the reported constant gene of each TCR either the pMSCV-PImC-TRBC1 vector or the pMSCV-PImC-TRBC2 vector was used for assembly.

3.4.4 Transformation into competent bacteria

For transformation, 1.5 – 3 µl DNA assembly product were added to 5 –10 µl of chemo-competent DH10b *E. coli* cells (kindly provided by Claudia Winter), mixed gently by flicking the tube and incubated for 30 minutes on ice. Subsequently, a heat shock was performed for 45 seconds at 42 °C. Afterwards, the bacteria were immediately cooled down on ice for 1 minute before 100 µl LB-medium (without antibiotics) were added and the cells were incubated for 1 h at 37 °C, shaking at 650 rpm. The cells were then plated on LB-agar plates containing 100 µg/ml ampicillin. The bacteria were grown over night at 37 °C until separate colonies were visible.
For retransformation of plasmid stocks, only 0.5 µl vector (0.3 – 1 µg/µl) were used for transformation and 10% of the competent bacteria were spread on ampicillin plates.

3.4.5 Screening of bacterial colonies by PCR

Transformed bacterial colonies were screened for the presence of the TCR alpha and beta genes by colony PCR. For this, bacterial colonies were picked, resuspended in 3 µl nuclease-free water and 1 µl of this suspension was used as template for PCR. Additionally, 1 µl of the bacterial suspension was spread on a LB-agar plate containing 100 µg/ml ampicillin and incubated overnight at 37 °C before storage at 4 °C.

The colony PCR was performed using the forward primer colP_Psi_in_F and the reverse primer $TRBC_{115\text{-}135}$, binding upstream and downstream of the insertion site, respectively (see Supplementary Table 10). The composition of the PCR reaction is listed in Table 12. The PCR cycling steps were performed as described in Table 13. Afterwards, the PCR products were analyzed by gel electrophoresis on a 2 % agarose gel, where a 2100 bp large band indicated

the presence of the complete TCR. To exclude sequences with PCR-induced point mutations, amplicons with the correct size were Sanger sequenced (Eurofins Genomics) using the colony PCR primers, and were subsequently aligned to the reference sequence.

Table 12: Composition of the colony PCR reaction for TCR alpha and beta

Reagent	Stock concentration	Final concentration	Volume (µl)
Nuclease-free water	-		16.2
PCR Buffer	[10x]	1x	2.00
5' primer	[50 µM]	0.5 µM	0.20
3' primer	[50 µM]	0.5 µM	0.20
dNTPs	[25 mM each]	0.25 mM	0.20
HotStarTaq	[5 U/µl]	0.05 U/µl	0.20
Template	-	-	1.00
Total			20.0

Table 13: PCR program of the colony PCR for TCR alpha and beta

Step	Temperature	Duration	Cycles
Initial denaturation	98 ˚C	10 min	1x
Denaturation	98 ˚C	30 sec	30x
Primer annealing	52 ˚C	40 sec	30x
Elongation	72 ˚C	3 min	30x
Final elongation	72 ˚C	10 min	1x
Keeping cold	4 ˚C	Hold	1x

3.4.6 Preparation of vector DNA

Single colonies of correct clones were used to inoculate 5 ml LB medium containing 75 µg/ml ampicillin. The bacteria were grown overnight at 37°C shaking (180 rpm) and either harvested the next day or, if larger DNA yields were required, used to inoculate 500 ml LB medium (75 µg/ml ampicillin) which were again grown overnight at 37°C shaking. The bacteria were purified using the NucleoSpin® Plasmid or NucleoBond® Xtra Midi / Maxi kit (Macherey-Nagel GmbH) according to the manufactures suggestions. The purification is based on the binding of plasmid DNA to a silica membrane. The DNA purity and concentration were measured with a NanoQuant plate using a Tecan M1000 Pro plate reader.

3.5 Co-receptor cloning

To stably introduce the TCR co-receptors CD3, CD4 and CD8 into Jurkat76 T cells, the co-receptors were amplified from human cDNA and cloned into retroviral expression vectors.

3.5.1 RNA isolation and reverse transcription

For cDNA synthesis, $5x10^6$ PBMCs were thawed as described before (3.1.2) and RNA was isolated using the RNeasy Mini Kit (Qiagen) according to the provider's instructions. Subsequently total RNA was reverse transcribed to cDNA using random hexamer primers and the SuperScript™ IV First-Strand Synthesis System (Invitrogen).

3.5.2 Amplification of co-receptor genes

In a next step, the co-receptors were amplified from cDNA using gene-specific primers containing overlaps and restriction sites required for integration into the expression vectors (Table 14, Supplementary Table 11). The retroviral expression plasmid pMIG-II-CD3-PT, containing the murine CD3Z gene as well as the human CD3D, CD3G and CD3E genes separated by 2A peptides, was kindly provided by Dr. Paul G. Thomas, St. Jude Children's Research Hospital, Memphis, USA (Supplementary Figure 19) [150]. To exchange the murine CD3Z gene with the human one, the human CD3Z gene was amplified from cDNA and joined to the CD3E-P2A fragment, which was amplified with overlaps from the pMIG-II-CD3-PT vector. For CD8, the alpha gene (CD8A) was amplified in two fragments with primers binding in the region encoding the transmembrane domain to exclude amplification of the secreted CD8A isoform. The composition of the PCR reaction and the cycling conditions are listed in Table 15 and Table 16, respectively. After PCR amplification, the samples were separated by agarose gel electrophoresis, excised and purified using the NucleoSpin Gel and PCR Clean-up kit (Macherey-Nagel GmbH).

Table 14: Primers, annealing temperatures and templates used to amplify the TCR co-receptor genes

Amplicon (size)	5' primer	3' primer	Annealing temp. [°C]	Template	Template amount
CD3E-P2A (318 bp)	hCD3E_F	hCD3E_P2A_R	65	pMIG-II-CD3-PT	5 ng
CD3Z (538 bp)	hCD3Z_F	hCD3Z_R	69	cDNA	2 µl
CD4 (1401 bp)	hCD4_MluI_F	hCD4_SalI_R	66	cDNA	2 µl
CD8A-1 (583 bp)	hCD8A_F	hCD8A_TMD_R	60	cDNA	2 µl
CD8A-2 (215 bp)	hCD8A_TMD_F	hCD8A_P2A_R	62	cDNA	2 µl
CD8B (702 bp)	hCD8B_P2A_F	hCD8B_R	61	cDNA	2 µl

Table 15: Composition of the PCR reaction for the amplification of the TCR co-receptor genes

Reagent	Stock concentration	Final concentration	Volume (µl)
Nuclease-free water	-		50 - x
PCR Buffer	[5x]	1x	10.0
5' primer	[50 µM]	0.5 µM	0.50
3' primer	[50 µM]	0.5 µM	0.50
dNTPs	[25 mM each]	0.20 mM	0.40
Phusion	[2 U/µl]	0.02 U/µl	0.50
Template	-	-	See Table 14
Total			50.0

Table 16: PCR cycling program for the amplification of the TCR co-receptor genes

Step	Temperature	Duration	Cycles
Initial denaturation	98 ˚C	1 min	1x
Denaturation	98 ˚C	20 sec	40x
Primer annealing	See Table 14	30 sec	40x
Elongation	72 ˚C	1 min	40x
Final elongation	72 ˚C	10 min	1x
Keeping cold	4 ˚C	Hold	1x

3.5.3 Restriction endonuclease digest of the retroviral expression vectors

To allow insertion of the co-receptor genes into the retroviral expression vectors, the vectors were cut-open with corresponding restriction endonucleases as suggested by the provider (Table 17). During PCR amplification, matching restriction sites were also added to the CD4 gene, which was digested for subsequent ligation into the backbone. As CD3 and CD8 were later inserted by DNA assembly, no digest was performed with these amplicons. Religation of the cut-open backbones was prevented by dephosphorylation of the open ends with the alkaline phosphatase CIP for 1 h at 37 ˚C. All digested fragments were separated by agarose gel electrophoresis, excised and purified using the NucleoSpin Gel and PCR Clean-up kit (Macherey-Nagel GmbH).

Table 17: Restriction endonuclease digests of TCR co-receptor genes and expression vectors

	Restriction endonuclease	Purified (size)	Cut out (size)	Usage
pMIG-II-CD3-PT	MfeI	Backbone (7894 bp)	Partial CD3E-2A-mCD3Z (788 bp)	Backbone for CD3E-2A-CD3Z
pMSCV-PIG-SSa-TRBC2	MluI, SalI	Backbone (5123 bp)	TCR-PIG (3115 bp)	Backbone for CD4 or CD8A-P2A-CD8B
CD4	MluI, SalI	CD4 (1389 bp)	-	CD4 insert

3.5.4 Integration of co-receptors into retroviral expression vectors

The co-receptors were inserted into the open expression vectors either by ligation with the T4 DNA ligase or by DNA assembly with the NEBuilder HiFi DNA assembly kit (New England BioLabs) according to provider's instructions (Table 18).

Table 18: Insertion of the co-receptors into the retroviral expression vectors

Vector	Inserts	Vector-insert ratio	Method	Final construct
pMIG-II-CD3-PT	CD3E-P2A, P2A-CD3Z	1:2	DNA assembly	pMIG-II-CD3
pMSCV	CD4	1:3	Ligation	pMSCV-CD4
pMSCV	CD8A-1, CD8A-2, CD8B	1:1	DNA assembly	pMSCV-CD8

3.5.5 Preparation of vector DNA and sequence verification

The expression vectors containing the co-receptors were transformed into chemically competent DH10b *E. coli* bacteria as described before (3.4.4). Afterwards, colonies were picked and used to inoculate 5 ml LB medium containing 75 µg/ml ampicillin for subsequent DNA preparation (3.4.6). The correctness of the sequences was verified by Sanger sequencing (Eurofins Genomics).

3.6 Stable expression of T cell receptors and co-receptors in T cells

To stably express TCRs and the TCR co-receptors CD3, CD4 and CD8 in TCR-deficient T cells, retroviral transduction was performed. The packaging cell line Phoenix Ampho was transfected with the retroviral expression vector containing, besides the target gene, a retroviral packaging sequence Psi as well as 5' and 3' long terminal repeats (LTRs). These components complemented the retroviral components present in the Phoenix Ampho cells and allowed production of amplification-deficient, amphotrophic retroviral particles containing the gene of interest. These retroviral particles were used to stably integrate the target genes into the T cell genome.

3.6.1 Culture of Phoenix Ampho cells

Adherent Phoenix Ampho cells were cultured in DMEM GlutaMAX medium containing 10% heat-inactivated FBS and 1% Penicillin/Streptomycin (=Phoenix medium). The cells were incubated at 37 ˚C and 5% CO_2 and passaged every 2-3 days. For passaging, cells were detached from the plates by addition of trypsin and incubation for 2-3 minutes at room temperature. Afterwards cells were seeded at a density of $2x10^5$ cells per ml into a new tissue culture flask.

3.6.2 Culture of Jurkat76 cells

The TCR-deficient T cell line Jurkat76 [151] (or derivates) was cultured at 37 ˚C and 5% CO_2 in RPMI medium containing 10% heat-inactivated FBS, 2 mM L-glutamine and 1% Penicillin/Streptomycin (=Jurkat medium). Every 2-3 days, cells were passaged and $3x10^5$ cells per ml were seeded into a new tissue culture flask.

3.6.3 Transfection of Phoenix Ampho cells

For transfection, $5x10^5$ Phoenix Ampho cells were seeded in 2 ml Phoenix medium into each well of a 6-well tissue culture plate and grown overnight at 37 ˚C and 5% CO_2. When the confluence reached 60-80%, cells were transfected using calcium chloride. For each transfection, 10 µl DNA (0.1 µg/µl) were incubated at 55 ˚C for 30 min before adding 102.5 µl nuclease-free water and 12.5 µl $CaCl_2$ (2.5 M). Then, 125 µl 2x HBS (pH 7.05) were added dropwise to the reaction while vortexing. The mixture was incubated for 10 minutes at room temperature. Meanwhile, the medium of the confluent Phoenix Ampho cells was aspirated and 2 ml Phoenix medium without antibiotics, containing 25 µM chloroquine, were added to the cells. The DNA/$CaCl_2$ mix (250 µl per well) was added dropwise to the cells and incubated for 6 h at 37 ˚C and 5% CO_2. Subsequently, the medium was aspirated and 2 ml Jurkat medium without antibiotics were added. The cells were incubated overnight at 37 ˚C and 5% CO_2 and the supernatant containing the retroviral particles was harvested the next day. The supernatant was centrifuged at 1000 g for 5 minutes at room temperature to remove cellular debris and then used for transduction of Jurkat76 cells.

3.6.4 Retroviral transduction of Jurkat76 cells

Jurkat76 cells (or derivates) were harvested and $5x10^5$ cells were resuspended in 1 ml retroviral supernatant (see section 3.6.3) containing 10 µg/ml protamine sulfate. For spin infection, the cell suspensions were plated into flat bottom 24-well plates and centrifuged at 2000 g and 32 ˚C for 1.5 h (without brakes). Afterwards, 1 ml Jurkat medium without antibiotics was added to each well and the cells were incubated for 2 days. If cells were transduced with expression vectors containing the puromycin resistance gene puromycin N-acetyltransferase (PAC), transduced cells were selected with Jurkat medium containing 0.8 µg/ml puromycin dihydrochloride for 7 days (see section 8.2).

3.6.5 Detection of TCR and co-receptor expression in transduced Jurkat76 cells

To detect the expression of proteins previously introduced into Jurkat76 cells by retroviral transduction, cells were analyzed by flow cytometry. $1\text{-}2x10^6$ cells were harvested and washed in FACS buffer (10% FBS in PBS). If stained in 96-well plates, all washing steps were performed with 200 µl FACS buffer and centrifugation for 2 minutes at 700 g and 4 ˚C. If stained in 1.5 ml Eppendorf tubes, cells were washed in 1 ml FACS buffer and centrifuged for

3 minutes at 1300 g and 4 ˚C. After washing, the cells were stained in 50 µl FACS buffer containing the respective antibodies (see Table 19) for 30-60 minutes at 4 ˚C in the dark. After subsequent washing, cells were stained with 50 µl of the 1:400 diluted live-dead marker 7-AAD (Invitrogen) for 10 minutes (CD3, CD4, CD8) or with 1:1000 diluted LIVE/DEAD Fixabable Near-IR Dead Cell Stain (Invitrogen) for 30 minutes (TCR) at 4 ˚C in the dark. Cells were washed and analyzed at the FACS Aria III (BD).

CD3, CD4 and CD8-transduced Jurkat76 cells with high expression levels of the respective protein were single-cell sorted into U-bottom 96-well tissue-culture plates containing 100 µl Jurkat medium and were cultured at 37 ˚C and 5% CO_2 for 6-8 weeks until rapidly growing monoclonal cell lines were established. The stable expression of the proteins was monitored over time by flow cytometry.

Table 19: Fluorescent markers used for analysis of transduced T cells

Antigen	Fluorochrome	Clone	Dilution
CD3-transduced T cells			
CD3	Detection via the co-expressed fluorescent protein Ametrine		
CD4-transduced T cells			
CD4	APC-Cy7	A161A1	1:100
CD8-transduced T cells			
CD8a	Alexa700	SK1	1:200
CD8b	APC	2ST8.5H7	1:100
TCR-transduced T cells			
TCRab	PE-Cy7	IL26	1:20

3.7 Functional characterization of T cell receptors

For the characterization of TCR specificities, TCR-transgenic T cells (generated as described in section 3.6) were co-cultured with immortalized autologous B cells presenting the antigens of interest. The degree of T cell stimulation was determined by measuring the IL-2 secretion by ELISA.

3.7.1 Generation of immortalized autologous B cells

The Epstein-Barr virus (EBV), used for B cell immortalization, was obtained from the B95-8 cell line (DSMZ). B95-8 cells, derived from a cotton-top tamarin, were described to release high titers of EBV and can therefore function as a source of EBV [152]. B95-8 cells were cultured in RPMI medium containing 10% heat-inactivated FBS, 2 mM L-glutamine and 1% Penicillin/Streptomycin at 37 ˚C and 5% CO_2. Every 2-3 days, B95-8 cells were passaged and seeded at densities of $5x10^6$ cells per ml. For the generation of EBV stocks, B95-8 cells were incubated for 7 days without exchanging the medium. Afterwards, the cell suspension was harvested and centrifuged at 500 g for 5 minutes to pellet the cells. The undiluted supernatant, containing EBV, was frozen in cryotubes and stored in liquid nitrogen.

For B cell immortalization, human B cells were isolated from PBMCs using fluorescence-activated cell sorting. $5x10^6$ PBMCs were thawed as described before (section 3.2.1) and washed by addition of 1 ml FACS buffer (10% FBS in PBS) and subsequent centrifugation for 3 minutes at 1300 g and 4 ˚C. The cells were stained with CD19-PE-Cy7 antibody (clone SJ25C1), diluted 1:20 in 100 µl FACS buffer, for 30 minutes at 4 ˚C in the dark. Cells were washed and incubated for 10 minutes with the live/dead marker 7-AAD (1:400 diluted in 100 µl FACS buffer) at 4 ˚C in the dark. Afterwards the cells were washed, resuspended in FACS buffer and analyzed with the FACS AriaIII (BD). All live B cells, defined as 7-AAD^- $CD19^+$ lymphocytes, were bulk sorted into 15 ml tubes, yielding 1-$3x10^5$ B cells per $5x10^6$ PBMCs. The B cells were washed by addition of 5 ml RPMI medium and centrifugation for 5 minutes at 500 g and 4 ˚C. Subsequently, cells were resuspended in 250 µl EBV-containing supernatant and 250 µl B cell medium (RPMI medium with 10% heat-inactivated FBS, 2 mM L-glutamine, 1% Penicillin/Streptomycin, 1% Non-essential Amino Acids and 1 mM pyruvate) supplemented with 1.25 µg/ml Resiquimod (TLR7/8 agonist). The addition of TLR agonists has been shown to improve the transformation efficiency by activating the B cells [153]. After 5 days of incubation at 37 ˚C and 5% CO_2, 500 µl fresh B cell medium with 1.25 µg/ml Resiquimod were added to the cells. On day 7 after the sort, the B cells were washed by centrifugation for 5 minutes at 500 g and resuspended in B cell medium without TLR agonist. From then on, the B cells were expanded every 2-3 days by adjusting the volume of B cell medium to reach a concentration of $5x10^5$ B cells per ml. Expanded cells were frozen in FBS containing 10% DMSO at concentrations of 2-$5x10^6$ cells per ml and stored in liquid nitrogen.

3.7.2 T cell stimulation

If not stated differently, TCR-transgenic T cells were stimulated as described below. For stimulation in 96-well tissue culture plates (U-bottom), $2.13x10^5$ immortalized autologous B cells were resuspended in 150 µl AIM-V medium and loaded with 5 µg/ml peptide for 2 h or 10 µg/ml protein for 18 h at 37 ˚C and 5% CO_2. Afterwards, $4.27x10^5$ TCR-transgenic Jurkat76 cells were resuspended in 50 µl AIM-V medium and added to the B cells. As positive control, 1 µg/ml Staphylococcal enterotoxin B was added to the B-T co-culture. After 24 h of stimulation at 37 ˚C and 5% CO_2 the plates were centrifuged for 2 min at 700 g and the supernatant was harvested for quantification of the IL-2 concentration.

3.7.3 Detection of T cell activation by IL-2 ELISA

The IL-2 concentration in the culture supernatant was determined by sandwich ELISA (enzyme-linked immunosorbent assay) using the human IL-2 ELISA MAX™ Deluxe kit (BioLegend). The ELISA was performed as suggested by the provider. Based on the IL-2 concentration, the supernatant was analyzed undiluted or up to 1:20 diluted. The OD_{450} was measured with a Bio-Rad Model 680 microplate reader.

3.8 Quantification of CSP-specific antibody titers

For the detection of CSP-reactive antibodies in the plasma, an ELISA was performed. Transparent high-binding 96-well plates were coated overnight at 4 °C with 100 µl PBS per well containing full-length CSP (0.4 µg/ml), CSP $NANP_5$ repeat (2 µg/ml), CSP N-terminus (2 µg/ml) or CSP C-terminus (2 µg/ml). The next day, the plates were washed three times in deionized water. Unspecific binding of antibodies was prevented by blocking the plates with 200 µl blocking buffer (4% BSA and 0.01% Tween in PBS) for 1 h at room temperature. The plasma samples were diluted in PBS containing 1% BSA and 0.05% Tween in seven 1:2 dilution steps, starting with a 1:200 dilution. After the blocking step, the plates were washed three times in deionized water and 50 µl of the diluted samples were added per well. The plates were incubated for 1-1.5 h at room temperature, washed three times and loaded with 50 µl horseradish peroxidase conjugated goat anti-human IgG, IgM or IgA antibody diluted 1:1000 in PBS with 1% BSA and 0.05% Tween. After the incubation, plates were washed again and developed by addition of 100 µl ABTS solution, consisting of 91 ml ABTS buffer,

one ABTS tablet (Roche) and 1 µl/ml H_2O_2. The absorbance at OD_{405} was measured with a M1000 Pro platereader (Tecan).

3.9 Sporozoite hepatocyte traversal assay

The capability of antibodies to prevent sporozoite traversal through hepatocytes was determined by an in vitro traversal assay, kindly performed by Dr. Rajagopal Murugan. In brief, the human hepatocyte cell line HC-04 was seeded into a 96-well plate at $6x10^4$ cells/well and incubated for 24 h at 37 ˚C and 5% CO_2 until 70% confluency was reached. 50,000 *Pf* sporozoites (strain NF54) were isolated from infected *Anopheles coluzzi* mosquitos and incubated with 100 µg/ml monoclonal antibody or serial dilutions of plasma samples of a total volume of 27.5 µl for 30 min on ice. Subsequently 27.5 µl dextran-rhodamine (1 mg/ml, Molecular Probes) were added to the sporozoites and 50 µl of this mixture were transferred to the hepatocytes. To measure the background noise, control cells were treated with dextran-rhodamine alone. Cells treated with sporozoites and dextran-rhodamine in absence of antibodies were used to quantify the maximal traversal rate. The monoclonal antibodies mGO53 and 2A10 were used as negative and positive control, respectively. The plate was centrifuged for 10 min at 3000 rpm without brake and acceleration and afterwards incubated for 2 h at 37 ˚C and 5% CO_2. The hepatocytes were washed three times with PBS, detached by trypsin treatment and resuspended in 10% FCS in PBS. The cells were centrifuged for 5 min at 3600 rpm and 4 ˚C and the pellet was resuspended in 1% PFA in PBS. The cells were analyzed by flow cytometry using a LSR II instrument to quantify the frequency of dextran-positive cells. After subtraction of the background signal, the inhibition of sporozoite traversal was calculated by normalization of the data to the maximal sporozoite traversal measured in the controls without antibodies.

3.10 gDNA preparation for HLA-typing

For gDNA preparation, PBMC samples were thawed (see section 3.1.2) and the gDNA was extracted using the DNeasy Blood & Tissue Kit (Qiagen) according to the provider's instructions. The HLA-typing was performed by the Institut für Immunologie und Genetik, Kaiserslautern, in cooperation with SEQ-IT GmbH.

3.11 Statistical analysis

Statistics were calculated using GraphPad Prism (Version 8.1.2) and R (Version 3.4.2). The corresponding statistical test used for each experiment is stated in the figure legend (*P < 0.05; **P < 0.01; ***P < 0.001; ****P < 0.0001).

4 Results

4.1 Development of a human TCR analysis platform

To study T cell responses induced during malaria vaccination in humans, we developed a platform that allows the in-depth characterization of T cells by directly linking the cellular phenotype with the T cell receptor repertoire and specificity on single-cell level (Figure 6). This method is based on the amplification of full-length, paired TCR alpha and beta genes from single-sorted T cells. To overcome the low throughput of single-cell approaches, we applied a barcoding system previously developed in our laboratory, which enabled the paralleled analysis of several thousand TCRs [154]. The development of an automated analysis pipeline facilitated the fast and comparable analysis of the TCR sequences. Furthermore, the amplification of full-length TCR genes allowed the direct cloning of large numbers of TCRs for functional assessment.

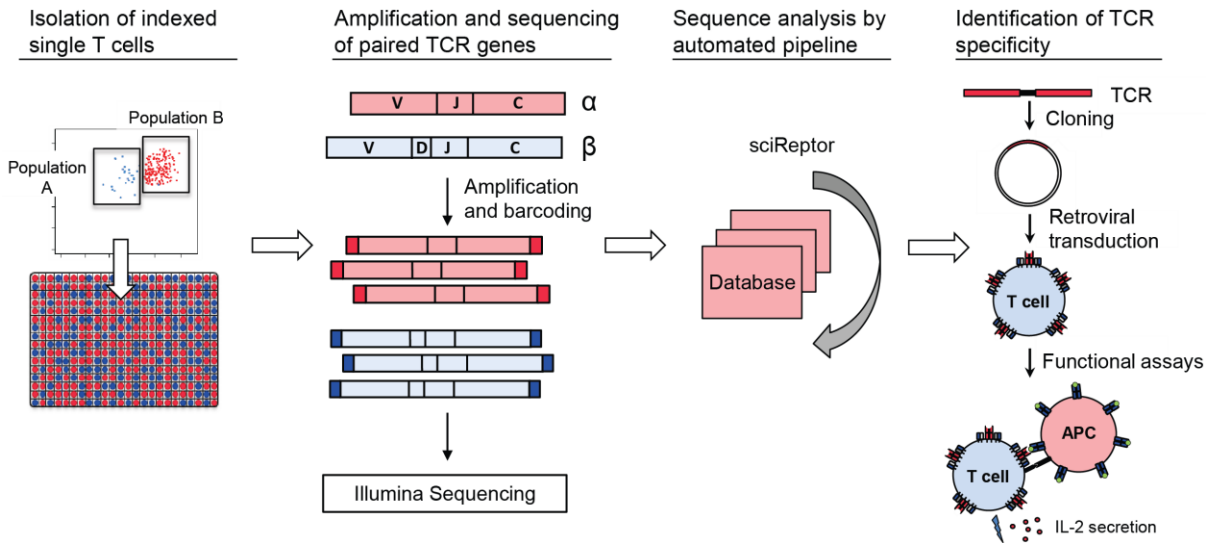

Figure 6: Schematic overview of the human TCR characterization platform. Single human T cells are index-sorted into 384-well plates, whereby the indexing-function records the phenotype of each sorted cell. The complete RNA of each cell is reverse transcribed and the resulting cDNA is used as template for the amplification of the full-length alpha and beta genes. During this amplification step barcodes are added to the DNA fragments to encode the position of each cell on the plate. Afterwards all PCR products are pooled and sequenced using Illumina MiSeq. The resulting sequencing reads are analyzed using the automated analysis pipeline sciReptor. TCRs of interest are cloned into a retroviral expression vector and stably introduced into TCR^{neg} T cells (Jurkat76) using retroviral transduction. The specificity of the TCRs is determined by co-cultures with antigen-presenting cells (APCs) presenting peptides of interest. The activity of T cells is monitored by detection of IL-2 secretion by ELISA.

4.1.1 Amplification and sequencing of human TCR alpha and beta transcripts

For TCR amplification single human T cells were sorted into 384-well plates using fluorescence-activated cell sorting. To allow the analysis of multiple T cell populations from limited biological samples, the index sorting function linked the phenotypic information to the position of the cell on the plate, enabling later discrimination of populations by position. Subsequently, total RNA was reverse transcribed from single cells using random hexamer primers, leaving the option for characterization of additional genes, e.g. cytokines (Figure 7A). The resulting cDNA was used as template for the amplification of the TCR alpha and beta genes, which was performed in two subsequent semi-nested PCRs. Mixes of 41 and 27 distinct V segment-specific forward primers, covering all functional V segments, were used to separately amplify the TCR alpha and beta genes, respectively (Supplementary Table 6 and Supplementary Table 7). To allow direct expression cloning of TCR genes after amplification, the forward primers were designed to bind directly downstream of the signal peptide sequence, thereby amplifying the complete sequence encoding the mature TCR chains [149]. Each forward primer further contained a common linker sequence at the 5' end, serving as primer binding site in the second PCR [141]. The reverse primer bound in the conserved constant region. To further increase the amount of TCR amplicon for sequencing, a second amplification step was performed using the first PCR product as template. In this second PCR, forward primers binding to the attached common linker sequence as well as nested reverse primers binding to the constant region were used. Furthermore, in this step information about the position of the cell on the plate was added to the amplicons to allow the pooling for next-generation sequencing without losing information about the TCR alpha and beta gene pairing as well as the associated cellular phenotype (Figure 7B). In detail, 16 bp long unique barcodes were added to the forward and reverse primers and were used along the row and column of a 384-well plate, resulting in a matrix of 384 unique row- and column-barcode combinations. By reading the barcodes from the amplicons, the position of a given cell in the 384-well plate could be indexed [154]. The throughput was further increased by designing 64 unique row and 72 unique column barcodes, which could distinguish positions on a matrix of 3x4 384-well plates. This barcoding and subsequent pooling of amplicons enabled the paralleled sequencing of hundreds to thousands of sequences. For the sequencing the Illumina MiSeq300 platform was used, as it could cover the complete amplicon sequence of maximal 550 bp. With this strategy, TCR alpha and beta genes could be amplified from 20-50% of the sorted $CD4^+$ T cells (Supplementary Figure 1A,B). This amplification efficiency was further increased by exchanging the reverse primer, as well as splitting the cDNA and performing two separate alpha and beta first PCRs (Supplementary Figure 1A-D). Furthermore, a drop of amplification efficiency, observed upon barcoding of second PCR primers, was rescued by

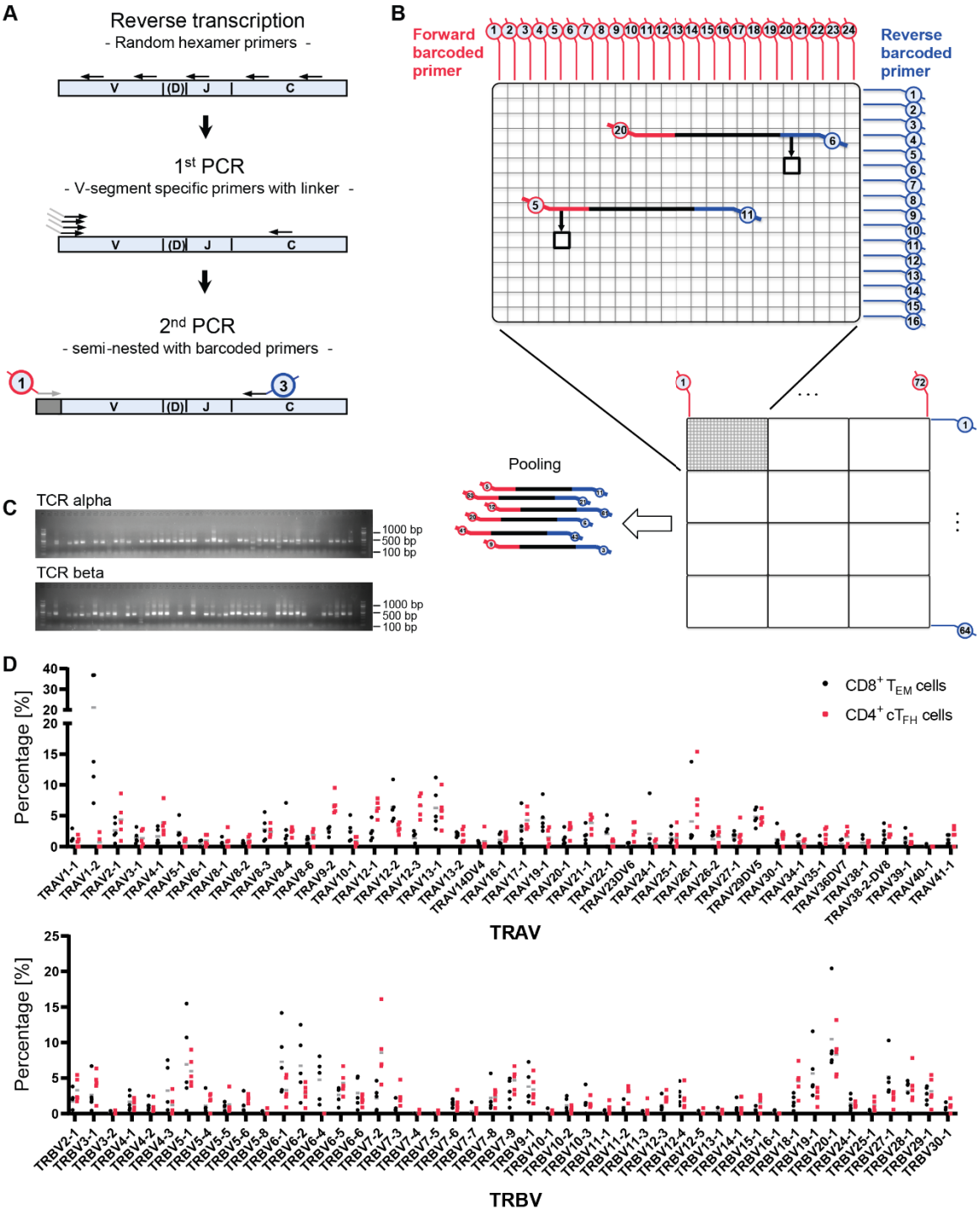

Figure 7: High-throughput, single-cell based human TCR alpha and beta gene amplification. (A) Schematic representation of the TCR gene amplification protocol. Single T cells are sorted into a 384-well plate and the mRNA is reverse transcribed using random hexamer primers. The TCR genes are amplified from the cDNA in two separate, semi-nested PCR reactions. The first PCR is carried out with a cocktail of V segment-specific forward primers, containing a common linker sequence at the 5' end, as well as a C segment-specific reverse primer. In the second PCR, barcoded linker-specific forward primers as well as barcoded C segment-specific reverse primers are used. (B) Overview of the primer matrix. Column- and row-specific barcodes are attached to the forward and reverse primers, respectively. During the PCR amplification, unique combinations of row and column barcodes are added to the amplicons which encode the position on the matrix, thereby enabling the pooling of all samples of a 3x4 384-well plate matrix for NGS sequencing. (C) Representative agarose gel electrophoresis picture showing the amplification efficiencies for TCR alpha and beta. (D) Alpha and beta V segment usage of $CD8^+$ T_{EM} cells and $CD4^+$ cT_{FH} cells isolated from PBMCs of healthy donors. Each dot represents an individual donor.

increasing the magnesium chloride concentration (Supplementary Figure 1E). With this optimized PCR protocol, the TCR alpha and beta genes could be amplified from 41-73% and 42-80% of the sorted T cells, respectively (Table 20, Figure 7C). Paired sequences of the alpha and beta genes could be gained from 24-62% of the sorted cells. Interestingly, the amplification efficiency was influenced stronger by the sample quality, assessed by measuring the cell viability, than the cellular phenotype (Supplementary Figure 2, Table 20). Next we wanted to confirm that our primers were able to amplify all published functional TCR alpha and beta V segments. Indeed, all 48 functional V beta segments could be identified with our primer set, whereas 43 of 45 functional V alpha segments were detected. The two functional V alpha segments that were not detected with our primer set were TRAV7-1 and TRAV18-1. Interestingly, other studies confirmed that TRAV7-1 and TRAV18-1 are very low abundant or not detectable, respectively, which is likely the reason why we did not detect them yet [141,155–158]. The frequencies at which we detected the remaining V alpha and beta segments also correlated with the frequencies observed in other studies (Figure 7D) [141,155–158]. Remarkably, we observed prominent differences in segment usage in two different T cell subsets, circulating T follicular helper cells (cT_{FH}) and $CD8^+$ effector memory T cells ($CD8^+$ T_{EM}), indicating that the analyzed population can have a strong impact on the detected segment usage (Figure 7D). This difference can be partly attributed to the presence of mucosal-associated invariant T cells (MAIT cells) in the $CD8^+$ T_{EM} subset, which preferentially use the TRAV1-2 segment paired with TRBV6 or TRBV20 segments [159,160]. In summary, we were able to efficiently amplify TCR alpha and beta genes from different T cell populations, covering 98% of the reported V segments.

Table 20: Combined efficiency of TCR alpha and beta gene amplification, sequencing and sciReptor annotation. T_{EM} = effector memory T cell; cT_{FH} = circulating T follicular helper cell.

Population	Phenotype	Number of experiments, number of cells	Efficiency (in %)		
			TCRα	TCRβ	TCRαβ
$CD8^+$ T_{EM}	$CD3^+$ $CD8^+$ $CD45RA^-$ $CCR7^-$	4, n=5376	43-49	42-57	24-32
Activated $CD8^+$ T_{EM}	$CD3^+$ $CD8^+$ $CD45RA^-$ $CCR7^-$ $PD\text{-}1^+$ $ICOS^+$	3, n=5568	58-69	48-74	38-49
Activated cT_{FH}	$CD3^+$ $CD4^+$ $CD45RA^-$ $CXCR5^+$ $PD\text{-}1^+$ $ICOS^+$	4, n=5267	41-76	57-80	27-62
Highly activated cT_{FH}	$CD3^+$ $CD4^+$ $CD45RA^-$ $CXCR5^+$ $PD\text{-}1^{++}$ $ICOS^+$	4, n=5170	56-66	70-77	45-55

4.1.2 Automated analysis pipeline for the processing of TCR sequence data

To enable the efficient analysis of the high-throughput sequencing data generated with our TCR amplification protocol, we developed an automated TCR analysis pipeline that is capable of handling large data sets, process and analyze TCR sequence features and link those to the donor- and cell-specific meta-information.

To achieve this, we made use of the analysis pipeline sciReptor, which was previously developed in our group and is capable of processing Ig sequences [146]. With the help of Dr. Christian Busse, sciReptor was modified to allow the analysis of TCR sequences (Figure 8A). In the first step, the analysis pipeline imports the NGS reads into a relational database. Subsequently, the V, D and J segments are identified by IgBLAST [148] and the constant region is identified by BLAST [161], which aligns the query sequence to the reference database. This reference database was generated by insertion of all TCR alpha and beta segments published on the Ensembl Genome Browser [149]. Next, the barcodes encoding the position of the cell on the 384-well plate are read by RazerS [162]. Reads with identical segment usage and barcodes are grouped and the two groups with most reads are separately aligned to form an error-corrected first and second consensus sequence by MUSCLE [163]. In a next step, the consensus sequences are analyzed, and the V, D, J as well as C segments are annotated as before. Furthermore, the locus is identified, mutations are recorded and framework and complementarity-determining regions are annotated. The sequence information is subsequently stored in a relational database and joined to the metadata, including the donor and sample-specific information as well as the flow cytometric indexing data. The data are stored in a standardized format and can be accessed for downstream analysis like the determination of segment usage, alpha and beta chain pairing and clonal expansion. Additionally, the pipeline performs a quality control to monitor the sequence quality and the pipeline run. This quality control system revealed that some TCR alpha sequencing runs had a 2-4 fold reduced efficiency in obtaining sequences from the sorted T cells (Figure 8B,C). This drop in efficiency was in line with a shift in the distribution of reads per well, which resulted in a strong overrepresentation of single wells, as well as a generally low read quality (Figure 8D,E). Interestingly, when a new library preparation and sequencing run was performed with the same pooled PCR products, a normal efficiency, read distribution and read quality was observed, indicating that the problem was independent on the PCR products (Figure 8F-H). This phenomenon occurred in 30-40% of the TCR alpha sequencing runs but was not detectable for TCR beta runs (Figure 8B). Hence, the problem was specific for the TCR alpha sequences and occurred either during library preparation or sequencing. Further investigations will address whether this is caused by an inefficient adaptor ligation and what

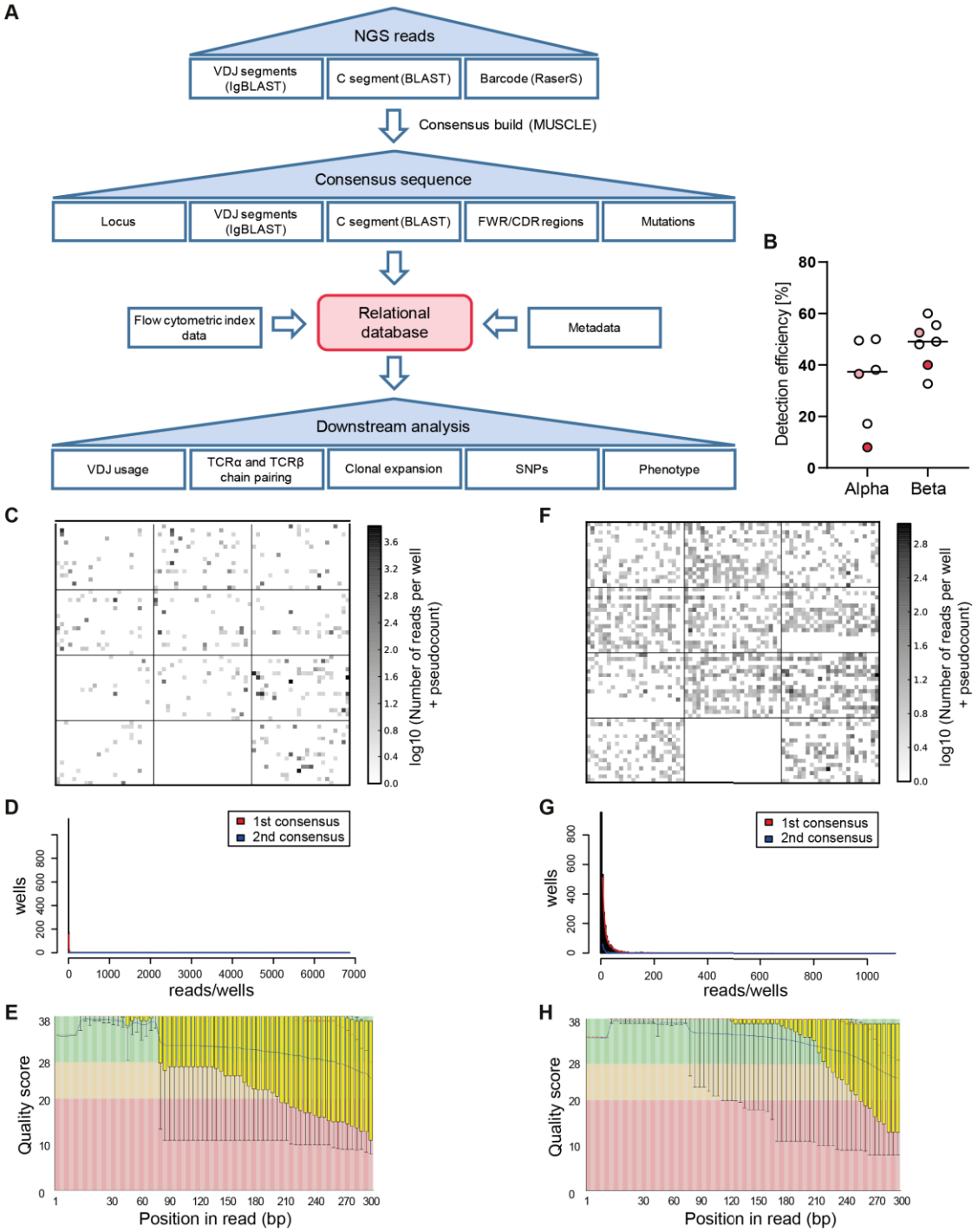

Figure 8: Automated T cell receptor sequence analysis with sciReptor. (A) Schematic workflow of the analysis pipeline sciReptor. First, raw reads from NGS are analyzed and grouped for consensus formation. Error-corrected consensus sequences are analyzed for annotation of T cell receptor sequence features. The sequence information is linked to the metadata and flow cytometric index data and stored in a relational database. (B) Efficiency of TCR sequencing of single-sorted T cells after TCR amplification, library preparation, NGS sequencing and sciReptor analysis. Each dot represents a separate library preparation and sequencing run. Dark red: sequencing run shown in C-E. Light red: sequencing run shown in F-H. 100,000 reads per sequencing run were analyzed. (C-H) sciReptor quality control (QC) output of a low efficiency (C-E) and high efficiency (F-H) TCR alpha sequencing run. (C, F) Reads obtained from each well on a 3x4 matrix of 384-well plates are shown. Filled squares indicate a successful sequencing and the darkness represents the number of reads yielded. 11 plates were analyzed in parallel and one position was intentionally left empty. (D, G) Distribution of reads per well for all reads (histogram), first consensus (red line) and second consensus reads (blue line). (E,H) Averaged Illumina quality scores per position in the read. For the Illumina QC, 442692 (E) and 509518 (H) reads were analyzed. Of these, 100,000 reads were randomly selected for the sciReptor analysis (C, D, F, G).

renders the alpha sequences more susceptible. In conclusion, the modified pipeline is a helpful tool for the fast and comparable TCR data analysis by linking the genetic information to the cellular phenotype and sample information. Its quality control mechanism allows the identification of alterations in the sequence quality which can influence the data interpretation.

4.1.3 Expression and functional analysis of human T cell receptors

To determine the specificity of the TCRs identified by the analysis pipeline, we next developed a method for the fast and efficient expression cloning of TCRs followed by screening for reactivity to different antigens.

To ensure an equimolar expression of both TCR chains, the TCR alpha and beta gene were joined head-to-tail with a porcine teschovirus-1 2A (P2A) peptide and cloned into a retroviral expression vector using Gibson assembly (Figure 9A) [164]. The expression vector contained parts of a common TCR alpha signal sequence as well as the TCR beta constant segment TRBC1 or TRBC2 (Supplementary Figure 17). The sequence overlaps required for Gibson assembly were introduced to the TCR alpha and beta genes by PCR using the first PCR product as template and primers binding to the V and C segments for amplification. Some V segment primers not only contained the required overlaps but also up to 26 bp of the corresponding V segment which were not amplified during the previous PCR (Supplementary Table 8 and Supplementary Table 9). The amplification with primers specific for each individual V segment not only introduced overlaps but also reverted mutations in the primer binding site that were introduced by the binding of degenerated primers in the previous PCR. After amplification, the TCR genes were joined together with a linker fragment, containing the TCR alpha constant region, the P2A peptide and the TCR beta signal sequence, as well as the backbone in a single reaction. The correctness of the sequence was confirmed by sequencing, where 54% of the analyzed TCR sequences were correct, whereas 46% showed point mutations, insertions or deletions (Figure 9B,C). Notably, the majority of incorrect TCR sequences carried 1-2 point mutations, which likely were generated by random errors of the polymerases used during TCR amplification. In summary, a maximum of 3 assembled sequences per TCR were sufficient to gain a correct sequence for almost all (95%) of the TCRs (Figure 9B).

In a next step the cloned TCRs were stably introduced into TCR^{neg} Jurkat76 (J76) cells by retroviral transduction, which resulted in long-term TCR expression and hence enabled repeated functional analysis for several weeks [151]. J76 cells are expressing only low levels of the co-receptors CD3, CD4 and CD8, which are known to play an important role in T cell

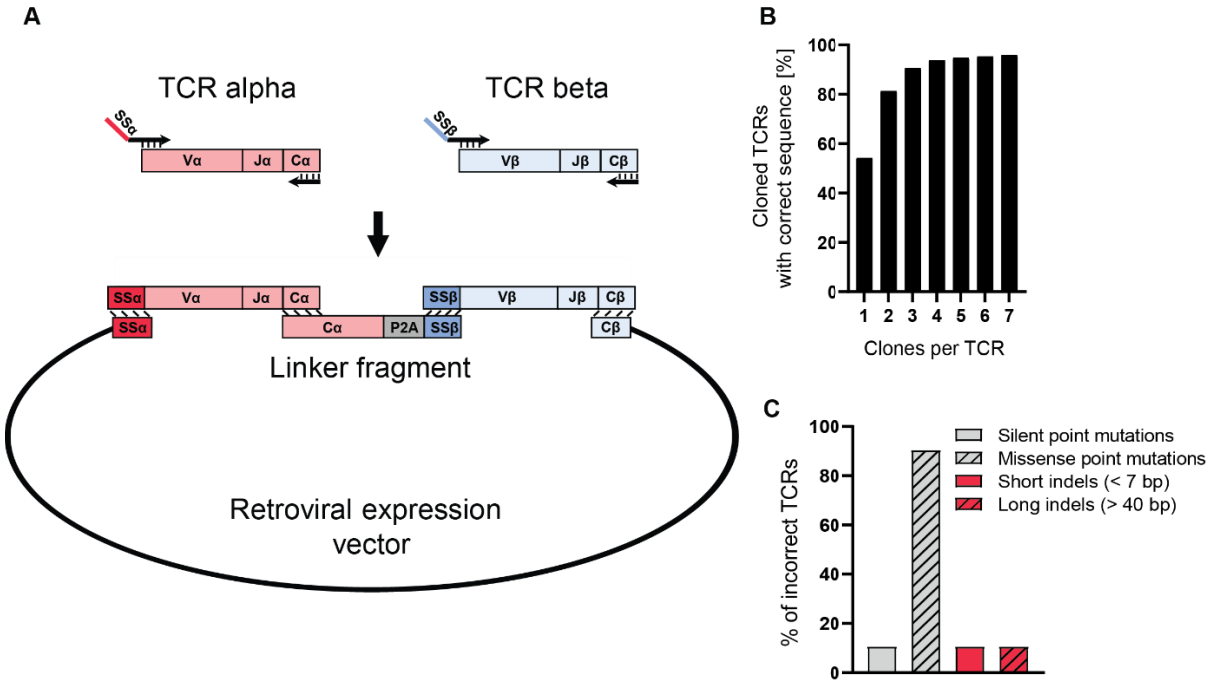

Figure 9: Cloning of selected human TCRs. (A) Schematic overview of the TCR cloning strategy. The TCR alpha and beta genes are amplified separately from first PCR products using V segment-specific forward primers and C segment-specific reverse primers. Forward primers carry a common signal sequence at the 5' end (Supplementary Table 8 and Supplementary Table 9). The amplified alpha and beta genes were joined head-to-tail with a linker fragment, containing a P2A sequence, as well as the retroviral expression vector in a single Gibson assembly reaction. Regions of sequence homology are indicated with dashes. (B) Cumulative frequency of correctly assembled, unmutated TCRs gained after sequencing multiple clones per TCR construct. (C) Frequencies of mutations detected in incorrect TCR sequences. Data of 192 (B) and 94 (C) TCRs from two independent experiments were pooled and analyzed. (B,C) Data were generated together with Rebecca Hundsdorfer and Julia Puchan. Indel = insertion or deletion.

activation [10,11,16,17,165]. Therefore, a monoclonal $CD3^+$ $CD4^+$ and $CD3^+$ $CD8^+$ J76 T cell line, hereafter referred to as J76-CD4 and J76-CD8, respectively, was generated by stable retroviral transduction of the co-receptors into J76 cells and subsequent single-cell sorting and expansion. The presence of the co-receptors was verified by flow cytometry (Figure 10A). To stably introduce TCRs into these J76-CD4/8 T cells, the cells were transduced with retroviruses carrying the TCR-containing expression plasmid. As control TCRs the MHC-II restricted HY-TCR, specific for the human $DDX3Y_{176-187}$ peptide (in J76-CD4 T cells), and the MHC-I restricted JM22-TCR, specific for the influenza A virus $M1_{58-66}$ peptide (in J76-CD8 T cells), were used [166–169]. Successfully transduced J76 cells were identified by the expression of a fluorescent protein (GFP/mCherry) and selected with puromycin, which resistance gene, puromycin N-acetyl-transferase (PAC), was encoded on the vector (Figure 10B, Supplementary Figure 17). The TCR expression was monitored by flow cytometry. Transduction of the J76-CD4 and J76-CD8 cells with the respective control TCR resulted in 10-60.4% transduced cells and 3.9-22.2% TCR-expressing cells (Figure 10C). Treatment of these cells with puromycin led to an increase in the frequency of transduced cells to 98-100%

and of TCR-expressing cells to 48.5-74%. The higher frequency of transduced cells compared to TCR-expressing cells was likely caused by differences in the promoter activity, as the expression of the TCR and the GFP/mCherry-IRES-PAC cassette were controlled by different promoters (Supplementary Figure 17). Next, TCRs with different segment usage and unknown specificity were cloned and expressed and the range of TCR^+ T cells was quantified (Figure 10C). Interestingly, 10% of the TCRs were expressed on less than 25% of the transduced T cells after puromycin treatment, which also correlated with reduced levels of surface TCR expression on the TCR^+ T cells (Supplementary Figure 3). One reason for this could be an erroneous cloning which might result in segment-specific dropouts, caused for example by an incorrect signal sequence prediction. This could be ruled out as weakly expressed TCRs used diverse V segments and for most V segments well and poorly expressed TCRs were observed (Supplementary Figure 4). An alternative explanation could be the presence of two functional alpha chains in one cell, which has been reported in 25% of T cells as a consequence of missing allelic exclusion [170]. As not always both functional alpha chains can be expressed on the surface to form a functional TCR with the beta chain, the cloning of the wrong alpha chain could also lead to the observed low expression level [171]. This was supported by the fact that of eight TCRs, for which two alpha chains were detected, only four could express both chains efficiently on the cell surface, whereas three could express only one alpha chain and one could express none of the two (Figure 10D). This suggests that the cloning of an alpha chain which cannot pair with the beta chain to form a functional receptor might explain some drop outs in TCR expression, but other mechanisms also seem to be in play as for one TCR none of the two alpha chains could be expressed. Interestingly, the alpha chain amplified more efficiently by PCR and NGS (first consensus sequence) was not necessarily the one expressed best, impeding the prediction of the correct chain by read counts.

After confirming that the cloning and expression of TCRs with diverse segment usage works with 90% efficiency, we established a T cell stimulation assay that allows the screening of large numbers of TCRs with varying sensitivities to the given antigen. To have a reliable source of MHC-matched antigen presenting cells (APCs), autologous B cells were bulk sorted and immortalized with Epstein-Barr-Virus (EBV). As B cells are efficiently taking up extracellular proteins and presenting them on their MHC-II, $CD4^+$ T cells could be stimulated with peptides or whole proteins. In contrast, B cells are inefficient in cross-presenting exogenous proteins on MHC-I molecules, hence $CD8^+$ T cells could only be screened for their reactivity to processed peptides which can be exchange on the surface of the MHC-I without cellular processing [172–174]. To estimate and optimize the sensitivity and specificity of the T cell stimulation assay the JM22-TCR, binding the $M1_{58\text{-}66}$ peptide with high affinity (K_D 5-6 µM), was introduced into J76-CD8 T cells [175,176]. The JM22-TCR transgenic J76-CD8 T cells were

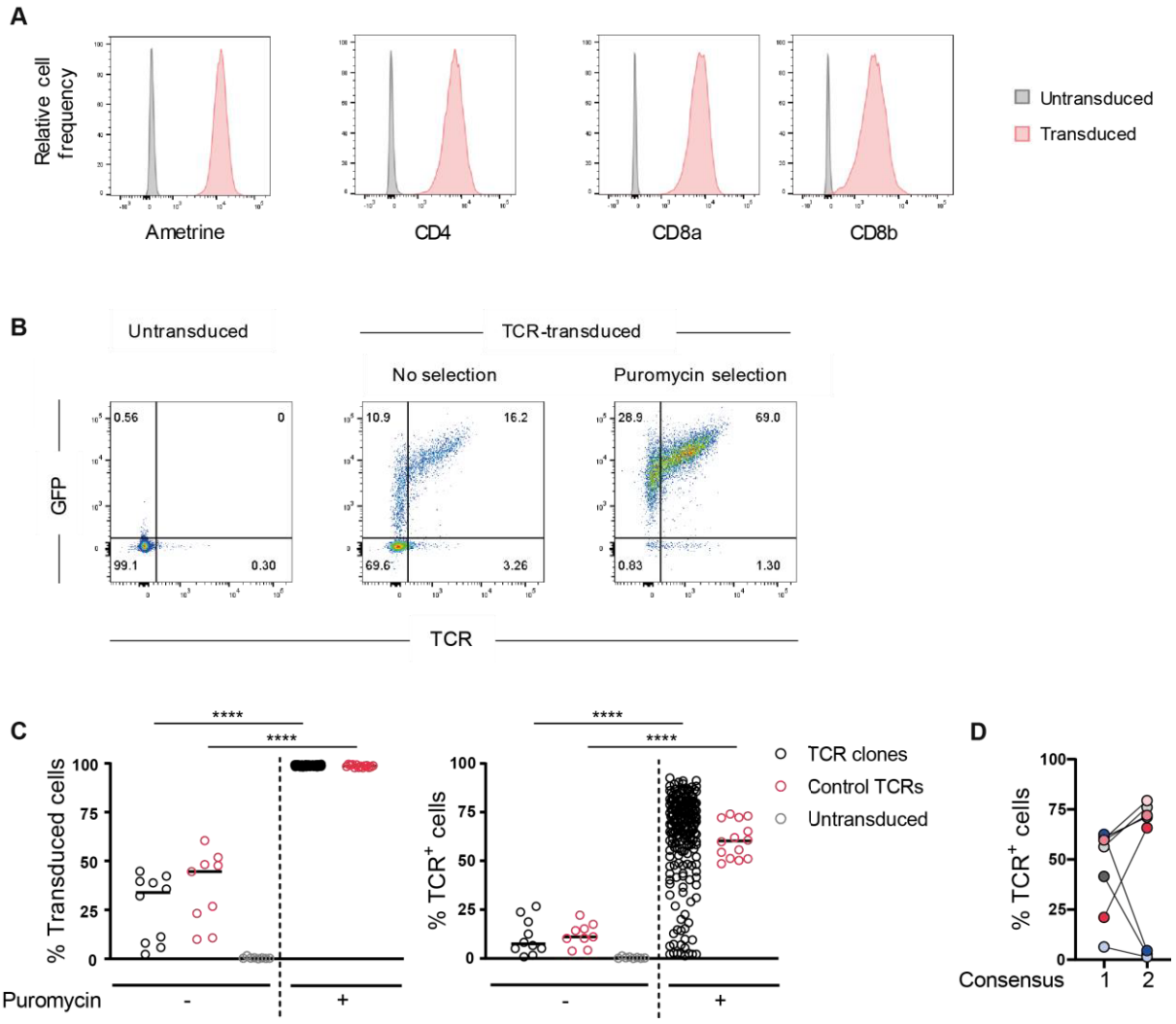

Figure 10: Expression of cloned TCRs in TCR-deficient T cells. (A) Stable monoclonal $CD3^+$ $CD4^+$ and $CD3^+$ $CD8^+$ Jurkat76 cell lines were generated by retroviral transduction and subsequent fluorescence-activated single-cell sorting and clonal expansion. The expression of CD3 was determined by detection of the co-expressed fluorescent protein Ametrine. The surface expression of CD4 and CD8a/CD8b was analyzed with fluorescently-labelled antibodies. Frequency distribution histograms are shown for Jurkat76 cells before and after retroviral transduction (pre-gated on live cells). (B) Representative gating strategy for the flow cytometric analysis of surface TCR-expression of Jurkat76 cells before and after retroviral transduction with cloned TCRs. Transduced cells were identified by co-expression of GFP or mCherry and were selected with puromycin. (C) Quantification of the frequency of transduced cells ($GFP/mCherry^+$) and TCR-expressing cells (TCR^+) in Jurkat76 cell lines that were transduced with TCR clones from a human malaria immunization trial and analyzed by flow cytometry before and after puromycin treatment. Negative control: Untransduced Jurkat76 cells. Positive control: Jurkat76 cells transduced with control TCRs (HY and JM22). Pooled data from two independent experiments are shown. (D) Selected TCR clones from (C), for which two alpha chains (connected with lines) paired with one beta chain were detected after sequencing. The alpha chains were ranked as first and second consensus sequence dependent on the read number obtained from NGS. (C,D) Experiments were performed together with Rebecca Hundsdorfer and Julia Puchan.**** $p < 0.0001$, two-tailed Mann-Whitney test.

subsequently stimulated for 24h with $M1_{58-66}$ peptide-pulsed autologous B cells. To allow the screening of large numbers of TCRs, the T cell stimulation assay was performed in 96-well plates and the T cell activation was determined by measuring the IL-2 secretion by ELISA. To increase the sensitivity of the assay different parameters were optimized to allow detection of TCRs with a lower affinity to their antigen than the JM22-TCR. First, the total cell number was titrated to identify the optimal range, where the cells are sufficiently dense for efficient interactions but not too dense to compete for nutrients. We found a concentration of $3.2x10^6$ cells/ml to be ideal for the T cell activation, as this led to the highest IL-2 production detected by ELISA (Figure 11A). As a positive control Staphylococcal enterotoxin B (SEB) was used, which can crosslink the TCR and the MHC molecules unspecifically [177]. Interestingly, the IL-2 production in response to SEB strongly resembled the one induced in response to the $M1_{58-66}$ peptide, confirming that all T cells expressing a TCR on the surface were also specific for the $M1_{58-66}$ peptide. No IL-2 secretion was detected in response to DMSO without peptide. Next, we assessed the best T:B cell ratio to quantify how many APCs would be required for T cell activation. Here we observed the highest IL-2 production at a T:B cell ratio of 2:1 (Figure 11B). Finally we titrated the minimal amount of peptide required for T cell activation, which is critical when pools of multiple peptides are used and the concentration of the toxic DMSO, in which most peptides are dissolved, should be kept as low as possible. We measured similar IL-2 secretion after stimulation with 0.5 – 10 µg/ml $M1_{58-66}$ peptide, indicating that for peptide pools the concentration of each peptide can be strongly reduced without impairing the sensitivity of the assay (Figure 11C). These results show that the T cell stimulation assay is able to identify antigen-specific responses of TCR-transduced T cells. Importantly, the strong IL-2 signal as well as the low background most likely allows also the discrimination of weaker signals resulting from lower affine TCRs.

In summary, we generated a platform for the high-throughput, single-cell characterization of human TCR repertoires, which links the genetic information of each TCR with the cellular phenotype and is furthermore able to identify specificities of selected TCRs. This platform allows the in-depth characterization of T cell responses induced to a variety of triggers, including vaccinations and infections and was used in a next step to characterize the T cell responses raised after successive malaria immunizations in healthy donors.

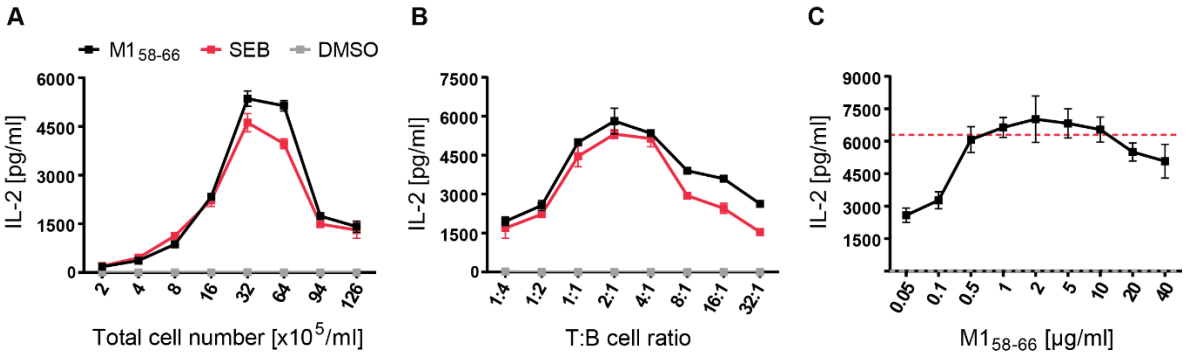

Figure 11: Optimization of the antigen-specific stimulation of TCR-transgene T cells. TCR-deficient J76-CD8 T cells were retrovirally transduced with the JM22-TCR specific for the $M1_{58-66}$ peptide. After puromycin selection, the TCR-transgenic T cells were co-cultured with peptide-pulsed B cells for 24 h and the IL-2 concentration in the supernatant was determined by ELISA. SEB and DMSO were used as positive and negative control, respectively. (A) Titration of the total cell number with a T:B cell ratio of 1:1 and 10 µg/ml $M1_{58-66}$ peptide. (B) IL-2 concentration for varying T:B cell ratios with a total cell concentration of $32x10^5$ cells/ml and 10 µg/ml $M1_{58-66}$ peptide. (C) Titration of the $M1_{58-66}$ peptide concentration used to stimulate $32x10^5$ cells/ml with a T:B cell ratio of 2:1. Dashed lines depict the SEB (red) and DMSO (gray) control.
One representative experiment of three is shown per titration. The mean and standard deviation of two technical replicates is plotted. Data were produced jointly with Sandro Hoffmann.

4.2 T cell responses to *Plasmodium falciparum*

Current advances in malaria vaccine development highlight the relevance of $CD4^+$ and $CD8^+$ T cell responses for the induction of sterile immunity [91,92,98,111,178]. While numerous studies focused on the identification of epitopes targeted by T cells, knowledge about the TCRs recognizing the antigens and how immunizations shape the T cell repertoire is still missing [115,116,122,123,126]. To shed light on the process of antigen-mediated activation of *Pf*-specific T cells, we aimed at characterizing the T cell repertoire of $CD8^+$ effector memory T cells and $CD4^+$ T follicular helper cells after successive malaria immunizations to search for signs of antigen-driven selection, such as clonal expansion of T cells or the enrichment of TCR sequence features associated with antigen binding.

4.2.1 Human malaria immunization trial MAVACHE A

To study T cell responses to *Plasmodium falciparum*, PBMC samples from the human malaria immunization trial MAVACHE A, which used radiation-attenuated *Plasmodium falciparum* sporozoites (*Pf* RAS) for immunization, were analyzed. The use of *Pf* RAS has two major advantages: First, they are known to induce strong immune responses which can be easily detected in the blood. Second, *Pf* RAS can only develop until the liver stage, thereby

facilitating the characterization of immune responses induced to the early stages of infection, which are most relevant for vaccine design. In the MAVACHE A trial, five healthy volunteers were immunized three times, on day 0, 7 and 28, with 900,000 radiation-attenuated sporozoites (Figure 12). Blood samples were taken 3 days before the first immunization (referred to as 0) and 7 days after each immunization (referred to as I, II and III). The study was conducted by Prof. Dr. Benjamin Mordmüller and colleagues in the Institute of Tropical Medicine, Tübingen, Germany.

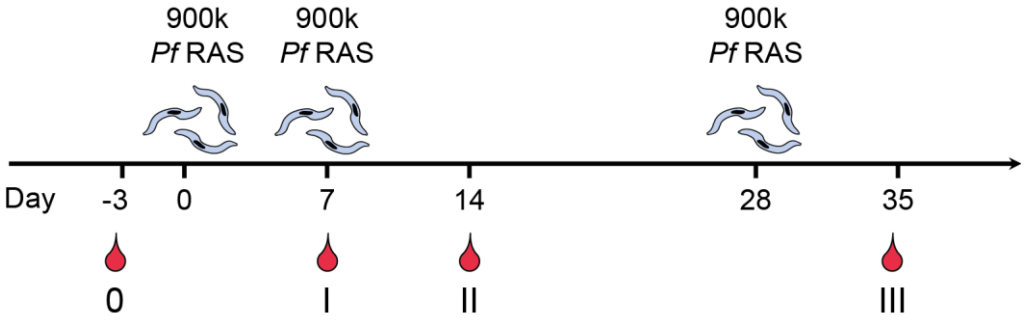

Figure 12: Schematic overview of the human malaria immunization trial MAVACHE A. Five human volunteers were immunized three times with 900,000 radiation-attenuated *Plasmodium falciparum* sporozoites (*Pf* RAS). The duration between the first and second immunization was 3 times shorter (7 days) than between the second and third immunization (21 days). Blood samples for analysis were taken three days before the first immunization (0) and seven days after each immunization (I, II and III). Due to the short immunization schedule, the time point I overlapped with the start of the second immunization, however blood was taken before application of *Pf* RAS. The study was conducted by Prof. Dr. Benjamin Mordmüller and colleagues in the Institute of Tropical Medicine, Tübingen, Germany.

4.2.2 CD8$^+$ effector T cell responses in *Pf* RAS immunization

As CD8$^+$ T cells play an important role in protection against *Pf* parasites by targeting infected hepatocytes, the platform for single-cell human TCR characterization was applied to investigate the CD8$^+$ T cell repertoire. The direct analysis of antigen-specific cells was impeded by the high diversity of *Pf* proteins and hence T cell epitopes, as well as MHC-alleles of the donors, making it impossible to gain comprehensive information using tetramer staining. Therefore, unselected effector memory T cells (T_{EM}) were analyzed, which were reported to contain, together with terminally differentiated effector memory cells (T_{EMRA}), most *Pf*-specific CD8$^+$ T cells in RAS immunization [91]. While the overall frequency of CD8$^+$ T_{EM} cells (CD45RA$^-$ CCR7$^-$) in the volunteers did not change over the course of immunizations, the mean fraction of activated T_{EM} cells (PD-1$^+$ ICOS$^+$) within CD8$^+$ T_{EM} cells increased slightly from 2.9% before immunization to 4.2 - 4.9% after immunization, suggesting antigen-mediated activation (Figure 13). Notably, statistical tests could not be performed to test the significance in difference over time, as a minimum of 6 donors would be required for significance using the paired, non-parametric Wilcoxon test.

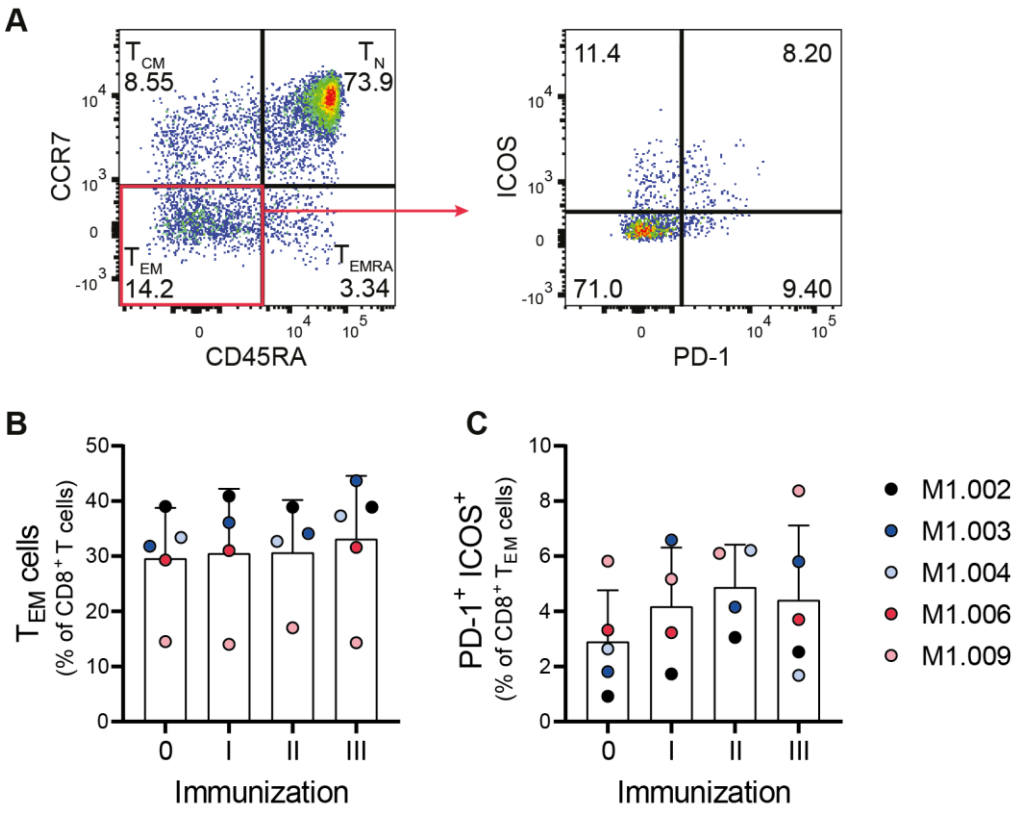

Figure 13: Frequencies of activated CD8⁺ T_{EM} cells after *Pf* RAS immunization. (A) Representative gating strategy for the flow cytometric analysis of PBMC samples from the malaria immunization trial MAVACHE A. PBMCs were pre-gated on single, live CD8⁺ T cells (for gating see Supplementary Figure 5A) and activated T_{EM} cells (CD45RA⁻ CCR7⁻ PD-1⁺ ICOS⁺) were single-cell sorted into 384-well plates for subsequent TCR repertoire analysis. Data are shown for donor M1.009 at III (B,C) Quantification of CD8⁺ T_{EM} cells (B) and activated CD8⁺ T_{EM} cells (C) in five volunteers before the first (0) and after each subsequent malaria immunization (I - III). Bar graphs show the mean and standard deviation, dots mark single donors. Samples M1.004 (I) and M1.006 (II) were excluded from analysis due to low sample quality (Supplementary Figure 5B).

Pf RAS immunization results in the recruitment of small T cell clones

To determine how the *Pf* RAS immunizations shaped the repertoire of CD8⁺ T cells, activated CD8⁺ T_{EM} cells were single-cell index sorted for subsequent TCR repertoire analysis. The newly developed protocol for paired, single-cell TCR amplification and subsequent Illumina MiSeq sequencing was applied to obtain TCR sequences. After sequence analysis with the modified analysis pipeline sciReptor, a total of 2500 paired TCR sequences were obtained from samples taken before (0) and after *Pf* RAS immunization (II, III) (Supplementary Table 1). Notably, this study focused on the analysis of the two later immunizations as they likely induced higher frequencies of *Pf*-specific T cell responses. In a next step, the TCR repertoire was analyzed for signs of antigen-driven selection. As activated T cells proliferate upon antigen encounter, the degree of clonal expansion is commonly used to identify antigen-specific cells. For simplicity, clones were defined by identical amino acid sequence of only the

TCR beta CDR3, as a single T cell could have sequences from two different alpha chains. Furthermore, the number of TCR sequences for analysis was increased by including TCR beta sequences with no detectable alpha gene instead of limiting the analysis only to paired sequences. Interestingly, the overall degree of clonal expansion in the TCR repertoire was rather high with around 60% clonally expanded cells before immunization (Figure 14A). Contrary to the assumption of clonal expansion being induced upon immunization, the frequency of clonally expanded cells decreased in all donors by 3-23% after the second immunization and increased again after the third to reach pre-immunization levels. This phenomenon was not due to differences in the number of TCR sequences as similar effects were detectable after random subsampling (Figure 14B, Supplementary Figure 6A). The increase of clonal expansion coincided with an increase of diversity of the clonally expanded cells as measured by Shannon diversity index (Figure 14C). Together, this indicates that the immunizations led to the emergence and recruitment of smaller clones, instead of fast expansion of pre-existing clones. This is in line with the fact that none of the five donors had a history of malaria infection and hence should not have *Pf*-specific memory T cells. The increased clonal expansion and decreased diversity after the third immunization could be mediated by T cell clones that were activated in response to the first and second immunization and were reactivated upon administering the third immunization. To examine these hypotheses, the kinetics of single clones were tracked over the course of immunizations. Indeed, upon immunization the emergence of new clones as well as the shrinkage of large pre-existing clones was observed, which is in agreement with the recruitment of new T cell clones into the immune response (Figure 14D, Supplementary Figure 6B). In contrast, there was no proof for the assumption that smaller clones expand with each immunization, as the larger clones present after the third immunization were, despite one exception, either not detected before or present already prior to immunization. It is possible, however, that infrequent T cell clones were not detected due to the low sampling depth, thereby underestimating the overlap of post-immunization samples. Overall, the overlap between pre- and post-immunization repertoires was highly comparable within each donor and ranged between 20-30%, indicating that even if there are shared clones emerging after immunization they are masked by the dominance of pre-existing memory cells from former infections (Figure 14E, Supplementary Figure 6C). A closer comparison between the pre-existing memory cells and the cells detected only after immunization revealed that the difference in diversity of clonally expanded cells, seen after second immunization, is indeed mediated by newly emerged cells, whereas the diversity among the pre-existing clones stayed highly comparable (Figure 15A). Furthermore, the newly raised T cell clones also showed a higher degree of activation compared to the pre-existing cells, which was reflected by an higher level of ICOS expression (mean fluorescence intensity, MFI), whereas no difference in the PD-1 expression

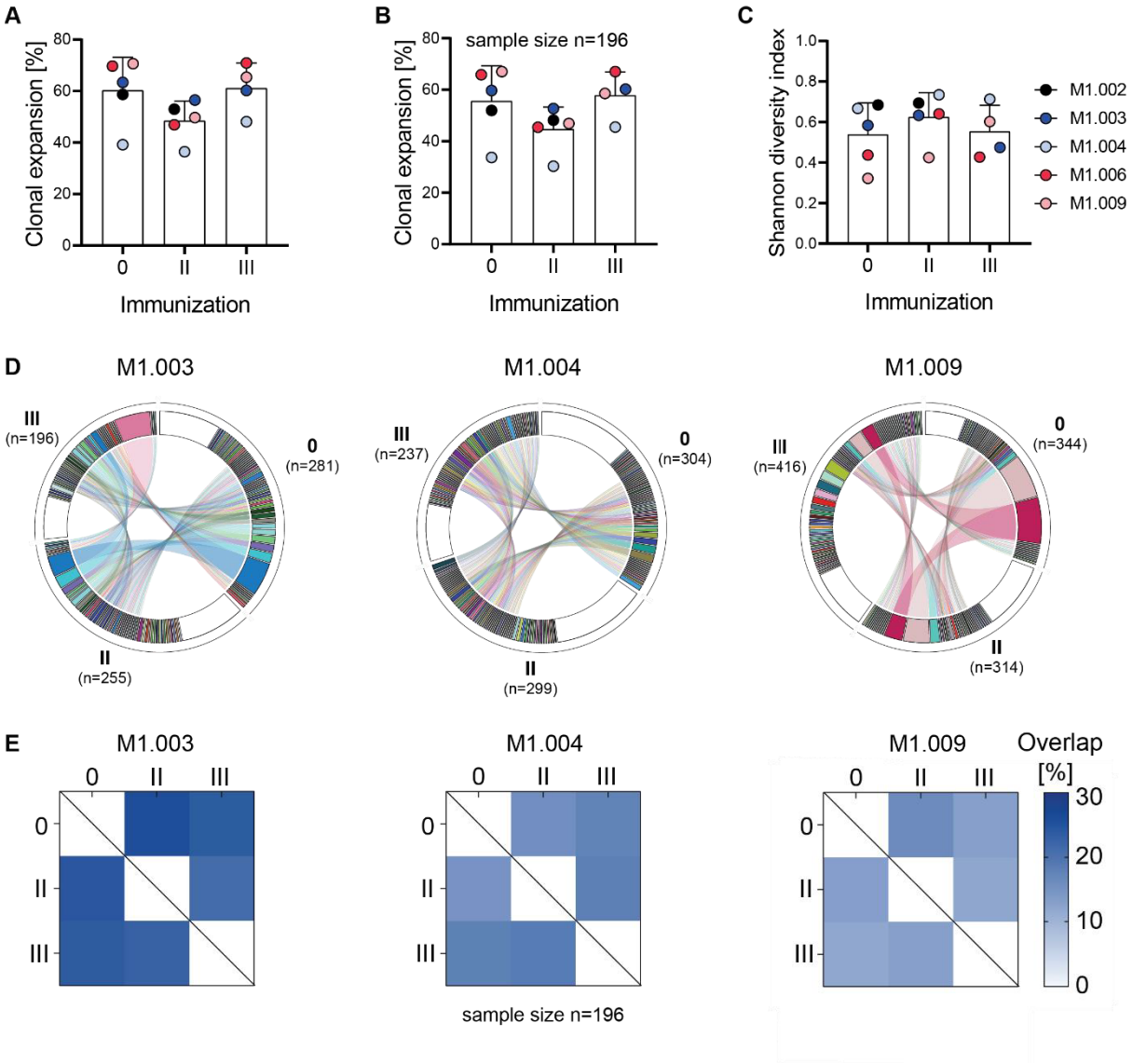

Figure 14: Strong clonal overlap of the TCR repertoire in CD8⁺ T_{EM} cells before and after *Pf* RAS immunizations. Single PD-1⁺ ICOS⁺ CD8⁺ T_{EM} cells were sorted and TCR genes were amplified and sequenced for subsequent repertoire analysis. Clones were defined by identical amino acid sequence of the TCR beta CDR3. The degree of clonal expansion was quantified at each time point (A). To account for differences in the number of available sequences per sample, sequences were 50 times randomly subsampled to the lowest sequence number observed (n=196) and the clonal expansion was quantified (B). Each dot represents the mean clonal expansion of the 50 subsamples. (C) Shannon diversity of clonally expanded sequences with 0 and 1 being completely monoclonal and polyclonal, respectively. To account for variations in sequence number, the diversity was normalized to the total number of expanded sequences. (D) Circos plots depicting the clonal overlap between pre- (0) and post-immunization (II, III) samples for three representative donors. Each color encodes for one expanded clone, whereas all non-expanded clones are depicted in white. Shared clones are connected by lines. Numbers of sequences analyzed per samples are given. (E) Heat map showing the percent clonal overlap of three representative donors. The mean of 50 random subsamples (n=196) was calculated.
(A-C) No TCR repertoire data were available for donor M1.002 after the third immunization (III).

was detectable (Figure 15B). Notably, a direct comparison of MFI values is only possible within but not between samples, as samples were recorded on different days. In summary, the data show that the CD8$^+$ T_{EM} repertoire is dominated by large clones, which are maintained over time and could be considered as steady state repertoire of T cells from previous infections. Upon *Pf* RAS immunization, smaller, new clones are recruited into the immune response. These newly recruited cells are more diverse, have a stronger activation phenotype and are rather restricted to single immunizations instead of expanding with each subsequent immunization.

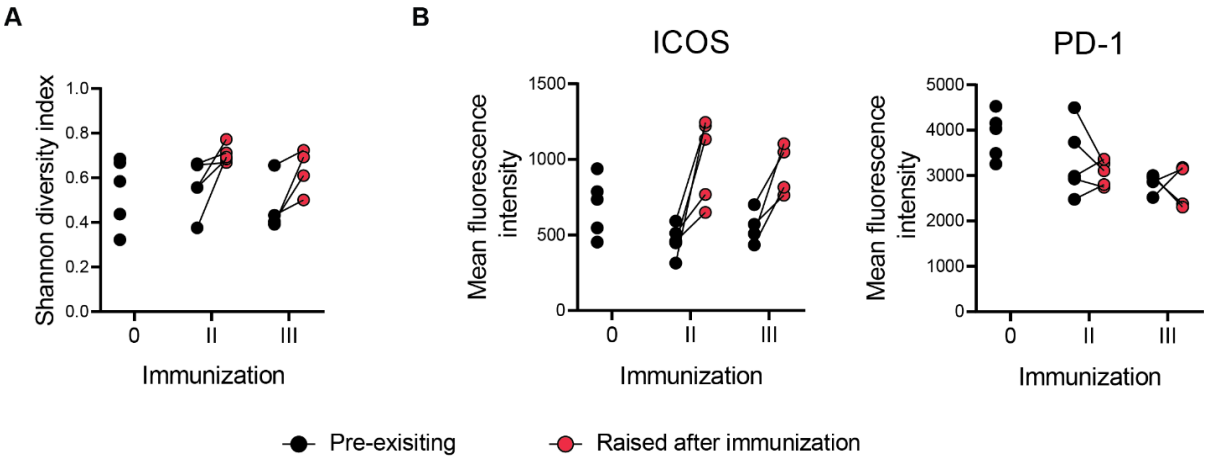

Figure 15: Comparison of TCRs existing before immunization to TCRs raised after immunization. TCRs of post-immunization samples were separated into pre-existing (at least one clone member detected before immunization) and raised after immunization (all clone members detected only in post-immunization samples). (A) Shannon diversity of clonally expanded cells normalized to the total number of expanded sequences. (B) Mean fluorescence intensity (MFI) of ICOS and PD-1 measured by index sorting. As samples from different immunizations were stained and analyzed on different days, MFIs may vary between immunizations. Each dot represents an individual donor.

The CD8$^+$ T_{EM} repertoire shows signs of antigen-driven selection

In a next step, the repertoire was analyzed for signs of antigen-driven selection of TCR sequence features involved in antigen binding. To this end, the V segment usage (Supplementary Figure 7), the preferential pairing of specific V and J segments (Supplementary Figure 8) as well as the CDR3 length distribution (Supplementary Figure 9) was analyzed for TCR alpha and beta to identify changes induced by subsequent immunizations. Overall, the repertoire was highly diverse and different between the individual donors. Interestingly, within donors the preferential enrichment of certain TCR features was observed after immunization, indicating antigen-specific selection. However, no universal

pattern was observed in all donors, which likely results from the restriction of TCRs to the donor-specific MHC-I alleles. To determine whether those donor-specific preferential TCR sequence features are indeed signatures of *Pf*-specific cells, individual TCRs were selected for cloning and functional analysis. Only clones isolated after immunization were considered for analysis and ranked according to clone size, usage of enriched TCR sequence features (e.g. segment usage), and ICOS expression level. In total, 96 TCRs were selected for analysis (Supplementary Table 2), cloned and stably expressed in J76-CD8 T cells using retroviral transduction. The TCR-transgenic T cell lines were subsequently co-cultured with immortalized autologous B cells loaded with 50 different peptides covering the most frequently detected epitopes of *Pf* (see section 8.5.2). A screening with complete proteins like CSP was not possible due to the lack of cross-presentation in B cells. None of the screened TCRs was reactive to the 50 different peptides (data not shown), which is likely a result of the technical limitation of the screening as the TCRs could be reactive to any other epitope of one of the 5300 proteins of *P. falciparum*. Hence the development of a broader screening approach would be required to identify antigen-specific $CD8^+$ T cells in the repertoire.

4.2.3 Humoral immune responses against CSP

To study the role of $CD4^+$ T follicular helper cell responses during *Pf* RAS immunization, the presence of robust anti-malarial antibody responses was first assessed by measuring blood plasma antibodies against the immunodominant *Pf* antigen CSP. Plasma samples from all volunteers were taken 7 days after the first and second immunization (I, II) and 11 days after the third immunization (III+) and the presence of CSP-specific antibodies was determined by ELISA (Figure 16A). In all donors, no CSP-specific antibodies were detected after the first immunization, indicating that 7 days are not sufficient to develop CSP-specific antibodies in malaria-naive donors. Interestingly, although the levels of antibodies varied between donors, the kinetics were very comparable, with IgM and IgA antibodies peaking after the second immunization and IgG being highest after the third immunization. However, as the plasma samples of the third immunization were taken 11 days post immunization instead of 7 days, it cannot be determined whether the different kinetics of IgM and IgG responses are due to the different sampling times or a consequence of different immunizations. Interestingly, donor M1.002 showed slightly different kinetics as the anti-CSP antibodies showed a delayed emergence with all isotypes peaking only after the third immunization. To gain insights into the regions of CSP that are targeted, antibodies against the central repeat region (NANP5), the C-terminal region (C-CSP) and the N-terminal region (N-CSP) were measured separately (Figure 16B). The central repeat region has been reported to contain most B-cell epitopes and

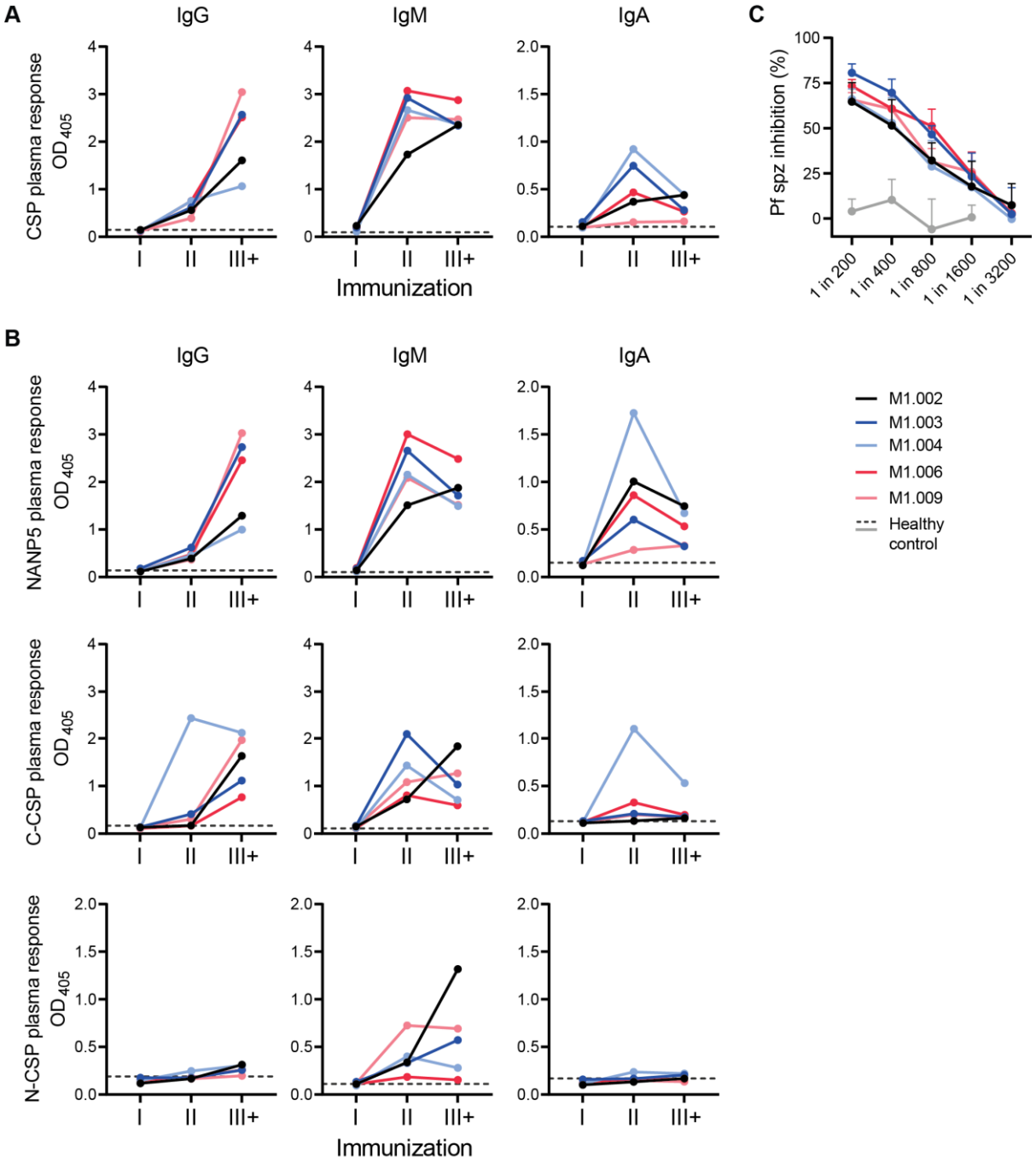

Figure 16: Strong CSP plasma response induced after immunization with *Pf* RAS. (A,B) Levels of IgG, IgM and IgA antibodies against CSP were determined after 1:1600 dilution of the plasma. Plasma samples were collected from immunized volunteers 7 days after the first and second immunization (I, II) and 11 days after the third immunization (III+). Dashed lines indicate the mean of three healthy controls. One representative plot of three independent experiments is shown. Data were generated together with Sandro Hoffmann. (A) Antibodies against full-length CSP. (B) Antibodies against NANP-repeats of CSP (NANP5), the C-terminus (C-CSP) or N-terminus (N-CSP) were measured separately. (C) Inhibition of *Pf* sporozoite traversal through hepatocytes by addition of plasma from immunized donors (III+), measured by *in vitro* traversal assay. The mean of three (dilution 1:200 – 1:1600) or two (dilution 1:3200) independent experiments is depicted. The traversal assay was kindly performed by Dr. Rajagopal Murugan and Dr. Giulia Costa.

dominate the anti-CSP antibody response [121,124,125]. In line with this, the kinetics of the NANP5-specific antibodies strongly mimicked the responses against the full-length CSP. Antibody responses against the C-CSP were also present and followed a similar pattern, however were detected at lower levels. An exception, however, is donor M1.004 that showed higher IgG and IgA antibody titers compared to the other donors. Almost no class-switched N-CSP-specific antibodies could be detected. In a next step, the function of the plasma antibodies was assessed by determining their ability to inhibit *Pf* sporozoite traversal through hepatocytes in an *in vitro* hepatocyte traversal assay [124]. The addition of plasma, isolated after the third immunization, to *Pf* sporozoites exhibited a strong, dose-dependent blockage of hepatocyte traversal (Figure 16C). Notably, all donors showed a comparable traversal inhibition, demonstrating that they all mounted antibodies that could potentially be protective by preventing hepatocyte infection and therefore arrest the parasite development.

In summary, the detailed analysis of the CSP-specific antibody response revealed that immunization with *Pf* RAS induced a high anti-CSP response in all donors. While the majority of antibodies is directed against the central repeat region, antibodies could also be detected against C-CSP and N-CSP, which are more relevant for T cell responses as they contain multiple T cell epitopes. The presence of plasma antibodies that can inhibit hepatocyte traversal highlights the relevance of antibody responses in protection against *Pf* infection and prompted us to characterize T_{FH} cell responses to better understand the emergence of *Pf*-specific antibodies upon *Pf* RAS immunization.

4.2.4 T follicular helper cell responses in *Pf* RAS immunization

Studies of T_{FH} cells in humans are often limited to their circulating counterparts (cT_{FH} cells) due to the limited accessibility of secondary lymphoid organs. Recent studies on cT_{FH} cell not only established a phenotypically and functional relationship between T_{FH} and cT_{FH} cells but also identified the activated cT_{FH} cells as the antigen-specific cT_{FH} compartment increasing upon various immunizations and being superior in providing help to B cells. To identify whether a similar increase of activated cT_{FH} cells occurs upon *Pf* RAS immunization, PBMCs isolated before and 7 days after each immunization were analyzed by flow cytometry. Indeed, while the overall frequency of cT_{FH} cells ($CD4^+$ $CD45RA^-$ $CXCR5^+$) only slightly increased upon immunization from 6.1% to 8-9%, the fraction of activated ($PD\text{-}1^+$ $ICOS^+$) and highly activated ($PD\text{-}1^{++}$ $ICOS^+$) cells among them increased strongly by 2-3 fold and peaked after the second and third immunization (Figure 17A-D). Notably, the analyzed numbers of highly activated cells were rather low, therefore the calculated frequencies have to be interpreted with caution

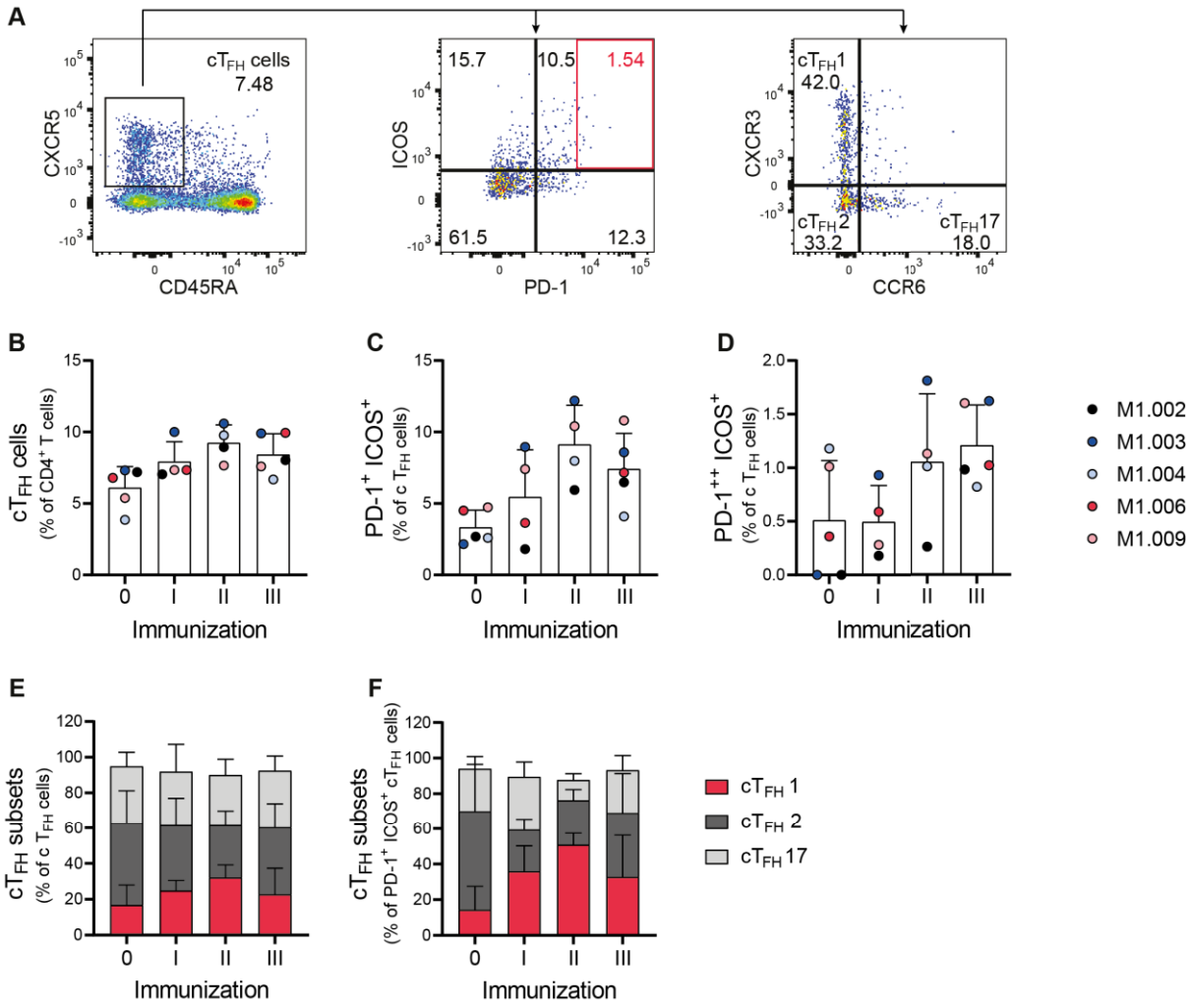

Figure 17: Successive *Pf* RAS immunizations enrich for activated cT_{FH} cells with a $cT_{FH}1$ phenotype. (A) Representative gating strategy for the flow cytometric analysis of PBMC samples collected during the malaria immunization trial. PBMCs were pre-gated on single, live $CD4^+$ T cells (for pre-gating see Supplementary Figure 5) and cT_{FH} cells were defined as $CXCR5^+$ $CD45RA^-$ $CD4^+$ T cells. The cT_{FH} cells were further characterized by their activation status (PD-1 and ICOS expression) as well as the chemokine receptor expression (CCR6 and CXCR3). Highly activated cT_{FH} cells ($CXCR5^+$ $CD45RA^-$ $PD\text{-}1^{++}$ $ICOS^+$, red gate) were single-cell sorted into 384-well plates for subsequent TCR repertoire analysis. Plots are shown for donor M1.009 at III. (B - D) Quantification of the frequency of cT_{FH} cells (B), activated cT_{FH} cells (C) and highly activated cT_{FH} cells in five volunteers before the first (0) and after each subsequent *Pf* RAS immunization (I - III). Bar graphs show the mean and standard deviation, dots mark single donors. (E, F) Quantification of $cT_{FH}1$ cells ($CXCR3^+$ $CCR6^-$), $cT_{FH}2$ cells ($CXCR3^-$ $CCR6^-$) and $cT_{FH}17$ cells ($CXCR3^-$ $CCR6^+$) among all cT_{FH} cells (E) or activated cT_{FH} cells (F). The mean of all donors as well as the standard deviation are shown.
(B-F) Samples M1.004 (I) and M1.006 (II) were excluded from analysis due to low sample quality.

(Figure 17D). cT_{FH} cells can be further subdivided into different subsets dependent on the expression of the chemokine receptors CXCR3 and CCR6 (Figure 17A). While the $cT_{FH}1$ subset ($CXCR3^+$ $CCR6^-$) is inferior in providing help to B cell compared to the $cT_{FH}2$ ($CXCR3^-$ $CCR6^-$) and $cT_{FH}17$ ($CXCR3^-$ $CCR6^+$) subset, recent studies showed an increased activation of this inefficient helpers in natural malaria infection [109]. In agreement with these data, *Pf* RAS immunization resulted in an increase of $cT_{FH}1$ cells among cT_{FH} cells from on average 16.8% to 32.1% (Figure 17E, Supplementary Figure 10A). This effect was even more pronounced among the activated cT_{FH} cells, where the mean $cT_{FH}1$ frequencies increased from 14.3% to 50.9% (Figure 17F, Supplementary Figure 10B). Interestingly, also for $CD4^+$ T_{EM} cells ($CD45RA^-$ $CCR7^-$) and $CD4^+$ T_{CM} cells ($CD45RA^-$ $CCR7^+$) an increase of activated cells with a T_H1-like phenotype was observed (Supplementary Figure 11). Together, the data show that *Pf* RAS immunization induced an activation of cT_{FH} cells as well as $CD4^+$ T_{EM} and T_{CM} cells with a T_H1-like phenotype. The strongest activation was seen after the second immunization, despite some donor-specific variations, which might be explained by the short timespan between the first and second immunization (7 days) compared to the second and third immunization (21 days).

Clonally expanded cells emerge in the dynamic, polyclonal cT_{FH} cell repertoire upon *Pf* RAS immunization

To characterize the repertoire of the activated and likely antigen-specific cT_{FH} cells, highly activated cT_{FH} cells ($PD\text{-}1^{++}$ $ICOS^+$) were single-cell index sorted and the TCRs were amplified and sequenced. After analysis with sciReptor, a total of 3013 paired TCR sequences were gained from samples of all donors and all sampling times (0, I, II and III) (Supplementary Table 3). Similar to $CD8^+$ T_{EM} cells, clones were defined by identical TCR beta CDR3 sequence. Furthermore, TCR beta sequences without a matching alpha chain were also included into the analysis. In contrast to the $CD8^+$ T_{EM} cell repertoire, the overall degree of clonal expansion was very low before immunization (0-14%) and increased strongly upon immunization, with the highest clonal expansion detected after the second and third immunization (10-52%) (Figure 18A). To account for variations in the number of sequences among samples, the clonal expansion was also calculated after performing random subsampling of the sequences (Figure 18B, Supplementary Figure 12A). After subsampling, a strong increase of clonal expansion was still visible after the second immunization but only to a minor extent after the third. The diversity of the clonally expanded compartment was overall high, with a moderate increase after the third immunization (Figure 18C). These findings together indicate that *Pf*-specific clones were activated during the primary immunization and further expanded during the

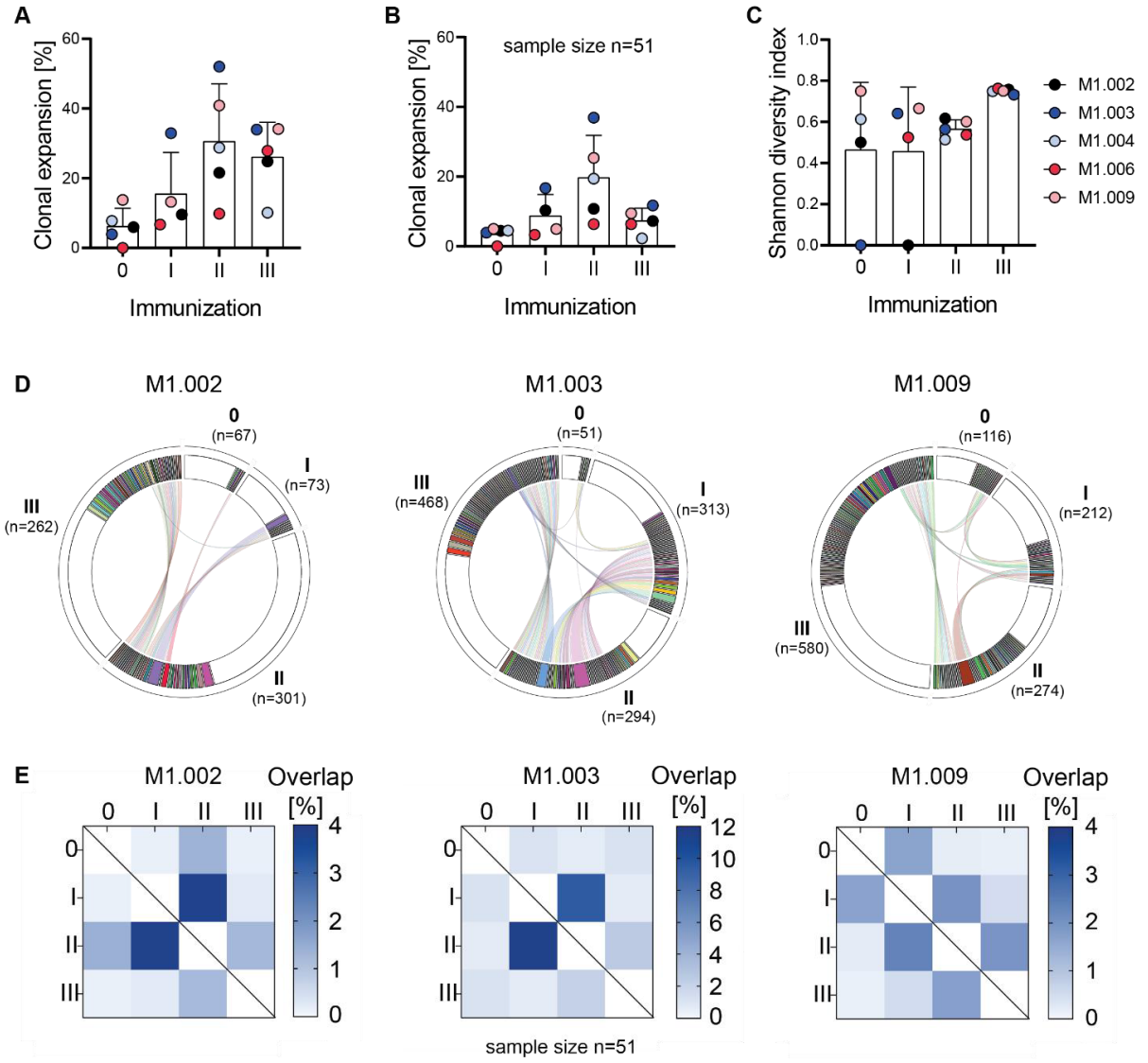

Figure 18: Increased clonal expansion and clonal overlap in activated cT_{FH} cells after *Pf* RAS immunizations. TCR repertoire analysis of single-sorted PD-1^{++} $ICOS^{+}$ cT_{FH} cells after TCR gene amplification and sequencing. Clones were defined by identical beta CDR3 amino acid sequence. (A) Percent of clonally expanded sequences. (B) Sequences were 50 times randomly subsampled to the lowest sequence number (n=51) and the mean clonal expansion was calculated. (C) Shannon diversity of clonally expanded cells normalized to the total sequence number of each sample. (D) Circos plots of three representative donors showing the clonal overlap of TCRs over the course of the immunization trial. Expanded clones are marked in different colors and overlapping clones are linked by lines. Non-expanded TCRs are shown in white. Numbers of sequences available per samples are given. (E) Percent clonal overlap of three representative donors shown in heat maps. The mean of 50 random subsamples (n=51) is shown.
(A-C) No TCR repertoire data were available for donor M1.004 after the first immunization (I).

second immunization. The lower clonal expansion and higher degree of diversity observed after the third immunization suggests that rather new, smaller clones were recruited into this response, probably due to the large timespan between the immunizations. These assumptions are in line with data revealed from kinetics of single clones over the course of immunization, which showed a strong overlap between the first and second immunization, with strongly expanded clones in the second immunization being already recruited after the first immunization (Figure 18D, Supplementary Figure 12B). In contrast, the majority of larger clones detected after the third immunization were newly recruited and hence comparably small. While clones overlapping between the second and third immunization were also frequently detected, the higher number of sequence available for later time points might overestimate this overlap. Interestingly, the size of expanded clones was in general rather smaller compared to the $CD8^+$ T_{EM} compartment and no clones overlapped between all samples. In general, the highest overlap was always observed between the time-wise closest repertoires. To determine whether the overlap between repertoires was solely dependent on time or was also influenced by the subsequent immunizations, the overlap of repertoires was calculate after random subsampling. This revealed that the overlap of repertoires was rather low with a maximum of 1%-12% dependent on the donor (Figure 18E, Supplementary Figure 12C). Interestingly, after subsampling a stronger overlap was evident between the cT_{FH} repertoires analyzed after the first and second immunization compared to the other time points. Overall this highlights that the *Pf* RAS immunization led to the emergence of clonally expanded cells that dominated the otherwise very polyclonal repertoire of the highly activated cT_{FH} cells. The overall low degree of overlap between the different samples further highlights the dynamic exchange of T cells in this compartment in contrast to the stable maintenance observed in the $CD8^+$ T_{EM} cells.

Identification of CSP-reactive cT_{FH} cells

To identify antigen-specific cells, the TCR repertoire was analyzed for features that might be associated with antigen-driven selection. As for $CD8^+$ T_{EM} cells, the V segment usage (Supplementary Figure 13), as well as the V and J segment pairing (Supplementary Figure 14) and CDR3 length (Supplementary Figure 15) were analyzed for the alpha and beta chain over the course of immunizations. In line with the data obtained from $CD8^+$ T_{EM} cells, the TCR repertoire of cT_{FH} cells was highly diverse within and between donors and only donor-specific enrichments of TCR sequence features were identified, without the presence of features enriched in all donors. To determine whether these features are associated with antigen-specificity, 192 TCRs were selected for subsequent cloning and analysis. This selection was

mainly based on clone size and the presence of enriched features. For some TCRs very similar counterparts were found in the repertoire and they were hence selected due to sequence similarity, although no extensive analysis of similarity patterns was performed. Notably, the phenotype and the cT_{FH} subset was not considered during the selection process. The selected TCRs were cloned and retrovirally expressed in J76-CD4 T cells, resulting in the successful generation of 183 TCR-transgenic T cell lines. Not all T cells within a TCR-transgenic T cell line expressed the TCR on their surface, and the frequency of TCR^+ T cells varied between 1 – 90% (Figure 10C). All T cell lines containing more that 5% of TCR^+ T cells were used for subsequent stimulation assays (175). To identify *Pf*-specific cells, TCR-transgenic T cell lines from donor M1.003 and M1.006 were screened for reactivity against CSP or the unrelated Ovalbumin (OVA) protein (negative control) by co-culture with antigen-presenting autologous B cells for 24 h. While no CSP-specific TCR was detected for donor M1.003 (0/54), 10 TCRs from donor M1.006 (10/37) were activated and secreted IL-2 above the detection limit of the IL-2 ELISA (7.8 pg/ml) in at least one of two subsequent stimulation experiments (Figure 19A). To verify that these are indeed CSP-specific TCRs and to identify the region within CSP which they recognize, those TCRs were stimulated with C-CSP, NANP5 or N-CSP. All TCRs except for one induced a strong T cell activation after stimulation with C-CSP (Figure 19B). No TCR was reactive to NANP5 and N-CSP, and one TCR did not react to any part of CSP and was therefore false positive in the previous stimulation. Interestingly, the IL-2 production in response to C-CSP was substantially stronger compared to full-length CSP and some TCRs even failed to produce IL-2 concentrations above the detection limit in one of the two repeated CSP stimulations, indicating that the stimulation with CSP induces T cell activation that is at or even below the detection limit of the IL-2 ELISA while the stimulation with the smaller poly-peptide C-CSP is more sensitive. Therefore, TCR-transgenic T cells of the remaining three donors were screened with C-CSP in addition to CSP and OVA. While no reactive TCR could be identified for donor M1.002 (0/26), in both M1.004 and M1.009 C-CSP-reactive TCR could be identified at frequencies of 25% (6/24) and 11% (5/46), respectively. Interestingly, in these stimulation experiments almost none of the C-CSP-reactive TCRs was able to induce IL-2 secretion above the threshold when stimulated with full-length CSP. In summary, the stimulation experiments showed that TCRs selected according to clone size and TCR sequence features contained antigen-specific cells in 3 of the 5 donors, and were all responding to the C-terminal region of CSP, known to contain the majority of T cell epitopes within the CSP protein [115,126]. Due to the limited sensitivity in stimulations using whole protein, a more detailed screening would be required to evaluate whether TCRs reactive to other CSP regions are also present. Importantly, the frequency of TCR^+ T cell within a certain TCR-transgenic T cell line also seemed to influence the sensitivity of the assay as cell lines containing fewer TCR^+ T cells also tended to secrete less IL-2 in response to C-CSP

(Supplementary Figure 16). The overall broad range of IL-2 concentrations detected upon stimulation of different TCRs may also reflect differences in TCR affinity.

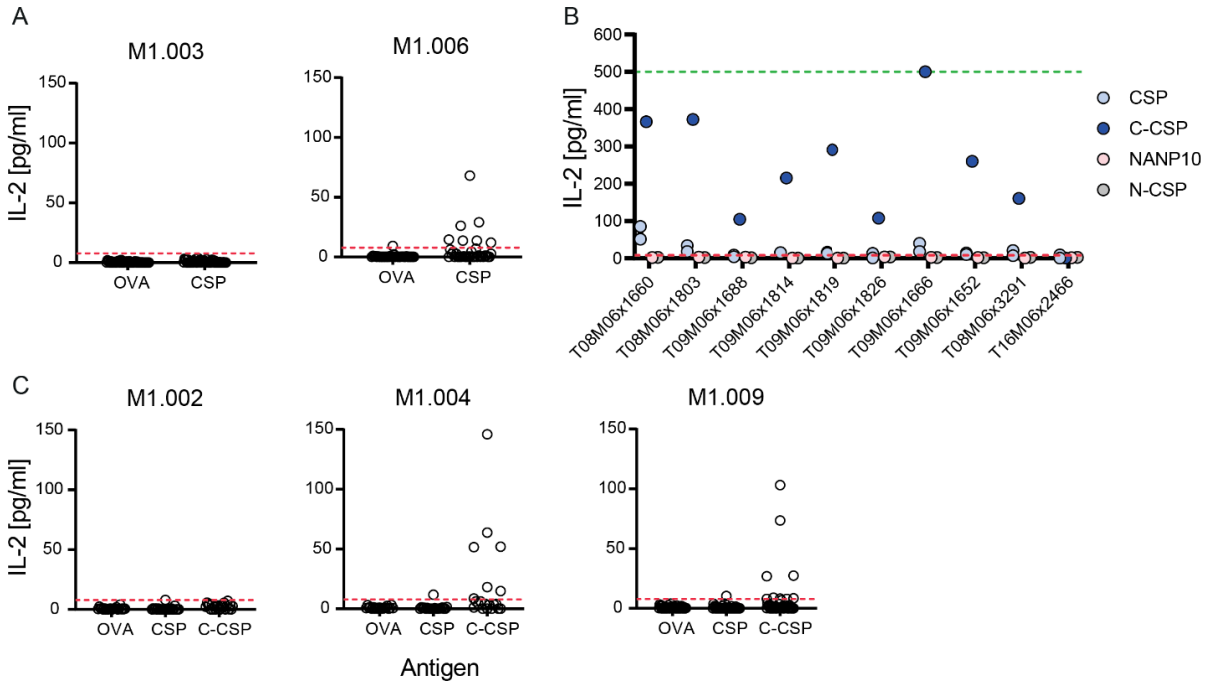

Figure 19: Identification of C-CSP-specific TCRs from three *Pf* RAS-immunized donors. TCR-transgene Jurkat76 T cell lines were generated by retroviral transduction and screened for their reactivity to different antigens by co-culture with autologous B cells. The activation of T cells was quantified by measuring the IL-2 concentration in the cell culture supernatant by ELISA. Dashed red and green lines indicate the lower and upper detection limit of the assay. Each dot represents an individual TCR-transgenic T cell line. (A) Stimulation of TCR-transgenic T cells with an unrelated antigen (OVA) or full-length CSP. The mean of two independent experiments is shown. (B) Ten potentially CSP-reactive T cell lines from donor M1.006 were screened for reactivity to full-length CSP and different CSP domains. Preliminary data of a single screening are shown. (C) Stimulation of TCR-transgenic T cells with an unrelated antigen (OVA), full-length CSP or the C-terminal region of CSP (C-CSP). The mean of two independent experiments is shown.
Data were generated jointly with Julia Puchan (A,B) and Rebecca Hundsdorfer (C).

C-CSP-specific T cell clones preferentially belong to the $cT_{FH}1$ subsets

After identifying 20 C-CSP-reactive TCRs, it was analyzed whether a certain cT_{FH} cell phenotype was associated with antigenicity, i.e. the $cT_{FH}1$ phenotype predominantly induced upon *Pf* RAS immunization (Figure 17E,F). Indeed, C-CSP-specific cT_{FH} cells were enriched for $cT_{FH}1$ cells compared to the entire repertoire (Figure 20), indicating that the emergence of activated $cT_{FH}1$ cells upon immunization is mediated by antigen-driven activation.

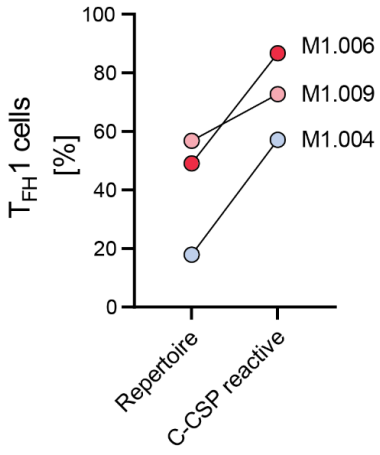

Figure 20: C-CSP-reactive T cell clones are preferentially of $T_{FH}1$ - type. The percentage of $T_{FH}1$ cells is compared between all cells sorted after immunization (complete repertoire) and the C-CSP-reactive clones using the index data recorded during sorting.

C-CSP-reactive cT_{FH} cell clones vary strongly in clone size

By making advantage of the extensive repertoire information, we wanted to analyze whether the C-CSP-specific T cell clones belong to expanded clones overlapping between immunizations, newly recruited, smaller clones or even unexpanded single cells. Surprisingly, although clonal expansion is often associated with antigen-specificity, the C-CSP-reactive TCRs showed a broad range of clone sizes, ranging from the second largest clones within an individual to a non-expanded single cell (Figure 21). C-CSP-specific cells were exclusively detected at the second and third immunization and the majority was not shared between multiple immunizations. While for donor M1.004 C-CSP-reactive T cells were detected mainly during the second immunization, C-CSP-reactive T cells of donor M1.006 and M1.009 originated predominantly from cells of the third immunization. Interestingly, so far none of the expanded T cell clones, overlapping between the first and second immunization, were identified to be C- CSP-reactive. Overall this highlights that clonal expansion and presence after multiple immunizations is not a direct measure for antigen-specificity.

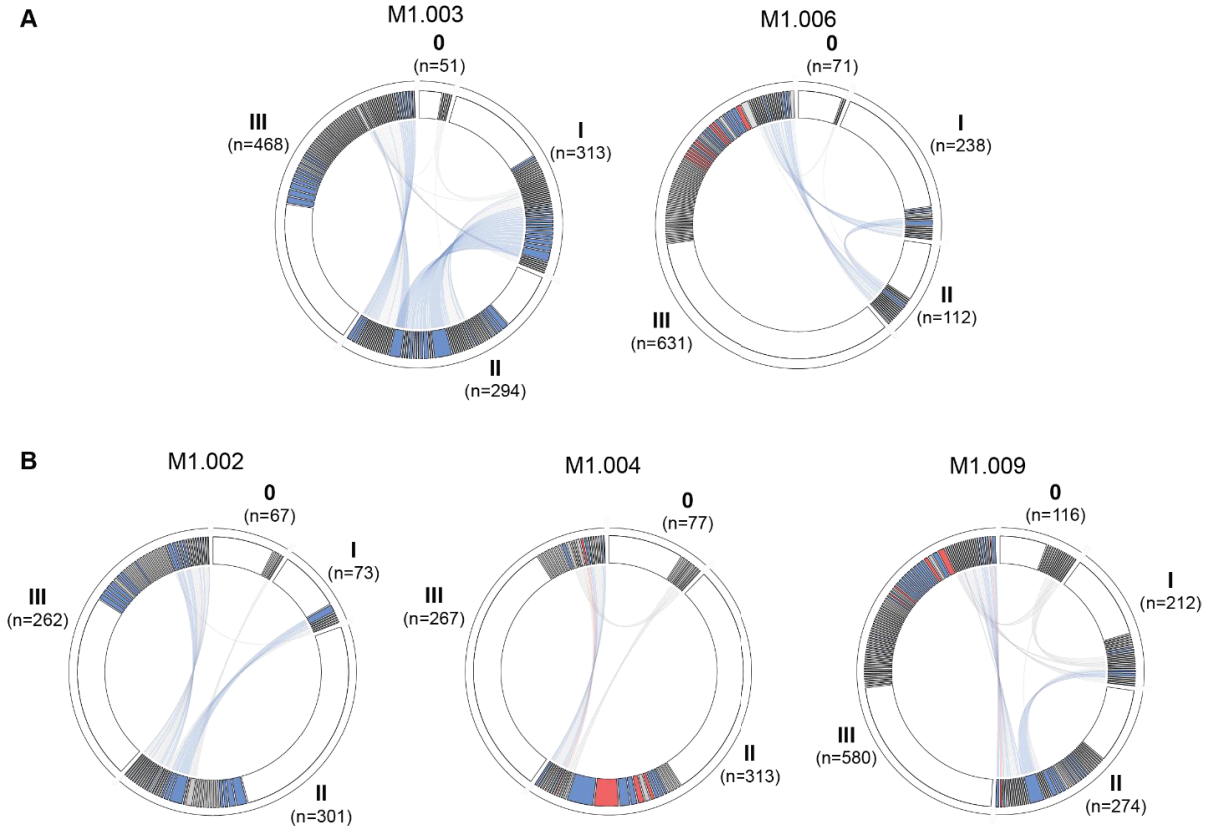

Figure 21: C-CSP-reactive TCRs are diverse in clone size. Circos plots depicting the clonal size and overlap between immunizations are shown for each donor. Each bar represents an individual T cell clone and overlapping clones are linked by lines. Non-expanded clones are shown in white. Cloned and screened TCRs are highlighted in colors. (A) Blue: non-reactive to CSP; red: reactive to CSP and C-CSP. (B) Blue: non-reactive to CSP and C-CSP, red: reactive to C-CSP. n = total number of sequences per sample.

C-CSP-reactive clones are highly diverse despite some signs of convergent selection

Next we wanted to evaluate how diverse the TCR sequence features of C-CSP-specific T cells are, given that they all bind to the same 124 amino acid long region of CSP. The sequences of the C-CSP-reactive TCRs were rather diverse within and between donors, reflecting the presence of multiple epitopes within C-CSP as well as the large MHC-II diversity (Table 21). One exception is the TCR beta segment TRBV20-1, which was used by one third of all C-CSP-reactive TCRs. Interestingly, some TCRs showed a strong sequence similarity that might reflect the recognition of identical epitopes. This was most prominent in a cluster of 4 different T cells clones, which all used the TRBV20 segment paired with TRAV24-1 and TRAJ48, and were present only in donor M1.006 after the third immunization. While the TCR alpha CDR3 sequences were almost identical among all clones, the beta CDR3 sequences showed more

Table 21: Sequence data and selection criteria of C-CSP-specific TCRs. For each donor, all TCRs with a clone size of 3 or larger were selected for cloning (green). Furthermore TCRs using segments which were more frequently used after immunization were selected (green). Preferential TRBV-TRAV pairing and TRAV-TRAJ pairing as reason for selection is highlighted with red squares. Green coloring of CDR3 sequences indicates the presence of closely related TCRs with similar CDR3 sequence in the post-immunization dataset.

			Beta chain				Alpha chain			
TCR	Donor	Clone size	V	J	CDR3	CDR3 length	V	J	CDR3	CDR3 length
T16M04x1709	M1.004	21	10-1	2-3	ASSELGTSGRPDTQY	15	25-1	48	AGLFGNEKLT	10
T08M04x4234	M1.004	2	20-1	2-1	SAKTSGRSVNEQF	13	13-2	49	AENAGNQFY	9
T16M04x1619	M1.004	2	20-1	2-7	SARDSGRSSYEQY	13	16-1	31	ALRGARLM	8
T16M04x1805	M1.004	1	20-1	1-2	SAPQGQKYGYT	11	26-1	52	IVKNGGTSYGKLT	13
T16M04x1732	M1.004	3	6-2	2-7	ASRWTGQTYEQY	12	21-1	8	AVGPRGTGFQKLV	13
T16M04x1590	M1.004	5	7-3	2-1	ASSRGGTGGNEQF	13	41-1	48	AVFNFGNEKLT	11
T09M06x1826	M1.006	2	20-1	2-7	SARDGGRSSYEQY	13	16-1	23	ALRGQGGKLI	10
T09M06x1819	M1.006	3	20-1	1-6	SAPGQRGNSPLH	12	24-1	48	AFNNFGNEKLT	11
T08M06x1803	M1.006	4	20-1	1-2	SAPRRRANYGYT	12	24-1	48	AWGNFGNEKLT	11
T09M06x1666	M1.006	3	20-1	1-5	SASPPRSNQPQH	12	24-1	48	AFTNFGNEKLT	11
T09M06x1652	M1.006	3	20-1	1-2	SATPRRVNYGYT	12	24-1	48	AFSNFGNEKLT	11
T09M06x1814	M1.006	3	4-2	1-3	ASSPTTGTTGNTIY	14	22-1	30	AVYGRDDKII	10
T08M06x1660	M1.006	3	4-3	1-6	ASSQAGTYNSPLH	13	29DV5	49	AASVPRNTGNQFY	13
T09M06x1688	M1.006	8	5-1	1-2	ASSPDGGTYGYT	12	13-2	43	AENRKGNNNDMR	12
T08M06x3291	M1.006	4	6-1	2-4	ASTLGQTYKNIQY	13	13-2	32	AENMGGYGGATNKLI	15
T09M09x2529	M1.009	4	24-1	1-1	ATSDLRRQVGAF	12	35-1	58	AGQEETSGSRLT	12
T08M09x2192	M1.009	13	5-1	2-3	ASSPGGRSDTQY	12	29DV5	48	AARTNFGNEKLT	12
T15M09x2180	M1.009	6	7-8	1-6	ASSPHRAGDSPLH	13	13-2	28	AENRRAGSYQLT	12
T08M09x2114	M1.009	3	7-9	2-3	ASSPGGRADTQY	12	25-1	45	AGNRDSGGGADGLT	14
T08M09x2191	M1.009	7	9-1	2-7	ASSVAGEDYEQY	12	8-1	5	AVKGTGRRALT	11

variability which can be attributed to the usage of different TRBJ segments (Figure 22). However key residues that might be involved in the peptide-MHC interaction were conserved in all clones. Moreover, the repertoire of the donor M1.006 contained 4 more clones that belong to this cluster, but have not yet been tested for reactivity to C-CSP. Besides this similarity of TCRs within a donor, the activation of TCRs with similar TCR sequence was also observed between different donors, as shown for a cluster of TCRs using TRBV20-1, TRBJ2-7 and TRAV16 segments (Table 22). While the beta CDR3 sequence was almost identical among the individual TCRs, the alpha CDR3 was rather diverse due to the use of different J segments. Whether those TCRs all react to C-CSP needs to be confirmed, as only two clones have been screened so far. Taken together, the majority of C-CSP-reactive TCRs shows a diverse segment usage indicative of the recognition of different peptides presented by different MHC-II alleles, whereas some highly similar TCRs within but also between different donors likely recognize the same epitope and suggest convergent recruitment of T cells upon *Pf* RAS immunization.

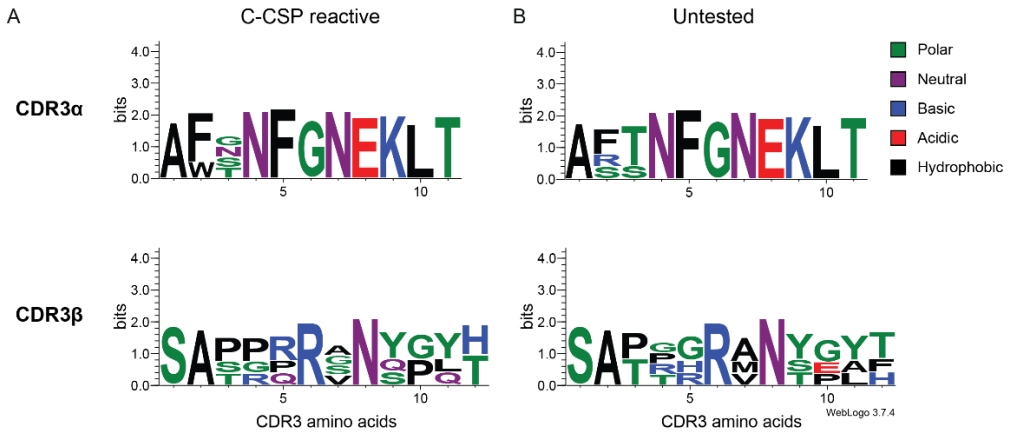

Figure 22: Strong amino acid sequence similarity in a group of C-CSP-reactive TCRs. WebLogo plots[179] comparing the CDR3 amino acid usage of TCRs encoded by TRBV20-1, TRAV24-1 and TRAJ48-1. The amino acids found at each position of the CDR3 are shown, with the symbol size representing the frequency at which each amino acid is found at this position. The overall height represents the sequence conservation per position. The chemical properties of the amino acids are encoded by colors. Analysis of four C-CSP-reactive TCRs (A) and four TCRs of unknown specificity (B) found after the last immunization (III) in the repertoire of donor M1.006.

Table 22: Highly similar T cell clones detected in two donors include C-CSP-specific TCRs.

			Beta chain			Alpha chain			
Donor	**Immunization**	**Clone size**	**V**	**J**	**CDR3**	**V**	**J**	**CDR3**	**C-CSP-reactive**
M1.004	III	1	20-1	2-7	SARDSGRSSYEQY	16-1	16	ALRGGQKLL	?
M1.006	III	2	20-1	2-7	SARDGGRSSYEQY	16-1	23	ALRGQGGKLI	Yes
M1.004	II,III	2	20-1	2-7	SARDSGRSSYEQY	16-1	31	ALRGARLM	Yes
M1.006	III	1	20-1	2-7	SARDGGRSSYEQY	16-1	31	ALRGSARLM	?
M1.004	II	1	20-1	2-7	SARDGGRSSYEQY	16-1	58	ALRVGGSRLT	?

4.2.5 Direct identification of *Pf*-specific T cells by *in vitro* stimulation

The characterization of unselected T cell repertoires during immunization can provide valuable insights into the kinetics of antigen-specific T cells and improves the understanding of the emergence and maintenance of reactive T cell clones. The identification of antigen-specific T cells from unselected repertoires, however, requires in-depth repertoire analysis and the determination of features predictive for antigen-specificity. The identification of TCR sequence features that are associated with binding to different *Pf*-antigens could strongly improve this selection process and increase the likelihood to identify antigen-specific cells in the large and diverse repertoire. For a fast detection of antigen-specific cells, PBMCs obtained after the third *Pf* RAS immunization were stimulated with either complete sporozoite lysate (*Pf* SPZ) or the CSP protein and incubated for 72 h until proliferation of activated T cells was detectable. The proliferation was tracked by the addition of a proliferation dye (cell trace violet, CTV), which is diluted upon each cell division. To determine background proliferation, PBMCs were also stimulated with PBS and lysate prepared from the salivary gland of uninfected mosquitos, serving as negative controls for CSP and *Pf* SPZ lysate (prepared from the salivary gland of *Pf* SPZ infected mosquitos), respectively. The *Pf* SPZ lysate and matching negative controls were kindly provided by Dr. Giulia Costa and Dr. Elena Levashina, MPI IB, Berlin. Proliferating T cells ($CD3^+$ CTV^{low}) were identified and quantified by flow cytometric analysis using a broad lymphocyte gate to account for phenotypic changes induced upon activation (Figure 23A). While no proliferation above the background of the negative control was observed in PBMCs obtained from three healthy controls, a clear increase in proliferation in the CSP and *Pf* SPZ-treated PBMCs was detectable in all immunized donors except for donor M1.003 (Figure 23B). The frequency of CSP and *Pf* SPZ-specific cells was around 0.1-0.4% of all T cells, which is in agreement with other *Pf* RAS immunization studies [91,180]. The fold change of frequencies of proliferating T cells in response to CSP and *Pf* SPZ compared to the respective negative control was around 1 for healthy controls and M1.003 and around 2 - 4 for the other immunized donors (Figure 23C). Notably, the PBS negative control of donor M1.006 showed an unexpectedly high degree of proliferation, which is likely caused by technical issues. The complete absence of a CSP- and *Pf* SPZ-specific T cell response in donor M1.003 requires further evaluation to determine whether it results from technical issues or is due to a general lack of *Pf*-specific T cell responses in this donor. Overall, a robust *Pf*-specific T cell response was detected in 4 of the 5 immunized donors, with no significant difference in strength between the CSP and *Pf* SPZ response.

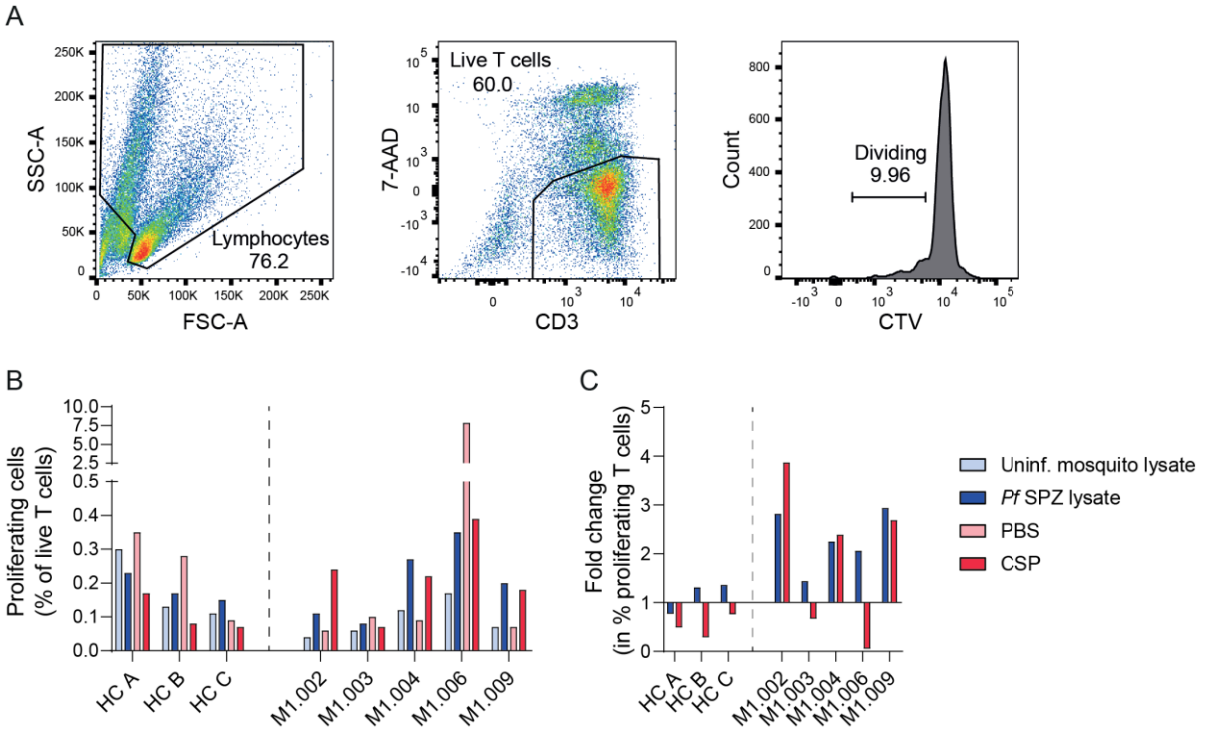

Figure 23: *Pf*-specific T cells detected in the blood of donors after the third *Pf* RAS immunization. PBMCs collected 7 days after the third immunization (III) were stained with a proliferation dye (CTV) and stimulated with CSP or *Pf* SPZ-lysate (collected from the salivary glands of infected mosquitos). As negative controls, PBS or lysate from salivary glands of uninfected mosquitos were used, respectively. (A) Gating strategy applied to identify proliferating, live T cells ($CCR7^{low}$ $7\text{-}AAD^{-}$ $CD3^{+}$) after stimulation of PBMCs with SEB (M1.003). (B) Quantification of proliferating T cells in immunized volunteers (M1.002-M1.009) compared to three healthy controls (HC). (C) Fold change of the frequency of proliferating T cells. Experiments were performed together with Julia Puchan.

To characterize the TCR repertoire of the *Pf*-specific T cells, live, proliferating T cells ($7\text{-}AAD^{-}$ $CD3^{+}$ CTV^{low}) were single-cell index sorted and TCRs were amplified, sequenced and analyzed. Due to the low frequency of antigen-specific cells, as well as low PCR amplification efficiency, likely caused by the generally lower viability of the cells, only 322 TCR beta sequences and 215 paired TCR alpha and beta sequences were obtained (Supplementary Table 5). Before analysis of the T cell repertoire, $CD4^{+}$ and $CD8^{+}$ T cells were distinguished using the recorded index data (Figure 24A). Furthermore cT_{FH} cells among the $CD4^{+}$ T cells were identified as $CD45RA^{-}$ $CXCR5^{+}$ cells (Figure 24B). Due to the low number of $CD8^{+}$ T cell sequences (37 paired sequences), only $CD4^{+}$ T cells were analyzed and the sequences of all donors were pooled. The analysis of the TCR alpha and beta V segment usage revealed a strong diversity in the TCR repertoire, despite the restriction to CSP and SPZ-specific cells (Figure 24C,D). Remarkably, the T cell response against CSP was not more focused than the T cell response against whole sporozoites, with both covering most of the functional V segments. Some V segments were preferentially used in the proliferating cells, i.e. members of the TRAV12 and TRAV13 family as well as TRBV5-1 and TRBV20-1, and whether these segments are crucial for binding to certain *Pf*-epitopes needs to be determined. The clonal

expansion in the antigen-specific T cells was relatively low (5.9% for $CD4^+$ T cells, 5.5% for $CD8^+$ T cells), which probably results from the overall low number of sequences. Interestingly, 20% (6/29) of the TCR sequences found in cells with a T_{FH} phenotype overlapped with the cT_{FH} repertoire data, in contrast to 0.9% of the non-T_{FH} cells (1/115), with overlapping cells being defined by identical TCR beta and TCR alpha CDR3 sequence. This indicates that despite 72 h stimulation the T_{FH} phenotype was still preserved. For $CD8^+$ T cells, 13.5% (5/37) of the stimulated cells overlapped with the $CD8^+$ T_{EM} repertoire, although 4 of these cells did not share a T_{EM} phenotype. Given the plasticity of the $CD8^+$ T cell compartment, it is not possible to infer whether those cells had a T_{EM} phenotype, which was changed during the 72 h

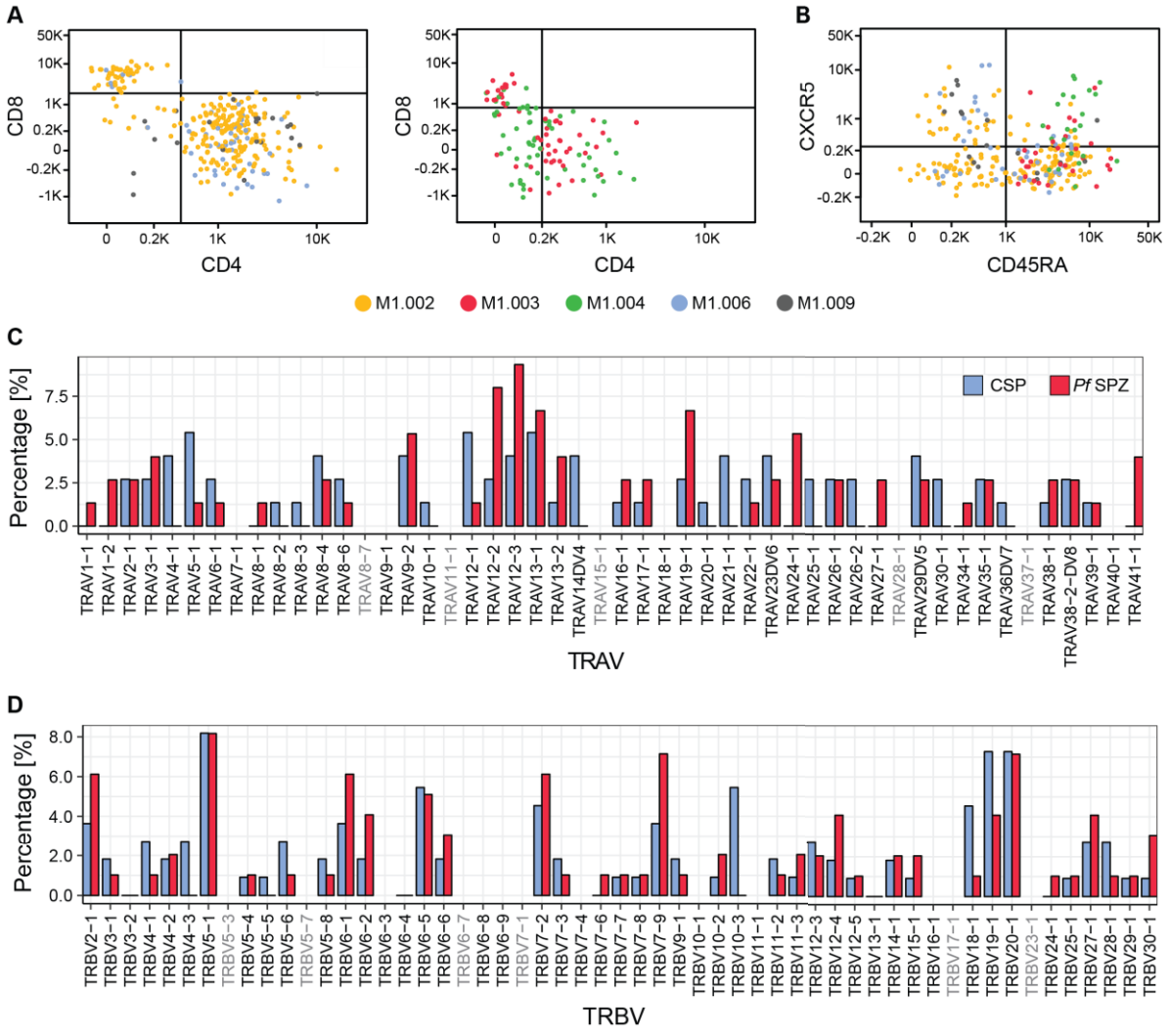

Figure 24: High diversity of TCRs reactive to *Pf* SPZ and CSP. T cells proliferating in response to *Pf* SPZ or CSP were single-cell index sorted and the TCR genes were amplified and sequenced. Discrimination of $CD4^+$ and $CD8^+$ T cells (A) as well as T_{FH} ($CD4^+$ $CD45RA^-$ $CXCR5^+$) cells (B) using index data. Segment usage of TRAV genes (C) and TRBV genes (D) in $CD4^+$ T cells stimulated with CSP or *Pf* SPZ lysate. Sequences of all donors were pooled.

stimulation, or whether they were phenotypically different already before stimulation. Overall, the TCR repertoire of stimulated T cells could serve as a reference dataset to improve the identification of *Pf*-specific cells in the unselected repertoire. Due to the low number of TCR sequences as well as high diversity, general TCR features involved in binding could not be defined, while the identification of *Pf*-specific cells based on sequence similarity may be a more promising approach. Importantly, the background proliferation in the negative controls implies that not all TCRs in the dataset are indeed *Pf*-specific and highlights the importance of functional screening to validate the reactivity.

5 Discussion

5.1 High-throughput, single-cell TCR repertoire analysis

For the in-depth characterization of human T cell responses, a high-throughput platform was developed which allows the molecular and functional analysis of T cell repertoires at single-cell level. The basis of this approach forms a single-cell amplification and sequencing strategy that is compatible with direct cloning and functional assessment of TCRs and thereby overcomes limitations of other sequencing strategies, which do not provide paired TCR alpha and beta sequences that can be accessed individually for cloning [132,133,138,143–145]. The low throughput, which is a major drawback of single-cell analysis, is overcome here by the barcoding of amplicons, which allows pooling of sequences for next-generation sequencing and thereby increases the number of TCRs that can be analyzed to several thousand. The modification of the existing analysis pipeline sciReptor enabled the fast, efficient and consistent analysis of TCR sequences and further linked the genetic information to the cellular phenotype recorded during index-sorting [146]. Although it was not exploited here, the reverse transcription of the entire mRNA during the TCR gene amplification procedure would allow an even deeper analysis of cellular phenotypes by measuring the expression of intracellular proteins, as it has been recently shown for cytokines [141].

The amplification of full-length TCR genes enables the highly efficient and fast cloning of large numbers of TCRs in parallel as it bypasses the need of plasmid libraries encoding missing parts of V segments, which is required for strategies where only the CDR3 sequence is amplified [165,181]. This is especially important as the cloning is one of the most time-consuming and rate-limiting steps. For expression and reactivity screenings of cloned TCRs, the TCR^{neg} T cell line Jurkat76 was used and high T cell activation was guaranteed by stable insertion of co-receptors required for proper T cell activation [182]. The absence of endogenous TCR expression in Jurkat76 cells allows the characterization of TCR specificity without background signaling [165,183]. By using autologous, immortalized B cells for antigen-presentation, we bypassed the need for cell lines engineered to express a variety of different MHC alleles and thereby could screen TCRs restricted to any of the multiple MHC alleles present in each donor [181,183,184]. The fact that B cells immortalized with EBV can also present EBV-derived peptides was negligible as in each stimulation experiment a matching negative control was included. While multiple studies introduced reporter cassettes into the TCR-transgenic T cells to efficiently identify antigen-specific T cells after activation, we found a rather low TCR-expression in Jurkat76-Nur77-GFP reporter cells (kindly provided by Dr. Paul Thomas, St.

Jude Children's Research Hospital, Memphis, USA) after retroviral transduction and therefore used the parental Jurkat76 cells without reporter cassette and detected antigen-specific cells via IL-2 ELISA [165,181].

Overall, the platform described here forms a powerful toolkit to characterize T cell responses to various cues and is especially powerful for the deep sampling of rare populations. The application and potency of this approach is further exemplified in this study where it is applied to characterize the kinetics of activated $CD8^+$ T_{EM} cells and $CD4^+$ cT_{FH} cells induced upon malaria parasite immunization to better understand the emergence and maintenance of antigen-specific T cell clones.

5.2 Activated $CD8^+$ T_{EM} cell responses in *Pf* RAS immunization

Results from efforts to develop a potent malaria vaccine that provides long-term sterile protection have highlighted the important role of $CD8^+$ T cell responses to prevent disease progression by targeting infected hepatocytes [91,92,99,101,102,178]. In this study, we aimed at characterizing how the repertoire of $CD8^+$ T_{EM} cells is shaped by subsequent immunizations with radiation-attenuated *Plasmodium falciparum* sporozoites (*Pf* RAS).

While most studies restrict the analysis to antigen-specific T cells identified by either tetramer staining or *in vitro* stimulation, these approaches have multiple drawbacks. The tetramer staining approach needs *a priori* knowledge of the epitope as well as HLA-type of the donor. Although this approach can be very powerful for the characterization of immune responses to simpler pathogens like viruses, it is hardly suitable for the analysis of complex parasites with large genomes, e.g. *Pf* with over 5300 genes, as only a minor fraction of the parasite-specific T cell response can be monitored [185,186]. *In vitro* stimulation, in contrast, allows the analysis of T cell responses to a variety of different antigens or even whole parasites. However, with increasing stimulation time the phenotype of cells changes. Furthermore, the clonal composition is altered due to progressive proliferation and cell death. To overcome these limitations, this study characterized $CD8^+$ T_{EM} responses without prior identification of antigen-specific cells.

In all donors, the overall frequencies of $CD8^+$ T_{EM} cells did not increase after successive immunizations, which is in agreement with the low frequencies of *Pf*-specific $CD8^+$ T cells (on average 0.2%) in the blood of RAS-immunized donors [91,92]. To enrich for potential antigen-specific cells, the analysis was restricted to $CD8^+$ T_{EM} cells expressing the co-stimulatory and co-inhibitory molecules ICOS and PD-1, respectively, which are transiently upregulated upon

TCR-mediated T cell activation [187–189]. After *Pf* RAS immunization, the frequencies of activated CD8$^+$ T_{EM} cells were moderately increased, indicating *Pf*-specific T cell activation in this compartment.

5.2.1 Dominance of large, persistent T cell clones in the CD8$^+$ T_{EM} repertoire

To identify and track *Pf*-specific T cells in the repertoire of activated CD8$^+$ T_{EM} cells, the platform for TCR repertoire analysis was used. As the memory compartment contains T cells activated during numerous infections throughout life, the analysis of T cells already present before immunization is indispensable to discriminate pre-existing cells from T cells induced upon immunization. The TCR repertoire of CD8$^+$ T_{EM} cells present before immunization showed a high degree of clonal expansion with single clones strongly dominating the repertoire. A similar distribution of clonally expanded cells as well as wide range of clone sizes has also been described by others analyzing the memory T cell compartment of healthy volunteers [190,191]. We found the large, pre-existing T cell clones to be maintained throughout all analyzed time points, although their frequency decreased upon successive immunizations, implying that they may not contribute to the *Pf*-specific immune response. As the immunization led to increased frequencies of activated CD8$^+$ T_{EM} cells, mediated by the emergence of smaller clones, it is likely that while the frequency of pre-existing clones decreased, their overall counts stayed rather constant. This assumption is supported by findings of other studies that analyzed changes in the T cell memory compartment over months to years and found the repertoire to be highly stable, especially concerning the strongly expanded clones [190,192,193]. The large, persistent clones are reported to often recognize antigens of viruses resulting in chronic infections, e.g. cytomegalovirus (CMV), Epstein-Barr virus (EBV) or human immunodeficiency virus (HIV) [128,193–195]. Whether the pre-existing clones identified here are also induced by chronic infections remains to be evaluated. A comparison with TCRs of known specificity, published on the open TCR database VDJdb, did not resolve this as often only either the TCR alpha or beta CDR3 was similar to one of the pre-existing clones and the predicted antigens ranged from likely targets as CMV or EBV to highly unlikely targets as HIV, for which all volunteers were negative upon study onset [196].

In contrast to the stable maintenance of pre-existing clones, clones induced upon immunization were rather small, highly diverse and showed a stronger activation phenotype. Interestingly, while newly recruited cells showed a higher expression of the co-stimulatory molecule ICOS, no difference in expression of the co-inhibitory molecule PD-1 was detectable. This likely reflects the heterogeneous composition of PD-1$^+$ CD8$^+$ T cells, which includes not

only recently activated T cells but also exhausted T cells that upregulate PD-1 expression and become functionally impaired due to chronic stimulation [197]. Exhausted $CD8^+$ T cells can be found in various persistent viral infections as HIV and hepatitis C virus infection, as well as among tumor-specific T cells [198–204]. In contrast, PD-1^+ exhausted $CD8^+$ T cells are absent in chronic CMV infections [205]. Overall, these results indicate that ICOS alone may be sufficient for the identification of recently activated cells, however a more stringent gating may further enrich for antigen-specific cells.

5.2.2 High diversity of the $CD8^+$ T_{EM} cell repertoire hampers the identification of *Pf*-specific cells

To identify *Pf*-specific T cells, the repertoire was analyzed for signs of antigen-specificity. As TCRs specific for the same epitope are often highly similar and are encoded by the same segments, the enrichment of certain TCR segments upon immunization is a good measure for antigen-specificity [206,207]. The TCR repertoire of activated $CD8^+$ T_{EM} cells was highly diverse between the volunteers, reflecting differences in immune history in the individuals as well as different MHC restriction. In agreement with this, only donor-specific changes in the TCR repertoire, i.e. segment usage, were detected upon immunization. The functional characterization of TCRs that use enriched segments and originate from highly activated ($ICOS^+$), expanded T cells did not lead to the discovery of *Pf*-specific T cells. This might reflect the low abundance of antigen-specific $CD8^+$ T cells in the blood of *Pf* RAS-immunized donors, as studies of RAS-immunized non-human primates report that the majority of *Pf*-specific $CD8^+$ T cells reside in the liver, targeting infected hepatocytes [92]. Furthermore, the limited amount of epitopes that could be used for $CD8^+$ T cell screening further reduced the likelihood of identifying antigen-specific cells. Importantly, so far most epitopes of $CD8^+$ T cells were identified from a limited number of proteins which are critical for pathogenicity, and therefore relevant for vaccine design [115,116]. This, however, likely covers only a small fraction of epitopes of *Pf*-specific $CD8^+$ T cells and leaves a large number of unknown epitopes to be identified.

5.3 Induction of antigen-specific cT_{FH} responses by *Pf* RAS immunization

The induction of long-lived, high-affine antibody responses forms the basis of most vaccines and strictly relies on help provided by antigen-specific T_{FH} cells in the GCs. Therefore, improving T_{FH} cell responses to vaccines has become a promising target for the enhancement

of protective antibody responses. Limited access to lymph nodes in humans, however, has fostered the characterization of the circulating counterparts of GC T_{FH} cells – cT_{FH} cells – during immune responses as a surrogate for GC T_{FH} cells. To better understand how protective antibody responses are formed during *Pf* RAS immunization, an in-depth analysis of cT_{FH} cell responses was performed in this study. By tracking the kinetics of antigen-specific cT_{FH} cells during successive immunizations, we gained detailed insights into the emergence and maintenance of *Pf*-specific T_{FH} cell responses.

5.3.1 *Pf* RAS immunization preferentially activates the inefficient B cell helpers

cT_{FH} cell responses characterized 7 days post *Pf* RAS immunization showed a profound increase of activated cT_{FH} cells indicative for the induction of *Pf*-specific cT_{FH} cells. Most of these activated cT_{FH} cells had a $cT_{FH}1$ phenotype, associated with poor B cell help [59,60]. Similar observations have been made for cT_{FH} cells in acute natural malaria infection indicating that *Pf* RAS immunizations and natural infections share common features of cT_{FH} cell responses [109]. Interestingly, characterization of T_{FH} cell responses in lymph nodes of mice infected with live *P. berghei* parasites revealed that T_{FH} cells in the SLO are also skewed towards T_H1 polarization in malaria infections, which has been associated with impaired antibody responses [108]. A T_H1 skewing was also present in infections with irradiated *P. berghei* parasites, although to a lesser extent. This highlights the relevance of studying cT_{FH} cell responses as a surrogate for GC T_{FH} cells. The polarization of T_{FH} cells to a T_H1-associated phenotype seems to be induced by a general T_H1-like inflammatory milieu as we and others show that all $CD4^+$ T cell responses are skewed towards T_H1 differentiation in response to *Pf* [108,110,111]. Similar observations have been made in other immunizations and diseases, where the cT_{FH} differentiation followed the general $CD4^+$ T cell polarization [59,62].

5.3.2 Clonally expanded cells dominate the polyclonal cT_{FH} cell repertoire upon *Pf* RAS immunization

Besides the phenotypical and functional similarity between cT_{FH} cells and GC T_{FH} cells, recent studies also confirmed the close relationship of these subsets on the TCR repertoire level [65,208,209]. Analysis of paired blood and lymph node or tonsil samples revealed the highest clonal overlap of GC T_{FH} cells with cT_{FH} cells, in contrast to $CXCR5^-$ subsets in the SLOs or circulation. Remarkably, the expression of the activation marker PD-1 on cT_{FH} cells positively

correlated with repertoire similarity to GC T_{FH} cells, demonstrating that activated cT_{FH} cells most closely resemble GC T_{FH} cells on the clonal level [208]. Therefore, the repertoire of highly activated (PD-1^{hi} $ICOS^{+}$) cT_{FH} cells was analyzed before and after *Pf* RAS immunization as a representative for GC T_{FH} cells. Interestingly, the cT_{FH} repertoire was highly dynamic with almost no clonal overlap between the pre- and post-immunization repertoire, which stands in contrast to the stable maintenance of persistent clones in the $CD8^{+}$ T_{EM} repertoire. This is, however, in agreement with data of Herati and colleagues, which reported a dynamic exchange of clones in the repertoire of activated cT_{FH} cells, while more stability was seen among non-activated cT_{FH} cells containing resting memory cells [210]. In agreement with the rapid exchange of clones in this compartment, the repertoire of activated cT_{FH} cells was highly diverse and polyclonal. Upon immunization, the clonal expansion increased and peaked after the second and third immunization, dependent on the donor. The increase in clonal expansion coincided with the general expansion of cT_{FH} cells, suggesting that the increase in activated cT_{FH} cells is mediated by the recruitment and expansion of antigen-specific T cells. Similar increases in clonal expansion of the cT_{FH} cell repertoire were also described after influenza vaccination, where the presence of antigen-specific cells within this subset was also confirmed experimentally [208,210]. The observation that in most donors the frequencies of activated cT_{FH} cells as well as the clonal expansion were highest after the second *Pf* RAS immunization instead of the third was unexpected, as higher numbers of booster immunizations have been shown to result in improved humoral and cellular immune responses and hence higher rates of protection [91]. This effect can be best explained by the different timespans between each immunization: 7 days between the first and second and 21 days between the second and third immunization. As the formation of GCs requires around 5-6 days, it is likely that the second immunization rather extended the lifespan of GCs induced upon the first immunization by increasing the antigen availability, instead of seeding new GCs [42]. This assumption is supported by the higher clonal overlap between the first and second immunization. In contrast, within the longer time between the second and third immunization, dynamic GCs likely changed in composition and even waned, requiring the re-seeding of new GCs in the third immunization and hence resulting in lower cT_{FH} cell responses compared to the second immunization.

5.3.3 Activated cT_{FH} cells are highly enriched for C-CSP-specific clones

To identify whether there are also qualitative differences in the immune responses induced by the different immunizations, the repertoire was deeper analyzed to identify *Pf*-specific cT_{FH} cells. Although the repertoire of cT_{FH} cells was highly diverse, the enrichment of specific TCR

segments as well as the preferential paring of segments could be detected with successive immunizations, indicating antigen-mediated selection and activation of the cells. TCR repertoires between donors were highly diverse and did not share a uniform immune response, which could be partly explained by differences in immune history and MHC allele restriction between donors. TCRs encoded by enriched V segments or belonging to expanded T cell clones were analyzed for their reactivity to CSP by detecting IL-2 secretion upon antigen-encounter. In 3 out of 5 donors TCRs reactive to CSP were detected at frequencies ranging from 11-25% of the tested TCRs. The fact that all CSP-reactive TCRs bound the C-terminal domain of CSP (C-CSP) confirmed the immunodominance of C-CSP in T cell responses. However, while C-CSP-reactive T cell clones secreted strong amounts of IL-2 upon stimulation with C-CSP, the stimulation with full-length CSP led to the induction of rather low IL-2 concentrations which were at or even below the detection limit of the assay. This suggest that the established stimulation assay is more sensitive to stimulation with subdomains instead of complete proteins. As most TCRs were screened for their reactivity to CSP or C-CSP, but not to other subdomains of CSP, the number of CSP-reactive TCRs might be underestimated. Hence, further tests with different subdomains for CSP are required to reliably capture all CSP-reactive TCRs. This might be especially relevant for donor M1.002 and M1.003, for which so far no CSP-reactive cT_{FH} cells could be identified. As both donors showed high titers of CSP-reactive antibodies, it is very likely that they also possess CSP-reactive T_{FH} cells which have not been spotted due to limited sensitivity of the assay or low numbers of analyzed TCRs. This is supported by the presence of CSP-reactive $CD4^+$ T cells in the blood of donor M1.002, which were detected by proliferation upon *in vitro* stimulation of PBMCs with CSP. Interestingly, in these stimulation experiments, no CSP-reactive T cells could be detected in the blood of donor M1.003. Whether this reflects a complete absence of CSP-reactive T cells in this donor or is caused by limitations of the *in vitro* stimulation needs to be analyzed further, although the strong CSP-specific antibody titers would suggest the latter to be more plausible. Overall, the low activation of T cells by stimulation with full-length protein was rather unexpected, as the assay was optimized to be highly sensitive. Although the optimization was performed with J76-CD8 T cells and the JM22-TCR, stimulated with peptide instead of proteins, a strong T cell activation could also be observed with J76-CD4 T cells expressing the HY-TCR (kindly provided by Dr. M.H.M. Heemskerk, LUMC Leiden, Netherlands), reactive to the $DDX3Y_{176\text{-}187}$ peptide, after stimulation with both, peptide or whole DDX3Y protein (data not shown) [167]. Seminal studies have established the dependency of T cell activation on TCR affinity, ligand availability and number of TCR molecules on the T cell surface [211–213]. While highly affine TCRs require less TCR-antigen interactions, and hence lower numbers of TCRs on the surface and protein in the co-culture, lower affine TCRs are highly dependent on the interaction of high numbers of TCR-pMHC complexes. Whether differences in the affinity can

explain the discrepancy between the control TCRs and the C-CSP-specific TCRs cannot be inferred from the data as only for the highly affine JM22-TCR affinities were available [175,176]. As some T cell lines contain low numbers of TCR^+ T cells, which have been shown to also have lower numbers of TCRs on their surface, this could further affect the sensitivity. This highlights that the numbers of reactive TCRs found for each donor might increase even further upon analysis with CSP subdomains. Despite these limitations in the stimulation assay, the numbers of C-CSP-reactive TCRs found in the three donors were remarkably high, given the low frequency of CSP- or *Pf*-reactive cells (<1%) among all T cells in the circulation of volunteers in this and other studies [91,92,98]. Interestingly, analysis of activated cT_{FH} cells induced after influenza vaccination revealed comparable numbers of antigen-specific cells in this compartment, with 2-10% binding to a limited number of tetramers and about 30-65% responding to the entire vaccine [62,64]. This confirms that activated cT_{FH} cells are in general highly enriched for cells responding to current antigens. However, the high frequency of cT_{FH} cells recognizing C-CSP is still surprising given the large number of possible antigens present in *Pf* parasites. This dominance of C-CSP in cT_{FH} responses is likely a result of the high abundance of CSP on sporozoites as well as the immunodominance of the C-terminal domain [115,117].

5.3.4 C-CSP-specific cT_{FH} cell clones follow different kinetics

To better understand the emergence of the C-CSP-reactive T cell clones, the clone size as well as the kinetics of those clones were analyzed. While some reactive TCRs belong to highly expanded clones, several belong to rather small clones or even single cells, indicating that they emerged at different time points during the immune response. Interestingly, donors seemed to respond differently regarding the immunization time points after which the C-CSP-reactive clones were isolated. In donor M1.006 and M1.009, the majority of C-CSP-reactive clones were isolated after the third immunization, whereas no C-CSP-reactive clones were so far detected among the expanded, overlapping clones shared between the first and second immunization. In contrast to this, most C-CSP-specific clones in donor M1.004 were detected after the second immunization. Whether this could explain the early emergence of class-switched C-CSP-specific antibodies after the second immunization, exclusively seen for donor M1.004, needs further confirmation by analysis of higher numbers of reactive cT_{FH} cells.

5.3.5 Some C-CSP-specific TCRs show high sequence similarity

To spot whether certain TCR segments are associated with C-CSP binding, a deeper analysis of the TCR sequences of C-CSP-reactive clones was conducted. Interestingly, C-CSP-reactive clones were highly diverse within and between donors, in line with the large number of different epitopes and MHC alleles, on which they could be presented. A similar diversity was also observed in T cells proliferating in response to *in vitro* stimulation with CSP or *Pf* lysate. Despite this high diversity, both approaches revealed an enrichment of TCRs encoded by TRBV20-1 and TRAV13 segments. However, due to the limited number of reactive clones as well as the missing epitope information, it is not possible to associate the features directly with CSP-reactivity. Interestingly, some TCRs encoded by the TRBV20-1 segment belong to clusters of highly similar TCRs, which were found within and between different donors. Given the high number of different TCR sequences that could be generated during random V(D)J recombination (10^{15}), this accumulation of highly similar sequences is remarkable, especially given the small number of TCRs available for analysis [5]. Experimental evidences show that although the TCR recombination is considered random, some TCRs have a higher probability to be generated and are therefore more frequently shared between multiple individuals (public TCRs) [214–217]. This raises the assumption that the highly similar TCRs detected in this study also have a higher generation probability. This idea is supported by findings of a recent TCR sequence analysis revealing that T cells specific for the same epitope can either contain highly similar TCRs that cluster together or more distant 'outsider' TCRs, with a strong correlation of cluster size with generation probability [207]. However, the presence of both, similar TCR alpha and beta chain, in one cell cannot be explained solely by higher generation probabilities but also reflects the convergent selection upon antigen-encounter. Together this confirms the relevance of TCR clustering by similarity for the identification of TCRs contributing in the ongoing immune response. Importantly, the assumption that the highly similar TCRs detected in this study recognize the same epitope presented on similar or identical MHC alleles still needs experimental verification. Notably, donor M1.004 and M1.006, which share one cluster of highly similar TCRs, also share two MHC-II alleles that are identical on amino acid level and could hence present the same peptides.

5.3.6 Can C-CSP-specific $cT_{FH}1$ cells impact protective antibody responses?

Overall, the in-depth analysis of cT_{FH} responses to *Pf* RAS immunization showed a strong activation of $cT_{FH}1$ cells, which are highly enriched for CSP-specific cells and have diverse TCRs with smaller clusters of highly similar TCRs, likely recognizing the same epitope.

However, one major question remains: What does this tell us about the T_{FH} response in the germinal center and the induction of the humoral immune response? One important notion is that, although cT_{FH} cells show the highest overlap with GC T_{FH} cells compared to any other subset, the overlap is lower than 5% [65,209]. However, all studies comparing the repertoire overlap of GC T_{FH} cells and cT_{FH} cells in humans were so far limited to samples from healthy volunteers without the context of immunization. In healthy volunteers, the low numbers of GC T_{FH} cells and activated cT_{FH} cells are likely residuals of former infections or induced in steady state and do therefore have a lower chance to overlap. This is supported by the analysis of Brenna and colleagues who found influenza-specific T cells from former infections among the few overlapping clones between GC T_{FH} and cT_{FH} cells [209]. Therefore the comparison of repertoires from both subsets in the context of an ongoing immune response is indispensable to estimate how strongly cT_{FH} cells resemble GC T_{FH} cells. To overcome the limitations in accessing lymphoid organs in humans, a recent report exploited the use of fine needle aspirations for the analysis of GC T_{FH} cell responses in humans and gained encouraging numbers of GC T_{FH} cells, confirming that this technique could shed more light on T_{FH} cell responses in humans and how strongly they relate to cT_{FH} cells [218].

The impact of cT_{FH} cells on B cell responses, on the other hand, has been widely analyzed and many studies reported a positive correlation between activated cT_{FH} cell frequencies and either protective antibodies or autoantibodies [58–62,65]. However, the induction of the most inefficient B cell helpers, $cT_{FH}1$ cells, in response to *Pf* RAS immunization raises the question whether they would also positively influence anti-*Pf* B cell responses. In natural malaria infection the induction of $cT_{FH}1$ cells does not correlate with B cell responses, however the overall lower immune response raised during natural infection might mask detectable effects [109]. Importantly, studies analyzing $cT_{FH}1$ responses to influenza vaccination also failed to observe a correlation of $cT_{FH}1$ and antibody responses upon the primary response in children, but found an important role in $cT_{FH}1$ cells in boosting pre-existing antibody responses to subsequent infections [62]. This is in agreement with data showing that $cT_{FH}1$ cells can provide help to memory B cells but not naive B cells [59,62]. Hence the C-CSP-reactive cT_{FH} cells detected in this study, which preferentially had a $cT_{FH}1$ phenotype, might play an important role in activating and orchestrating B cell responses to subsequent malaria infections and thereby contribute to protection. The identification of epitopes targeted by these cT_{FH} cells can further help to guide the development of new vaccines by restricting the administered antigen to the most potent epitopes and thereby further focusing the immune response.

6 Outlook

The synchronized changes in the $CD8^+$ T_{EM} repertoire, induced upon *Pf* RAS immunization, imply the presence of *Pf*-specific T cells in this compartment. However, none of the cloned TCRs was reactive to one of the 50 published epitopes tested in this study. Therefore, a broader screening approach would be required to identify the targets of the cloned TCRs. This was so far limited by the inability of B cells to efficiently cross-present extracellular proteins on their MHC-I complexes. As cross-presentation has been reported for B cells that internalized antigens via specific binding to the B cell receptor, the stable insertion of CSP-specific B cell receptors into autologous B cells could enable BCR-mediated CSP uptake and cross-presentation of peptides [219]. Thereby, cloned TCRs could be screened for all epitopes of CSP in parallel. Furthermore, cloning and reactivity tests of TCRs originating from $CD8^+$ T cells that proliferated in response to CSP could accelerate the identification of CSP-specific T cells and could guide the selection of TCRs for cloning.

In the cT_{FH} cell compartment, the identification of TCRs reactive to the C-terminal domain of CSP opens many new questions that could be addressed in further studies. One major question is which epitopes within C-CSP are targeted by the TCRs. Are certain regions within C-CSP predominantly targeted and hence essential for vaccine formulations? And do clusters of similar TCRs indeed target identical epitopes? These questions could be addressed in future by stimulation of TCRs with overlapping peptide libraries covering the entire C-CSP. Once epitopes recognized by individual TCRs are identified, the MHC allele information of the donors can be used to predict the alleles that are involved in peptide presentation. This information is crucial for the interpretation of donor-specific differences in T cell responses. Furthermore, it can be used to measure binding affinities of the TCRs to peptide-MHC complexes by surface plasmon resonance (SPR), to qualitatively assess differences in T cell responses.

A major difficulty in vaccine development is the high diversity of different *Plasmodium falciparum* strains, as vaccines inducing protection only against the immunizing strain are not likely to protect from subsequent infection with other strains. Therefore, it would be crucial to investigate whether the CSP-specific TCRs identified in this study target only epitopes of the immunizing strain, *Pf* Nf54, or could also bind related epitopes of other *Pf* strains and hence could show some degree of cross-protection from heterologous infections.

Lastly, the identification of more CSP- and *Pf*-specific TCRs would broaden our understanding of T cell responses induced by *Pf* RAS immunization. For this, cloned TCRs could be screened for reactivity to other CSP-domains, i.e. N-CSP and the central repeat region. To detect TCRs

that are recognizing other proteins of *Pf*, stimulation of TCRs with whole sporozoite lysate could be exploited. However, this would require the optimization of the T cell stimulation assay, as stimulation with full-length CSP resulted in T cell activation that was already at the detection limit of the assay. For this, either the use of high sensitivity ELISAs or the detection of alternative readouts like the upregulation of activation-induced markers, e.g. CD69, could be investigated. As for $CD8^+$ T cells, the analysis of $CD4^+$ TCRs from the *in vitro* PBMC stimulation with CSP or sporozoite lysate could accelerate the identification of *Pf*-specific TCRs and could help identifying features relevant to predict *Pf*-specificity.

Overall, the determination of specificities of CSP-, but also non-CSP-specific T cells in the repertoire could provide helpful insights into future vaccine design by addressing critical questions about the dominance of CSP in the *Pf*-specific T cell response as well as the relevance of other proteins for subunit vaccines. Furthermore, assessing the capacity of CSP-specific T cells to recognize epitopes of related *Pf* strains could provide further information about protection from heterologous infections. This knowledge could be used to optimize vaccines by reducing the administered antigens to regions that are highly conserved and induce potent T cell expansion, thereby focusing the T cell responses to epitopes that can protect from infection with different *Pf* strains, which is still a major obstacle in current malaria vaccines like RTS,S [220].

7 References

1. Roth, D. B. V(D)J Recombination: Mechanism, Errors, and Fidelity. *Microbiol. Spectr.* **2**, (2014).
2. Lafaille, J. J., DeCloux, A., Bonneville, M., Takagaki, Y. & Tonegawa, S. Junctional sequences of T cell receptor γδ genes: Implications for γδ T cell lineages and for a novel intermediate of V-(D)-J joining. *Cell* **59**, 859–870 (1989).
3. Alt, F. W. & Baltimore, D. Joining of immunoglobulin heavy chain gene segments: Implications from a chromosome with evidence of three D-J(H) fusions. *Proc. Natl. Acad. Sci. U. S. A.* **79**, 4118–4122 (1982).
4. Candéias, S., Muegge, K. & Durum, S. K. Junctional diversity in signal joints from T cell receptor beta and delta loci via terminal deoxynucleotidyl transferase and exonucleolytic activity. *J. Exp. Med.* **184**, 1919–1926 (1996).
5. Davis, M. M. & Bjorkman, P. J. The T cell receptor genes and T cell recognition. *Nature* **334**, 395–402 (1988).
6. Bianconi, E. *et al.* An estimation of the number of cells in the human body. *Ann. Hum. Biol.* **40**, 463–471 (2013).
7. Klein, L., Kyewski, B., Allen, P. M. & Hogquist, K. A. Positive and negative selection of the T cell repertoire: What thymocytes see (and don't see). *Nat. Rev. Immunol.* **14**, 377–391 (2014).
8. De Simone, M., Rossetti, G. & Pagani, M. Single cell T cell receptor sequencing: Techniques and future challenges. *Front. Immunol.* **9**, 1638 (2018).
9. Meuer, S. C., Schlossman, S. F. & Reinherz, E. L. Clonal analysis of human cytotoxic T lymphocytes: T4+ and T8+ effector T cells recognize products of different major histocompatibility complex regions. *Proc. Natl. Acad. Sci. U. S. A.* **79**, 4395–4399 (1982).
10. Janeway, C. A. The T cell receptor as a multicomponent signalling machine: CD4/CD8 coreceptors and CD45 in T cell activation. *Annu. Rev. Immunol.* **10**, 645–674 (1992).
11. Li, Y., Yin, Y. & Mariuzza, R. A. Structural and biophysical insights into the role of CD4 and CD8 in T cell activation. *Front. Immunol.* **4**, 206 (2013).
12. Garcia, K. C. *et al.* An αβ T cell receptor structure at 2.5 Å and its orientation in the TCR-MHC complex. *Science (80-.).* **274**, 209–219 (1996).
13. Garboczi, D. N. *et al.* Structure of the complex between human T-cell receptor, viral peptide and HLA-A2. *Nature* **384**, 134–141 (1996).
14. Ding, Y. H. *et al.* Two human T cell receptors bind in a similar diagonal mode to the HLA- A2/Tax peptide complex using different TCR amino acids. *Immunity* **8**, 403–411 (1998).
15. Reinherz, E. L. *et al.* The crystal structure of a T cell receptor in complex with peptide and MHC class II. *Science (80-.).* **286**, 1913–1921 (1999).
16. Garcia, K. C. *et al.* CD8 enhances formation of stable T-cell receptor/MHC class I molecule complexes. *Nature* **384**, 577–581 (1996).
17. Yin, Y., Wang, X. X. & Mariuzza, R. A. Crystal structure of a complete ternary complex of T-cell receptor, peptide-MHC, and CD4. *Proc. Natl. Acad. Sci. U. S. A.* **109**, 5405–5410 (2012).
18. Guy, C. S. & Vignali, D. A. A. Organization of proximal signal initiation at the TCR:CD3 complex. *Immunol. Rev.* **232**, 7–21 (2009).
19. June, C. H., Ledbetter, J. A., Gillespie, M. M., Lindsten, T. & Thompson, C. B. T-cell proliferation involving the CD28 pathway is associated with cyclosporine-resistant interleukin 2 gene expression. *Mol. Cell. Biol.* **7**, 4472–4481 (1987).
20. Linsley, P. S., Clark, E. A. & Ledbetter, J. A. T-cell antigen CD28 mediates adhesion with B cells by interacting with activation antigen B7/BB-1. *Proc. Natl. Acad. Sci. U. S. A.* **87**, 5031–5035 (1990).
21. Azuma, M. *et al.* B70 antigen is a second ligand for CTLA-4 and CD28. *Nature* **366**, 76–79 (1993).
22. Alderson, M. R. *et al.* Molecular and biological characterization of human 4- 1BB and its ligands. *Eur. J. Immunol.* **24**, 2219–2227 (1994).

23. Zhu, J., Yamane, H. & Paul, W. E. Differentiation of Effector CD4 T Cell Populations. *Annu. Rev. Immunol.* **28**, 445–489 (2010).

24. Pashine, A., John, B., Rath, S., George, A. & Bal, V. T(h)1 dominance in the immune response to live Salmonella typhimurium requires bacterial invasiveness but not persistence. *Int. Immunol.* **11**, 481–489 (1999).

25. Kaplan, M. H., Whitfield, J. R., Boros, D. L. & Grusby, M. J. Th2 cells are required for the Schistosoma mansoni egg-induced granulomatous response. *J. Immunol.* **160**, 1850–1856 (1998).

26. Acosta-Rodriguez, E. V. *et al.* Surface phenotype and antigenic specificity of human interleukin 17-producing T helper memory cells. *Nat. Immunol.* **8**, 639–646 (2007).

27. Schaerli, P. *et al.* CXC chemokine receptor 5 expression defines follicular homing T cells with B cell helper function. *J. Exp. Med.* **192**, 1553–1562 (2000).

28. Breitfeld, D. *et al.* Follicular B helper T cells express CXC chemokine receptor 5, localize to B cell follicles, and support immunoglobulin production. *J. Exp. Med.* **192**, 1545–1551 (2000).

29. Chen, W. J. *et al.* Conversion of Peripheral CD4+CD25- Naive T Cells to CD4+CD25+ Regulatory T Cells by TGF-β Induction of Transcription Factor Foxp3. *J. Exp. Med.* **198**, 1875–1886 (2003).

30. Fantini, M. C. *et al.* Cutting Edge: TGF-β Induces a Regulatory Phenotype in CD4 + CD25 − T Cells through Foxp3 Induction and Down-Regulation of Smad7 . *J. Immunol.* **172**, 5149–5153 (2004).

31. Dutton, R. W., Bradley, L. M. & Swain, S. L. T cell memory. *Annu. Rev. Immunol.* **16**, 201–223 (1998).

32. Sallusto, F., Lenig, D., Förster, R., Lipp, M. & Lanzavecchia, A. Two subsets of memory T lymphocytes with distinct homing potentials and effector functions. *Nature* **401**, 708–712 (1999).

33. Farber, D. L., Yudanin, N. A. & Restifo, N. P. Human memory T cells: Generation, compartmentalization and homeostasis. *Nat. Rev. Immunol.* **14**, 24–35 (2014).

34. Kambayashi, T. & Laufer, T. M. Atypical MHC class II-expressing antigen-presenting cells: Can anything replace a dendritic cell? *Nat. Rev. Immunol.* **14**, 719–730 (2014).

35. Lee, S. K. *et al.* B cell priming for extrafollicular antibody responses requires Bcl-6 expression by T cells. *J. Exp. Med.* **208**, 1377–1388 (2011).

36. Kerfoot, S. M. *et al.* Germinal Center B Cell and T Follicular Helper Cell Development Initiates in the Interfollicular Zone. *Immunity* **34**, 947–960 (2011).

37. Ansel, B. K. M., Mcheyzer-williams, L. J., Ngo, V. N., Mcheyzer-williams, M. G. & Cyster, J. G. In vivo-activated CD4 T cells upregulate CXC chemokine receptor 5 and reprogram their response to lymphoid chemokines. *J. Exp. Med.* **190**, 1123–1134 (1999).

38. Gunn, M. D. *et al.* A B-cell-homing chemokine made in lymphoid follicles activates Burkitt's lymphoma receptor-1. *Nature* **391**, 799–803 (1998).

39. Garside, P. *et al.* Visualization of specific B and T lymphocyte interactions in the lymph node. *Science (80-.).* **281**, 96–99 (1998).

40. Okada, T. *et al.* Antigen-engaged B cells undergo chemotaxis toward the T zone and form motile conjugates with helper T cells. *PLoS Biol.* **3**, 1047–1061 (2005).

41. Vinuesa, C. G., Linterman, M. A., Yu, D. & Maclennan, I. C. M. Follicular Helper T Cells. *Annu. Rev. Immunol.* **34**, 335–368 (2016).

42. Jacob, J., Kassir, R. & Kelsoe, G. In situ studies of the primary immune response to (4-hydroxy-3-nitrophenyl)acetyl. I. The architecture and dynamics of responding cell populations. *J. Exp. Med.* **173**, 1165–1175 (1991).

43. Smith, K. G. C., Hewitson, T. D., Nossal, G. J. V. & Tarlinton, D. M. The phenotype and fate of the antibody-forming cells of the splenic foci. *Eur. J. Immunol.* **26**, 444–448 (1996).

44. Hosokawa, T. Studies on B-cell memory. II. T-cell independent antigen can induce B-cell memory. *Immunology* **38**, 291–299 (1979).

45. Victora, G. D. & Nussenzweig, M. C. Germinal centers. *Annu. Rev. Immunol.* **30**, 429–57 (2012).

46. Stavnezer, J., Guikema, J. E. J. & Schrader, C. E. Mechanism and Regulation of Class Switch Recombination. *Annu. Rev. Immunol.* **26**, 261–292 (2008).

47. Jacob, J., Kelsoe, G., Rajewsky, K. & Weiss, U. Intraclonal generation of antibody mutants in germinal centres. *Nature* **354**, 389–392 (1991).

48. Berek, C., Berger, A. & Apel, M. Maturation of the immune response in germinal centers. *Cell* **67**, 1121–1129 (1991).

49. Teng, G. & Papavasiliou, F. N. Immunoglobulin somatic hypermutation. *Annu. Rev. Genet.* **41**, 107–20 (2007).

50. Allen, C. D. C., Okada, T., Tang, H. L. & Cyster, J. G. Imaging of germinal center selection events during affinity maturation. *Science (80-.).* **315**, 528–531 (2007).

51. Batista, F. D., Iber, D. & Neuberger, M. S. B cells acquire antigen from target cells after synapse formation. *Nature* **411**, 489–494 (2001).

52. Mandel, T. E., Phipps, R. P., Abbot, A. P. & Tew, J. G. Long-term antigen retention by dendritic cells in the popliteal lymph node of immunized mice. *Immunology* **43**, 353–62 (1981).

53. Shulman, Z. *et al.* Germinal centers: Dynamic signaling by T follicular helper cells during germinal center B cell selection. *Science (80-.).* **345**, 1058–1062 (2014).

54. Crotty, S. Follicular helper CD4 T cells (TFH). *Annu. Rev. Immunol.* **29**, 621–63 (2011).

55. Phan, T. G. *et al.* High affinity germinal center B cells are actively selected into the plasma cell compartment. *J. Exp. Med.* **203**, 2419–2424 (2006).

56. Weisel, F. J., Zuccarino-Catania, G. V., Chikina, M. & Shlomchik, M. J. A Temporal Switch in the Germinal Center Determines Differential Output of Memory B and Plasma Cells. *Immunity* **44**, 116–130 (2016).

57. Zotos, D. & Tarlinton, D. M. Determining germinal centre B cell fate. *Trends Immunol.* **33**, 281–288 (2012).

58. Simpson, N. *et al.* Expansion of circulating T cells resembling follicular helper T cells is a fixed phenotype that identifies a subset of severe systemic lupus erythematosus. *Arthritis Rheum.* **62**, 234–244 (2010).

59. Morita, R. *et al.* Human Blood CXCR5+ CD4+ T Cells Are Counterparts of T Follicular Cells and Contain Specific Subsets that Differentially Support Antibody Secretion. *Immunity* **34**, 108–121 (2011).

60. Locci, M. *et al.* Human Circulating PD1+ CXCR3- CXCR5+ Memory Tfh Cells Are Highly Functional and Correlate with Broadly Neutralizing HIV Antibody Responses. *Immunity* **39**, 758–769 (2013).

61. He, J. *et al.* Circulating Precursor CCR7lo PD-1hi CXCR5+ CD4+ T Cells Indicate Tfh Cell Activity and Promote Antibody Responses upon Antigen Reexposure. *Immunity* **39**, 770–781 (2013).

62. Bentebibel, S. E. *et al.* Induction of ICOS+ CXCR3+ CXCR5+ TH cells correlates with antibody responses to influenza vaccination. *Sci. Transl. Med.* **5**, 1–11 (2013).

63. Chevalier, N. *et al.* CXCR5 Expressing Human Central Memory CD4 T Cells and Their Relevance for Humoral Immune Responses. *J. Immunol.* **186**, 5556–5568 (2011).

64. Herati, R. S. *et al.* Successive annual influenza vaccination induces a recurrent oligoclonotypic memory response in circulating T follicular helper cells. *Sci. Immunol.* **2**, (2017).

65. Heit, A. *et al.* Vaccination establishes clonal relatives of germinal center T cells in the blood of humans. *J. Exp. Med.* **214**, 2139–2152 (2017).

66. Bossaller, L. *et al.* ICOS Deficiency Is Associated with a Severe Reduction of CXCR5+ CD4 Germinal Center Th Cells. *J. Immunol.* **177**, 4927–4932 (2006).

67. Vella, L. A. *et al.* T follicular helper cells in human efferent lymph retain lymphoid characteristics. *J. Clin. Invest.* **129**, 3185–3200 (2019).

68. White, N. J. *et al.* Malaria. *Lancet* **383**, 723–735 (2014).

69. Cowman, A. F., Healer, J., Marapana, D. & Marsh, K. Malaria : Biology and Disease. *Cell* **167**, 610–624 (2016).

70. Mok, S. *et al.* Population transcriptomics of human malaria parasites reveals the mechanism of artemisinin resistance. *Science (80-.).* **347**, 431–435 (2015).

71. Mbengue, A. *et al.* A molecular mechanism of artemisinin resistance in Plasmodium falciparum malaria.

Nature **520**, 683–687 (2015).

72. Singh Sidhu, A. B., Verdier-Pinard, D. & Fidock, D. A. Chloroquine resistance in Plasmodium falciparum malaria parasites conferred by pfcrt mutations. *Science (80-.).* **298**, 210–213 (2002).

73. Amino, R. *et al.* Quantitative imaging of Plasmodium transmission from mosquito to mammal. *Nat. Med.* **12**, 220–224 (2006).

74. Vanderberg, J. P. & Frevert, U. Intravital microscopy demonstrating antibody-mediated immobilisation of Plasmodium berghei sporozoites injected into skin by mosquitoes. *Int. J. Parasitol.* **34**, 991–996 (2004).

75. Formaglio, P., Tavares, J., Ménard, R. & Amino, R. Loss of host cell plasma membrane integrity following cell traversal by Plasmodium sporozoites in the skin. *Parasitol. Int.* **63**, 237–244 (2014).

76. Hopp, C. S. *et al.* Longitudinal analysis of plasmodium sporozoite motility in the dermis reveals component of blood vessel recognition. *Elife* **4**, e07789 (2015).

77. Shin, S. C. J., Vanderberg, J. P. & Terzakis, J. A. Direct Infection of Hepatocytes by Sporozoites of Plasmodium berghei. *J. Protozool.* **29**, 448–454 (1982).

78. Yuda, M. & Ishino, T. Liver invasion by malarial parasites - How do malarial parasites break through the host barrier? *Cell. Microbiol.* **6**, 1119–1125 (2004).

79. Sturm, A. *et al.* Manipulation of host hepatocytes by the malaria parasite for delivery into liver sinusoids. *Science (80-.).* **313**, 1287–1290 (2006).

80. Dvorak, J. A., Miller, L. H., Whitehouse, W. C. & Shiroishi, T. Invasion of erythrocytes by malaria merozoites. *Science (80-.).* **187**, 748–750 (1975).

81. Riglar, D. T. *et al.* Super-resolution dissection of coordinated events during malaria parasite invasion of the human erythrocyte. *Cell Host Microbe* **9**, 9–20 (2011).

82. Hafalla, J. C., Silvie, O. & Matuschewski, K. Cell biology and immunology of malaria. *Immunol. Rev.* **240**, 297–316 (2011).

83. Doolan, D. L., Dobaño, C. & Baird, J. K. Acquired immunity to Malaria. *Clin. Microbiol. Rev.* **22**, 13–36 (2009).

84. Bull, P. C. *et al.* Parasite antigens on the infected red cell surface are targets for naturally acquired immunity to malaria. *Nat. Med.* **4**, 358–360 (1998).

85. Wipasa, J. *et al.* Long-lived antibody and B cell memory responses to the human malaria parasites, Plasmodium falciparum and Plasmodium vivax. *PLoS Pathog.* **6**, e1000770 (2010).

86. Fowkes, F. J. I., Richards, J. S., Simpson, J. A. & Beeson, J. G. The relationship between anti-merozoite antibodies and incidence of Plasmodium falciparum malaria: A systematic review and meta-analysis. *PLoS Med.* **7**, e1000218 (2010).

87. Tran, T. M. *et al.* An intensive longitudinal cohort study of malian children and adults reveals no evidence of acquired immunity to plasmodium falciparum infection. *Clin. Infect. Dis.* **57**, 40–47 (2013).

88. Nussenzweig, R. S., Vanderberg, J. P., Most, H. & Orton, C. Protective Immunity produced by the Injection of X-irradiated Sporozoites of Plasmodium berghei. *Nature* **216**, 160–162 (1967).

89. Itsara, L. S. *et al.* The Development of Whole Sporozoite Vaccines for Plasmodium falciparum Malaria. *Front. Immunol.* **9**, 2748 (2018).

90. Hoffman, S. L. *et al.* Protection of Humans against Malaria by Immunization with Radiation-Attenuated Plasmodium falciparum Sporozoites. *J. Infect. Dis.* **185**, 1155–1164 (2002).

91. Seder, R. A. *et al.* Protection Against Malaria by Intravenous Immunization with a Nonreplicating Sporozoite Vaccine. *Science (80-.).* **341**, 1359–65 (2013).

92. Ishizuka, A. S. *et al.* Protection against malaria at 1 year and immune correlates following PfSPZ vaccination. *Nat. Med.* **22**, 614–23 (2016).

93. Clyde, D., Most, H., McCarthy, V. & Vanderberg, J. Immunization of man against sporozite-induced falciparum malaria. *Am. J. Med. Sci.* **266**, 169–177 (1973).

94. Olotu, A. *et al.* Seven-year efficacy of RTS, S/AS01 malaria vaccine among young african children. *N. Engl. J. Med.* **374**, 2519–2529 (2016).

95. The RTSS Clinical Trials Partnership. First Results of Phase 3 Trial of RTS,S/AS01 Malaria Vaccine in African Children. *N. Engl. J. Med.* **365**, 1863–1875 (2011).

96. The RTSS Clinical Trials Partnership. A phase 3 trial of RTS,S/AS01 malaria vaccine in African infants. *N. Engl. J. Med.* **367**, 2284–2295 (2012).

97. The RTSS Clinical Trials Partnership. Efficacy and safety of RTS,S/AS01 malaria vaccine with or without a booster dose in infants and children in Africa: final results of a phase 3, individually randomised, controlled trial. *Lancet* **386**, 31–45 (2015).

98. Mordmüller, B. *et al.* Sterile protection against human malaria by chemoattenuated PfSPZ vaccine. *Nature* **542**, 445–449 (2017).

99. Sedegah, M. *et al.* Naturally acquired CD8 + cytotoxic T lymphocytes against the Plasmodium falciparum circumsporozoite protein. *J. Immunol.* **149**, 966–971 (1992).

100. Doolan, D. L. *et al.* Degenerate cytotoxic T cell epitopes from P. falciparum restricted by multiple HLA-A and HLA-B supertype alleles. *Immunity* **7**, 97–112 (1997).

101. Cockburn, I. A. *et al.* In vivo imaging of CD8+ T cell-mediated elimination of malaria liver stages. *Proc. Natl. Acad. Sci. U. S. A.* **110**, 9090–9095 (2013).

102. Kimura, K. *et al.* CD8+ T cells specific for a malaria cytoplasmic antigen form clusters around infected hepatocytes and are protective at the liver stage of infection. *Infect. Immun.* **81**, 3825–3834 (2013).

103. Mellouk, S. *et al.* Inhibitory activity of interferons and interleukin 1 on the development of Plasmodium falciparum in human hepatocyte cultures. *J. Immunol.* **139**, 4192–4195 (1987).

104. Seguin, B. M. C. *et al.* Induction of nitric oxide synthase protects against malaria in mice exposed to irradiated Plasmodium berghei infected mosquitoes: involvement of interferon gamma and CD8+ T cells. *J. Exp. Med.* **180**, 353–358 (1994).

105. Hollingdale, M. R., Zavala, F., Nussenzweig, R. S. & Nussenzweig, V. Antibodies to the protective antigen of Plasmodium berghei sporozoites prevent entry into cultured cells. *J. Immunol.* **128**, 1929–1930 (1982).

106. Hollingdale, M. R., Nardin, E. H., Tharavanij, S., Schwartz, A. L. & Nussenzweig, R. S. Inhibition of entry of Plasmodium falciparum and P. vivax sporozoites into cultured cells; an in vitro assay of protective antibodies. *J. Immunol.* **132**, 909–13 (1984).

107. Pérez-Mazliah, D. *et al.* Follicular Helper T Cells are Essential for the Elimination of Plasmodium Infection. *EBioMedicine* **24**, 216–230 (2017).

108. Ryg-cornejo, V. *et al.* Severe Malaria Infections Impair Germinal Center Responses by Inhibiting T Follicular Helper Cell Article Severe Malaria Infections Impair Germinal Center Responses by Inhibiting T Follicular Helper Cell Differentiation. *Cell Rep.* **14**, 1–14 (2016).

109. Obeng-adjei, N. *et al.* Circulating Th1-Cell-type Tfh Cells that Exhibit Impaired B Cell Help Are Preferentially Activated during Acute Malaria in Children. *Cell Rep.* **13**, 425–439 (2015).

110. Troye-Blomberg, M. *et al.* Production of IL 2 and IFN-gamma by T cells from malaria patients in response to Plasmodium falciparum or erythrocyte antigens in vitro. *J. Immunol.* **135**, 3498–3504 (1985).

111. Kurup, S. P., Butler, N. S. & Harty, J. T. T cell- mediated immunity to malaria. *Nat. Rev. Immunol.* (2019) doi:10.1038/s41577-019-0158-z.

112. Horowitz, A. *et al.* Cross-Talk between T Cells and NK Cells Generates Rapid Effector Responses to Plasmodium falciparum - Infected Erythrocytes . *J. Immunol.* **184**, 6043–6052 (2010).

113. Blanchette, J., Jaramillo, M. & Olivier, M. Signalling events involved in interferon-γ-inducible macrophage nitric oxide generation. *Immunology* **108**, 513–522 (2003).

114. Gardner, M. J. *et al.* Genome sequence of the human malaria parasite Plasmodium falciparum. *Nature* **419**, 498–511 (2002).

115. Vaughan, K. *et al.* Meta-analysis of immune epitope data for all Plasmodia: Overview and applications for malarial immunobiology and vaccine-related issues. *Parasite Immunol.* **31**, 78–97 (2009).

116. Heide, J., Vaughan, K. C., Sette, A., Jacobs, T. & Schulze, J. Comprehensive Review of Human Plasmodium falciparum -Specific CD8 + T Cell Epitopes. *Front. Immunol.* **10**, (2019).

117. Potocnjak, P., Zavala, F., Nussenzweig, R. & Nussenzweig, V. Inhibition of idiotype-anti-idiotype

interaction for detection of a parasite antigen: a new immunoassay. *Science (80-.).* **215**, 1637–1639 (1982).

118. Cerami, C. *et al.* The basolateral domain of the hepatocyte plasma membrane bears receptors for the circumsporozoite protein of plasmodium falciparum sporozoites. *Cell* **70**, 1021–1033 (1992).

119. Dame, J. *et al.* Structure of the gene encoding the immunodominant surface antigen on the sporozoite of the human malaria parasite Plasmodium falciparum. *Science (80-.).* **225**, 593–599 (1984).

120. Wang, Q., Fujioka, H. & Nussenzweig, V. Mutational analysis of the GPI-anchor addition sequence from the circumsporazoite protein of Plasmodium. *Cell. Microbiol.* **7**, 1616–1626 (2005).

121. Zavala, F. *et al.* Rationale for development of a synthetic vaccine against Plasmodium falciparum malaria. *Science (80-.).* **228**, 1436–1440 (1985).

122. Nardin, E. *et al.* Conserved repetitive epitope recognized by CD4+ clones from a malaria-immunized volunteer. *Science (80-.).* **246**, 1603–1606 (1989).

123. Sedegah, M. *et al.* Identification of minimal human MHC-restricted CD8+ T-cell epitopes within the Plasmodium falciparum circumsporozoite protein (CSP). *Malar. J.* **12**, 185 (2013).

124. Triller, G. *et al.* Natural Parasite Exposure Induces Protective Human Anti-Malarial Antibodies. *Immunity* **47**, 1197-1209.e10 (2017).

125. Murugan, R. *et al.* Clonal selection drives protective memory B cell responses in controlled human malaria infection. *Sci. Immunol.* **3**, eaap8029 (2018).

126. Reece, W. H. H. *et al.* A CD4+ T-cell immune response to a conserved epitope in the circumsporozoite protein correlates with protection from natural Plasmodium falciparum infection and disease. *Nat. Med.* **10**, 406–410 (2004).

127. Wendel, B. S. *et al.* The receptor repertoire and functional profile of follicular T cells in HIV-infected lymph nodes. *Sci. Immunol.* **3**, eaan8884 (2018).

128. Klarenbeek, P. L. *et al.* Deep Sequencing of Antiviral T-Cell Responses to HCMV and EBV in Humans Reveals a Stable Repertoire That Is Maintained for Many Years. *PLoS Pathog.* **8**, e1002889 (2012).

129. Bradley, P. & Thomas, P. G. Using T Cell Receptor Repertoires to Understand the Principles of Adaptive Immune Recognition. *Annu. Rev. Immunol.* **37**, 547–570 (2019).

130. Altman, J. D. *et al.* Phenotypic analysis of antigen-specific T lymphocytes. *Science (80-.).* **274**, 94–96 (1996).

131. Vollers, S. S. & Stern, L. J. Class II major histocompatibility complex tetramer staining: Progress, problems, and prospects. *Immunology* vol. 123 305–313 (2008).

132. Tumeh, P. C. *et al.* PD-1 blockade induces responses by inhibiting adaptive immune resistance. *Nature* **515**, 568–571 (2014).

133. Wu, D. *et al.* High-throughput sequencing detects minimal residual disease in acute T lymphoblastic leukemia. *Sci. Transl. Med.* **4**, 134ra63 (2012).

134. Cha, E. *et al.* Improved survival with T cell clonotype stability after anti-CTLA-4 treatment in cancer patients. *Sci. Transl. Med.* **6**, 238ra70 (2014).

135. Freeman, J. D., Warren, R. L., Webb, J. R., Nelson, B. H. & Holt, R. A. Profiling the T-cell receptor beta-chain repertoire by massively parallel sequencing. *Genome Res.* **19**, 1817–24 (2009).

136. Zhou, D. *et al.* High throughput analysis of TCR-beta rearrangement and gene expression in single T cells. *Lab. Invest.* **86**, 314–21 (2006).

137. Warren, R. L. *et al.* Exhaustive T-cell repertoire sequencing of human peripheral blood samples reveals signatures of antigen selection and a directly measured repertoire size of at least 1 million clonotypes. *Genome Res.* **21**, 790–7 (2011).

138. Britanova, O. V *et al.* Age-related decrease in TCR repertoire diversity measured with deep and normalized sequence profiling. *J. Immunol.* **192**, 2689–98 (2014).

139. Sherwood, A. M. *et al.* Deep sequencing of the human TCRγ and TCRβ repertoires suggests that TCRβ rearranges after αβ and γδ T cell commitment. *Sci. Transl. Med.* **3**, 90ra61 (2011).

140. Paillard, F., Sterkers, G., Bismuth, G., Gomard, E. & Vaquero, C. Lymphokine mRNA and T cell

multireceptor mRNA of the Ig super gene family are reciprocally modulated during human T cell activation. *Eur. J. Immunol.* **18**, 1643–6 (1988).

141. Han, A., Glanville, J., Hansmann, L. & Davis, M. M. Linking T-cell receptor sequence to functional phenotype at the single-cell level. *Nat. Biotechnol.* **32**, 684–692 (2014).

142. Kim, S. M. *et al.* Analysis of the paired TCR α- and β-chains of single human T cells. *PLoS One* **7**, (2012).

143. Turchaninova, M. A. *et al.* Pairing of T-cell receptor chains via emulsion PCR. *Eur. J. Immunol.* **43**, 2507–15 (2013).

144. Howie, B. *et al.* High-throughput pairing of T cell receptor a and b sequences. *Sci. Transl. Med.* **7**, 301ra131 (2015).

145. Mcdaniel, J. R., Dekosky, B. J., Tanno, H., Ellington, A. D. & Georgiou, G. Ultra-high-throughput sequencing of the immune receptor repertoire from millions of lymphocytes. *Nat. Protoc.* **11**, 429–442 (2016).

146. Imkeller, K., Arndt, P. F., Wardemann, H. & Busse, C. E. sciReptor: analysis of single-cell level immunoglobulin repertoires. *BMC Bioinformatics* **17**, 67 (2016).

147. Masella, A. P., Bartram, A. K., Truszkowski, J. M., Brown, D. G. & Neufeld, J. D. PANDAseq: paired-end assembler for illumina sequences. *BMC Bioinformatics* **13**, 31 (2012).

148. Ye, J., Ma, N., Madden, T. L. & Ostell, J. M. IgBLAST: an immunoglobulin variable domain sequence analysis tool. *Nucleic Acids Res.* **41**, W34-40 (2013).

149. Zerbino, D. R. *et al.* Ensembl 2018. *Nucleic Acids Res.* **46**, D754–D761 (2018).

150. Guo, X. J. *et al.* Rapid cloning , expression , and functional characterization of paired αβ and γδ T-cell receptor chains from single-cell analysis. 1–12 (2016) doi:10.1038/mtm.2015.54.

151. Heemskerk, M. H. M. *et al.* Redirection of antileukemic reactivity of peripheral T lymphocytes using gene transfer of minor histocompatibility antigen HA-2 – specific T-cell receptor complexes expressing a conserved alpha joining region. *Blood* **102**, 3530–3540 (2003).

152. Miller, G., Shope, T., Lisco, H., Stitt, D. & Lipman, M. Epstein-Barr virus: transformation, cytopathic changes, and viral antigens in squirrel monkey and marmoset leukocytes. *Proc. Natl. Acad. Sci. U. S. A.* **69**, 383–387 (1972).

153. Sadreddini, S. *et al.* Evaluation of EBV transformation of human memory B-cells isolated by FACS and MACS techniques. *J. Immunotoxicol.* **13**, 490–497 (2016).

154. Busse, C. E., Czogiel, I., Braun, P., Arndt, P. F. & Wardemann, H. Single-cell based high-throughput sequencing of full-length immunoglobulin heavy and light chain genes. *Eur. J. Immunol.* **44**, 597–603 (2014).

155. Emerson, R. *et al.* Estimating the ratio of CD4 + to CD8 + T cells using high-throughput sequence data. *J. Immunol. Methods* **391**, 14–21 (2013).

156. Liu, P. *et al.* Characterization of human αβTCR repertoire and discovery of D-D fusion in TCRβ chains. *Protein Cell* **5**, 603–615 (2014).

157. Kitaura, K., Shini, T., Matsutani, T. & Suzuki, R. A new high-throughput sequencing method for determining diversity and similarity of T cell receptor (TCR) α and β repertoires and identifying potential new invariant TCR α chains. *BMC Immunol.* **17**, (2016).

158. Chen, X., Poncette, L. & Blankenstein, T. Human TCR-MHC coevolution after divergence from mice includes increased nontemplate-encoded CDR3 diversity. *J. Exp. Med.* **214**, 3417–3433 (2017).

159. Gapin, L. Check MAIT. *J. Immunol.* **192**, 4475–4480 (2014).

160. Godfrey, D. I., Koay, H. F., McCluskey, J. & Gherardin, N. A. The biology and functional importance of MAIT cells. *Nat. Immunol.* **20**, 1110–1128 (2019).

161. Altschul, S. F., Gish, W., Miller, W., Myers, E. W. & Lipman, D. J. Basic local alignment search tool. *J. Mol. Biol.* **215**, 403–410 (1990).

162. Weese, D., Holtgrewe, M. & Reinert, K. RazerS 3: faster, fully sensitive read mapping. *Bioinformatics* **28**, 2592–9 (2012).

163. Edgar, R. C. MUSCLE: multiple sequence alignment with high accuracy and high throughput. *Nucleic Acids Res.* **32**, 1792–1797 (2004).

164. Kim, J. H. *et al.* High Cleavage Efficiency of a 2A Peptide Derived from Porcine Teschovirus-1 in Human Cell Lines, Zebrafish and Mice. *PLoS One* **6**, e18556 (2011).

165. Guo, X.-Z. J. *et al.* Rapid cloning, expression, and functional characterization of paired αβ and γδ T-cell receptor chains from single-cell analysis. *Mol. Ther. Methods Clin. Dev.* **3**, 15054 (2016).

166. Vogt, M. H. J. *et al.* The DBY gene codes for an HLA-DQ5–restricted human male-specific minor histocompatibility antigen involved in graft-versus-host disease. *Blood* **99**, 3027–3032 (2002).

167. van der Veken, L. T. *et al.* HLA class II restricted T-cell receptor gene transfer generates CD4+ T cells with helper activity as well as cytotoxic capacity. *Gene Ther.* **12**, 1686–1695 (2005).

168. Moss, P. A. *et al.* Extensive conservation of alpha and beta chains of the human T-cell antigen receptor recognizing HLA-A2 and influenza A matrix peptide. *Proc. Natl. Acad. Sci. U. S. A.* **88**, 8987–90 (1991).

169. Lehner, P. J. *et al.* Human HLA-A0201-restricted cytotoxic T lymphocyte recognition of influenza A is dominated by T cells bearing the V beta 17 gene segment. *J. Exp. Med.* **181**, 79–91 (1995).

170. Malissen, M. *et al.* Regulation of TCR α and β gene allelic exclusion during T-cell development. *Immunol. Today* **13**, 315–322 (1992).

171. Kuida, K. *et al.* Post-translational attainment of allelic exclusion of the T cell receptor α chain in a T cell clone. *Int. Immunol.* **3**, 75–82 (1991).

172. Rock, K. L., Gamble, S. & Rothstein, L. Presentation of exogenous antigen with class I major histocompatibility complex molecules. *Science (80-.).* **249**, 918–921 (1990).

173. Schumacher, T. N. M. *et al.* Direct binding of peptide to empty MHC class I molecules on intact cells and in vitro. *Cell* **62**, 563–567 (1990).

174. Eisen, H. N. *et al.* Promiscuous binding of extracellular peptides to cell surface class I MHC protein. *Proc. Natl. Acad. Sci. U. S. A.* **109**, 4580–4585 (2012).

175. Ishizuka, J. *et al.* The Structural Dynamics and Energetics of an Immunodominant T Cell Receptor Are Programmed by Its Vβ Domain. *Immunity* **28**, 171–182 (2008).

176. Willcox, B. E. *et al.* TCR binding to peptide-MHC stabilizes a flexible recognition interface. *Immunity* **10**, 357–365 (1999).

177. Rödström, K. E. J., Elbing, K. & Lindkvist-Petersson, K. Structure of the superantigen staphylococcal enterotoxin B in complex with TCR and peptide-MHC demonstrates absence of TCR-peptide contacts. *J. Immunol.* **193**, 1998–2004 (2014).

178. Hafalla, J. C. R., Cockburn, I. A. & Zavala, F. Protective and pathogenic roles of CD8+ T cells during malaria infection. *Parasite Immunol.* **28**, 15–24 (2006).

179. Crooks, G., Hon, G., Chandonia, J. & Brenner, S. WebLogo: a sequence logo generator. *Genome Res* **14**, 1188–1190 (2004).

180. Mordmüller, B. *et al.* Sterile protection against human malaria by chemoattenuated PfSPZ vaccine. *Nat. Publ. Gr.* **1**, 1 (2016).

181. Hu, Z. *et al.* A cloning and expression system to probe T-cell receptor specificity and assess functional avidity to neoantigens. *Blood* **132**, 1911–1921 (2018).

182. Heemskerk, M. H. M. *et al.* Redirection of antileukemic reactivity of peripheral T lymphocytes using gene transfer of minor histocompatibility antigen HA-2-specific T-cell receptor complexes expressing a conserved alpha joining region. *Blood* **102**, (2003).

183. Simon, P. *et al.* Functional TCR Retrieval from Single Antigen-Specific Human T Cells Reveals Multiple Novel Epitopes. *Cancer Immunol. Res.* **2**, 1230–1244 (2014).

184. Kobayashi, E. *et al.* A new cloning and expression system yields and validates TCRs from blood lymphocytes of patients with cancer within 10 days. *Nat. Med.* **19**, 1542–6 (2013).

185. Klenerman, P., Cerundolo, V. & Dunbar, P. R. Tracking T cells with tetramers: New tales from new tools. *Nat. Rev. Immunol.* **2**, 263–272 (2002).

186. Wolf, K. *et al.* Identifying and Tracking Low-Frequency Virus-Specific TCR Clonotypes Using High-

Throughput Sequencing. *Cell Rep.* **25**, 2369-2378.e4 (2018).

187. Agata, Y. *et al.* Expression of the PD-1 antigen on the surface of stimulated mouse T and B lymphocytes. *Int. Immunol.* **8**, 765–72 (1996).

188. Hutloff, A. *et al.* ICOS is an inducible T-cell co-stimulator structurally and functionally related to CD28. *Nature* **397**, 263–266 (1999).

189. Beier, K. C. *et al.* Induction, binding specificity and function of human ICOS. *Eur. J. Immunol.* **30**, 3707–3717 (2000).

190. Baron, V. *et al.* The repertoires of circulating human CD8+ central and effector memory T cell subsets are largely distinct. *Immunity* **18**, 193–204 (2003).

191. de Greef, P. C. *et al.* The naive T-cell receptor repertoire has an extremely broad distribution of clone sizes. *Elife* **9**, e49900 (2020).

192. Chu, N. D. *et al.* Longitudinal immunosequencing in healthy people reveals persistent T cell receptors rich in highly public receptors. *BMC Immunol.* **20**, (2019).

193. Neller, M. A., Burrows, J. M., Rist, M. J., Miles, J. J. & Burrows, S. R. High Frequency of Herpesvirus-Specific Clonotypes in the Human T Cell Repertoire Can Remain Stable over Decades with Minimal Turnover. *J. Virol.* **87**, 697–700 (2013).

194. Miles, J. J. *et al.* T-cell grit: Large clonal expansions of virus-specific CD8+ T cells can dominate in the peripheral circulation for at least 18 years. *Blood* **106**, 4412–4413 (2005).

195. van Bockel, D. J. *et al.* Persistent Survival of Prevalent Clonotypes within an Immunodominant HIV Gag-Specific CD8 + T Cell Response . *J. Immunol.* **186**, 359–371 (2011).

196. Bagaev, D. V. *et al.* VDJdb in 2019: database extension, new analysis infrastructure and a T-cell receptor motif compendium. *Nucleic Acids Res.* **48**, D1057–D1062 (2020).

197. Wherry, E. J. & Kurachi, M. Molecular and cellular insights into T cell exhaustion. *Nat. Rev. Immunol.* **15**, 486–499 (2015).

198. Trautmann, L. *et al.* Upregulation of PD-1 expression on HIV-specific CD8+ T cells leads to reversible immune dysfunction. *Nat. Med.* **12**, 1198–1202 (2006).

199. Day, C. L. *et al.* PD-1 expression on HIV-specific T cells is associated with T-cell exhaustion and disease progression. *Nature* **443**, 350–354 (2006).

200. Petrovas, C. *et al.* PD-1 is a regulator of virus-specific CD8+ T cell survival in HIV infection. *J. Exp. Med.* **203**, 2281–2292 (2006).

201. Urbani, S. *et al.* PD-1 Expression in Acute Hepatitis C Virus (HCV) Infection Is Associated with HCV-Specific CD8 Exhaustion. *J. Virol.* **80**, 11398–11403 (2006).

202. Radziewicz, H. *et al.* Liver-Infiltrating Lymphocytes in Chronic Human Hepatitis C Virus Infection Display an Exhausted Phenotype with High Levels of PD-1 and Low Levels of CD127 Expression. *J. Virol.* **81**, 2545–2553 (2007).

203. Greenough, T. C. *et al.* Programmed death-1 expression on epstein barr virus specific CD8+ T Cells varies by stage of infection, epitope specificity, and T-cell receptor usage. *PLoS One* **5**, e12926 (2010).

204. Ahmadzadeh, M. *et al.* Tumor antigen-specific CD8 T cells infiltrating the tumor express high levels of PD-1 and are functionally impaired. *Blood* **114**, 1537–1544 (2009).

205. Hertoghs, K. M. L. *et al.* Molecular profiling of cytomegalovirus-induced human CD8+ T cell differentiation. *J. Clin. Invest.* **120**, 4077–4090 (2010).

206. Glanville, J. *et al.* Identifying specificity groups in the T cell receptor repertoire. *Nature* **547**, 94–98 (2017).

207. Dash, P. *et al.* Quantifiable predictive features define epitope-specific T cell receptor repertoires. *Nature* **547**, 89–93 (2017).

208. Hill, D. L. *et al.* The adjuvant GLA-SE promotes human Tfh cell expansion and emergence of public TCRβ clonotypes. *J. Exp. Med.* **216**, 1857–1873 (2019).

209. Brenna, E. *et al.* CD4+ T Follicular Helper Cells in Human Tonsils and Blood Are Clonally Convergent but Divergent from Non-Tfh CD4+ Cells. *Cell Rep.* **30**, 137-152.e5 (2020).

210. Herati, R. S. *et al.* Successive annual influenza vaccination induces a recurrent oligoclonotypic memory response in circulating T follicular helper cells. *Sci. Immunol.* **2**, (2017).

211. Schodin, B. A., Tsomides, T. J. & Kranz, D. M. Correlation between the number of T cell receptors required for T cell activation and TCR-ligand affinity. *Immunity* **5**, 137–146 (1996).

212. Viola, A. & Lanzavecchia, A. T cell activation determined by T cell receptor number and tunable thresholds. *Science (80-.).* **273**, 104–106 (1996).

213. Lanzavecchia, A., Iezzi, G. & Viola, A. From TCR engagement to T cell activation: A kinetic view of T cell behavior. *Cell* **96**, 1–4 (1999).

214. Murugan, A., Mora, T., Walczak, A. M. & Callan, C. G. Statistical inference of the generation probability of T-cell receptors from sequence repertoires. *Proc. Natl. Acad. Sci. U. S. A.* **109**, 16161–16166 (2012).

215. Venturi, V. *et al.* TCR β-Chain Sharing in Human CD8 + T Cell Responses to Cytomegalovirus and EBV . *J. Immunol.* **181**, 7853–7862 (2008).

216. Quigley, M. F. *et al.* Convergent recombination shapes the clonotypic landscape of the naïve T-cell repertoire. *Proc. Natl. Acad. Sci. U. S. A.* **107**, 19414–19419 (2010).

217. Elhanati, Y., Sethna, Z., Callan, C. G., Mora, T. & Walczak, A. M. Predicting the spectrum of TCR repertoire sharing with a data-driven model of recombination. *Immunol. Rev.* **284**, 167–179 (2018).

218. Havenar-Daughton, C. *et al.* Normal human lymph node T follicular helper cells and germinal center B cells accessed via fine needle aspirations. *J. Immunol. Methods* **479**, 112746 (2020).

219. Ke, Y. & Kapp, J. A. Exogenous antigens gain access to the major histocompatibility complex class I processing pathway in B cells by receptor-mediated uptake. *J. Exp. Med.* **184**, 1179–1184 (1996).

220. Neafsey, D. E. *et al.* Genetic diversity and protective efficacy of the RTS,S/AS01 malaria vaccine. *N. Engl. J. Med.* **373**, 2025–2037 (2015).

8 Supplement

8.1 Supplementary Figures

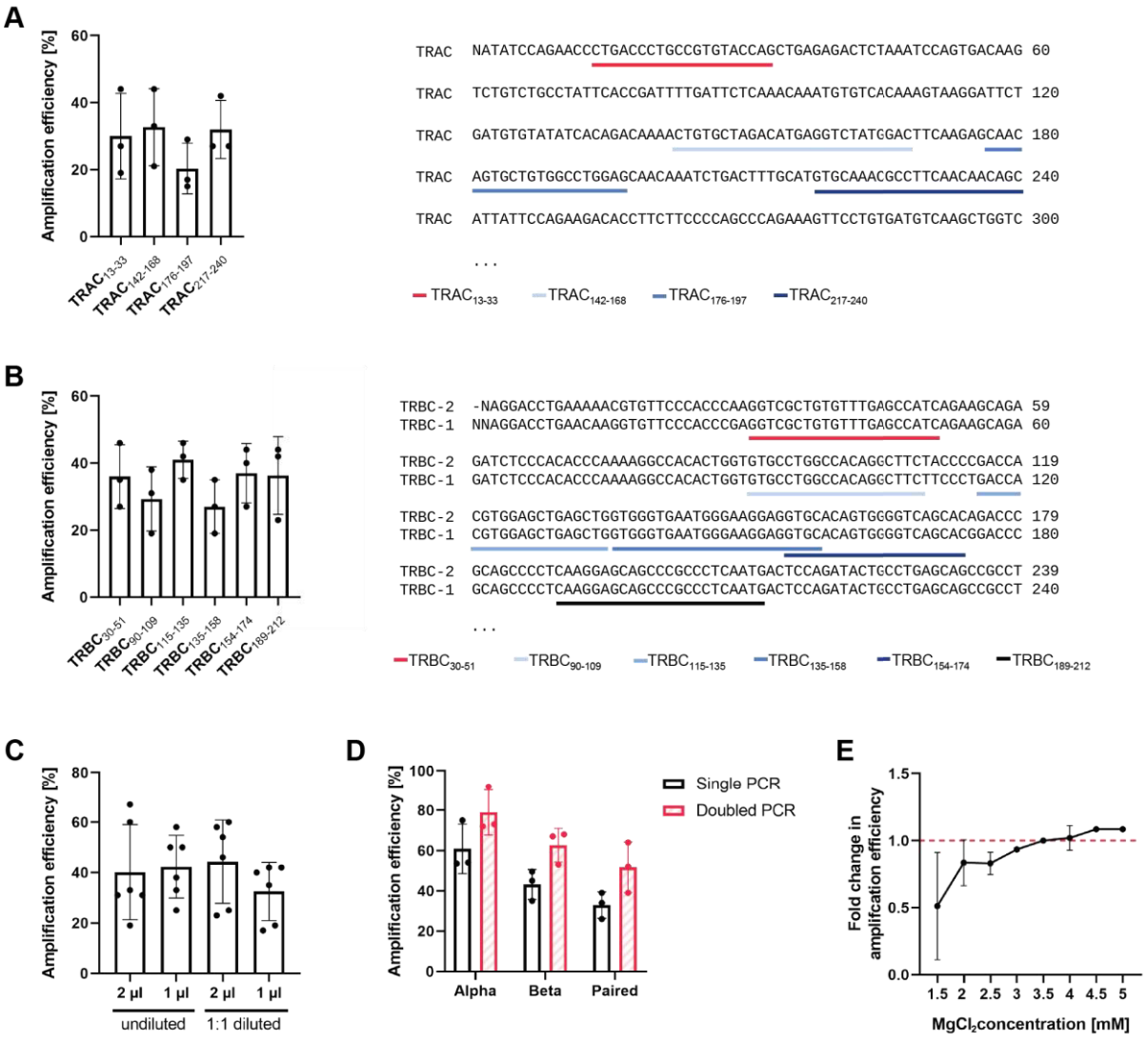

Supplementary Figure 1: Optimization of the human TCR alpha and beta gene amplification protocol. Amplification efficiency of TCRs amplified in two subsequent PCRs from single CD4⁺ T cells sorted in 384-well plates. (A,B) Different reverse primers tested for the first PCR of TCR alpha (A) and beta genes (B). The positions of the reverse primers in the C segment gene are shown in the right panel. The alpha reverse primer $TRAC_{217\text{-}240}$ and the beta reverse primer $TRBC_{115\text{-}135}$ were used in all subsequent experiments. (C) To titrate the minimal cDNA amount required as template for the first PCR, the TCR beta amplification efficiency was determined after serial dilution of the cDNA. (D) TCR alpha and beta amplification efficiencies quantified after performing single or doubled first PCRs per chain. Paired efficiencies quantify cells where both, TCR alpha and beta genes, were amplified. 2 µl of 1:1 diluted cDNA were used as template for the first PCR. (E) To rescue a drop in amplification efficiency observed upon barcoding of the second PCR primers, the magnesium chloride ($MgCl_2$) concentration was titrated. The fold change in alpha gene amplification efficiency achieved with barcoded primers as compared to non-barcoded primers (red dashed line) was calculated for different $MgCl_2$ concentrations. The mean of two experiments is shown. All subsequent second PCR reactions were performed with 4 mM $MgCl_2$.
(A-D) Each dot represents an individual experiment. (A-C, E) 48 cells per experiment. (D) 96 cells per experiment.

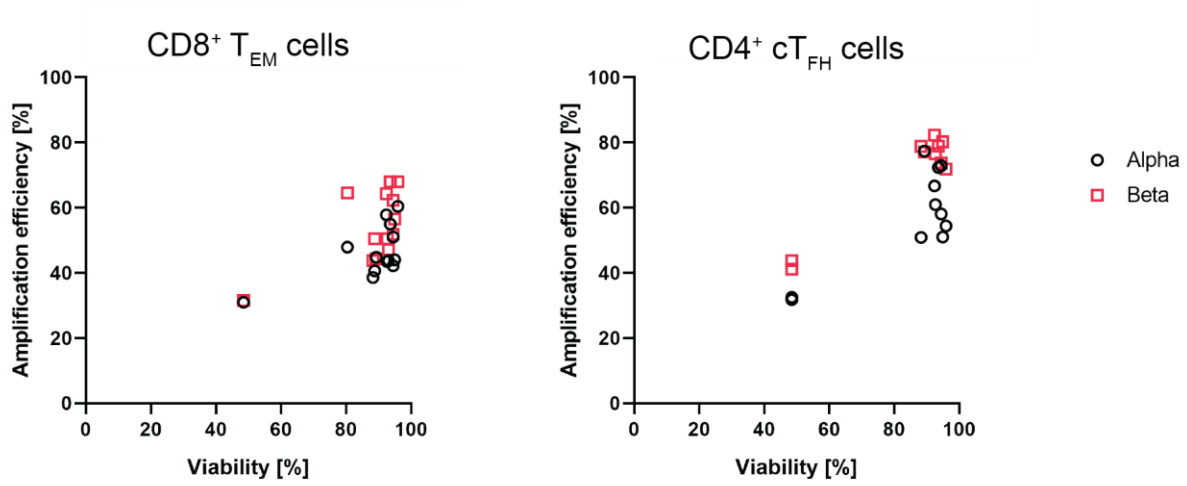

Supplementary Figure 2: Drop in amplification efficiency caused by low viability. The viability was determined by flow cytometry as the frequency of live cells per sample. Of each sample, single, live T cells were sorted and TCR alpha and beta were amplified. Each dot represents an individual sample.
T_{EM} = effector memory T cell; cT_{FH} = circulating T follicular helper cell**.**

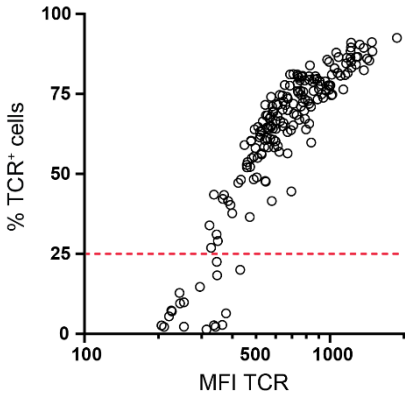

Supplementary Figure 3: Correlation of frequencies of TCR⁺ cells with the level of TCR surface expression. TCR^{neg} Jurkat 76 cells, retrovirally transduced with different TCR clones of unknown specificity, were selected with puromycin and the frequency of TCR^+ cells as well as the TCR expression level (MFI) of these TCR^+ cells were determined by flow cytometry. 192 different TCRs from two independent experiments were analyzed. Each dot represents an individual TCR. Red line: threshold for TCR-expression at 25%. Data were produced jointly with Rebecca Hundsdorfer and Julia Puchan.

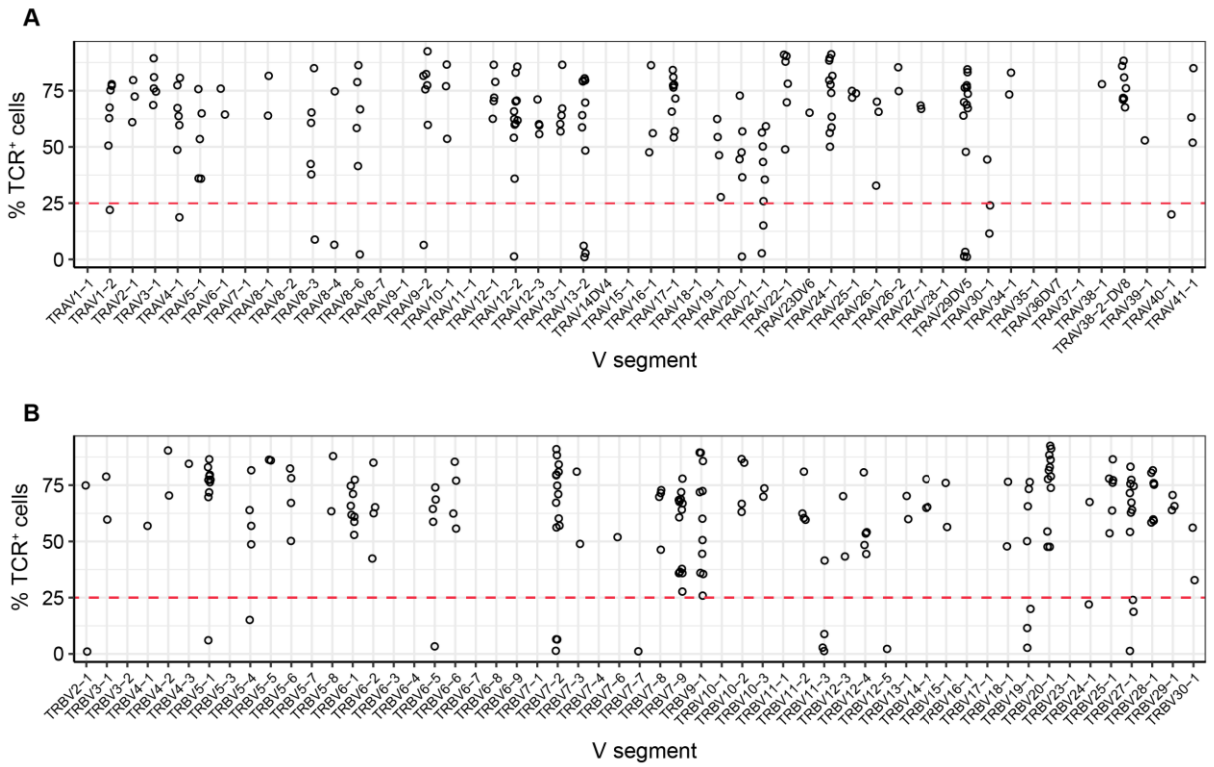

Supplementary Figure 4: TCR expression is independent on TCR alpha and beta V segment usage. TCR^{neg} Jurkat76 T cells were retrovirally transduced with cloned TCRs and selected with puromycin. The frequency of TCR^{+} cells was quantified by flow cytometry and compared to the annotated TCR alpha (A) and beta (B) V segment gene. Each dot represents an individual TCR. Red line: threshold for TCR-expression. 192 TCRs from two independent experiments are shown.

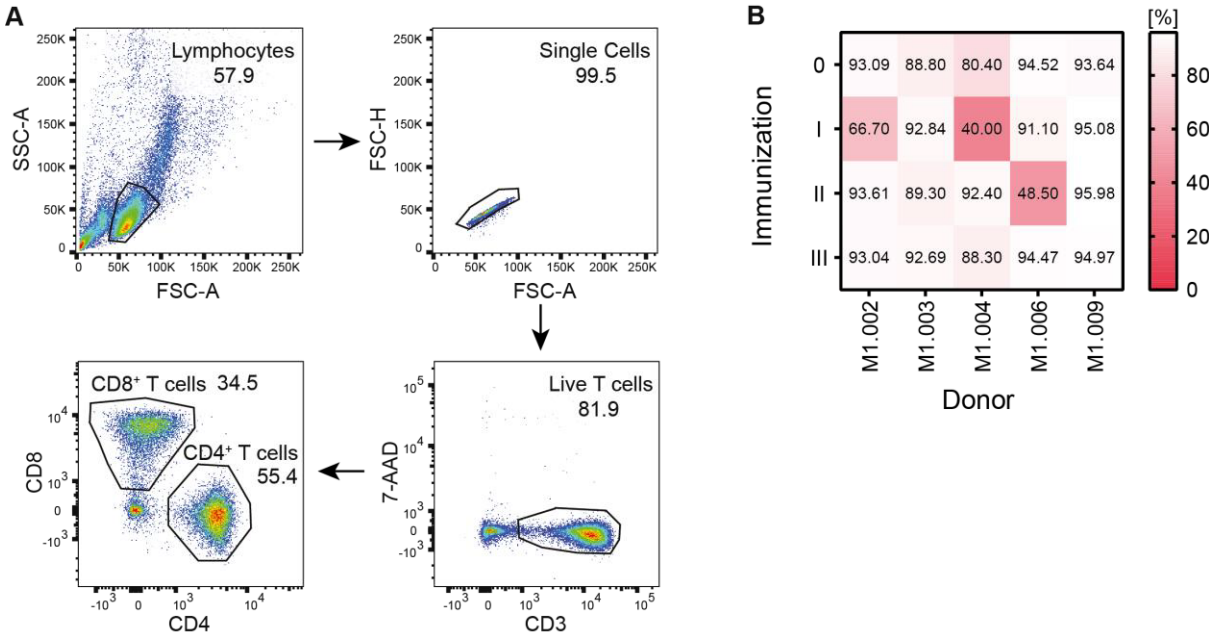

Supplementary Figure 5: Flow cytometric analysis of CD8⁺ and CD4⁺ T cells. (A) Gating strategy for the analysis of single, live CD8⁺ and CD4⁺ T cells. Donor M1.009 at time point III is shown. (B) Viability scores defined by the percentage of all live (7-AAD negative) cells in PBMC samples of five volunteers collected during the malaria immunization trial. Samples with a viability < 50% were excluded from further analysis.

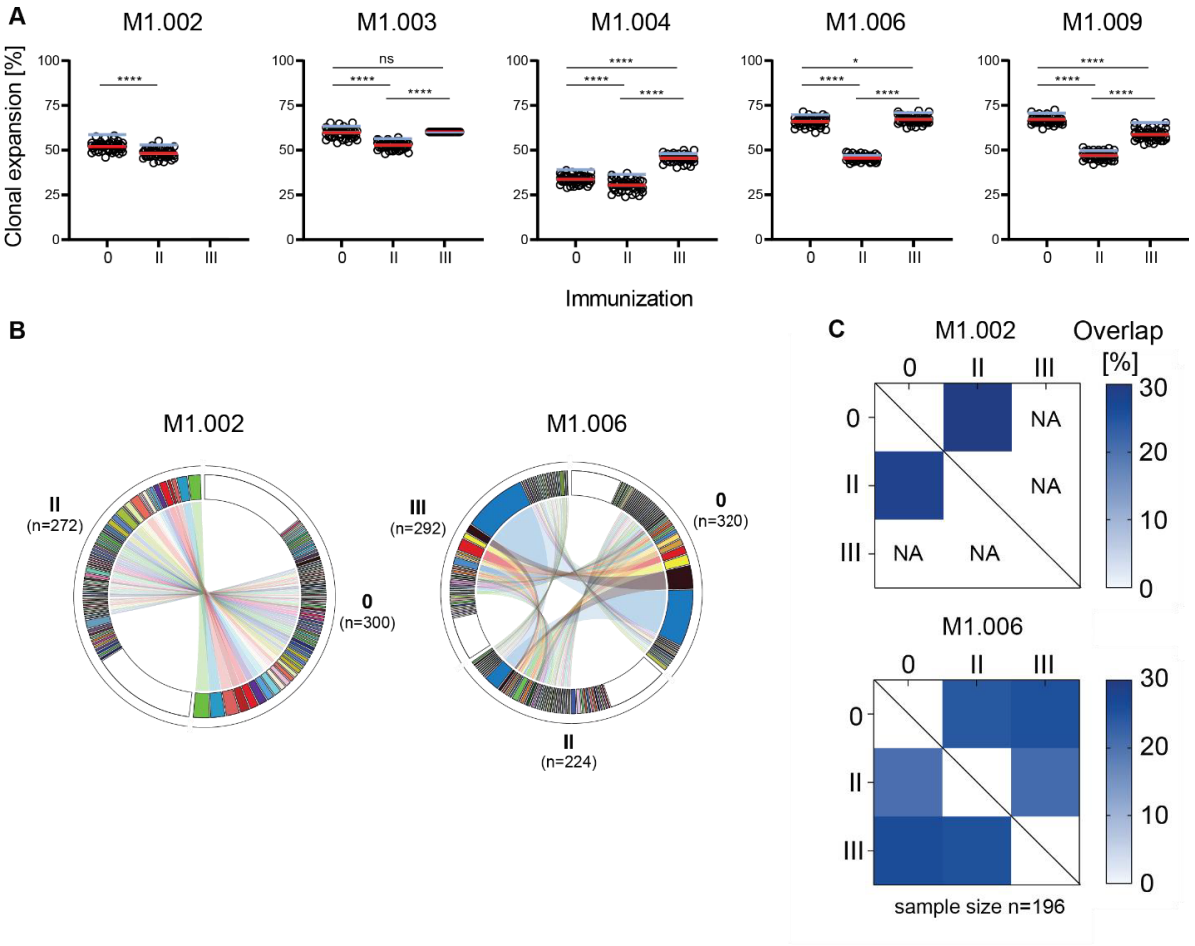

Supplementary Figure 6: Analysis of expanded clones of CD8⁺ T_{EM} cells before and after successive *Pf* RAS immunizations. TCR repertoire analysis of single PD-1⁺ ICOS⁺ CD8⁺ T_{EM} cells. Clones were defined by identical beta CDR3 amino acid sequences. (A) Clonal expansion calculated for 50 random subsamples (n=196). Red line marks the mean, the blue line the degree of clonal expansion observed without subsampling. **** $p < 0.0001$, * $p < 0.05$, ns: non-significant, two-tailed Mann-Whitney test. (B) Circos plots of two donors depicting clonally expanded (colored) and non-expanded (white) T cells. Overlapping clones are connected by lines. (C) Percent of clonal overlap calculated as the mean of 50 random subsamples (n=196). NA marks missing sequence data (M1.002, III).

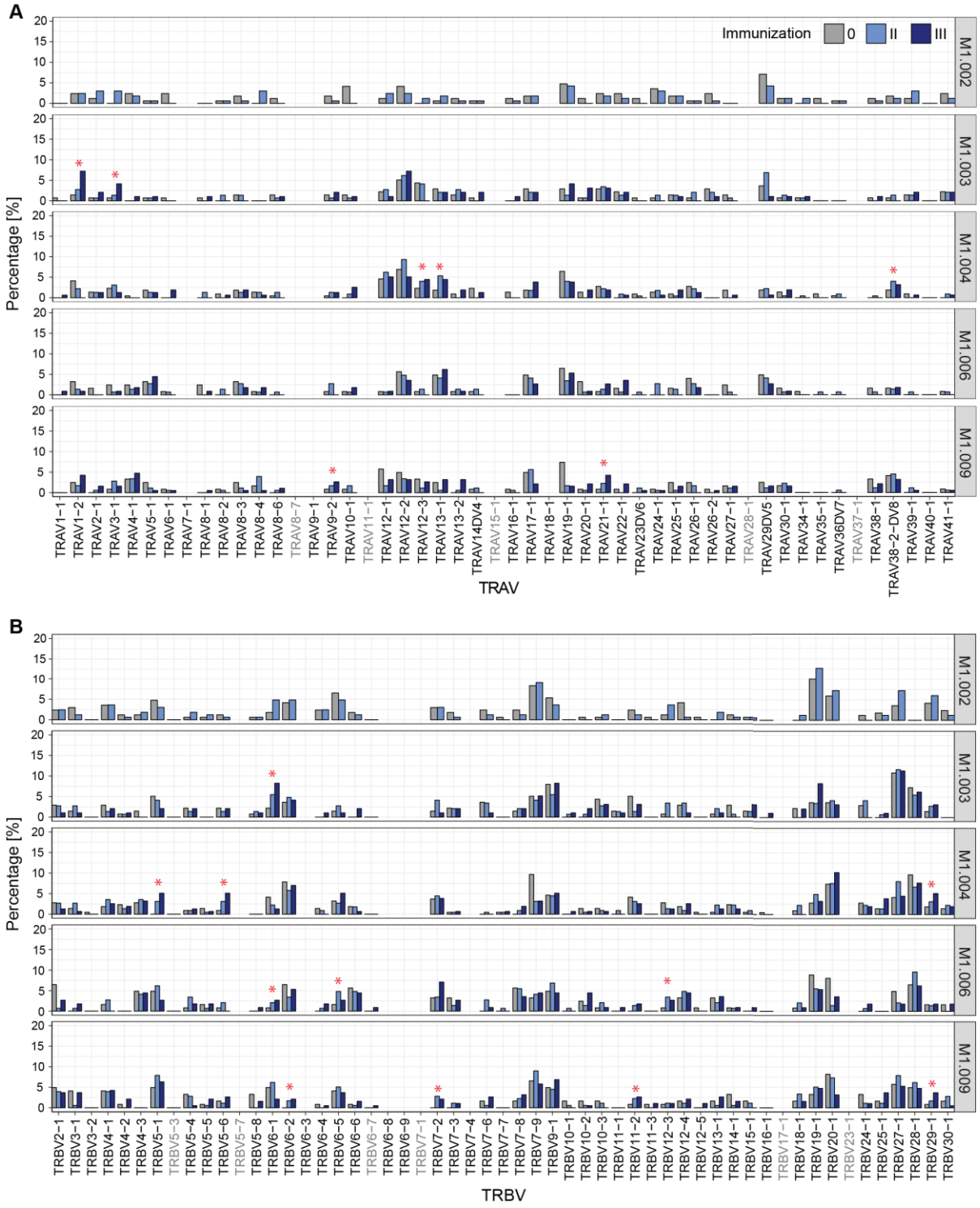

Supplementary Figure 7: Donor-specific changes in TCR segment usage in CD8⁺ T_{EM} cells after immunization. TRAV (A) and TRBV (B) segment usage quantified over time in each donor. Expanded clones were collapsed and only counted once (clonal reduction). Non-functional segments or pseudogenes are marked in grey. For donor M1.002 no sequence data were available after the third immunization (III). Red asterisks mark enriched segments that guided the selection of TCRs for cloning

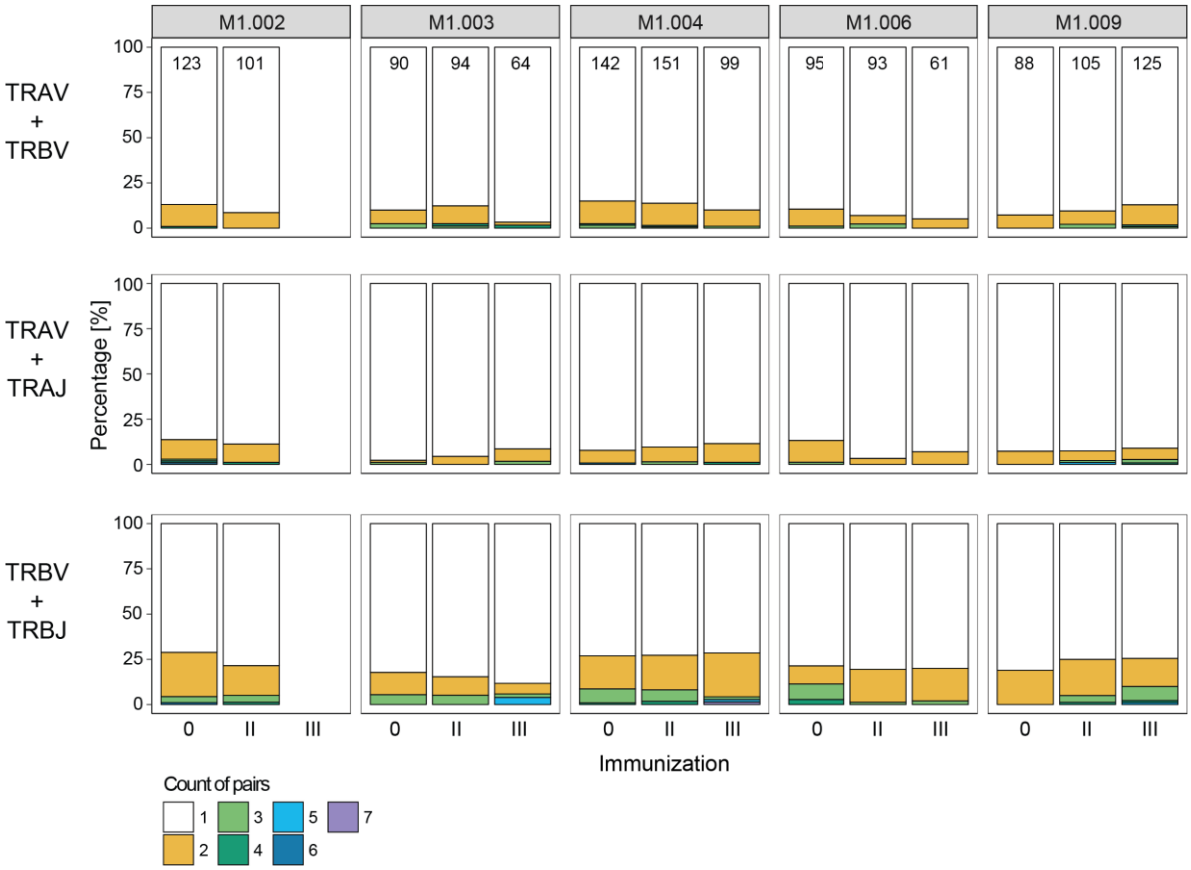

Supplementary Figure 8: Highly diverse pairing of TCR alpha and beta segments in CD8⁺ T_{EM} cells. The combination of TRAV and TRBV segments (A), TRAV and TRAJ segments (B) and TRBV and TRBJ segments in TCRs within the repertoire was quantified after clonal reduction. The percentage of pairs found once (white) or multiple times (colored) is shown to highlight the high diversity of the sequences. The number of sequences per donor and sample are listed in the upper graph.

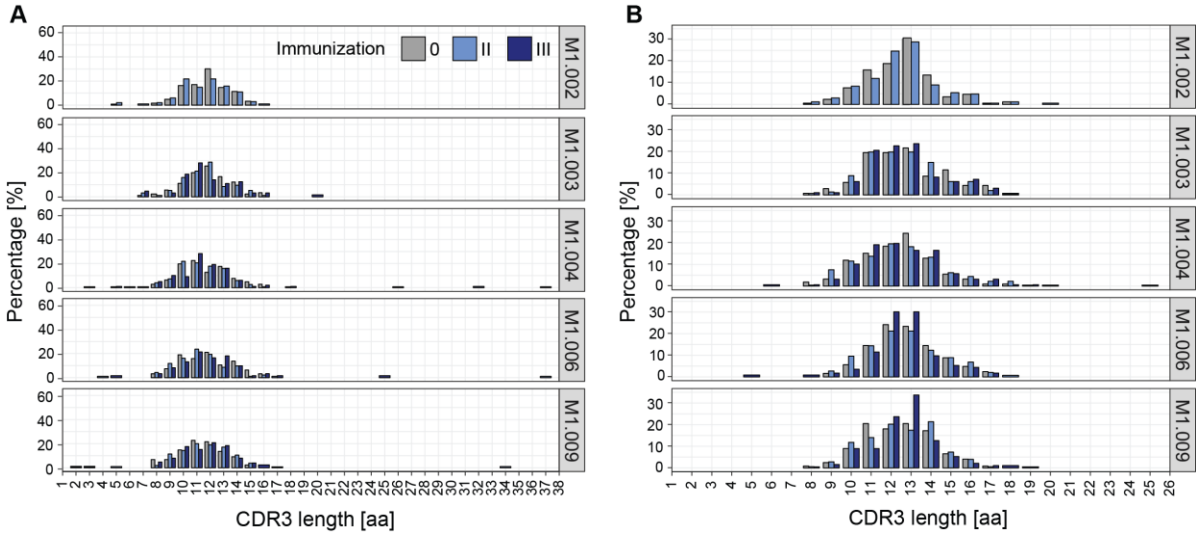

Supplementary Figure 9: CDR3 amino acid length distribution in CD8⁺ T_{EM} cells. The distribution of CDR3 lengths of TCR alpha (A) and beta (B) sequences was quantified after clonal reduction for each donor over time. No sequence data were available for donor M1.002 after the third immunization (III).

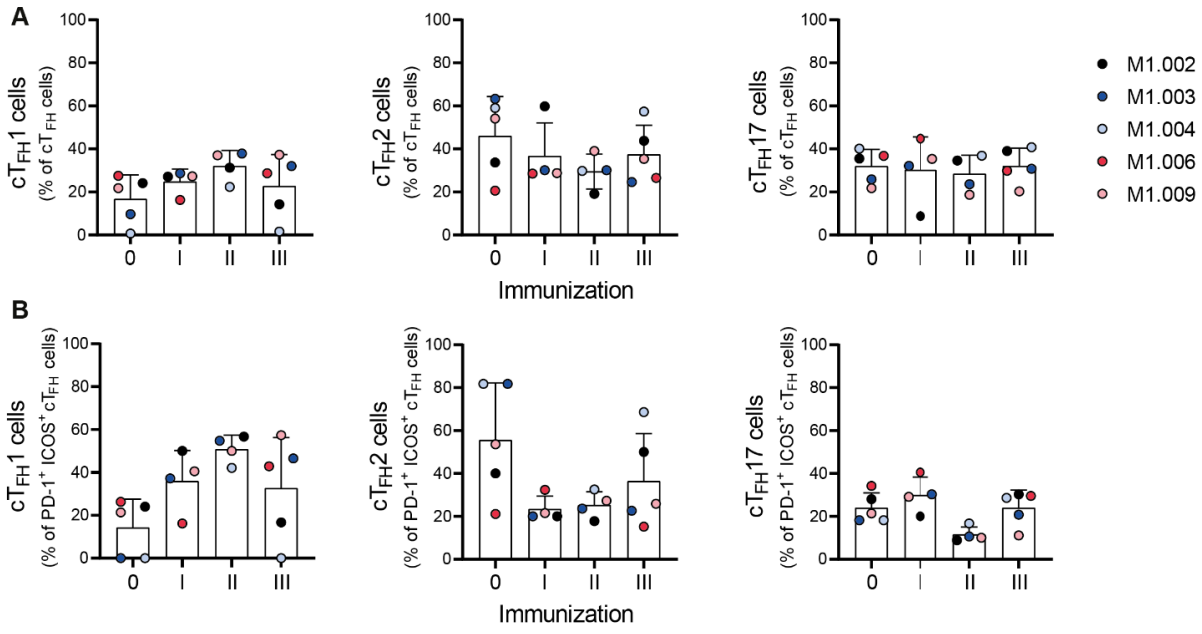

Supplementary Figure 10: Increase of $cT_{FH}1$ cells after successive *Pf* RAS immunizations. (A,B) Flow cytometric quantification of frequencies of $cT_{FH}1$ ($CXCR3^+$ $CCR6^-$), $cT_{FH}2$ ($CXCR3^-$ $CCR6^-$) and $cT_{FH}17$ ($CXCR3^-$ $CCR6^+$) cells among all cT_{FH} cells (A) or activated ($PD\text{-}1^+$ $ICOS^+$) cT_{FH} cells (B) in PBMCs collected from five donors during the *Pf* RAS immunization trial. Bar graphs show the mean and standard deviation, dots mark single donors. Samples M1.004 (I) and M1.006 (II) were excluded from analysis due to low sample quality.

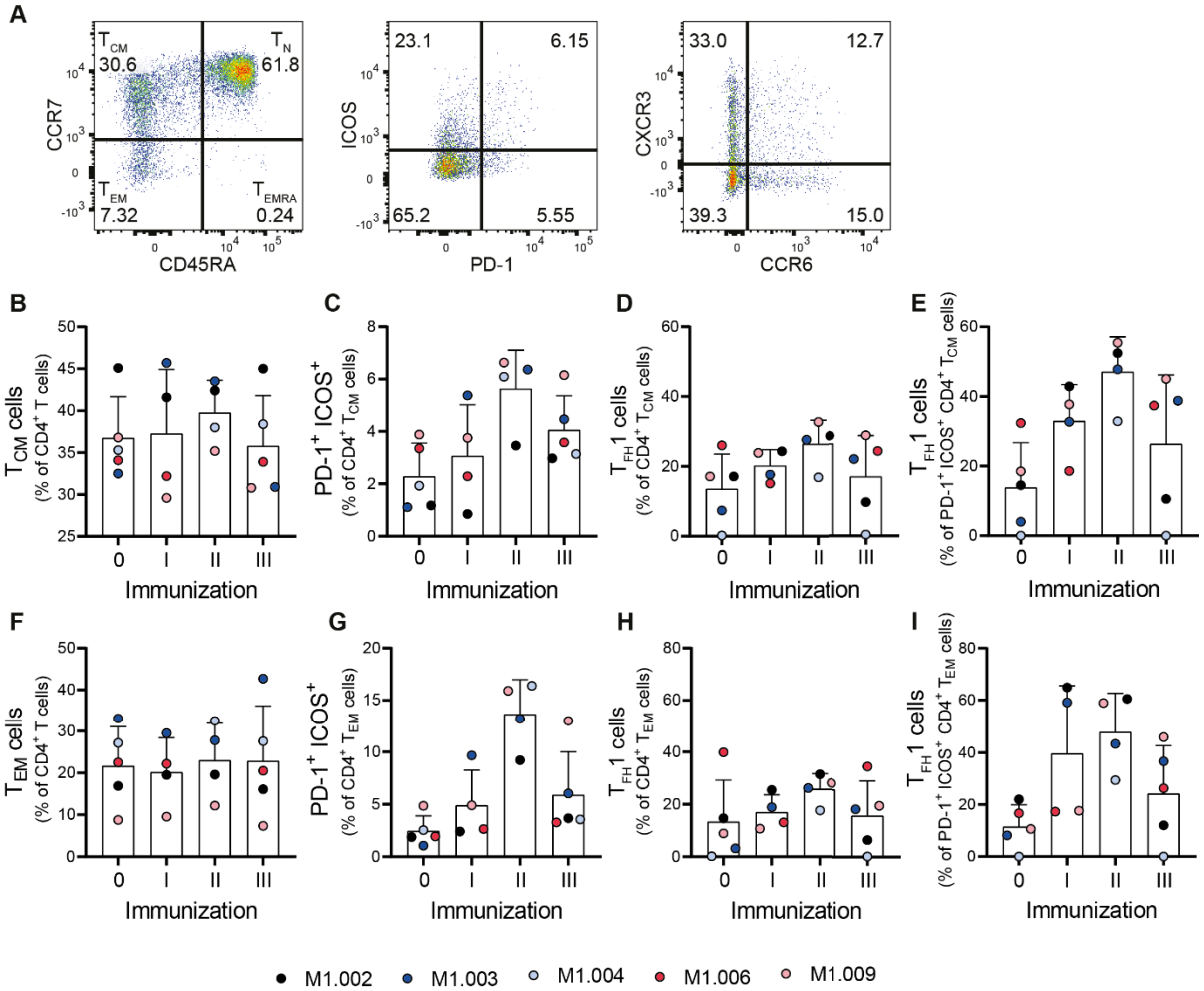

Supplementary Figure 11: CD4⁺ T cell responses to *Pf* RAS immunizations are skewed towards a T_H1 phenotype. (A) Representative gating strategy for the identification of $CD4^+$ T_{CM} cells ($CD45RA^-$ $CCR7^+$) and $CD4^+$ T_{EM} cells ($CD45RA^-$ $CCR7^-$), depicted for donor M1.009 after the third immunization. Cells were pre-gated on single, live $CD4^+$ T cells (for pre-gating see Supplementary Figure 5). T_{CM} and T_{EM} cells were further characterized by their activation status (PD-1 and ICOS) as well as their chemokine receptor profile (CXCR3 and CCR6). The analysis for T_{CM} cells and T_{EM} cells is shown in (B-E) and (F-I), respectively. Frequencies of T_{CM} (B) and T_{EM} cells (F) as well as activated $PD\text{-}1^+$ $ICOS^+$ T_{CM} (C) and T_{EM} (G) were quantified. The increase in frequencies of cells with T_H1 phenotype (CXCR3 expression) during subsequent immunizations was moderate among all T_{CM} (D) and T_{EM} cells (H) and strong among the $PD\text{-}1^+$ $ICOS^+$ T_{CM} (E) and T_{EM} (I) cells.
(B-I) Bar graphs show the mean and standard deviation, dots mark single donors. Samples M1.004 (I) and M1.006 (II) were excluded from analysis due to low sample quality

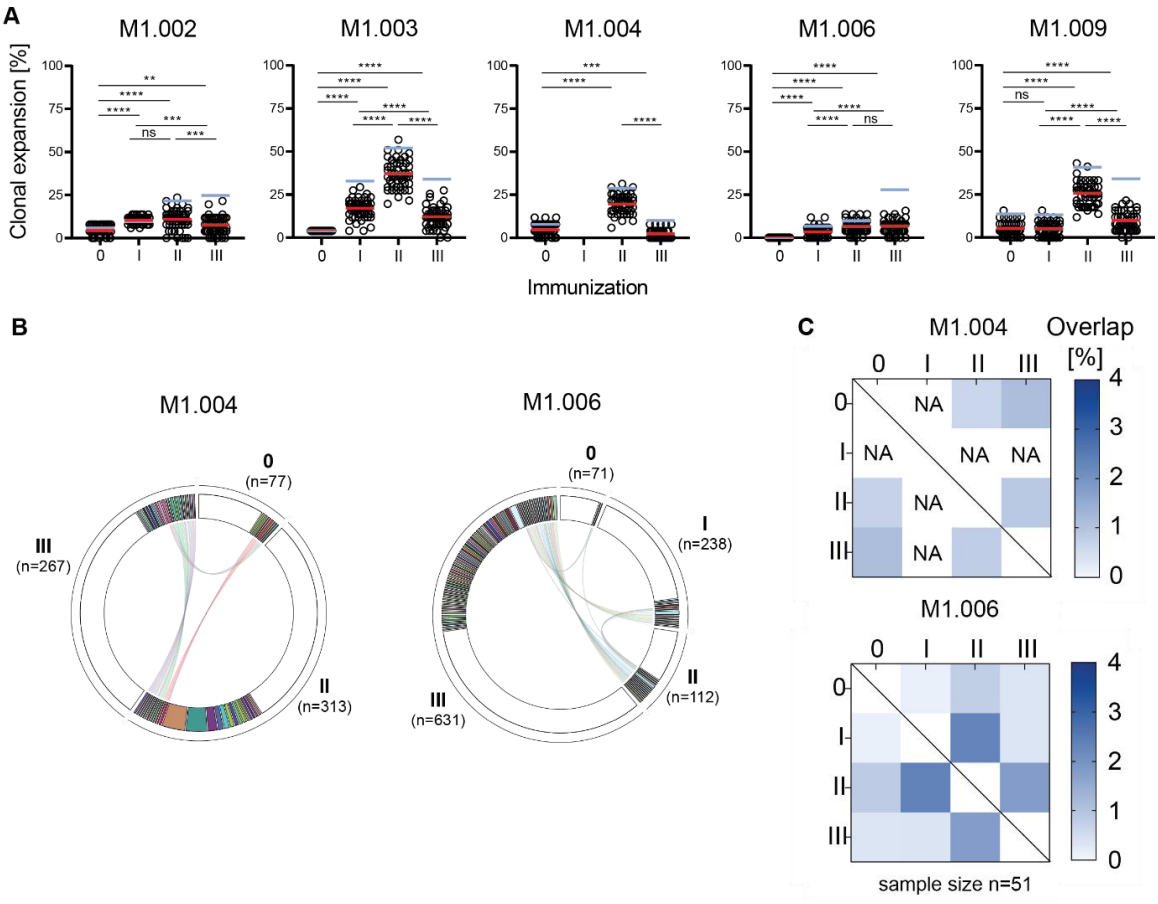

Supplementary Figure 12: Analysis of expanded clones of activated cT_{FH} cells before and after successive *Pf* RAS immunizations. Clones were defined by identical beta CDR3 amino acid sequences. (A) Clonal expansion calculated for 50 random subsamples (n=51). The mean is highlighted with a red line, whereas the degree of clonal expansion without subsampling is marked with a blue line. **** $p < 0.0001$, *** $p < 0.001$, ** $p < 0.01$, ns: non-significant, two-tailed Mann-Whitney test. (B) Circos plots of two donors showing the clonal overlap between pre- and post-immunization samples. Expanded clones are shown in different colors and shared clones were linked by lines. Non-expanded cells are shown in white. (C) Percent overlap calculated as mean of 50 random subsamples (n=51) for two donors. NA marks missing sequence data.

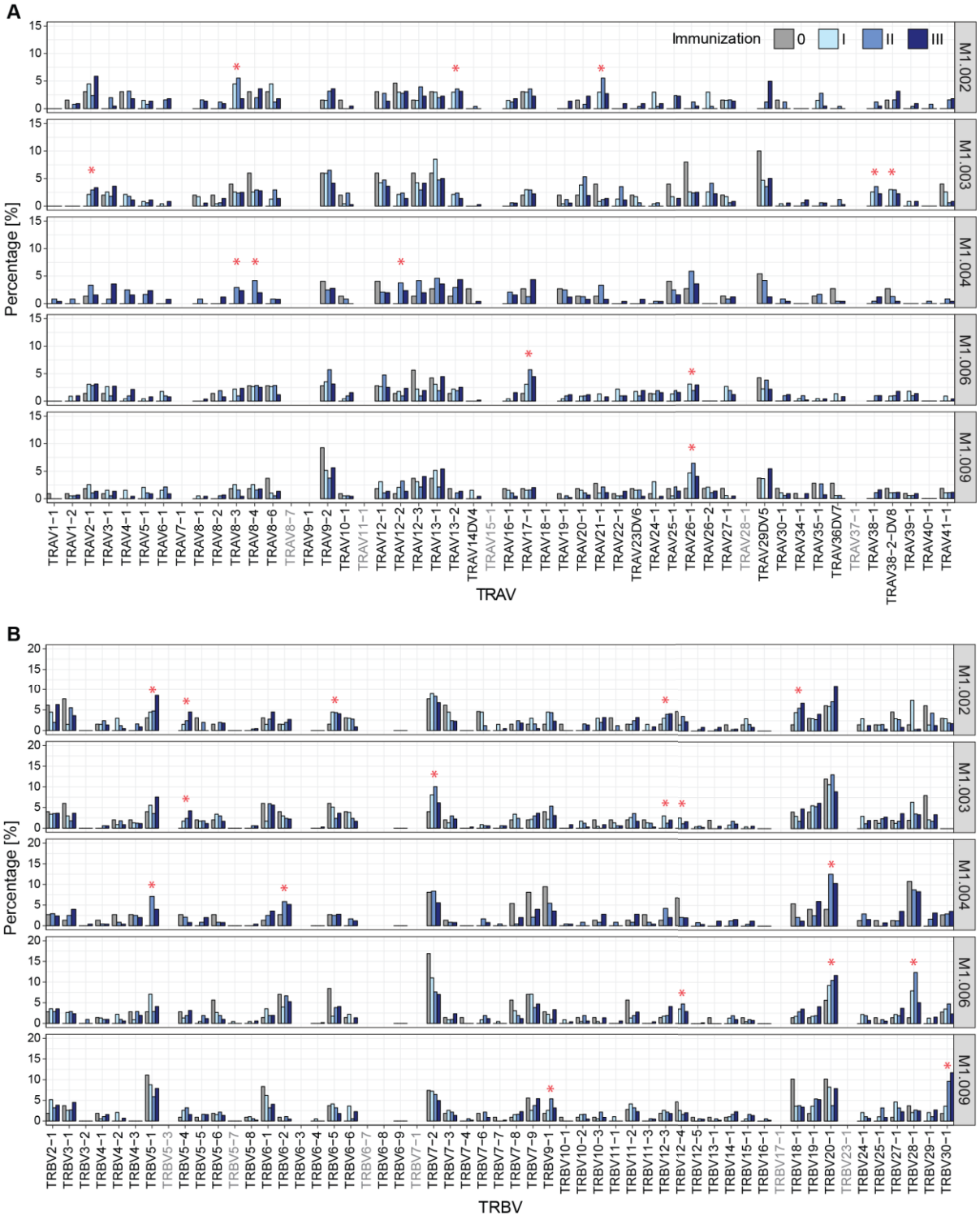

Supplementary Figure 13: Donor-specific changes in TCR V segment usage in cT$_{FH}$ cells after malaria immunization. Quantification of TRAV (A) and TRBV (B) segment usage after clonal reduction. Non-functional segments or pseudogenes are marked in grey. For donor M1.004 no sequence data were available for the first immunization (I). Red asterisks highlight enriched segments that led to the preferential selection of TCRs for cloning.

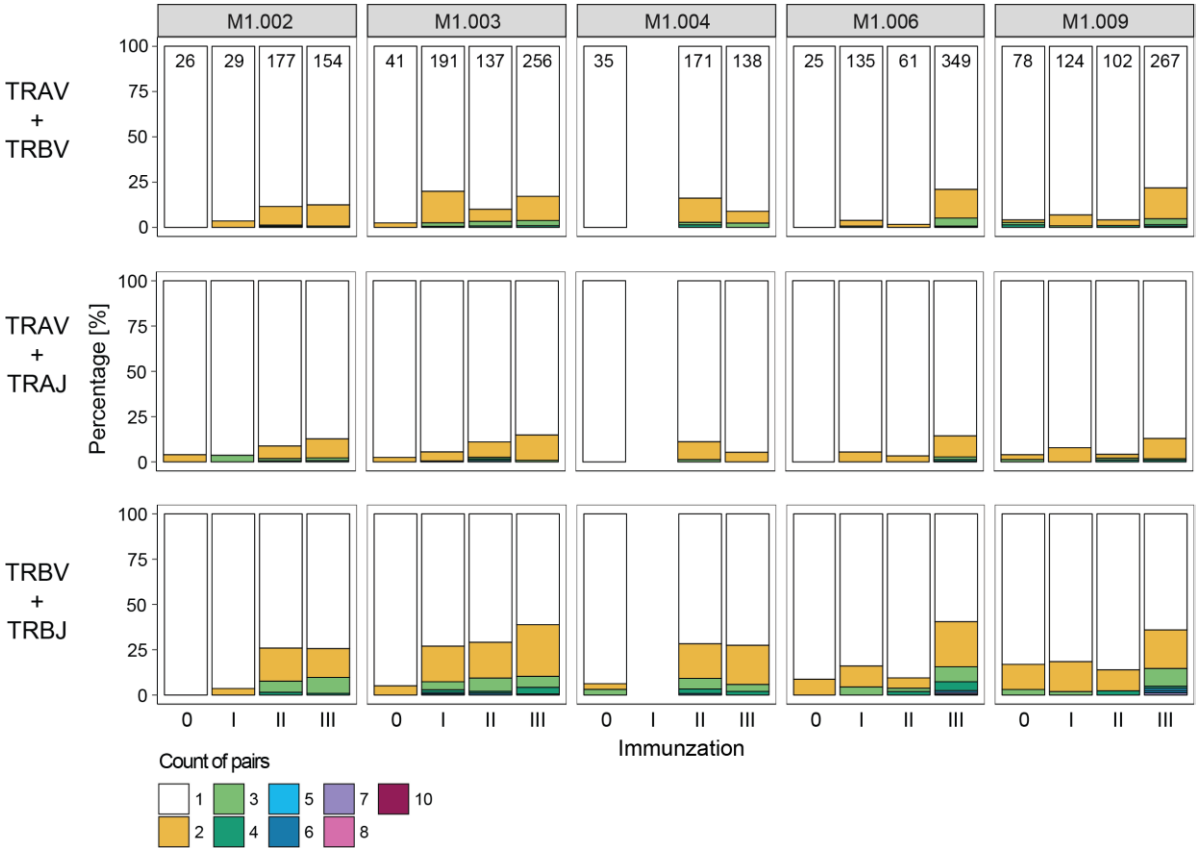

Supplementary Figure 14: Highly diverse pairing of TCR alpha and beta segments in cT_{FH} cells. Quantification of TRAV and TRBV segment pairs (A), TRAV and TRAJ segment pairs (B) and TRBV and TRBJ segment pairs (C) after clonal reduction. The percentage of unique pairs (white) and pairs found more than once (colored) is shown for each donor. The number of sequences per donor and sample are listed in the upper graph.

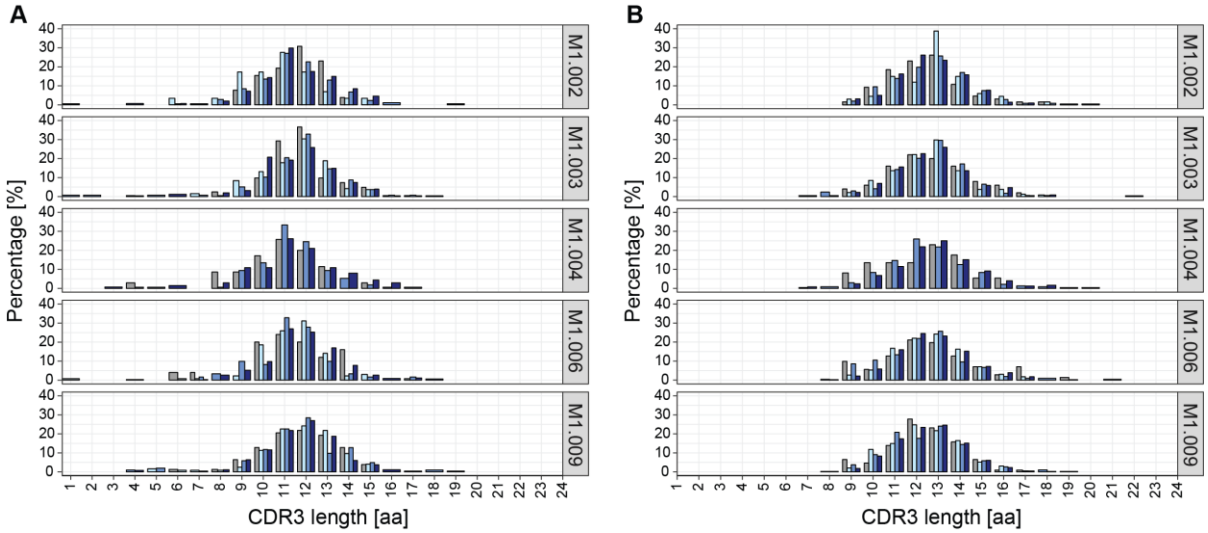

Supplementary Figure 15: Donor-specific changes in CDR3 length distribution in TCRs of cT_{FH} cells after malaria immunization. TCR alpha (A) and beta (B) CDR3 amino acid length distribution after clonal reduction was quantified for each donor over the course of the immunization trial. No sequence data were available for donor M1.004 after the first immunization (I).

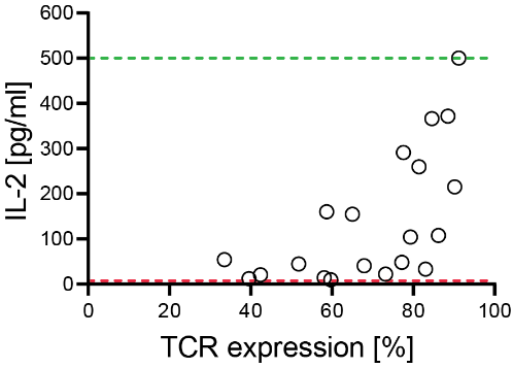

Supplementary Figure 16: Correlation of the IL-2 secretion capacity and the frequency of TCR^+ T cells in each T cell line. The IL-2 secretion of C-CSP-specific T cell lines after 24 h co-culture with C-CSP loaded autologous B cells was measured by IL-2 ELISA. Each dot represents an individual TCR-transgenic T cell line. Pooled data from two independent experiments are shown. Dashed red and green lines indicate the lower and upper detection limit of the assay.

8.2 Expression vector maps

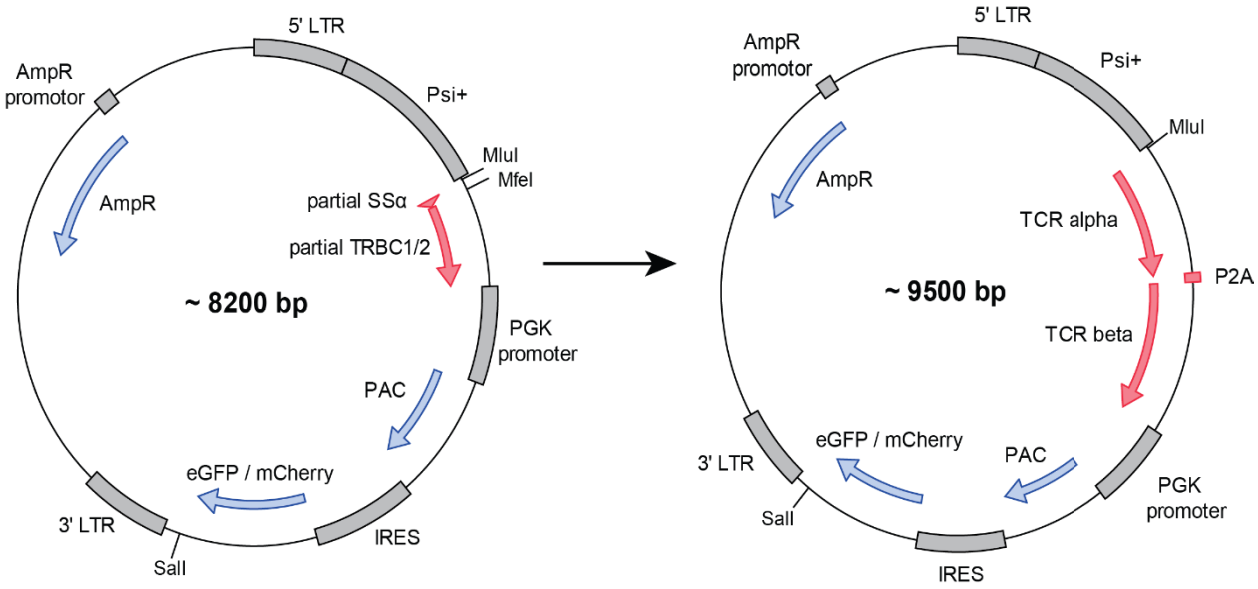

Supplementary Figure 17: Expression vector map for pMSCV-PIG/mC-TRBC1/2. Different versions of the pMSCV-based expression vector contain either the TRBC1 or TRBC2 segment combined with the fluorescent protein eGFP (pMSCV-PIG) or mCherry (pMSCV-PImC). The assembled TCRs are inserted into the expression vector after MfeI digest. The TCR alpha and beta chain are linked with a P2A peptide.
Abbreviations: LTR = long terminal repeats; Psi+ = extended packaging sequence; SSα = TCR alpha signal sequence; PGK = phosphoglycerate kinase 1; PAC = puromycin N-acetyltransferase; IRES = internal ribosomal entry site; GFP = green fluorescent protein; AmpR = ampicillin resistance.

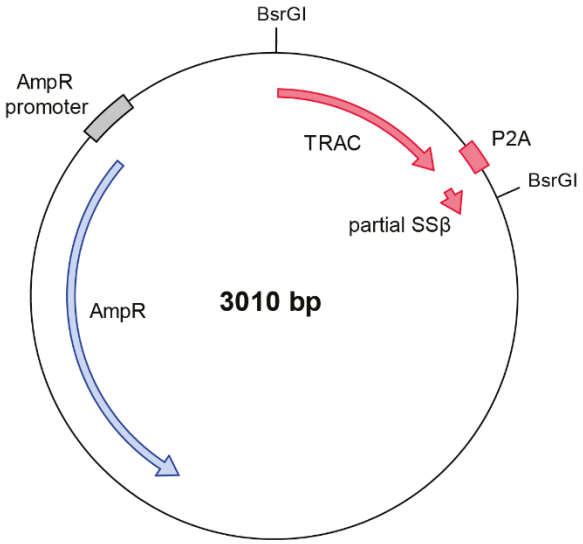

Supplementary Figure 18: Map of the pEX-A128-TRAC-2A-SSb vector containing the linker segment for joining the TCR alpha and beta genes. The vector was purchased from Eurofins Genomics.
Abbreviations: SSβ = TCR beta signal sequence; AmpR = ampicillin resistance.

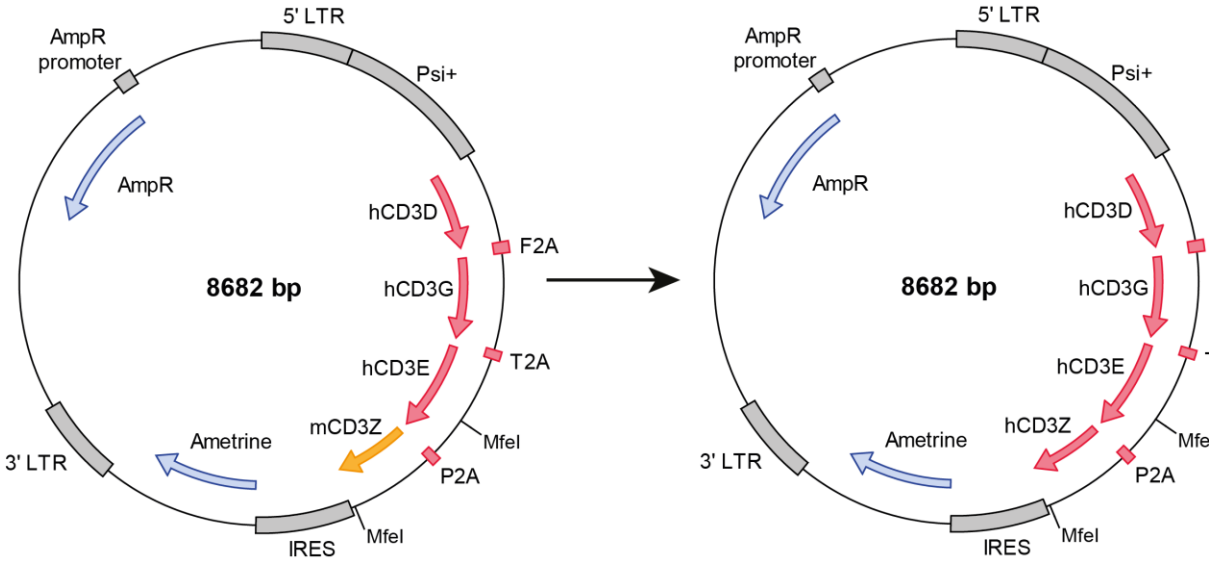

Supplementary Figure 19: Maps of the retroviral expression vectors pMIG-II-CD3-PT (left) and pMIG-II-CD3 (right). The pMIG-II-CD3-PT vector was kindly provided by Dr. Paul Thomas, St. Jude Children's Research Hospital, Memphis, USA. The vector was modified by the replacement of the murine CD3Z gene with the human CD3Z gene. All CD3 genes were linked by 2A peptides.
Abbreviations: LTR = long terminal repeats; Psi+ = extended packaging sequence; IRES = internal ribosomal entry site; AmpR = ampicillin resistance.

8.3 Supplementary Tables

Supplementary Table 1: Number of paired TCR sequences and cloned TCRs from activated CD8 T_{EM} cells. TCRs were analyzed before immunization (0) and after immunization II and III in each donor.

Donors	Paired TCR sequences			Cloned TCRs
	0	II	III	
M1.002	202	147	0	0
M1.003	166	138	141	14
M1.004	191	190	141	24
M1.006	205	123	137	20
M1.009	250	198	271	32

Supplementary Table 2: TCR sequence features and reactivity of TCRs cloned from activated $CD8^+$ T_{EM} cells. The TCR cloning and screening was performed together with Sandro Hoffmann.

TCR	Donor	Immunization	TRBV	TRBJ	TRBC	CDR3β length	TRAV	TRAJ	CDR3α length	Clone size	TCR expression [%]	CD8 peptide pool
T08M03x0018	M1.003	III	6-1	2-7	2	11	12-2	5	12	2	65.8	Not reactive
T08M03x0085	M1.003	III	12-4	2-1	2	10	5-1	22	14	2	53.5	Not reactive
T08M03x0132	M1.003	III	9-1	2-5	2	16	1-2	13	12	2	50.6	Not reactive
T08M03x0173	M1.003	III	7-9	2-1	2	11	12-2	15	10	3	63.5	Not reactive
T08M03x0244	M1.003	III	28-1	1-2	1	12	1-2	20	10	3	75.2	Not reactive
T08M03x0317	M1.003	III	10-3	2-7	2	12	16-1	56	11	2		
T08M03x0352	M1.003	III	6-1	2-7	2	11	12-2	5	13	1	61.8	Not reactive
T13M03x3464	M1.003	II	7-2	1-5	1	13	39-1	48	12	2		
T13M03x3498	M1.003	II	6-2	1-1	1	11	12-3	6	12	2		
T13M03x3622	M1.003	II	5-8	2-2	2	12	24-1	47	10	1	63.4	Not reactive
T13M03x3628	M1.003	II	11-2	1-1	1	10	3-1	34	13	1	81	Not reactive
T13M03x3647	M1.003	II	12-3	1-5	1	15	21-1	15	11	2	43.3	Not reactive
T13M03x3684	M1.003	II	6-5	2-3	2	11	29DV5	7	9	3	3.35	
T13M03x3700	M1.003	II	2-1	2-2	2	11	13-2	34	13	1	1.04	
T13M03x3714	M1.003	II	7-9	2-5	2	11	5-1	4	10	1	35.9	Not reactive
T13M03x3793	M1.003	II	27-1	1-3	1	12	12-2	32	13	3	1.31	
T13M03x3837	M1.003	II	7-6	1-4	1	13	41-1	43	10	3	51.9	Not reactive
T08M04x3841	M1.004	III	20-1	2-7	2	18	19-1	23	11	5	54.4	Not reactive
T08M04x3935	M1.004	III	6-2	2-1	2	11	8-3	54	11	5	42.4	Not reactive
T08M04x3942	M1.004	III	7-9	2-5	2	12	19-1	30	13	2	27.7	Not reactive
T08M04x3978	M1.004	III	11-2	2-1	2	10	12-2	43	8	3	60.4	Not reactive
T08M04x4012	M1.004	III	6-6	2-1	2	14	12-3	15	9	2	55.7	Not reactive
T08M04x4013	M1.004	III	25-1	1-6	1	11	38-2-DV8	54	11	2	76.1	Not reactive

T08M04x4033	M1.004	III	27-1	2-7	2	10	30-1	57	14	2	24	Not reactive
T08M04x4057	M1.004	III	5-1	2-2	2	13	17-1	22	13	1	77.3	Not reactive
T08M04x4059	M1.004	III	5-6	1-2	1	11	13-1	36	10	2	67.1	Not reactive
T08M04x4069	M1.004	III	4-2	2-7	2	13	12-1	5	11	3	70.4	Not reactive
T08M04x4189	M1.004	III	20-1	2-5	2	9	20-1	33	11	4	47.6	Not reactive
T13M04x1157	M1.004	II	29-1	1-2	1	10	12-2	31	10	1	70.6	Not reactive
T13M04x1173	M1.004	II	27-1	2-7	2	12	38-2-DV8	30	12	1	71.5	Not reactive
T13M04x1210	M1.004	II	27-1	1-1	1	13	1-2	20	11	4	62.8	Not reactive
T13M04x1211	M1.004	II	5-6	1-5	1	12	22-1	38	11	6	78.1	Not reactive
T13M04x1213	M1.004	II	12-4	2-7	2	12	30-1	48	13	9	44.4	Not reactive
T13M04x1214	M1.004	II	30-1	2-1	2	10	26-1	17	12	6	32.8	Not reactive
T13M04x1261	M1.004	II	7-2	2-3	2	17	24-1	13	13	6	56.2	Not reactive
T13M04x1297	M1.004	II	27-1	2-1	2	13	13-1	6	13	1	64	Not reactive
T13M04x1314	M1.004	II	9-1	2-2	2	14	12-3	12	11	3	60.1	Not reactive
T13M04x1369	M1.004	II	5-1	2-2	2	15	13-1	13	10	3		
T13M04x1418	M1.004	II	6-2	2-7	2	9	12-1	39	9	1	62.5	Not reactive
T13M04x1476	M1.004	II	13-1	2-7	2	11	12-2	23	10	2	59.9	Not reactive
T13M04x1507	M1.004	II	25-1	2-7	2	12	10-1	18	13	3	53.6	Not reactive
T13M04x1533	M1.004	II	5-1	2-7	2	11	38-2-DV8	28	15	5	71.8	Not reactive
T08M06x3759	M1.006	III	7-8	2-7	2	13	17-1	32	14	3	71.5	Not reactive
T09M06x1369	M1.006	III	7-8	2-5	2	13	19-1	42	16	2	46.3	Not reactive
T09M06x1379	M1.006	III	7-9	2-7	2	11	8-3	43	12	2	37.8	Not reactive
T09M06x1420	M1.006	III	5-4	2-7	2	12	4-1	39	11	1	48.7	Not reactive
T09M06x1508	M1.006	III	12-4	2-2	2	13	13-2	6	10	3	48.4	Not reactive
T09M06x1527	M1.006	III	6-6	2-5	2	13	19-1	52	10	1	62.4	Not reactive
T13M06x0778	M1.006	II	10-3	1-5	1	10	29DV5	21	10	2	69.9	Not reactive
T13M06x0823	M1.006	II	10-2	1-1	1	9	8-6	40	11	3	66.7	Not reactive
T13M06x0865	M1.006	II	6-5	1-6	1	14	24-1	47	10	1	58.7	Not reactive
T13M06x0888	M1.006	II	5-4	2-7	2	13	21-1	58	12	1	15.1	Not reactive
T13M06x0896	M1.006	II	7-6	1-5	1	12	8-6	15	12	3		
T13M06x0926	M1.006	II	6-1	1-1	1	13	9-2	21	9	2	77.4	Not reactive
T13M06x0933	M1.006	II	24-1	2-1	2	12	1-2	8	13	3	22	Not reactive
T13M06x2337	M1.006	II	12-3	2-7	2	15	26-1	8	13	1	70.1	Not reactive
T13M06x2378	M1.006	II	28-1	2-7	2	10	8-6	29	11	3	58.4	Not reactive
T13M06x2397	M1.006	II	6-5	1-6	1	17	24-1	32	10	3	74	Not reactive
T13M06x2399	M1.006	II	10-3	1-5	1	12	29DV5	21	10	1	73.6	Not reactive
T13M06x2435	M1.006	II	12-4	2-4	2	12	12-2	10	13	5	54.1	Not reactive
T13M06x2460	M1.006	II	7-9	1-1	1	12	38-2-DV8	49	12	4	67.6	Not reactive
T13M06x2465	M1.006	II	7-7	2-5	2	12	29DV5	16	11	2	1.14	
T13M06x2471	M1.006	II	6-6	1-1	1	12	10-1	49	9	3	77	Not reactive
T08M09x1929	M1.009	III	5-6	2-7	2	18	21-1	48	11	17	50.2	Not reactive
T08M09x1961	M1.009	III	13-1	1-1	1	12	12-2	6	12	5	70.2	Not reactive
T08M09x1982	M1.009	III	27-1	2-1	2	12	4-1	8	12	18	67.3	Not reactive
T08M09x1986	M1.009	III	24-1	2-1	2	13	1-2	31	12	11	67.5	Not reactive
T08M09x1989	M1.009	III	11-3	2-1	2	14	8-3	6	13	4	8.82	Not reactive
T08M09x2018	M1.009	III	9-1	2-1	2	12	5-1	23	11	3	36	Not reactive

T08M09x2020	M1.009	III	5-1	2-1	2	12	13-2	23	9	2	6.05	Not reactive
T08M09x2058	M1.009	III	6-1	1-5	1	12	39-1	58	12	5	52.9	Not reactive
T08M09x2061	M1.009	III	29-1	2-2	2	14	8-1	20	12	2	63.9	Not reactive
T08M09x2064	M1.009	III	6-5	2-2	2	14	3-1	48	12	3	68.6	Not reactive
T08M09x2067	M1.009	III	27-1	1-6	1	10	17-1	57	16	6	54.2	Not reactive
T09M09x1120	M1.009	III	3-1	2-1	2	15	4-1	17	13	4	59.7	Not reactive
T09M09x1940	M1.009	III	25-1	1-4	1	13	1-2	26	12	2	77.9	Not reactive
T09M09x1995	M1.009	III	4-1	2-1	2	13	20-1	38	14	4	56.9	Not reactive
T09M09x2019	M1.009	III	27-1	2-1	2	12	9-2	52	14	4	75.6	Not reactive
T09M09x2022	M1.009	III	7-2	2-3	2	14	8-4	45	14	1	6.5	Not reactive
T09M09x2089	M1.009	III	11-2	2-7	2	12	12-2	29	8	28	62.4	Not reactive
T09M09x2110	M1.009	III	19-1	2-7	2	13	24-1	27	11	5	50.1	Not reactive
T09M09x2174	M1.009	III	11-2	2-7	2	15	12-3	17	11	3	59.6	Not reactive
T09M09x2201	M1.009	III	14-1	2-1	2	13	8-3	28	13	15	65.3	Not reactive
T09M09x2204	M1.009	III	19-1	2-2	2	14	30-1	29	10	2	11.5	Not reactive
T09M09x2211	M1.009	III	9-1	2-1	2	13	21-1	43	10	3	35.5	Not reactive
T09M09x2213	M1.009	III	11-2	2-7	2	13	9-2	48	13	4		
T09M09x2246	M1.009	III	25-1	1-4	1	13	1-2	26	12	7	77.2	Not reactive
T09M09x2249	M1.009	III	11-3	2-1	2	13	20-1	41	13	5	1.26	
T09M09x2251	M1.009	III	5-1	1-1	1	12	13-2	23	9	1	69.7	Not reactive
T09M09x2254	M1.009	III	27-1	2-5	2	11	4-1	33	10	5	18.7	Not reactive
T09M09x2255	M1.009	III	5-1	1-1	1	13	4-1	15	13	14	77.4	Not reactive
T09M09x2299	M1.009	III	28-1	1-5	1	10	21-1	34	12	2	59.2	Not reactive
T09M09x2300	M1.009	III	9-1	2-1	2	13	21-1	43	10	6	25.9	Not reactive
T13M09x1547	M1.009	II	19-1	2-1	2	13	26-1	26	13	3	65.6	Not reactive
T13M09x1635	M1.009	II	7-2	2-2	2	11	17-1	28	11	1	57	Not reactive
T13M09x1777	M1.009	II	6-5	1-3	1	15	6-1	42	13	3	64.4	Not reactive

Supplementary Table 3: Number of paired TCR sequences and cloned TCRs from activated cT_{FH} cells.
TCRs were analyzed before immunization (0) and after immunization I, II and III in each donor.

Donors	Paired TCR sequences				Cloned TCRs
	0	I	II	III	
M1.002	26	33	214	181	25
M1.003	41	246	230	318	56
M1.004	36	0	205	147	22
M1.006	25	143	63	404	37
M1.009	82	138	148	333	42

Supplementary Table 4: TCR sequence features and reactivity of TCRs cloned from activated cT_{FH} cells. CSP- and C-CSP-reactive TCRs are highlighted in gray. The TCR cloning and screening was performed together with Rebecca Hundsdorfer and Julia Puchan.

TCR	Donor	Immunization	TRBV	TRBJ	TRBC	CDR3β length	TRAV	TRAJ	CDR3α length	Clone size	TCR expression [%]	CSP [pg/ml]	C-CSP [pg/ml]
T07M02x1022	M1.002	III	11-2	2-7	2	11	2-1	39	11	7	45.6	0.0	0.0
T07M02x1073	M1.002	III	2-1	2-6	2	14	29DV5	42	14	4	75.2	0.7	2.8
T07M02x1107	M1.002	III	7-2	1-2	1	12	21-1	3	13	5	29.0	0.0	0.0
T07M02x1113	M1.002	III	20-1	2-1	2	13	8-1	29	11	6	75.4	0.1	5.5
T07M02x1128	M1.002	III	18-1	2-1	2	14	13-1	31	10	2	79.9	0.0	0.1
T07M02x1142	M1.002	III	6-2	1-5	1	11	25-1	45	13	3	73.4	0.1	0.0
T07M02x1383a1	M1.002	III	3-1	1-1	1	12	5-1	32	12	4	21.1	0.0	0.0
T07M02x1383a2	M1.002	III	3-1	1-1	1	12	8-1	27	11	4	65.8	0.2	5.6
T07M02x1408	M1.002	III	5-1	2-3	2	12	5-1	15	11	4	74.7	0.0	0.2
T07M02x2795	M1.002	III	24-1	2-3	2	12	12-2	52	15	4	68.2	0.0	2.3
T07M02x3019	M1.002	III	5-1	2-5	2	12	5-1	15	11	4	67.1	0.9	4.5
T07M02x3061	M1.002	III	7-3	2-4	2	11	13-2	40	11	2	73.4	0.0	3.9
T07M02x981	M1.002	III	27-1	2-5	2	11	9-2	53	13	3	86.8	0.0	0.0
T15M02x2397	M1.002	I	7-6	2-5	2	11	8-3	21	11	20	44.0	0.0	0.0
T16M02x1206	M1.002	II	5-1	1-1	1	12	21-1	31	11	3	78.6	0.0	4.2
T16M02x1218	M1.002	II	10-2	2-7	2	11	41-1	48	9	3			
T16M02x1223	M1.002	II	20-1	2-5	2	14	21-1	22	10	3	63.5	7.9	3.8
T16M02x1257	M1.002	II	12-4	2-1	2	13	29DV5	30	12	5	75.0	0.0	2.5
T16M02x1313a1	M1.002	II	12-3	2-1	2	11	26-1	52	13	6			
T16M02x1313a2	M1.002	II	12-3	2-1	2	11	12-3	40	12	6	45.6	0.0	7.2
T16M02x1367	M1.002	II	7-3	2-1	2	11	13-2	40	11	1			
T16M02x1369	M1.002	II	10-2	1-1	1	10	12-2	13	9	3	85.0	0.0	2.6
T16M02x1381	M1.002	II	6-5	2-1	2	13	35-1	54	12	10	74.0	0.8	2.9
T16M02x1384	M1.002	II	20-1	1-3	1	10	3-1	15	11	1	78.3	3.2	2.2
T16M02x1524	M1.002	II	9-1	2-3	2	12	12-1	32	12	3	72.5	0.0	3.2
T16M02x1526	M1.002	II	7-8	1-1	1	12	8-2	42	10	3	79.5	0.9	3.1
T07M03x1993	M1.003	III	7-9	2-5	2	12	29DV5	45	14	3	68.8	0.8	
T07M03x2168	M1.003	III	27-1	2-1	2	14	29DV5	42	14	2	77.5	0.6	
T07M03x2210	M1.003	III	5-1	1-1	1	13	34-1	29	11	8	83.1	0.6	
T07M03x2283	M1.003	III	5-8	2-7	2	11	22-1	37	12	5	87.8	1.0	
T07M03x3863a1	M1.003	III	15-1	2-3	2	14	21-1	27	11	11	56.2	0.1	
T07M03x3863a2	M1.003	III	15-1	2-3	2	14	3-1	48	14	11	76.2	0.2	
T07M03x3876	M1.003	III	20-1	1-2	1	10	9-2	30	10	3	92.3	0.2	
T07M03x4078	M1.003	III	7-9	2-1	2	12	8-3	27	12	3	60.7	0.1	
T07M03x4127	M1.003	III	6-1	1-4	1	13	12-3	7	11	4			
T07M03x4147	M1.003	III	9-1	1-2	1	12	12-2	22	12	6	85.6	0.5	
T07M03x4225	M1.003	III	9-1	2-5	2	12	3-1	18	13	4	89.3	0.3	
T07M03x4236	M1.003	III	6-1	1-3	1	13	8-4	47	10	4	74.4	0.9	
T07M03x4341	M1.003	III	9-1	2-1	2	12	25-1	48	12	3	72	0.3	

T07M03x4359	M1.003	III	5-1	2-1	2	13	12-1	52	12	6	86.5	0.6	
T07M03x4368	M1.003	III	7-3	2-3	2	17	22-1	26	11	6	49.5	1.1	
T07M03x4446	M1.003	III	7-2	1-2	1	13	29DV5	42	9	12	67.3	0.8	
T07M03x4460	M1.003	III	20-1	1-6	1	11	25-1	33	36	4	73.7	0.2	
T07M03x4464	M1.003	III	2-1	1-1	1	11	25-1	21	8	5	74.9	0.2	
T07M03x4484	M1.003	III	29-1	1-2	1	11	17-1	53	12	3	65.9	1.5	
T07M03x4487	M1.003	III	18-1	2-3	2	14	29DV5	43	8	12	48.3	0.2	
T07M03x4521	M1.003	III	12-3	2-4	2	12	26-1	32	15	3			
T07M03x4608	M1.003	III	5-1	2-3	2	12	29DV5	48	12	8	76.4	0.4	
T14M03x1192	M1.003	II	7-2	2-2	2	13	26-2	47	14	5	74.9	0.0	
T14M03x1214a1	M1.003	II	11-3	2-2	2	13	8-6	26	9	26	41.9	0.0	
T14M03x1214a2	M1.003	II	11-3	2-2	2	13	13-2	23	7	26	2.79		
T14M03x1215	M1.003	II	7-9	2-7	2	12	12-1	22	15	3	72	3.0	
T14M03x1257	M1.003	II	6-6	2-2	2	13	26-2	37	12	3	85.6	0.0	
T14M03x1263b1	M1.003	II	12-5	1-5	1	18	8-6	40	12	12	2.39		
T14M03x1263b2	M1.003	II	3-1	1-1	1	10	8-6	40	12	12	78.7	0.0	
T14M03x1277	M1.003	II	7-8	1-3	1	15	20-1	49	9	4	72.7	0.0	
T14M03x1281	M1.003	II	20-1	2-1	2	12	16-1	47	10	7	47.7	1.6	
T14M03x1300	M1.003	II	7-3	2-3	2	14	12-1	5	12	3			
T14M03x1324a1	M1.003	II	7-2	1-6	1	12	13-1	35	23	37	59.8	0.0	
T14M03x1324a2	M1.003	II	7-2	1-6	1	12	13-2	10	11	37	79.4	0.3	
T14M03x1331	M1.003	II	5-5	1-5	1	13	8-6	32	13	6	86.2	0.4	
T14M03x1400	M1.003	II	7-3	1-6	1	15	17-1	22	12	3	80.9	0.0	
T14M03x1430a1	M1.003	II	6-1	2-5	2	13	2-1	9	12	9	61	0.0	
T14M03x1430a2	M1.003	II	6-1	2-5	2	13	12-3	40	10	9	71.1	0.0	
T14M03x1439	M1.003	II	5-4	2-2	2	14	8-1	37	13	6	81.6	0.1	
T14M03x1453	M1.003	II	28-1	1-1	1	13	9-2	53	12	4	81.3	0.3	
T14M03x1479	M1.003	II	25-1	1-2	1	9	13-1	34	10	8	86.5	0.0	
T14M03x1481	M1.003	II	7-2	1-5	1	12	38-2-DV8	49	13	10	70.9	0.0	
T14M03x1485	M1.003	II	9-1	2-5	2	11	20-1	52	15	1	44.9	1.1	
T14M03x1486	M1.003	II	7-9	2-2	2	11	13-2	52	12	4	64.3	0.0	
T14M03x1520	M1.003	II	10-2	1-2	1	11	10-1	49	11	4	86.5	0.1	
T14M03x1533	M1.003	II	5-5	2-7	2	14	38-2-DV8	32	13	6	86.1	0.3	
T14M03x2321	M1.003	I	6-2	1-5	1	11	8-3	20	10	8	85	2.9	
T14M03x2391	M1.003	I	10-2	1-2	1	11	41-1	17	9	13	84.9	0.5	
T14M03x2443	M1.003	I	7-2	1-1	1	12	17-1	54	12	3	84.1	1.6	
T14M03x2453	M1.003	I	7-2	1-2	1	12	38-2-DV8	28	12	19	88.1	3.2	
T14M03x2470	M1.003	I	25-1	1-2	1	9	4-1	5	13	14	63.7	2.2	
T14M03x2471	M1.003	I	7-2	1-2	1	11	24-1	43	10	4	79.7	1.8	
T14M03x2507	M1.003	I	7-9	1-5	1	14	20-1	20	11	9	36.4	3.0	
T14M03x2512	M1.003	I	10-2	1-2	1	11	41-1	49	9	1	63.6	1.8	
T14M03x2537	M1.003	I	18-1	1-1	1	13	29DV5	42	12	15	76.5	2.1	
T14M03x2549a1	M1.003	I	7-2	2-7	2	13	9-2	17	10	3	6.76	2.6	
T14M03x2549a2	M1.003	I	7-2	2-7	2	13	29DV5	33	16	3	1.58		
T14M03x2561	M1.003	I	28-1	1-6	1	14	5-1	4	13	8	75.9	3.6	
T14M03x2679	M1.003	I	20-1	1-2	1	14	12-2	7	10	3	82.9	2.5	

T08M04x2499	M1.004	III	2-1	2-7	2	13	38-1	40	12	4			
T08M04x2566	M1.004	III	5-1	2-5	2	13	5-1	9	9	2			
T08M04x2662	M1.004	III	28-1	2-5	2	13	13-2	54	12	4	43.5	0.0	4.0
T08M04x4234	M1.004	III	20-1	2-1	2	13	13-2	49	9	2	65.0	11.7	145.9
T08M04x4268	M1.004	III	5-5	1-2	1	11	13-2	56	12	1	66.9	0.9	6.2
T08M04x4269	M1.004	III	28-1	2-2	2	18	9-2	3	12	2			
T08M04x4338	M1.004	III	6-1	2-7	2	11	12-2	47	11	5	67.7	0.7	6.1
T08M04x4345	M1.004	III	7-9	1-1	1	16	25-1	16	11	1	55.8	1.2	8.5
T08M04x4443	M1.004	III	20-1	1-2	1	15	19-1	5	13	3	70.9	0.0	4.1
T16M04x1568	M1.004	II	7-2	2-1	2	12	26-1	18	15	2	71.9	0.0	0.0
T16M04x1590	M1.004	II	7-3	2-1	2	13	41-1	48	11	5	42.4	0.0	18.1
T16M04x1597	M1.004	II	7-7	2-7	2	12	8-6	13	11	9	25.5	0.6	0.0
T16M04x1619	M1.004	II	20-1	2-7	2	13	16-1	31	8	3	33.5	1.5	51.5
T16M04x1634	M1.004	II	6-5	2-1	2	13	16-1	58	11	2	47.9	0.0	4.1
T16M04x1641	M1.004	II	12-5	2-2	2	12	36DV7	11	14	5	50.1	0.8	3.5
T16M04x1709	M1.004	II	10-1	2-3	2	15	25-1	48	10	21	58.1	0.0	14.9
T16M04x1717	M1.004	II	28-1	1-2	1	8	8-3	29	13	2	65.1	0.0	3.4
T16M04x1718	M1.004	II	18-1	2-1	2	13	9-2	17	11	3	74.7	0.4	0.0
T16M04x1732	M1.004	II	6-2	2-7	2	12	21-1	8	13	3	51.8	0.1	51.9
T16M04x1754	M1.004	II	9-1	1-2	1	13	26-1	27	10	3	32.4	0.2	1.1
T16M04x1760	M1.004	II	9-1	2-3	2	15	8-4	5	12	1	71.7	0.0	0.1
T16M04x1786	M1.004	II	7-6	2-1	2	10	13-2	40	11	4			
T16M04x1803	M1.004	II	7-2	2-7	2	13	38-1	49	10	23	42.5	0.0	0.0
T16M04x1805	M1.004	II	20-1	1-2	1	11	26-1	52	13	1	83.0	0.7	63.6
T08M06x1547	M1.006	III	9-1	2-6	2	13	2-1	31	12	6	72.4	2.5	
T08M06x1597	M1.006	III	7-2	1-1	1	12	38-2-DV8	57	11	5	80.9	0.0	
T08M06x1634	M1.006	III	5-6	1-4	1	14	9-2	45	12	3	82.3	0.0	
T08M06x1653	M1.006	III	27-1	1-4	1	13	29DV5	33	11	3	83	0.0	
T08M06x1660	M1.006	III	4-3	1-6	1	13	29DV5	49	13	3	84.6	68.1	366.0
T08M06x1676	M1.006	III	30-1	1-6	1	14	16-1	4	13	3	55.9	0.2	
T08M06x1715	M1.006	III	27-1	2-7	2	15	3-1	26	12	4	74.7	0.0	
T08M06x1768	M1.006	III	28-1	1-1	1	14	13-2	53	12	2	80.3	0.0	
T08M06x1795	M1.006	III	19-1	1-2	1	14	21-1	35	8	3	2.89		
T08M06x1803	M1.006	III	20-1	1-2	1	12	24-1	48	11	4	88.5	26.0	371.9
T08M06x1895	M1.006	III	5-4	1-2	1	11	29DV5	56	11	2	64.1	0.0	
T08M06x3165	M1.006	III	28-1	1-6	1	13	9-2	42	14	4	60.1	0.4	
T08M06x3195	M1.006	III	14-1	2-2	2	14	5-1	23	12	3	64.9	0.0	
T08M06x3288	M1.006	III	19-1	2-7	2	12	40-1	53	15	7	20.3	0.5	
T08M06x3291	M1.006	III	6-1	2-4	2	13	13-2	32	15	4	58.7	13.6	160.3
T08M06x3432	M1.006	III	9-1	1-6	1	12	24-1	44	11	4	89.4	0.5	
T08M06x3456	M1.006	III	14-1	2-2	2	14	17-1	34	12	7	77.7	4.2	
T09M06x1594	M1.006	III	7-9	2-1	2	13	27-1	27	12	3	68.4	2.7	
T09M06x1618	M1.006	III	5-4	2-5	2	13	13-1	13	11	1	56.9	0.0	
T09M06x1652	M1.006	III	20-1	1-2	1	12	24-1	48	11	3	81.4	11.9	259.7
T09M06x1666	M1.006	III	20-1	1-5	1	12	24-1	48	11	3	91.2	29.0	500.0

T09M06x1670	M1.006	III	5-1	1-5	1	13	13-2	30	9	2	79.7	0.0	
T09M06x1688	M1.006	III	5-1	1-2	1	12	13-2	43	12	8	79.3	6.2	104.4
T09M06x1742	M1.006	III	19-1	1-5	1	16	17-1	34	12	1	76.2	0.0	
T09M06x1753	M1.006	III	19-1	2-2	2	15	34-1	26	10	6	73.5	0.0	
T09M06x1814	M1.006	III	4-2	1-3	1	14	22-1	30	10	3	90.2	13.7	215.2
T09M06x1819	M1.006	III	20-1	1-6	1	12	24-1	48	11	3	77.6	14.6	291.0
T09M06x1826	M1.006	III	20-1	2-7	2	13	16-1	23	10	4	86.2	6.9	107.5
T13M06x1015	M1.006	II	7-2	2-1	2	9	2-1	20	9	2	79.5	1.2	
T13M06x1020	M1.006	II	20-1	2-5	2	12	12-1	31	11	2	78.7	0.0	
T13M06x2507	M1.006	II	6-2	2-5	2	12	23DV6	48	9	2	65.1	2.5	
T16M06x2384	M1.006	I	12-4	2-7	2	11	4-1	15	12	12	80.5	0.1	
T16M06x2394	M1.006	I	7-9	1-3	1	13	27-1	42	13	2	67.1	0.5	
T16M06x2466	M1.006	I	7-9	2-7	2	12	38-1	49	11	2	77.8	4.6	0.2
T16M06x2581	M1.006	I	28-1	2-1	2	14	6-1	21	12	2	75.3	0.1	
T16M06x3056	M1.006	I	7-8	2-7	2	9	22-1	43	7	3	69.7	1.1	
T16M06x3068	M1.006	I	7-2	1-4	1	12	22-1	40	12	3	91	1.1	
T08M09x2114	M1.009	III	7-9	2-3	2	12	25-1	45	14	3	39.6	0.3	26.9
T08M09x2133	M1.009	III	5-5	2-7	2	13	29DV5	29	12	6	58.6	0.0	0.2
T08M09x2138	M1.009	III	9-1	2-7	2	13	3-1	48	13	13	70.5	0.0	4.4
T08M09x2139	M1.009	III	7-2	2-1	2	13	13-2	11	9	3	26.9	0.0	3.7
T08M09x2141	M1.009	III	6-5	2-7	2	11	8-6	53	13	3	68.7	0.0	3.1
T08M09x2188	M1.009	III	5-1	2-7	2	12	29DV5	48	12	6	72.2	0.0	1.2
T08M09x2189a1	M1.009	III	30-1	2-2	2	12	29DV5	43	11	9	59.7	0.0	8.4
T08M09x2189a2	M1.009	III	30-1	2-2	2	12	17-1	54	10	9	72.0	0.0	7.9
T08M09x2191	M1.009	III	9-1	2-7	2	12	8-1	5	11	7	73.2	0.0	27.3
T08M09x2192	M1.009	III	5-1	2-3	2	12	29DV5	48	12	13	67.9	0.4	103.1
T08M09x2206	M1.009	III	5-1	2-5	2	13	38-2-DV8	53	16	5	80.3	0.0	0.0
T08M09x2209	M1.009	III	30-1	2-1	2	13	13-2	49	13	5	64.8	0.0	0.0
T08M09x2221	M1.009	III	7-9	2-1	2	13	13-1	4	13	1	50.8	0.0	0.0
T08M09x2236	M1.009	III	30-1	2-2	2	12	14DV4	54	12	4	76.1	0.1	0.0
T08M09x2242	M1.009	III	18-1	2-3	2	14	29DV5	43	8	2	14.7	0.0	8.2
T08M09x2280	M1.009	III	30-1	1-6	1	11	6-1	39	13	3	77.1	0.6	0.0
T09M09x2312	M1.009	III	30-1	2-1	2	14	14DV4	40	10	6	56.4	1.2	0.0
T09M09x2313	M1.009	III	30-1	1-4	1	13	26-2	32	12	6	78.7	10.4	0.2
T09M09x2525	M1.009	III	30-1	1-2	1	10	17-1	56	12	5	79.2	1.8	2.3
T09M09x2528	M1.009	III	29-1	2-2	2	12	21-1	42	13	5	51.8	0.0	1.8
T09M09x2529	M1.009	III	24-1	1-1	1	12	35-1	58	12	4	59.7	1.5	9.0
T09M09x2536	M1.009	III	9-1	2-7	2	12	12-1	30	12	3	10.0	0.0	0.6
T09M09x2560	M1.009	III	7-3	2-3	2	16	8-3	12	12	7			
T09M09x2635	M1.009	III	7-2	2-7	2	13	29DV5	28	11	3	54.0	1.0	0.8
T09M09x2661	M1.009	III	7-9	2-3	2	14	21-1	54	11	5	40.1	2.0	0.1
T09M09x499	M1.009	III	30-1	1-2	1	11	10-1	40	12	5	63.6	4.0	0.1
T09M09x616	M1.009	III	12-4	2-1	2	13	26-1	34	11	3	73.3	0.0	0.0
T09M09x635	M1.009	III	7-7	1-5	1	11	29DV5	54	11	3	16.2	0.2	0.0
T09M09x643	M1.009	III	20-1	1-2	1	11	19-1	57	12	1	67.4	0.0	0.0

T15M09x1971	M1.009	II	15-1	1-2	1	10	26-1	41	12	4	70.4	0.0	0.8
T15M09x1974	M1.009	II	9-1	2-5	2	11	20-1	52	15	3			
T15M09x1985	M1.009	II	5-6	2-6	2	13	36DV7	42	10	3	67.2	0.0	6.6
T15M09x1987	M1.009	II	12-3	2-6	2	13	36DV7	48	12	3	49.9	0.0	0.8
T15M09x2061	M1.009	II	9-1	2-1	2	11	20-1	52	15	6	60.5	0.3	0.0
T15M09x2124	M1.009	II	7-2	1-5	1	13	12-3	26	12	3	65.3	2.1	0.7
T15M09x2172	M1.009	II	7-2	2-3	2	14	26-1	48	12	6	68.8	0.0	7.9
T15M09x2177	M1.009	II	15-1	2-7	2	15	23DV6	42	14	10	26.6	0.0	0.3
T15M09x2180	M1.009	II	7-8	1-6	1	13	13-2	28	12	6	77.2	3.7	73.4
T15M09x2186	M1.009	II	11-2	2-7	2	12	25-1	10	11	3	64.7	1.6	0.3
T15M09x2221	M1.009	II	7-4	1-6	1	16	26-1	30	11	4	17.5	0.7	0.4
T15M09x2249	M1.009	II	30-1	1-3	1	10	26-1	42	14	3	77.2	0.0	0.0
T16M09x2696	M1.009	I	6-6	1-1	1	11	12-1	39	11	3	71.7	0.3	1.8
T16M09x2934a1	M1.009	I	9-1	2-5	2	11	23DV6	27	13	35			
T16M09x2934a2	M1.009	I	9-1	2-5	2	11	20-1	52	15	35	62.5	0.0	2.6
T16M09x2984	M1.009	I	7-9	2-3	2	13	2-1	6	11	3	16.3	0.0	1.6
T16M09x2998	M1.009	I	7-2	1-1	1	13	9-2	9	11	5	73.6	0.0	1.7

Supplementary Table 5: Number of sorted T cells and amplified paired TCR genes after stimulation of PBMCs with malarial antigens.

Donors	Sorted proliferating T cells			Paired TCR sequences		
	CSP	*Pf* SPZ lysate	Uninfected mosquito lysate	CSP	*Pf* SPZ lysate	Uninfected mosquito lysate
M1.002	209	175	17	81	34	2
M1.003	49	47	11	9	13	7
M1.004	122	253	21	0	15	9
M1.006	98	145	2	9	16	2
M1.009	113	127	5	11	7	0

8.4 Primer sequences

Supplementary Table 6: PCR primers for generation of TCR alpha amplicons. The common linker sequence is highlighted in red.

First PCR forward primers

hTRAV1-1	CCAGGGTTTTCCCAGTCACGACCTGCAGGACAAAGCCTTGAGC
hTRAV1-2	CCAGGGTTTTCCCAGTCACGACGATGGGAGGCACTACAGGAC
hTRAV2	CCAGGGTTTTCCCAGTCACGACGCAAGGACCAAGTGTTTCAGCC
hTRAV3	CCAGGGTTTTCCCAGTCACGACGAGAGCTCAGTCAGTGGCTCAGC
hTRAV4	CCAGGGTTTTCCCAGTCACGACCCTTGCTAAGACCACCCAGCC
hTRAV5	CCAGGGTTTTCCCAGTCACGACGAGTAGAGGAGAGGATGTGGAGC
hTRAV6	CCAGGGTTTTCCCAGTCACGACGTGGACTGGGTGAAGAGCC
hTRAV7	CCAGGGTTTTCCCAGTCACGACGTCTTGGCTGGGCAAATGGAG
hTRAV8-1	CCAGGGTTTTCCCAGTCACGACGATGCCAGAGCCCAGTCTGTG
hTRAV8-2,4,6	CCAGGGTTTTCCCAGTCACGACGGAGGAACCAGAGCCCAGTC
hTRAV8-3	CCAGGGTTTTCCCAGTCACGACCCAGAGCCCAGTCAGTGACC
hTRAV9-1	CCAGGGTTTTCCCAGTCACGACGGAGATTCAGTGGTCCAGACAG
hTRAV9-2	CCAGGGTTTTCCCAGTCACGACCGTGGAGATTCAGTGACCCAG
hTRAV10	CCAGGGTTTTCCCAGTCACGACGGGAATGGCAAAAACCAAGTGG
hTRAV12-1	CCAGGGTTTTCCCAGTCACGACGAGCCAACGGAAGGAGGTG
hTRAV12-2,3	CCAGGGTTTTCCCAGTCACGACGAGCCAACAGAAGGAGGTGG
hTRAV13-1	CCAGGGTTTTCCCAGTCACGACGGAGAGAATGTGGAGCAGCATCC
hTRAV13-2	CCAGGGTTTTCCCAGTCACGACGGTGAGCAGAGGAGAGAGTGTGG
hTRAV14DV4	CCAGGGTTTTCCCAGTCACGACGGCATTGCCCAGAAGATAACTC
hTRAV16	CCAGGGTTTTCCCAGTCACGACGGAACAAGAGCCCAGAGAGTGAC
hTRAV17	CCAGGGTTTTCCCAGTCACGACGAACAGTCAACAGGGAGAAGAGG
hTRAV18	CCAGGGTTTTCCCAGTCACGACCCAGTGGAGACTCGGTTACCCAG
hTRAV19	CCAGGGTTTTCCCAGTCACGACGGCTCAGAAGGTAACTCAAGCG
hTRAV20	CCAGGGTTTTCCCAGTCACGACGAGTGGAGAAGACCAGGTGACGC
hTRAV21	CCAGGGTTTTCCCAGTCACGACGAGCAGCAAACAGGAGGTGACG
hTRAV22	CCAGGGTTTTCCCAGTCACGACGGAATACAAGTGGAGCAGAGTCC
hTRAV23DV6	CCAGGGTTTTCCCAGTCACGACGTGAGTGGCCAACAGAAGGAG
hTRAV24	CCAGGGTTTTCCCAGTCACGACGTGAGCAGCATACTGAACGTGG
hTRAV25	CCAGGGTTTTCCCAGTCACGACGGTGAATGGACAACAGGTAATGC
hTRAV26-1	CCAGGGTTTTCCCAGTCACGACGATGCTAAGACCACCCAGCC
hTRAV26-2	CCAGGGTTTTCCCAGTCACGACGTGATGCTAAGACCACACAGCC
hTRAV27	CCAGGGTTTTCCCAGTCACGACGGTGAGCACCCAGCTGCTG
hTRAV29DV5	CCAGGGTTTTCCCAGTCACGACGTCAACAGAAGAATGATGACCAGC
hTRAV30	CCAGGGTTTTCCCAGTCACGACGAGAAGCCAACAACCAGTGCAG
hTRAV34	CCAGGGTTTTCCCAGTCACGACCAGTAGCCAAGAACTGGAGCAG
hTRAV35	CCAGGGTTTTCCCAGTCACGACGACATGGGTCAGTGGTCAACAG
hTRAV36DV7	CCAGGGTTTTCCCAGTCACGACGTGAGCAGTGAAGACAAGGTGG
hTRAV38-1,2	CCAGGGTTTTCCCAGTCACGACGGCYCAGACAGTCACTCAGTCTC
hTRAV39	CCAGGGTTTTCCCAGTCACGACGGTTAAGTGGAGAGCTGAAAGTGG

hTRAV40	CCAGGGTTTTCCCAGTCACGACCCAGCAGCAATTCAGTCAAGC
hTRAV41	CCAGGGTTTTCCCAGTCACGACCAGCTAAGCTGTGTAAGTGCCG

First PCR reverse primer

$TRAC_{217-240}$	GCTGTTGTTGAAGGCGTTTGCAC

Alternative first PCR reverse primers tested during optimization phase

$TRAC_{142-168}$	GTCCATAGACCTCATGTCTAGCACAG
$TRAC_{176-197}$	CTCCAGGCCACAGCACTGTTG

Second PCR forward primer

Linker	CCAGGGTTTTCCCAGTCACGAC

Second PCR reverse primer

$TRAC_{13-33}$	CTGGTACACGGCAGGGTCAG

Supplementary Table 7: PCR primers for generation of TCR beta amplicons. The common linker sequence is highlighted in red.

First PCR forward primers

hTRBV2	CCAGGGTTTTCCCAGTCACGACCACAGAACCTGAAGTCACCCAG
hTRBV3	CCAGGGTTTTCCCAGTCACGACGGACACAGCTGTTTCCCAGACTC
hTRBV4-1,2,3	CCAGGGTTTTCCCAGTCACGACACACCTGGTCATGGGAATGAC
hTRBV5-1,4,5,6,8	CCAGGGTTTTCCCAGTCACGACCTGATCAAAACGAGAGGACAGC
hTRBV6-1,2,3,5,6,8,9	CCAGGGTTTTCCCAGTCACGACGAATGCTGGTGTCACTCAGACCC
hTRBV6-4	CCAGGGTTTTCCCAGTCACGACGACTGCTGGGATCACCCAGG
hTRBV7-2,3	CCAGGGTTTTCCCAGTCACGACCCAGTAACAAGGTCACAGAGAAGG
hTRBV7-4,6,7,8	CCAGGGTTTTCCCAGTCACGACGGTGCTGGAGTCTCCCAGTC
hTRBV7-9	CCAGGGTTTTCCCAGTCACGACGATACTGGAGTCTCCCAGGACCC
hTRBV9	CCAGGGTTTTCCCAGTCACGACGGATTCTGGAGTCACACAAACCC
hTRBV10	CCAGGGTTTTCCCAGTCACGACGGATGCTGRAATCACCCAGAGC
hTRBV11-1	CCAGGGTTTTCCCAGTCACGACGAAGCTGAAGTTGCCCAGTCCC
hTRBV11-2	CCAGGGTTTTCCCAGTCACGACGAAGCTGGAGTTGCCCAGTCTCC
hTRBV11-3	CCAGGGTTTTCCCAGTCACGACGAAGCTGGAGTGGTTCAGTCTCC
hTRBV12-3,4,5	CCAGGGTTTTCCCAGTCACGACGGTGACAGAGATGGGACAAGAAG
hTRBV13	CCAGGGTTTTCCCAGTCACGACGGCTGCTGGAGTCATCCAGTC
hTRBV14	CCAGGGTTTTCCCAGTCACGACGAAGCTGGAGTTACTCAGTTCCC
hTRBV15	CCAGGGTTTTCCCAGTCACGACGGATGCCATGGTCATCCAG
hTRBV16	CCAGGGTTTTCCCAGTCACGACGGTGAAGAAGTCGCCCAGACTC
hTRBV18	CCAGGGTTTTCCCAGTCACGACGGCGTCATGCAGAACCCAAG
hTRBV19	CCAGGGTTTTCCCAGTCACGACGGATGGTGGAATCACTCAGTCC

hTRBV20	CCAGGGTTTTCCCAGTCACGACGCTTGGTGCTGTCGTCTCTCAAC
hTRBV24	CCAGGGTTTTCCCAGTCACGACGGATGCTGATGTTACCCAGACCC
hTRBV25	CCAGGGTTTTCCCAGTCACGACGGAAGCTGACATCTACCAGACCC
hTRBV27	CCAGGGTTTTCCCAGTCACGACGGAAGCCCAAGTGACCCAGAAC
hTRBV28	CCAGGGTTTTCCCAGTCACGACGCCTCGTAGATGTGAAAGTAACCC
hTRBV29	CCAGGGTTTTCCCAGTCACGACGGACTAGGCTCTGTGTTCAGTGC
hThRBV30	CCAGGGTTTTCCCAGTCACGACCCTGGGCACTTTCTTTGGG

First PCR reverse primer

$TRBC_{115-135}$	CAGCTCAGCTCCACGTGGTC

Alternative first PCR reverse primers tested during optimization phase

$TRBC_{90-109}$	GAAGCCTGTGGCCAGGCAC
$TRBC_{135-158}$	GCACCTCCTTCCCATTCACCCAC
$TRBC_{154-174}$	GTGCTGACCCCACTGTGCAC
$TRBC_{189-212}$	CATTGAGGGCGGGCTGCTCCTTG

Second PCR forward primer

Linker	CCAGGGTTTTCCCAGTCACGAC

Second PCR reverse primer

$TRBC_{30-51}$	GATGGCTCAAACACAGCGACC

Supplementary Table 8: Specific PCR primers for amplification and subsequent cloning of TCR alpha genes. The sequences encoding parts of the TRAV13-1 signal peptide, used as overlap for Gibson assembly cloning, are highlighted in blue.

Specific PCR forward primers

TRAV1-1_sPCR	TCCTGTGGCTGCAGCTGGACTTGGTGAATGGACAAAGCCTTGAGCAGCCC
TRAV1-2_sPCR	TCCTGTGGCTGCAGCTGGACTTGGTGAATGGACAAAACATTGACCAGCCCA
TRAV2-1_sPCR	TCCTGTGGCTGCAGCTGGACTTGGTGAATGGAAAGGACCAAGTGTTTCAGCC
TRAV3-1_sPCR	TCCTGTGGCTGCAGCTGGACTTGGTGAATGGACAGTCAGTGGCTCAGCCG
TRAV4-1_sPCR	TCCTGTGGCTGCAGCTGGACTTGGTGAATGGAAAGACCACCCAGCCCATC
TRAV5-1_sPCR	TCCTGTGGCTGCAGCTGGACTTGGTGAATGGAGAGGATGTGGAGCAGAGTCTT
TRAV6-1_sPCR	TCCTGTGGCTGCAGCTGGACTTGGTGAATGGACAAAAGATAGAACAGAATTCCGAGG
TRAV7-1_sPCR	TCCTGTGGCTGCAGCTGGACTTGGTGAATGGAGAAAACCAGGTGGAGCACA
TRAV8-1_sPCR	TCCTGTGGCTGCAGCTGGACTTGGTGAATGGACAGTCTGTGAGCCAGCATAACC
TRAV8-2_sPCR	TCCTGTGGCTGCAGCTGGACTTGGTGAATGGACAGTCGGTGACCCAGCTT
TRAV8-3_sPCR	TCCTGTGGCTGCAGCTGGACTTGGTGAATGGACAGTCAGTGACCCAGCCTG
TRAV8-4_sPCR	TCCTGTGGCTGCAGCTGGACTTGGTGAATGGACAGTCGGTGACCCAGCTT
TRAV8-6_sPCR	TCCTGTGGCTGCAGCTGGACTTGGTGAATGGACAGTCTGTGACCCAGCTTGA
TRAV8-7_sPCR	TCCTGTGGCTGCAGCTGGACTTGGTGAATGGACAGTCGGTGACCCAGCTT
TRAV9-1_sPCR	TCCTGTGGCTGCAGCTGGACTTGGTGAATGGAGATTCAGTGGTCCAGACAGAAG

TRAV9-2_sPCR	TCCTGTGGCTGCAGCTGGACTTGGTGAATGGAGATTCAGTGACCCAGATGGA
TRAV10-1_sPCR	TCCTGTGGCTGCAGCTGGACTTGGTGAATGGAAAAAACCAAGTGGAGCAGAGTC
TRAV12-1_sPCR	TCCTGTGGCTGCAGCTGGACTTGGTGAATGGACAACGGAAGGAGGTGGAG
TRAV12-2_sPCR	TCCTGTGGCTGCAGCTGGACTTGGTGAATGGACAACAGAAGGAGGTGGAGC
TRAV12-3_sPCR	TCCTGTGGCTGCAGCTGGACTTGGTGAATGGACAACAGAAGGAGGTGGAGC
TRAV13-1_sPCR	TCCTGTGGCTGCAGCTGGACTTGGTGAATGGAGAGAATGTGGAGCAGCATCC
TRAV13-2_sPCR	TCCTGTGGCTGCAGCTGGACTTGGTGAATGGAGAGAGTGTGGGGCTGCAT
TRAV14DV4_sPCR	TCCTGTGGCTGCAGCTGGACTTGGTGAATGGACAGAAGATAACTCAAACCCAACC
TRAV16-1_sPCR	TCCTGTGGCTGCAGCTGGACTTGGTGAATGGACAGAGAGTGACTCAGCCCGA
TRAV17-1_sPCR	TCCTGTGGCTGCAGCTGGACTTGGTGAATGGACAACAGGGAGAAGAGGATCC
TRAV18-1_sPCR	TCCTGTGGCTGCAGCTGGACTTGGTGAATGGAGACTCGGTTACCCAGACAGAA
TRAV19-1_sPCR	TCCTGTGGCTGCAGCTGGACTTGGTGAATGGACAGAAGGTAACTCAAGCGCA
TRAV20-1_sPCR	TCCTGTGGCTGCAGCTGGACTTGGTGAATGGAGAAGACCAGGTGACGCAG
TRAV21-1_sPCR	TCCTGTGGCTGCAGCTGGACTTGGTGAATGGAAAACAGGAGGTGACGCAGA
TRAV22-1_sPCR	TCCTGTGGCTGCAGCTGGACTTGGTGAATGGAATACAAGTGGAGCAGAGTCCTCC
TRAV23DV6_sPCR	TCCTGTGGCTGCAGCTGGACTTGGTGAATGGACAACAGAAGGAGAAAAGTGACCA
TRAV24-1_sPCR	TCCTGTGGCTGCAGCTGGACTTGGTGAATGGAATACTGAACGTGGAACAAAGTCC
TRAV25-1_sPCR	TCCTGTGGCTGCAGCTGGACTTGGTGAATGGACAACAGGTAATGCAAATTCCTCA
TRAV26-1_sPCR	TCCTGTGGCTGCAGCTGGACTTGGTGAATGGAAAGACCACCCAGCCCAC
TRAV26-2_sPCR	TCCTGTGGCTGCAGCTGGACTTGGTGAATGGAAAGACCACACAGCCAAATTCA
TRAV27-1_sPCR	TCCTGTGGCTGCAGCTGGACTTGGTGAATGGACAGCTGCTGGAGCAGAGC
TRAV29DV5_sPCR	TCCTGTGGCTGCAGCTGGACTTGGTGAATGGACAACAGAAGAATGATGACCAGC
TRAV30-1_sPCR	TCCTGTGGCTGCAGCTGGACTTGGTGAATGGACAACAACCAGTGCAGAGTCC
TRAV34-1_sPCR	TCCTGTGGCTGCAGCTGGACTTGGTGAATGGACAAGAACTGGAGCAGAGTCCT
TRAV35-1_sPCR	TCCTGTGGCTGCAGCTGGACTTGGTGAATGGACAACAGCTGAATCAGAGTCCTC
TRAV36DV7_sPCR	TCCTGTGGCTGCAGCTGGACTTGGTGAATGGAGAAGACAAGGTGGTACAAAGCC
TRAV38-1,2_sPCR	TCCTGTGGCTGCAGCTGGACTTGGTGAATGGACAGACAGTCACTCAGTCTCAACC
TRAV39-1_sPCR	TCCTGTGGCTGCAGCTGGACTTGGTGAATGGAGAGCTGAAAGTGGAACAAAACC
TRAV40-1_sPCR	TCCTGTGGCTGCAGCTGGACTTGGTGAATGGAAATTCAGTCAAGCAGACGGG
TRAV41-1_sPCR	TCCTGTGGCTGCAGCTGGACTTGGTGAATGGAGCCAAAAATGAAGTGGAGC

Specific PCR reverse primer

$TRAC_{13-33}$	CTGGTACACGGCAGGGTCAG

Supplementary Table 9: Specific PCR primers for amplification and subsequent cloning of TCR beta genes. The sequences encoding parts of the TRBV5-1 signal peptide, used as overlap for Gibson assembly cloning, are highlighted in blue. Orange marks sequences of the respective V gene which are missing in the template sequence and were attached during specific PCR.

Specific PCR forward primers

TRBV2-1_sPCR	AGCAGGCCCAGTAAAGGCTGAACCTGAAGTCACCCAGACTC
TRBV3-1_sPCR	AGCAGGCCCAGTAAAGGCTGCTGTTTCCCAGACTCCAAA
TRBV4-1_sPCR	AGCAGGCCCAGTAAAGGCTGAAGTTACCCAGACACCAAAACACCTGGTCATGGGAATGAC
TRBV4-2,3_sPCR	AGCAGGCCCAGTAAAGGCTGGAGTTACGCAGACACCAAGACACCTGGTCATGGGAATGAC
TRBV5-1_sPCR	AGCAGGCCCAGTAAAGGCTGGAGTCACTCAAACTCCAAGATATCTGATCAAAACGAGAGGACAGC
TRBV5-(3-7)_sPCR	AGCAGGCCCAGTAAAGGCTGGAGTCACCCAAAGTCCCACACACCTGATCAAAACGAGAGGACAGC
TRBV5-8_sPCR	AGCAGGCCCAGTAAAGGCTGGAGTCACACAAAGTCCCACACACCTGATCAAAACGAGAGGACAGC
TRBV6-(1-3),(5-9)_sPCR	AGCAGGCCCAGTAAAGGCTGGTGTCACTCAGACCCCAA
TRBV6-4_sPCR	AGCAGGCCCAGTAAAGGCTGGGATCACCCAGGCACCA
TRBV7-1_sPCR	AGCAGGCCCAGTAAAGGCTGGAGTCTCCCAGTCCCTGA
TRBV7-2_sPCR	AGCAGGCCCAGTAAAGGCTGGAGTCTCCCAGTCCCCCAGTAACAAGGTCACAGAGAAGG
TRBV7-3_sPCR	AGCAGGCCCAGTAAAGGCTGGAGTCTCCCAGACCCCCAGTAACAAGGTCACAGAGAAGG
TRBV7-4_sPCR	AGCAGGCCCAGTAAAGGCTGGAGTCTCCCAGTCCCCAA
TRBV7-6,7_sPCR	AGCAGGCCCAGTAAAGGCTGGAGTCTCCCAGTCTCCCA
TRBV7-8_sPCR	AGCAGGCCCAGTAAAGGCTGGAGTCTCCCAGTCCCCTAG
TRBV7-9_sPCR	AGCAGGCCCAGTAAAGGCTGGAGTCTCCCAGGACCCCA
TRBV9-1_sPCR	AGCAGGCCCAGTAAAGGCTGGAGTCACACAAACCCCAA
TRBV10-1_sPCR	AGCAGGCCCAGTAAAGGCTGAAATCACCCAGAGCCCAA
TRBV10-2,3_sPCR	AGCAGGCCCAGTAAAGGCTGGAATCACCCAGAGCCCA
TRBV11-1_sPCR	AGCAGGCCCAGTAAAGGCTGAAGTTGCCCAGTCCCCCA
TRBV11-2_sPCR	AGCAGGCCCAGTAAAGGCTGGAGTTGCCCAGTCTCCCA
TRBV11-3_sPCR	AGCAGGCCCAGTAAAGGCTGGAGTGGTTCAGTCTCCCAG
TRBV12-3_sPCR	AGCAGGCCCAGTAAAGGCTGGAGTTATCCAGTCACCCCGCCATGAGGTGACAGAGATGGGACAAGA
TRBV12-4_sPCR	AGCAGGCCCAGTAAAGGCTGGAGTTATCCAGTCACCCCGGCACGAGGTGACAGAGATGGGACAAGA
TRBV12-5_sPCR	AGCAGGCCCAGTAAAGGCTAGAGTCACCCAGACACCAAGGGACAAGGTGACAGAGATGGGACAAGA
TRBV13-1_sPCR	AGCAGGCCCAGTAAAGGCTGGAGTCATCCAGTCCCCAA
TRBV14-1_sPCR	AGCAGGCCCAGTAAAGGCTGGAGTTACTCAGTTCCCCAGC
TRBV15-1_sPCR	AGCAGGCCCAGTAAAGGCTATGGTCATCCAGAACCCAAG
TRBV16-1_sPCR	AGCAGGCCCAGTAAAGGCTGAAGAAGTCGCCCAGACTCC

TRBV18-1_sPCR	AGCAGGCCCAGTAAAGGCTGGCGTCATGCAGAACCCA
TRBV19-1_sPCR	AGCAGGCCCAGTAAAGGCTGGAATCACTCAGTCCCCAAA
TRBV20-1_sPCR	AGCAGGCCCAGTAAAGGCTGCTGTCGTCTCTCAACATCCG
TRBV24-1_sPCR	AGCAGGCCCAGTAAAGGCTGATGTTACCCAGACCCCAAGG
TRBV25-1_sPCR	AGCAGGCCCAGTAAAGGCTGACATCTACCAGACCCCAAGATACC
TRBV27-1_sPCR	AGCAGGCCCAGTAAAGGCTCAAGTGACCCAGAACCCAAG
TRBV28-1_sPCR_S	AGCAGGCCCAGTAAAGGCTAAAGTAACCCAGAGCTCGAGATATC
TRBV29-1_sPCR	AGCAGGCCCAGTAAAGGCTGCTGTCATCTCTCAAAAGCCA
TRBV30-1_sPCR	AGCAGGCCCAGTAAAGGCTCAGACTATTCATCAATGGCCAGC

Specific PCR reverse primer

$TRBC_{30-51}$	GATGGCTCAAACACAGCGACC

Supplementary Table 10: Primers used for colony PCR of cloned TCR genes.

Forward primer	
colP_Psi_in_F	CAAGCCCTTTGTACACCCT
Reverse primer	
$TRBC_{115-135}$	CAGCTCAGCTCCACGTGGTC

Supplementary Table 11: Primers used for the cloning of the co-receptors CD3, CD4 and CD8. Blue highlights regions inserted for Gibson assembly cloning whereas green marks restriction enzyme recognition sites.

Forward primers	
hCD3E_F	GAGATGGATGTGATGTCGGTG
hCD3Z_F	TGGAAGAAAACCCCGGTCCCATGAAGTGGAAGGCGCTTTTCAC
hCD4_MluI_F	GCTACGCGTGACATGAACCGGGGAGTCCCT
hCD8A_F	GGAATTAGATCTCGAACGCGTCTGATGGCCTTACCAGTGACC
hCD8A_TMD_F	GCCTGTGATATCTACATCTGGG
hCD8B_P2A_F	TCTCTGTTAAAGCAAGCAGGAGACGTGGAAGAAAACCCCGGTCCCATGCGGCCGCG GCTGTG
Reverse primers	
hCD3E_P2A_R	GGGACCGGGGTTTTCTTC
hCD3Z_R	CGGAATTGATCCTCGAGCAATTGTTAGCGAGGGGGCAGGG
hCD4_SalI_R	GCTGTCGACACTTCAAATGGGGCTACATGTCTTCT
hCD8A_TMD_R	CCCAGATGTAGATATCACAGGC
hCD8A_P2A_R	TCTTCCACGTCTCCTGCTTGCTTTAACAGAGAGAAGTTCGTGGCTTCGACGTATCTCG CCGA
hCD8B_R	TAAGCTTGGCTGCAGGTCGACGGTTCATTTGTAAAATTGTTTCATGAAACGAAGCC

8.5 Supplementary Material

8.5.1 Antibodies

ELISA capture antibody

Goat anti-human IgG, Fcγ	Jackson, ImmunoResearch Laboratories, West Grove, PA, USA
Goat anti-human IgA, α Chain	Jackson, ImmunoResearch Laboratories, West Grove, PA, USA
Goat anti-human IgM, Fc5μ	Jackson, ImmunoResearch Laboratories, West Grove, PA, USA

ELISA secondary antibodies

Goat anti-human IgG, Fcγ (HRP conjugated)	Jackson, ImmunoResearch Laboratories, West Grove, PA, USA
Goat anti-human IgM, Fc5μ (HRP conjugated)	Jackson, ImmunoResearch Laboratories, West Grove, PA, USA
Goat anti-human IgA, α Chain (HRP conjugated)	Jackson, ImmunoResearch Laboratories, West Grove, PA, USA

FACS analysis antibodies & reagents

CellTrace™ Violet Cell Proliferation Kit	Invitrogen GmbH, Karlsruhe, Germany
7-AAD	Invitrogen GmbH, Karlsruhe, Germany
LIVE/DEAD™ Fixable Near-IR Dead Cell Stain Kit	Invitrogen GmbH, Karlsruhe, Germany
Mouse anti-human CD3 (FITC-conjugated, clone OKT3)	BioLegend GmbH, Fell, Germany
Rat anti-human CD4 (APC-Cy7-conjugated , clone A161A1)	BioLegend GmbH, Fell, Germany
Rat anti-human CD4 (PE-Cy7-conjugated , clone A161A1)	BioLegend GmbH, Fell, Germany
Mouse anti-human CD8a (AF700-conjugated, clone SK1)	BioLegend GmbH, Fell, Germany
Mouse anti-human CD8b (APC-conjugated, clone 2ST8.5H7)	BD Biosciences GmbH, Heidelberg, Germany
Mouse anti-human CD19 (PE-Cy7-conjugated, clone SJ25C1)	BD Biosciences GmbH, Heidelberg, Germany
Mouse anti-human CD45RA (BV510-conjugated, clone HI100)	BioLegend GmbH, Fell, Germany
Mouse anti-human CD45RA (PE-conjugated, clone HI100)	BioLegend GmbH, Fell, Germany
Mouse anti-human CD183/CXCR3 (BV421-conjugated, clone G025H7)	BioLegend GmbH, Fell, Germany
Rat anti-human CD185/CXCR5 (AF647-conjugated, clone RF8B2)	BD Biosciences GmbH, Heidelberg, Germany

Mouse anti-human CD196/CCR6 (PE-conjugated, clone G034E3)	BioLegend GmbH, Fell, Germany
Mouse anti-human CD197/CCR7 (BV711-conjugated, clone G043H7)	BioLegend GmbH, Fell, Germany
Hamster anti-human CD278/ICOS (PE-Cy7-conjugated, clone C398.4A)	BioLegend GmbH, Fell, Germany
Mouse anti-human CD279/PD-1 (BV605-conjugated, clone EH12.2H7)	BioLegend GmbH, Fell, Germany
Mouse anti-human TCR alpha/beta (PE-Cy7-conjugated, clone IL26)	BioLegend GmbH, Fell, Germany

8.5.2 Antigens

CSP, C-terminus	EMBL Protein Expression and Purification Core Facility, Heidelberg, Germany
CSP, full-length	EMBL Protein Expression and Purification Core Facility, Heidelberg, Germany
CSP, N-terminus	EMBL Protein Expression and Purification Core Facility, Heidelberg, Germany
DDX3Y	Creative Biomart Inc., Shirley, NY, USA
$DDX3Y_{176-187}$	PSL GmbH, Heidelberg, Germany
$M1_{58-66}$	PSL GmbH, Heidelberg, Germany
$NANP_5$, $NANP_{10}$	Alpha Diagnostic Intl. Inc., Texas, USA
Ovalbumin	InvivoGen, San Diego, CA, USA
Plasmodium falciparum sporozoite lysate	Kind gift from Dr. Giulia Costa and Dr. Elena Levashina, Dept. Vector Biology, Max Planck Institute for Infection Biology, Berlin, Germany
Staphylococcal enterotoxin B	Sigma Aldrich Chemie GmbH, Steinheim, Germany

CD8 peptide pool

$AMA1_{391-399}$ (KSHGKGYNW)	PSL GmbH, Heidelberg, Germany
$AMA1_{520-528}$ (NEVVVKEEY)	PSL GmbH, Heidelberg, Germany
$AMA1_{499-508}$ (NSTCRFFVCK)	PSL GmbH, Heidelberg, Germany
CSP_{1-10} (MMRKLAILSV)	PSL GmbH, Heidelberg, Germany
CSP_{4-72} (SLKKNSRSL)	PSL GmbH, Heidelberg, Germany
CSP_{7-16} (ILSVSSFLFV)	PSL GmbH, Heidelberg, Germany
CSP_{86-94} (LRKPKHKKL)	PSL GmbH, Heidelberg, Germany
$CSP_{285-293}$ (MPNDPNRNV)	PSL GmbH, Heidelberg, Germany
$CSP_{310-319}$ (EPSDKHIKEY)	PSL GmbH, Heidelberg, Germany

$CSP_{319-327}$ (YLNKIQNSL)	PSL GmbH, Heidelberg, Germany
$CSP_{336-345}$ (VTCGNGIQVR)	PSL GmbH, Heidelberg, Germany
$CSP_{353-360}$ (KPKDELDY)	PSL GmbH, Heidelberg, Germany
$CSP_{386-394}$ (GLIMVLSFL)	PSL GmbH, Heidelberg, Germany
$EXP1_{2-10}$ (KILSVFFLA)	PSL GmbH, Heidelberg, Germany
$EXP1_{10-18}$ (ALFFIIFNK)	PSL GmbH, Heidelberg, Germany
$EXP1_{77-84}$ (ATSVLAGL)	PSL GmbH, Heidelberg, Germany
$EXP1_{83-91}$ (GLLGVVSTV)	PSL GmbH, Heidelberg, Germany
$EXP1_{91-100}$ (VLLGGVGLVL)	PSL GmbH, Heidelberg, Germany
$LSA1_{4-12}$ (ILYISFYFI)	PSL GmbH, Heidelberg, Germany
$LSA1_{11-20}$ (FILVNLLIFH)	PSL GmbH, Heidelberg, Germany
$LSA1_{59-68}$ (HVLSHNSYEK)	PSL GmbH, Heidelberg, Germany
$LSA1_{84-92}$ (LTMSNVKNV)	PSL GmbH, Heidelberg, Germany
$LSA1_{94-102}$ (QTNFKSLLR)	PSL GmbH, Heidelberg, Germany
$LSA1_{105-113}$ (GVSENIFLK)	PSL GmbH, Heidelberg, Germany
$LSA1_{191-199}$ (KLQEQQSDL)	PSL GmbH, Heidelberg, Germany
$LSA1_{1655-1663}$ (RLEIPAIEL)	PSL GmbH, Heidelberg, Germany
$LSA1_{1786-1794}$ (KPIVQYDNF)	PSL GmbH, Heidelberg, Germany
$LSA1_{1850-1857}$ (KPNDKSLY)	PSL GmbH, Heidelberg, Germany
$LSA1_{1854-1861}$ (KSLYDEHI)	PSL GmbH, Heidelberg, Germany
$LSA3_{111-119}$ (DLLEEGNTL)	PSL GmbH, Heidelberg, Germany
$LSA3_{662-670}$ (KLEELHENV)	PSL GmbH, Heidelberg, Germany
$LSA3_{750-758}$ (VLDKVEETV)	PSL GmbH, Heidelberg, Germany
$LSA3_{829-837}$ (GLLNKLENI)	PSL GmbH, Heidelberg, Germany
$LSA3_{1029-1037}$ (MEKLKELEK)	PSL GmbH, Heidelberg, Germany
$LSA3_{1293-1301}$ (EPKDEIVEV)	PSL GmbH, Heidelberg, Germany
$LSA3_{1437-1445}$ (APFISAVAA)	PSL GmbH, Heidelberg, Germany
$Pfs16_{77-85}$ (MPLETQLAI)	PSL GmbH, Heidelberg, Germany
$STARP_{513-521}$ (MINAYLDKL)	PSL GmbH, Heidelberg, Germany
$TRAP_{3-11}$ (HLGNVKYLV)	PSL GmbH, Heidelberg, Germany
$TRAP_{51-59}$ (LLMDCSGSI)	PSL GmbH, Heidelberg, Germany
$TRAP_{107-115}$ (ASKNKEKAL)	PSL GmbH, Heidelberg, Germany
$TRAP_{109-117}$ (KNKEKALII)	PSL GmbH, Heidelberg, Germany
$TRAP_{122-130}$ (LSTNLPYGK)	PSL GmbH, Heidelberg, Germany
$TRAP_{303-311}$ (QPRPRGDNF)	PSL GmbH, Heidelberg, Germany
$TRAP_{305-313}$ (RPRGDNFAV)	PSL GmbH, Heidelberg, Germany
$TRAP_{515-523}$ (GIAGGLALL)	PSL GmbH, Heidelberg, Germany
$TRAP_{523-531}$ (LACAGLAYK)	PSL GmbH, Heidelberg, Germany
$TRAP_{539-548}$ (TPYAGEPAPF)	PSL GmbH, Heidelberg, Germany
$TRAP_{558-567}$ (DLDEPEQFRL)	PSL GmbH, Heidelberg, Germany

8.5.3 Bacteria

E.coli DH10B	Clonetech Inc., Palo Alto, CA, USA

8.5.4 Bacterial culture media

Ampicillin	Sigma Aldrich Chemie GmbH, Steinheim, Germany
LB agar (35 g/l)	Sigma Aldrich Chemie GmbH, Steinheim, Germany
Lysogeny broth (LB) (25 g/l)	Sigma Aldrich Chemie GmbH, Steinheim, Germany

8.5.5 Buffers, solutions and chemicals

2x HBS (pH 7.05)	50 mM HEPES 280 mM sodium chloride 0.78 mM disodium phosphate
ABTS buffer (pH 4.2)	0.1 M citric acid 0.2 M disodium phosphate 1 ABTS tablet/91 ml ABTS buffer
ABTS tablets	Roche Diagnostics GmbH, Mannheim, Germany
Bovine serum albumin fraction V (BSA)	Carl Roth GmbH & Co. KG, Karlsruhe, Germany
Calcium chloride dihydrate ($CaCl_2$ x 2 H_2O)	Sigma Aldrich Chemie GmbH, Steinheim, Germany
Chloroquine diphosphate salt	Sigma Aldrich Chemie GmbH, Steinheim, Germany
Citric acid ($C_6H_8O_7$) (≥ 99.5 %)	Sigma Aldrich Chemie GmbH, Steinheim, Germany
Dimethyl sulfoxide (DMSO)	Genaxxon bioscience GmbH, Ulm, Germany
Disodium phosphate (Na_2HPO_4)	Carl Roth GmbH & Co. KG, Karlsruhe, Germany
Ethanol	VWR International, Leicestershire, UK
Ficoll-Paque™ PLUS	GE Healthcare Life Sciences, Freiburg, Germany
Gel Loading Dye, Purple (6X)	New England Biolabs GmbH, Frankfurt am Main, Germany
GIBCO™ 10x PBS (pH 7.4)	Life Technologies GmbH, Karlsruhe, Germany
GIBCO™ 1x PBS (pH 7.4)	Life Technologies GmbH, Karlsruhe, Germany
GIBCO™ Trypan Blue Stain 0.4%	Life Technologies GmbH, Karlsruhe, Germany
HEPES	Sigma Aldrich Chemie GmbH, Steinheim, Germany
Hydrogen peroxide solution (H_2O_2), 30%	AppliChem, Darmstadt, Germany
PegGREEN	PEQLAB Biotechnologie GmbH, Erlangen, Germany
Protamine sulfate	MP Biomedicals, Santa Ana, California, USA
Puromycin dihydrochloride	Sigma Aldrich Chemie GmbH, Steinheim, Germany
Resiquimod (R848)	Sigma Aldrich Chemie GmbH, Steinheim, Germany
SeaKem® LE Agarose	Lonza, Rockland, ME, USA
Sodium chloride (NaCl)	Sigma Aldrich Chemie GmbH, Steinheim, Germany
TAE Buffer (50x)	PanReac AppliChem, Darmstadt, Germany
Tween® 20 ($C_{58}H_{114}O_{26}$)	Carl Roth GmbH & Co. KG, Karlsruhe, Germany

8.5.6 Cell lines

B95-8	DSMZ (ACC 100)
Jurkat76	Kind gift from Dr. Mirjam Heemskerk, LUMC, Leiden, Netherlands
Phoenix Ampho cells	Kind gift from Florian Salopiata, DKFZ, Heidelberg, Germany

8.5.7 Cell culture media

AIM V Medium	Life Technologies GmbH, Karlsruhe, Germany
GIBCO™ DMEM GlutaMAX™	Life Technologies GmbH, Karlsruhe, Germany
GIBCO™ FBS	Life Technologies GmbH, Karlsruhe, Germany
GIBCO™ L-glutamine	Life Technologies GmbH, Karlsruhe, Germany
GIBCO™ MEM Non-Essential Amino Acids Solution	Life Technologies GmbH, Karlsruhe, Germany
GIBCO™ PenStrep	Life Technologies GmbH, Karlsruhe, Germany
GIBCO™ RPMI	Life Technologies GmbH, Karlsruhe, Germany
GIBCO™ Sodium Pyruvate	Life Technologies GmbH, Karlsruhe, Germany
GIBCO™ Trypsin EDTA 1x	Life Technologies GmbH, Karlsruhe, Germany

8.5.8 Commercial kits

DNeasy Blood & Tissue Kit	Qiagen AG, Hilden, Germany
ELISA MAX™ Deluxe Set Human IL-2	BioLegend GmbH, Fell, Germany
KAPA Library Quant Kit	Roche Diagnostics GmbH, Mannheim, Germany
NEBuilder HIFI DNA Assembly	New England Biolabs GmbH, Frankfurt am Main, Germany
NucleoBond® Xtra Midi / Maxi	Macherey-Nagel GmbH & Co. KG, Düren, Germany
NucleoSpin® Gel and PCR Clean-up	Macherey-Nagel GmbH & Co. KG, Düren, Germany
NucleoSpin® Plasmid Kit	Macherey-Nagel GmbH & Co. KG, Düren, Germany
RNeasy Mini Kit	Qiagen AG, Hilden, Germany
SuperScript™ IV First-Strand Synthesis System	Invitrogen GmbH, Karlsruhe, Germany
TruSeq Nano DNA LT	Illumina, San Diego, CA, USA

8.5.9 Enzymes and additives

Cloning

BsrGI, MfeI, MluI, SalI	New England Biolabs GmbH, Frankfurt am Main, Germany

Calf Intestinal Alkaline Phosphatase (CIP)	New England Biolabs GmbH, Frankfurt am Main, Germany
Cutsmart buffer 10x	New England Biolabs GmbH, Frankfurt am Main, Germany
NEBuffer 2.1	New England Biolabs GmbH, Frankfurt am Main, Germany
T4 DNA Ligase	New England Biolabs GmbH, Frankfurt am Main, Germany
T4 DNA Ligase buffer 10x	New England Biolabs GmbH, Frankfurt am Main, Germany

RT and PCRs

10x PCR buffer	Qiagen AG, Hilden, Germany
5x First strand buffer (RT)	Life Technologies GmbH, Karlsruhe, Germany
5X Phusion HF Buffer	New England Biolabs GmbH, Frankfurt am Main, Germany
DTT	Life Technologies GmbH, Karlsruhe, Germany
Hotstart *Taq* DNA polymerase	Qiagen GmbH, Hilden, Germany
Magnesium chloride ($MgCl_2$)	Qiagen GmbH, Hilden, Germany
NP-40	Sigma Aldrich Chemie GmbH, Steinheim, Germany
Nuclease free water	Eppendorf AG, Hamburg, Germany
Phusion® High-Fidelity DNA Polymerase	New England Biolabs GmbH, Frankfurt am Main, Germany
RNAsin®	Promega Inc., Madison, WI, USA
SuperScript™ IV Reverse Transcriptase	Life Technologies GmbH, Karlsruhe, Germany

8.5.10 Nucleotides and nucleic acids

100 bp DNA Ladder	New England Biolabs GmbH, Frankfurt am Main, Germany
1kb Plus DNA Ladder	New England Biolabs GmbH, Frankfurt am Main, Germany
Desoxynucleotide Triphosphates (dNTPs)	Life Technologies GmbH, Karlsruhe, Germany
Oligonucleotides	Eurofins Genomics Germany GmbH, Ebersberg, Germany
Random Hexamer Primers	Roche Diagnostics GmbH, Mannheim, Germany

8.5.11 Instruments and consumables

1.5 ml reaction tubes	Sarstedt AG, Nümbrecht, Germany
2 ml reaction tubes	Sarstedt AG, Nümbrecht, Germany
13 ml tubes	Sarstedt AG, Nümbrecht, Germany
96-well semi-skirted PCR plate	4titude, Surrey, UK
Adhesive aluminum foil seal	4titude, Surrey, UK
BD FACSAria™ III	BD Biosciences GmbH, Heidelberg, Germany
Cell culture 6-well plate	Greiner Bio-One GmbH, Frickenhausen, Germany
Cell culture 24-well plate	Corning Inc., Corning, NY, USA
Cell culture 96-well plate, U-bottom	TPP, Trasadingen, Switzerland
CellStar sterile serological pipettes 2 ml, 5 ml, 10 ml, 25 ml, 50 ml	Greiner Bio-One GmbH, Frickenhausen, Germany
Centrifuge 5427 R (rotor FA-45-30-11)	Eppendorf
Centrifuge mikro 200R (rotor 2424-B)	Andreas Hettich GmbH & Co.KG, Tuttlingen, Germany
Centrifuge rotina 420R (rotor 4784-A)	Andreas Hettich GmbH & Co.KG, Tuttlingen, Germany
Centrifuge universal 320R (rotor 1689-A)	Andreas Hettich GmbH & Co.KG, Tuttlingen, Germany
Centrifuge 5180R (rotor 5-4-104, rotor A-2-DWP-AT)	Eppendorf AG, Hamburg, Germany
CO_2 Incubator CB210	Binder GmbH, Tüttlingen, Germany
CO_2 Incubator Heracell™ 240i	Thermo Scientific Inc., Rochester, NY, USA
CoolCell LX / FTS30	Corning Inc., Corning, NY, USA
CountessTM II FL Automated Cell Counter	Life Technologies GmbH, Karlsruhe, Germany
CountessTM Cell Counting Chamber Slides	Life Technologies GmbH, Karlsruhe, Germany
CryoTube™ Vials, 1.8 ml	Thermo Fisher Scientific Inc., Darmstadt, Germany
EC 300 XL power supply	Thermo Scientific Inc., Rochester, NY, USA
ELISA plates (96-well, flat bottom)	Costar Inc., Corning, Action, MA, USA
FrameStar® 384	4titude, Surrey, UK
Freedom Evo200 automation platform	Tecan, Crailsheim, Germany
Gel Doc™ XR+	Bio-Rad Laboratories GmbH, München, Germany
Luna Automated Cell Counter	Logos Biosystems Inc., Anyang, Korea
Luna Vell Counting Slides	Logos Biosystems Inc., Anyang, Korea
M1000Pro plate reader	Tecan, Crailsheim, Germany
Mastercycler® ep Gradient S	Eppendorf AG, Hamburg, Germany
Mastercycler® Pro 384	Eppendorf AG, Hamburg, Germany
Microscope Primovert	ZEISS Microscopy, Oberkochen, Germany
Model 680 Microplate Reader	Bio-Rad Laboratories GmbH, München, Germany
Multichannel pipets Eppendorf Research® plus	Eppendorf AG, Hamburg, Germany

0.5-10 µl, 10-100 µl, 30-300 µl, 120-1200 µl Multipette plus	Eppendorf AG, Hamburg, Germany
Multiply - µStrip Pro 8-strip (PCR tube strip)	Sarstedt AG, Nümbrecht, Germany
Multitron Pro (Bacteria shaker)	Infors HT, Bottmingen, CH
NanoQuant plate™	Tecan, Crailsheim, Germany
Neubauer Counting Chamber by Marienfeld	Carl Roth GmbH & Co. KG, Karlsruhe, Germany
OWL A3-1, OWL B3, OWL Easycast B1A	Thermo Scientific Inc., Rochester, NY, USA
PC	LG Electronics Deutschland GmbH, Ratingen, Germany
PCR foil seal	4titude, Surrey, UK
Petri dishes (100 mm)	Greiner Bio-One GmbH, Frickenhausen, Germany
Pipetboy acu 2	Integra Biosciences GmbH, Fernwald, Germany
Gilson™ PIPETMAN Classic™ 0.1-2 µl, 2-20 µl, 20-200 µl, 100-1000 µl	Gilson S.A.S., Villiers-le-Bel, France
Polyolefin sealing foil for microtiterplate	HJ-Bioanalytik GmbH, Erkelenz, Germany
Polypropylene tubes (15 ml, 50 ml)	Sarstedt AG, Nümbrecht, Germany
Polystyrene round bottom tube (5 ml) with cell strainer cap	BD Biosciences GmbH, Heidelberg, Germany
T25 / T75 / T150 cm^2 flask	TPP, Trasadingen, Switzerland
Thermomixer comfort	Eppendorf AG, Hamburg, Germany
Vortex genie 2	Scientific Industries Inc., Bohemia, NY, USA
Water bath with thermostat	Memmert GmbH + Co. KG, Schwabach, Germany

8.5.12 Software

Clone Manager Professional 9	Scientific & Educational Software, Westminster, USA
FlowJo v10.6	Treestar Systems Inc., Ashland, USA
GraphPad Prism Version 8.1.2	GraphPad Software Inc., La Jolla, USA
Illustrator® CS6	Adobe Inc., San Jose, CA, USA
Mendeley Desktop	Mendeley Ltd, London, UK
Microsoft® Office 2013/2016	Microsoft GmbH, Stuttgart, Germany
Pearl	Version 12.5, open source distribution
R	Version 3.4.2
Rstudio version 0.99.484	RStudio, Inc., Boston, MA USA

8.5.13 Web Resources

Clustal Omega	http://www.ebi.ac.uk/Tools/msa/clustalo/
Ensemble Genome Browser	http://www.ensembl.org/index.html

Expasy SIB Bioinformatics Resource Portal	http://expasy.org/
IMGT®	http://www.imgt.org/
NCBI Ig Blast	http://www.ncbi.nlm.nih.gov/igblast/
PlasmoDB	http://plasmodb.org/plasmo/
SignalP-4.1 Server	http://www.cbs.dtu.dk/services/SignalP/
VDJdb	https://vdjdb.cdr3.net/search

9 Acknowledgment

First of all I want to thank Prof. Dr. Hedda Wardemann for giving me the opportunity to perform my PhD thesis in the Department of B cell Immunology – and work on T cells. Thanks for the scientific guidance, great support and inspiring discussions throughout my PhD and for always being open to my ideas.

I want to thank Prof. Dr. Hans-Reimer Rodewald and Prof. Dr. Benjamin Mordmüller for the advice and scientific discussions during my thesis advisory committee meetings. Further I want to thank Prof. Hans-Reimer Rodewald, Prof. Dr. Thomas Höfer and Prof. Dr. Ralf Bartenschlager for offering to review my PhD thesis and being part of my thesis examination committee.

The work presented in this thesis would not have been possible without the work of Prof. Dr. Benjamin Mordmüller and the clinical team in Tübingen, as well as the courage of the trial volunteers – thank you! Further I want to thank Dr. Giulia Costa and Dr. Elena Levashina for sharing the sporozoite lysate with me.

I also want to deeply thank Sandro Hoffmann, Rebecca Hundsdorfer and Julia Puchan for helping me with the experiments and sharing the scientific excitement about this project. Further I want to thank Dorien Foster, Claudia Winter and Julia Gärtner for all the support in the lab. I thank Dr. Julia Ludwig and Dr. Rajagopal Murugan for the helpful scientific and non-scientific discussions and for supporting me especially during stressful phases. A special thanks goes to Dr. Christian Busse, for introducing me into the world of Perl and for patiently teaching me almost everything I know about bioinformatics. I also want to thank all members of the Department of B cell Immunology for the nice working atmosphere and for sharing my coffee addiction.

Lastly, I want to thank my family, my friends and Flo for all the patience and support during the last years.